

# Colorado - New Mexico Regional Extreme Precipitation Study

## Summary Report

### Volume III

#### Regional Precipitation-Frequency Estimation

November 30, 2018

- 1
- 2
- 3
- 4
- 5
- 6
- 7



*This page left intentionally blank*

---

# Colorado – New Mexico Regional Extreme Precipitation Study

---

## Summary Report

### Volume III

#### Regional Precipitation-Frequency Estimation

Prepared by:

*MetStat, Inc.*

*and*

*MGS Engineering Consultants, Inc.*

*and*

*Applied Climate Services*

November 30, 2018

Revised July, 2019



**COLORADO**  
Division of Water Resources  
Department of Natural Resources



*This page left intentionally blank*

# Table of Contents

List of Figures .....	iii
List of Tables.....	ix
Appendices .....	xii
Glossary .....	xiii
1. Executive Summary .....	1
2. Overview.....	3
2.1. Regional Frequency Analysis and Storm Typing for Data Homogeneity .....	10
2.2. L-moment Statistics.....	10
2.3. Regional Growth Curve .....	11
2.4. Regional Probability Distribution .....	12
2.5. Spatial Mapping of L-Moment Statistics .....	16
2.6. Point Precipitation-Frequency .....	17
2.7. Watershed Precipitation-Frequency Relationships.....	17
2.8. Risk-Informed Decision-Making (RIDM) Framework .....	19
2.8.1 History of Uses and Application by Federal Agencies/Dam Owners.....	21
2.8.2 Application and Use by State Regulatory Agencies .....	22
3. Data Description and Sources .....	24
3.1. Precipitation Gauge Data .....	24
3.2. Meteorological Variables for Storm Typing.....	25
3.3. Mapping Datasets.....	27
3.4. Storm Data .....	29
3.5. Temporal Distribution Datasets .....	31
3.6. Temperature Time Series .....	32
4. Methodology.....	32
4.1. Storm Types of Interest .....	32
4.1.1 Local Storms (LS) .....	34
4.1.2 Mesoscale Storms with Embedded Convection (MEC) .....	34
4.1.3 Mid-Latitude Cyclone (MLC) .....	34
4.1.4 Tropical Storms and Remnants (TSR) .....	35
4.2. Storm Typing Procedures .....	35
4.2.1 Manual Storm Typing .....	37
4.2.2 Automated Storm Typing.....	44

4.3.	Annual Maximum Series Assembly and Quality Control .....	46
4.3.1	Key Durations for Storm Types .....	46
4.3.2	Assembly of Precipitation AMS .....	47
4.3.3	Data Quality Checking .....	49
4.4.	Regional Point Precipitation Frequency (PF) Analysis .....	52
4.4.1	Heterogeneous Super Regions .....	53
4.4.2	Homogeneous Sub-Regions .....	56
4.4.3	Spatial Mapping of L-Moment Statistics .....	57
4.4.4	Identification of the Regional Probability Distribution .....	64
4.4.5	Equivalent Independent Record Length (EIRL) .....	67
4.4.6	Spatial Mapping of Point Precipitation-Frequency Estimates .....	67
4.4.7	Uncertainties in Point Precipitation-Frequency Estimates .....	68
4.5.	Watershed Precipitation Frequency Relationships .....	68
4.5.1	Uncertainties in Watershed Precipitation-Frequency Estimates .....	71
4.6.	Development of Watershed PF Relationships via a Scaling Procedure .....	72
4.7.	Spatial and Temporal Distributions for Each Storm Type .....	73
4.7.1	Temporal Precipitation .....	73
4.7.2	Spatial Precipitation .....	75
4.7.3	Temperature Time Series .....	76
4.8.	Storm Seasonality .....	77
5.	Results .....	79
5.1.	Point Precipitation-Frequency .....	79
5.1.1	48-Hour Mid-Latitude Cyclones .....	79
5.1.2	2-hour Local Storms .....	105
5.1.3	6-hour Mesoscale Storms with Embedded Convection .....	125
5.2.	Watershed Precipitation Frequency Scaling .....	144
5.3.	Representative Temporal, Spatial, and Temperature Patterns .....	147
5.3.1	Temporal .....	147
5.3.2	Spatial .....	148
5.3.3	Freezing Levels .....	148
6.	Comparisons .....	149
6.1.	NOAA Atlas 14 .....	149
6.2.	Estimates of Annual Exceedance Probability for Historical Storms .....	160
7.	Uncertainty in Precipitation Frequency Estimates .....	162

8. Limitations ..... 165

9. Conclusions and Applications..... 165

10. Deliverables ..... 166

11. References ..... 166

## List of Figures

Figure 1. Example of Hyetograph Shape for Local Storm (LS) recorded at Cucharas Dam Colorado on July 12, 1953 ..... 4

Figure 2. Example of the spatial extent of a Local Storm (LS) on July 28, 2014..... 4

Figure 3. Example of Hyetograph Shape for Mesoscale Storm with Embedded Convection (MEC) recorded at Eads Colorado on August 15, 1968 ..... 5

Figure 4. Example of the spatial extent of a Mesoscale Storm with Embedded Convection (MEC) storm on July 19, 2007 ..... 5

Figure 5. Example of Hyetograph Shape for Mid-Latitude Cyclone (MLC) recorded near Hobbs New Mexico on August 22-23, 1966 ..... 6

Figure 6. Example of the spatial extent of a Mid-latitude Cyclone (MLC) storm on September 8, 2013 ..... 6

Figure 7. Depiction of three Macro Regions formed by major mountain barriers delineating areas with distinct differences in precipitation-frequency, temporal and spatial characteristics, and storm seasonality..... 9

Figure 8. Example of a Regional Growth Curve ..... 11

Figure 9. Example of effect of changes in L-Cv on Regional Growth Curve ..... 12

Figure 10. Example of effect of changes in L-Skewness on Regional Growth Curve ... 12

Figure 11. L-Moment ratio diagram depicting regional L-Skewness and L-Kurtosis values for homogeneous sub-regions in the Eastern region of the project area for 48-Hour precipitation maxima for MLCs..... 14

Figure 12. L-Moment Ratio Diagrams for L-Skewness, L-Kurtosis and L-Cinco for the Local Storm type for each Macro Region ..... 15

Figure 13. L-Moment Ratio Diagrams for L-Skewness, L-Kurtosis, and L-Cinco for the Mid-Latitude Cyclone (MLC) storm type for each Macro Region ..... 16

Figure 14. Example Watershed Precipitation-Frequency relationship for an 800-mi<sup>2</sup> watershed on the eastern face of the Rocky Mountains near Denver ..... 19

Figure 15. Project area and the defined Storm Typing Zones. (The NW and NNW Zones were typed based on Zone 1.) ..... 26

Figure 16. Hydroclimatic regions of Colorado used to describe and characterize extreme precipitation events ([https://ccc.atmos.colostate.edu/pdfs/Climo\\_97-1\\_Extreme\\_ppt.pdf](https://ccc.atmos.colostate.edu/pdfs/Climo_97-1_Extreme_ppt.pdf)) ..... 28

Figure 17. Selected Watersheds for computing scalable ARFs ..... 29

Figure 18. Seasonal Distribution of storm types for 1895-2014 period from DDST where the y-axis is the total number of days across the Storm Typing Zones (Figure 15) for each type where MLCs are red, TSRs are green, MECs are light blue and hybrid

MLC/MEC are purple. The data are grouped into larger general macro-climatic areas- West, East and South ..... 33

Figure 19. Time series of Tropical Storms and Remnants that affected the Colorado-New Mexico Project Area for 1853-2014 period ..... 35

Figure 20. Project Area depicting Storm Detection Network of daily precipitation stations (black dots) and 17 Storm Typing Zones (red boxes) ..... 38

Figure 21. Selected tropical storm tracks (from IBTrACs database) used to define days with TSR influence over the CO-NM Project Area ..... 39

Figure 22. Excerpt of Storm Typing Application panels ..... 41

Figure 23. Example of four panel display of 500-mb (upper left) and 850-mb (upper right) Height Contour Maps, Pw (lower left) and CAPE (lower right) used during manual storm typing ..... 42

Figure 24. Storm Tying Application panels for May 26th, 1996 MLC event ..... 43

Figure 25. Storm Tying Application panels for July 21st, 1972 MEC event ..... 44

Figure 26. Flowchart of Automated Storm Typing Algorithm ..... 46

Figure 27. Spatial plot of 1-day observations showing 4.53" at Hope, NM (294112) and some corroborating rain, up to 1.27", nearby on June 8th, 1992 ..... 51

Figure 28. Original COOP Observation Form showing 4.53" recorded on June 8th, 1992 at Hope, NM (294112) with comments related to severe thunderstorms ..... 52

Figure 29. Heterogeneous Climatic Super Regions and PRISM Mean Annual Precipitation ..... 54

Figure 30. Heterogeneous Climatic Regions with aspects associated with slopes >2 degrees ..... 54

Figure 31. Final Heterogeneous (Climatic) Super Regions ..... 56

Figure 32. Scatterplot of sample 48-Hour at-site means for MLCs for Super Regions in Mapping Area A in New Mexico for stations with record lengths of 20-years or more . 59

Figure 33. Comparison of regression-predicted 48-hour at-site means and sample 48-hour at-site means for Super Regions 30, 31, 45 and 55 for MLCs ..... 60

Figure 34. Comparison of spatially mapped 48-hour at-site means and sample 48-hour at-site means for Super Regions 30, 31, 45, 55 in mapping Area A for MLCs ..... 60

Figure 35. Map of 48-hour at-site means for the MLC storm type showing where Super Regions were combined into Mapping Areas ..... 61

Figure 36. Second order polynomial fitted to regional L-Cv values for homogeneous sub-regions (groupings of stations shown as blue dots) in Mapping Area A in Rio Grande Macro Region ..... 63

Figure 37. Mapping Areas used for mapping L-Cv and L-Skewness throughout the project area ..... 64

Figure 38. L-Moment ratio diagram depicting regional L-Skewness and L-Kurtosis values for homogeneous sub-regions for 48-hour precipitation maxima for MLCs in the West Macro Region ..... 66

Figure 39. Precipitation field for MEC storm of September 21, 2014 showing separate storm center zones and spatial precipitation patterns for the 6-hour duration ..... 70

Figure 40. Watershed precipitation-frequency relationship and 90 percent uncertainty bounds for 86-mi<sup>2</sup> watershed near Ft Collins for LS storm type ..... 71

Figure 41. Example of relative contribution to total uncertainty from various sources of uncertainty in developing Watershed Precipitation-Frequency Relationship for the MEC Storm Type in the East Macro Region ..... 72

Figure 42. Example of Watershed Precipitation-Frequency Areal Reduction Factors for the three storm types for the West Macro Region ..... 73

Figure 43. Example of synthetic temporal pattern for Local Storm type for East Macro Region ..... 75

Figure 44. The ratio of the PRISM precipitation relative to the watershed mean clipped to the watershed (top) and precipitation amounts scaled to a selected AEP (bottom) ..... 76

Figure 45. Example time series of freezing-level height (ZL) and 1000-mb temperatures (1000T) for the Rio Grande Macro Region ..... 77

Figure 46. Seasonality Sub-areas used to provide seasonal information for extreme storms of each Storm Type ..... 78

Figure 47. Location of daily and hourly precipitation stations used in the precipitation-frequency analysis for MLCs and the seasonal mean precipitation used in the predictor equations for the West Macro Region ..... 80

Figure 48. Histogram of data years for stations used in the precipitation-frequency analysis for MLCs ..... 81

Figure 49. Scatterplot of station sample values of 48-Hour at-site means for MLCs against seasonal mean precipitation for East Macro Region ..... 82

Figure 50. Comparison of observed and mapped 48-Hour at-site means for MLC storm type for three Macro Regions..... 84

Figure 51. Map of at-site means for 48-Hour duration for MLCs ..... 85

Figure 52. Example of variation of regional L-Cv with latitude for 48-hour MLCs in the East Macro Region ..... 88

Figure 53. Comparison of observed regional L-Cv and mapped regional L-Cv for 192 homogeneous sub-regions for 48-Hour MLCs using latitude and DEM elevation as explanatory variables..... 88

Figure 54. Map of regional L-Cv for 48-hour duration for MLCs..... 89

Figure 55. Map of regional L-Skewness for 48-hour precipitation annual maxima for MLCs ..... 90

Figure 56. L-Moment ratio diagrams depicting regional L-Skewness and L-Kurtosis pairings for homogeneous sub-regions for 48-Hour duration for MLCs for each of the Macro Regions..... 91

Figure 57. Map of regional Hondo for 48-hour precipitation annual maxima for MLCs 92

Figure 58. Probability plots of historical 2-day precipitation annual maxima for MLC storm type for stations located in the three Macro Regions and comparison with regional precipitation-frequency relationship for those locations ..... 94

Figure 59. Isopluvial map of 48-hour precipitation maxima for an AEP of 1:100 for MLCs ..... 95

Figure 60. Isopluvial map of 48-hour precipitation maxima for an AEP of 1:1,000 for MLCs ..... 96

Figure 61. Frequency histograms for seasonality of extreme 48-hour duration MLCs.. 97

Figure 62. Probability graphics depicting magnitude of dimensionless uncertainty bounds for point MLC precipitation-frequency estimates ..... 101

Figure 63. Long-term index stations used to develop 24-hour and 72-hour relationships to apply to 48-hour MLC AEP ..... 103

Figure 64. Comparison of 24-hour, 48-hour and 72-hour precipitation-frequency estimates for 1:1000 AEP for 48-hour MLCs ..... 104

Figure 65. Comparison of the magnitudes of TSR and MLC 48-hour annual maxima and a comparison of TSR and MLC annual maximum precipitation magnitudes relative to the at-site mean at stations in the CO-NM project area where the whiskers extend four times the Interquartile Range ..... 105

Figure 66. Location of hourly precipitation stations used in the precipitation-frequency analysis for Local Storms (LS) and the seasonal mean precipitation used in the predictor equations ..... 106

Figure 67. Histogram of data years for stations used in the precipitation-frequency analysis for Local Storms ..... 107

Figure 68. Comparison of station values and mapped values of 2-Hour at-site means for all Mapping Areas for Local Storms ..... 108

Figure 69. Map of at-site means for 2-hour duration for Local Storms ..... 109

Figure 70. Comparison of observed regional L-Cv and mapped regional L-Cv for 2-hour duration for homogeneous sub-regions for Local Storms ..... 111

Figure 71. Comparison of observed regional L-Skew and mapped regional L-Skew for 2-hour duration for homogeneous sub-regions for Local Storms ..... 112

Figure 72. Map of regional L-Cv for 2-hour duration for Local Storms ..... 113

Figure 73. Map of regional L-Skewness for 2-hour precipitation annual maxima for Local Storms ..... 114

Figure 74. L-Moment ratio diagrams depicting regional L-Skewness and L-Kurtosis values for homogeneous sub-regions for 2-Hour duration for Local Storms for each of the Macro Regions ..... 115

Figure 75. Map of regional Hondo for 2-hour precipitation annual maxima for Local Storms ..... 116

Figure 76. Probability plots of historical 2-hour precipitation annual maxima for Local Storm type for stations located in the three Macro Regions and comparison with regional precipitation-frequency relationship for those locations ..... 118

Figure 77. Isopluvial map of 2-hour precipitation maxima for an AEP of 1:100 for Local Storms ..... 119

Figure 78. Isopluvial map of 2-hour precipitation maxima for an AEP of 1:1000 for Local Storms ..... 120

Figure 79. Frequency histograms for seasonality of extreme 2-hour duration Local Storms ..... 122

Figure 80. Probability graphics depicting magnitude of dimensionless uncertainty bounds for point LS precipitation-frequency estimates ..... 125

Figure 81. Location of hourly precipitation stations used in the precipitation-frequency analysis for MECs and the seasonal mean precipitation used in the predictor equations ..... 126

Figure 82. Histogram of data years for stations used in the precipitation-frequency analysis for MECs ..... 127

Figure 83. Scatter plot of the observed 6-hour MEC at-site means with the mapped at-site means ..... 128

Figure 84. Map of at-site means for 6-hour duration for MECs ..... 129

Figure 85. Comparison of observed regional L-Cv and mapped regional L-Cv for 6-hour duration for homogeneous sub-regions for MEC Storms..... 130

Figure 86. Map of regional L-Cv for 6-hour duration for MECs ..... 132

Figure 87. Map of regional L-Skewness for 6-hour precipitation annual maxima for MECs ..... 133

Figure 88. Map of regional Hondo for 6-hour precipitation annual maxima for MECs 135

Figure 89. Probability plots of historical 6-hour precipitation annual maxima for MEC storm type for stations located in the three Macro Regions and comparison with regional precipitation-frequency relationship for those locations ..... 137

Figure 90. Isopluvial map of 6-hour precipitation maxima for an AEP of 1:100 for MECs ..... 138

Figure 91. Isopluvial map of 6-hour precipitation maxima for an AEP of 1:1000 for MECs ..... 139

Figure 92. Frequency histograms for seasonality of extreme 6-hour duration MECs . 141

Figure 93. Probability graphics depicting magnitude of dimensionless uncertainty bounds for point MEC precipitation-frequency estimates ..... 144

Figure 94. Watershed ARFs for LS, MEC, and MLC storm types for the East Macro Region ..... 145

Figure 95. Watershed ARFs for LS, MEC, and MLC storm types for the West Macro Region ..... 146

Figure 96. Watershed ARFs for LS, MEC, and MLC storm types for the Rio Grande Macro Region ..... 146

Figure 97. Point comparisons in each Macro Region between NOAA Atlas 14 and the results of CO-NM REPS (1 of 3) ..... 151

Figure 98. Point comparisons in each Macro Region between NOAA Atlas 14 and the results of CO-NM REPS (2 of 3) ..... 152

Figure 99. Point comparisons in each Macro Region between NOAA Atlas 14 and the results of CO-NM REPS (3 of 3) ..... 153

Figure 100. 1 in 100 AEP 2- and 6-hour LS and MEC comparison to NOAA Atlas 14 in Colorado; areas without color represent areas where REPs best estimates are within NOAA-14 confidence limits ..... 154

Figure 101. 1 in 100 AEP 2- and 6-hour LS and MEC Comparison to NOAA Atlas 14 in New Mexico; areas without color represent areas where REPs best estimates are within NOAA-14 confidence limits ..... 155

Figure 102. One in 100 AEP 48-hour MLC/TSR comparison to NOAA Atlas 14 in Colorado and New Mexico; areas without color represent areas where REPs best estimates are within NOAA-14 confidence limits ..... 156

Figure 103. 1 in 100 AEP 2- and 6-hour LS and MEC comparison to NOAA Atlas 14 in Colorado; areas without color represent areas where NOAA-14 best estimates are within REPs confidence limits ..... 157

Figure 104. 1 in 100 AEP 2- and 6-hour LS and MEC comparison to NOAA Atlas 14 in New Mexico; areas without color represent areas where NOAA-14 best estimates are within REPs confidence limits ..... 158

Figure 105. 1 in 100 AEP 48-hour LS and MEC comparison to NOAA Atlas 14 in Colorado and New Mexico; areas without color represent areas where NOAA-14 best estimates are within REPs confidence limits ..... 159

Figure 106. Example of relative contribution to total uncertainty from various sources of uncertainty in developing Watershed Precipitation-Frequency Relationship for the MEC Storm Type in the East Macro Region ..... 163

Figure 107. Probability graphics depicting magnitude of dimensionless uncertainty bounds for point MEC precipitation-frequency estimates ..... 164

## List of Tables

Table 1. Number of spatial storm patterns used for calculating PF-ARFs.....	18
Table 2. Storm Types and their key durations for the Colorado-New Mexico area.....	24
Table 3. List of data sources and reporting interval for precipitation gauge data. (ALERT data are Automatic Local Evaluation in Real Time rain gauges that do not report at regular intervals but were converted to hourly increments.).....	24
Table 4. List of SPAS storm analyses (Volume 2) which were used to provide storm spatial patterns and their associated Macro Region (Figure 7) .....	30
Table 5. List of storms from HRRR model output (Volume 4) which were used to provide storm patterns and their associated Macro Region (Figure 7) .....	31
Table 6. Storm Types and Numerical Codes Used in Storm Typing and DDST .....	36
Table 7. Observational period adjustments for number of observational periods.....	48
Table 8. Observational period adjustments for gauge types and durations .....	49
Table 9. Uncertainty Characteristics for Point Precipitation-Frequency Estimates for a site in the East Macro Region for the MLC storm type .....	68
Table 10. Additional uncertainty characteristics for Watershed Precipitation- Frequency for the LS and MEC storm types .....	71
Table 11. Number of Stations and data years for stations with 20 or more data years used in the precipitation-frequency analysis for MLCs.....	81
Table 12. Listing of explanatory variables for 48-Hour at-site means for MLCs and Relative RMSE for predictive equations .....	83
Table 13. Listing of number of homogeneous sub-regions for each mapping area for 48-hour L-Cv for MLCs and RMSE for regional prediction equations .....	86
Table 14. Listing of number of homogeneous sub-regions for each mapping area for 48-hour L-Skewness for MLCs and RMSE for regional prediction equations .....	86
Table 15. Summary statistics for spatial mapping of 48-hour duration regional L-Cv and L-Skewness for MLCs within contributing watershed area .....	87
Table 16. Estimate of EIRL for 48-Hour duration for MLCs .....	98
Table 17. Comparison of actual number of exceedances for selected AEPs with expected number from binomial distribution for Mid-Latitude Cyclone (MLC) storm type for West Macro Region .....	99
Table 18. Comparison of actual number of exceedances for selected AEPs with expected number from binomial distribution for Mid-Latitude Cyclone (MLC) storm type for Rio Grande Macro Region.....	99
Table 19. Comparison of actual number of exceedances for selected with expected number from binomial distribution for Mid-Latitude Cyclone (MLC) storm type for East Macro Region.....	99
Table 20. Number of Stations and data years for stations with 20 or more data years used in the precipitation-frequency analysis for Local Storms .....	107
Table 21. Listing of explanatory variables for 2-hour at-site means for Local Storms and RMSE for regional prediction equations .....	108
Table 22. Listing of number of homogeneous sub-regions for each mapping area for 2- hour L-Cv for Local Storms and RMSE for predictive equations.....	110

Table 23. Listing of number of homogeneous sub-regions for each mapping area for 2-hour L-Skewness for Local Storms and RMSE for regional prediction equations ..... 111

Table 24. Summary statistics for spatial mapping of 2-hour duration regional L-Cv and L-Skewness for Local Storms within contributing watershed area ..... 111

Table 25. Estimate of EIRL for 2-Hour duration for Local Storms ..... 123

Table 26. Comparison of actual number of exceedances for selected with expected number from binomial distribution for Local Storm (LS) storm type for West Macro Region ..... 123

Table 27. Comparison of actual number of exceedances for selected AEPs with expected number from binomial distribution for Local Storm (LS) storm type for Rio Grande Macro Region ..... 124

Table 28. Comparison of actual number of exceedances for selected AEPs with expected number from binomial distribution for Local Storm (LS) storm type for East Macro Region ..... 124

Table 29. Number of Stations and data years for stations with 20 or more data years used in the precipitation-frequency analysis for MECs ..... 127

Table 30. Listing of explanatory variables for 6-hour at-site means for MECs and RMSE for predictive equations ..... 128

Table 31. Listing of number of homogeneous sub-regions for each mapping area (the Macro Regions in this case) for 6-hour L-Cv for MEC Storms and RMSE for predictive equations ..... 130

Table 32. Listing of number of homogeneous sub-regions for each mapping area (the Macro Regions in this case) for 6-hour L-Skewness for MEC Storms and RMSE for predictive equations ..... 131

Table 33. Summary statistics for spatial mapping of 6-hour duration regional L-Cv and L-Skewness for MECs within contributing watershed area ..... 131

Table 34. Estimate of EIRL for 6-Hour duration for MECs ..... 142

Table 35. Comparison of actual number of exceedances for selected AEPs with expected number from binomial distribution for Mesoscale Storm with Embedded Convection (MEC) storm type for West Macro Region ..... 142

Table 36. Comparison of actual number of exceedances for selected AEPs with expected number from binomial distribution for Mesoscale Storm with Embedded Convection (MEC) storm type for Rio Grande Macro Region ..... 143

Table 37. Comparison of actual number of exceedances for selected AEPs with expected number from binomial distribution for Mesoscale Storm with Embedded Convection (MEC) storm type for East Macro Region ..... 143

Table 38. Watershed size limits for application of PF-ARFs ..... 145

Table 39. PF-ARF equations ..... 147

Table 40. Number of Storms Analyzed (Total = 134) as part of Temporal Distribution Analysis ..... 148

Table 41. Number of scalable historical storms (Total = 44) for use in MetPortal ... 148

Table 42. Number of scalable synthetic storms (Total = 12) for use in MetPortal .... 148

Table 43. Summary of the number of events of each storm type for a given macro-region and duration contained within the sample set of NOAA Atlas 14 AMS. Ratios are expressed in station-years to the total station-years of record. Stations selected include Ft Collins, CO and Pueblo Memorial AP, CO (East); Rienhardt Ranch, NM and

Santa Fe, NM (Rio Grande); Cedaredge, CO, Durango, CO, and Grand Junction  
Regional AP, CO (West). ..... 150  
Table 44. AEPs for the most extreme historical storms observed in the project area.  
NA's indicate the storm center was outside of our spatial mapping domain. Local  
storms are 2-hours, MECs are 6-hour and MLCs 48-hour. .... 160  
Table 45. List of Storm Types and associated durations available via the MetPortal 166

# Appendices

Appendix A. Excerpt of the L-RAP User's Manual

Appendix B. Metadata and sample L-moment statistics for stations used analysis

Appendix C. Schaefer-Wallis-Taylor (SWT) approach of the climate region method for regional precipitation-frequency analysis

Appendix D. Development of a watershed PF relationship and uncertainty bounds using the Stochastic Storm Transposition Method (STTM), also known as Move-the-Earth

Appendix E. Storms used in Temporal Analysis and figures of available scalable storms

## Document Revision History

Release Date	Description
November 2018	Primary release
July 2019	Update to Section 5.1.3 and Appendix E

# Glossary

**ANNUAL EXCEEDANCE PROBABILITY (AEP)** - The probability associated with exceeding a given amount in any given year once or more than once; the inverse of AEP provides a measure of the average time between years (and not events) in which a particular value is exceeded at least once; the term is associated with analysis of annual maximum series.

**ANNUAL MAXIMUM SERIES (AMS)** - Time series of the largest precipitation amounts in a continuous 12-month period (calendar or water year) for a specified duration at a given station.

**AT-SITE** - The term used to distinguish the analyses/data at a specific station/site from the regional analyses/data.

**BIAS** - The bias of an estimator is the difference between an expected value (mean value) of the estimator ( $e$ ) and the true value of the parameter being estimated ( $q$ ). In this study, bias was computed as part of spatial mapping of L-Moment statistics to assess the difference between expected values from a predictor equation and the observed values of the L-Moments. In this application, the true values of the L-moments statistics are unknown and a measure is desired as an indicator of how well a predictor equation for spatial mapping is matching the observed values. Bias ( $e$ ) is computed as the expected value (mean) of  $(e-q)$ , where  $e$  is the predicted value from the predictor equation and  $q$  is the observed value, where the mean of the collection of observed values is assumed to represent the true values. Mean bias is computed as the mean value for all pairings of predicted and observed values.

**DATA YEARS** - Number of years in which enough precipitation data existed to extract meaningful and usable annual maximum in a station's period of record (or data years).

**DISTRIBUTION FUNCTION (CUMULATIVE DISTRIBUTION FUNCTION)** - Mathematical description that completely describes frequency distribution of a random variable, here precipitation. distribution functions commonly used to describe precipitation data include 3-parameter distributions such as Generalized Extreme Value (GEV), Generalized Normal, Generalized Pareto, Generalized Logistic and Pearson type III, the 4-parameter Kappa distribution, and the 5-parameter Wakeby distribution.

**ESRI ASCII GRID** - Grid format with a 6-line header, which provides location and size of the grid and precedes the actual grid data. The grid is written as a series of rows, which contain one ASCII integer or floating point value per column in the grid. The first element of the grid corresponds to the upper-left corner of the grid. This format was developed by Environmental Systems Research Institute (ESRI).

**FREQUENCY** - General term for specifying the average recurrence interval or annual exceedance probability associated with specific precipitation magnitude for a given duration.

**FREQUENCY ANALYSIS** - Process of derivation of a mathematical model that represents the relationship between precipitation magnitudes and their frequencies.

**HONDO** - The second shape parameter of the 4-parameter Kappa probability distribution.

**HYETOGRAPH** - Graphical representation of time series of precipitation intensity; see Temporal Pattern.

**L-MOMENTS** - L-moments are summary statistics for probability distributions and data samples. They are analogous to ordinary moments, providing measures of location, dispersion, skewness, kurtosis, and other aspects of the shape of probability distributions or data samples, but are computed from linear combinations of the ordered data values (hence the prefix L).

**LS** - The term given to Local Storms which are relatively small-scale convective events (thunderstorms) in this project which occur in the warm season in the absence of any larger-scale atmospheric circulation. The areal coverage and duration of these storms are limited, typically less than a nominal 100 mi<sup>2</sup> and only one hour in duration.

**LOCAL STORM PMP** - NWS Hydrometeorological Report 49 introduced Local Storm Probable Maximum Precipitation (PMP) applicable to localized convective storms where there is high-intensity short-duration convective (thunderstorm) precipitation over localized areas capable of producing flash flooding. In HMR 49, Local Storm PMP had a nominal duration of 6-hours and an areal coverage of 500-square miles. Other HMRs in the western U.S., west of the Continental Divide, (HMRs 55A, 57, 58, 59) continued the practice of defining local storms with a nominal duration of 6-hours and an areal coverage of 500 miles. However, closer scrutiny shows the majority of Local Storm PMP in these western HMRs to fall within 1 to 2-hours with high-intensities over an area much smaller than 500 square miles. HMR 51 for the eastern U.S., east of the Continental Divide, predated the identification of Mesoscale Convective Complexes (MCCs) and other complex clustering of convective (thunderstorm) cells. High-intensity localized thunderstorm precipitation in HMR-51 was treated as convection embedded within a long-duration general storm. If Local Storm PMP were to be separated out from General Storm PMP in the eastern U.S., it would take the form of MCCs and other complex thunderstorm activity with duration of 6 to 12 hours and areal coverage on the order of 500 square miles to 1,000 square miles. In summary, short-duration high-intensity thunderstorm precipitation west of the Continental Divide (western U.S.) has shorter duration and smaller areal coverage than east of the Continental Divide (eastern U.S.). The criteria for definition of Local Storm (LS) and Mesoscale Storm with Embedded Convection (MEC) determined via Storm Typing (Task 2 of this study) is more definitive/restrictive with regard to duration and areal coverage than the generic definition of Local Storm PMP which originated with HMR 49.

**MACRO REGIONS** - The three climatologically and statistically distinct geographically contiguous regions, used in this project, formed by major mountain barriers: the East Macro Region for areas east of the Continental Divide and east of the crestline of the Sangre de Cristo range; the Rio Grande Macro Region for areas between the Continental Divide and Sangre de Cristo range and south of the Mogollon Rim; and the West Macro Region for areas west of the Continental Divide and north of the Mogollon Rim.

**MAPPING AREAS** - Groupings of stations/regions delineated for the development of predictor equations, in this project, that have similar characteristics leading to a single predictive equation.

**MEAN ANNUAL PRECIPITATION (MAP)** - The average precipitation for a year (usually calendar) based on the whole period of record or for a selected period (usually 30-year period such as 1981 through 2010).

**MEC** - The generic storm type in this project, Mesoscale storms with Embedded Convection, that is intended to include traditionally-defined Mesoscale Convective Complexes (MCCs) and other organized warm-season mesoscale and sub-synoptic scale storms with embedded convective cells (thunderstorms). The duration of the storm is generally about 6 hours and can occur within larger synoptic-scale storms if the Convective Available Potential Energy (CAPE) is high. This is a storm type that can produce large floods on intermediate size watersheds, less than about 1,000 mi<sup>2</sup> for the Colorado and New Mexico project area. This is generally a warm season event occurring from April through October.

**MLC** - Mid-Latitude Cyclones are large, synoptic-scale low-pressure systems with cyclonic circulations that form in the mid-latitudes (i.e., 30°N to 60°N). MLCs and associated frontal systems can produce precipitation for several days over very large areas. Conditions ripe for MLCs are mostly predominant in the cool season over the project area.

**PARAMETER-ELEVATION REGRESSIONS ON INDEPENDENT SLOPES MODEL (PRISM)** -Hybrid statistical-geographic approach to mapping climate data developed by Oregon State University's PRISM Climate Group.

**PRECIPITATION (RAINFALL) FREQUENCY ESTIMATE** - Precipitation (rainfall) magnitude associated with specific annual exceedance probability for a given duration.

**REGIONAL GROWTH CURVE/FACTOR** - A magnitude-frequency curve that is applicable to all sites within a homogeneous region. The regional growth factor, times the mean, provides a precipitation frequency estimate.

**RELATIVE ROOT MEAN SQUARE ERROR** - A dimensionless measure of the Root Mean Square Error (RMSE). In this study, relative RMSE was normalized by the true value of the parameter being estimated; and as such can be expressed as a percentage. Relative RMSE is often expressed as a percentage which for the spatial mapping of L-moments can be thought of as the standard deviation of the predicted values relative to the observed values. (See also Bias and Root Mean Square Error.)

**ROOT MEAN SQUARE ERROR (RMSE)** - A measure of the accuracy of a predictor; the variability of an estimator compared to the true value ( $e = \text{predicted} - \text{true}$ ) of the parameter being estimated. RMSE is computed in a manner to reflect both bias and variance of  $e$ . RMSE is computed as  $\text{SQRT} [\text{Bias } (e)^2 + \text{Variance } (e)]$ .

**STATION** - An instrumented location with precipitation measurements and perhaps other meteorological variables. The term station, gauge, and site are often used interchangeably.

**TEMPORAL PATTERN** - Time series of precipitation magnitudes for a given storm; in this project, representative patterns are comprised of a representative sample of the characteristics of historical storms; synthetic patterns are assembled from storm characteristics that are typically observed for the given storm type in each Macro Region.

**UNCERTAINTY BOUNDS FOR WATERSHED PRECIPITATION-FREQUENCY** - 90 percent uncertainty bounds are provided for the best-estimate watershed Precipitation-Frequency (PF) relationship. These bounds equate to the 5<sup>th</sup> and 95<sup>th</sup> percentiles for plausible watershed PF curves based on uncertainty characterizations for all of the parameters/factors considered in the uncertainty analysis. These are statistical measures wherein 90 percent of the 90 percent uncertainty bounds generated through computer simulations will contain the true watershed PF relationship. Also, 95 percent of the 95<sup>th</sup> percentile values generated through computer simulations will reside above the true watershed PF relationship.

## 1. Executive Summary

MGS Engineering Consultants, Inc. and MetStat, Inc. conducted the regional precipitation-frequency (PF) analyses as part of the Regional Extreme Precipitation Study (REPS) for the states of Colorado and New Mexico. The Precipitation Frequency (PF) products developed as part of this project will be used for several purposes. The primary purpose is to provide the hydrometeorological information needed to conduct flood analyses for watersheds using conventional hydrologic models. This allows for the assessment of the performance of spillways at dams and other water resource infrastructure. The hydrometeorological products are provided in a frequency-based format that will support both standards-based and Risk-Informed Decision-Making (RIDM) within the State Dam Safety programs. In addition, there is sufficient hydrometeorological information for engineers to conduct detailed stochastic flood analyses and develop hydrologic hazard curves for complex projects that warrant very detailed flood analyses for use in RIDM. Lastly, the findings of the precipitation-frequency analyses are used to provide an estimate of the annual exceedance probability (AEP) of the deterministically-derived Probable Maximum Precipitation (PMP) rainfall depths; this information served a critical, independent method of evaluating the reasonableness of the PMP estimates.

One of the key goals of the precipitation-frequency project was to provide increased accuracy in the estimation of extreme precipitation for use in hydrologic modeling of extreme floods, in particular AEPs well beyond 1 in 1000. Achievement of this goal was accomplished by several methods. Storm typing was used to assemble homogeneous precipitation annual maxima datasets for specific meteorological phenomenon. The Schaefer-Wallis-Taylor (SWT) method of regional analysis was used to minimize the effects of sampling variability and reduce uncertainties wherever possible. Each of these approaches was targeted at reducing the width of uncertainty bounds for estimation of extreme precipitation.

Specifically, a variety of storm types can produce floods in Colorado and New Mexico for watersheds of various sizes. These include: Local Storms (LS), Mesoscale Storms with Embedded Convection (MEC), Mid-Latitude Cyclones (MLC), and Tropical Storm Remnants (TSR). Each of these storm types has different spatial, temporal, and seasonal characteristics which must be maintained for realistic modeling of floods. Therefore, it was necessary to conduct separate precipitation-frequency analyses for each storm type in order to reduce uncertainties caused by mixed-populations of storm types. Storm Typing was accomplished by using meteorological criteria to identify the storm type for each day in the period from 1895 through 2014 for locations within a 2° by 2° grid-cell network for the project area. A Database of Daily Storm Types (DDST) was produced with the storm type listed for each day and each 2° by 2° grid-cell in the project area. The DDST was then used in assembling precipitation annual maxima data series for each observing station for each of the storm types. There were an insufficient number of Tropical Storm Remnants for a separate PF analysis, therefore TSRs were grouped with MLCs for analysis because both are synoptic-scale storm types with similar spatial and temporal characteristics.

Separate regional analyses were conducted to produce precipitation-frequency estimates for each of the storm types. A key duration was identified for each storm type which was representative of the typical duration for the meteorological phenomenon producing the

given storm type. The key durations identified were 48-hours for the synoptic scale MLC and TSR storm types, 6-hours for the MEC storm type, and 2-hours for the LS type.

Findings from the regional precipitation-frequency analyses resulted in the identification of three distinct Macro Regions formed by major mountain barriers. This included: The East Macro Region for areas east of the Continental Divide and east of the crestline of the Sangre de Cristo range; the Rio Grande Macro Region for areas between the Continental Divide and Sangre de Cristo range and south of the Mogollon Rim; and the West Macro Region for areas west of the Continental Divide and north of the Mogollon Rim. Each of the three Macro Regions has distinctive sources of atmospheric moisture along with differences in spatial and temporal storm patterns and storm seasonality. The three Macro Regions in combination with a set of heterogeneous super-regions provided a framework for investigating the spatial behavior of the L-Moment statistics.

Regional analyses and subsequent spatial mapping of L-Moment statistics were used to develop the point precipitation-frequency relationships for locations throughout the project area. This included spatial mapping to produce gridded datasets of the at-site means, regional L-moment ratio statistics L-Coefficient of Variation (L-Cv) and L-Skewness, and identification of the regional probability distribution. Isopluvial grids were prepared from this information for point precipitation maxima for annual exceedance probabilities (AEPs) of  $10^{-1}$ ,  $10^{-2}$ ,  $10^{-3}$ ,  $10^{-4}$ ,  $10^{-5}$ ,  $10^{-6}$ , and  $10^{-7}$  for the key durations for each storm type.

The gridded datasets described above along with spatial patterns from historical storms were used to develop Precipitation-Frequency Areal Reduction Factors (PF-ARFs) to convert point precipitation-frequency information into watershed-average precipitation-frequency relationships. This was accomplished using stochastic storm transposition methods for a range of watershed sizes and shapes. This approach provided for a scaling procedure to be developed utilizing PF-ARFs for each storm type and each Macro Region that allow direct conversion from point to areal precipitation for a watershed of interest. The watershed-average precipitation-frequency relationships in combination with dimensionless spatial and temporal representative patterns (or patterns from historical storm events) allow simulation of flood events that may be shorter or longer than the key duration. This approach allows greater variability in total storm duration for hydrological modeling consistent with durations observed in the historical record of storms.

Equivalent Independent Record Length (EIRL) analyses were conducted for each storm type to help quantify the benefit of regional analyses in what is referred to as trading space-for-time sampling. Specifically, EIRL is a measure of the effective record length of the statistical information for the storms contained in the regional datasets because annual maxima at stations throughout the project area are produced by the many separate storms that occur in a given year. EIRL is used in the uncertainty analyses for development of uncertainty bounds for both point and watershed-specific precipitation-frequency relationships.

Seasonality analyses were conducted to provide a description of the likelihood for storms to occur at various times throughout the year. This information is important in conducting flood analyses because soil moisture conditions and reservoir levels vary with storm seasonality for the various storm types.

In summary, the methods employed in the Regional Precipitation-Frequency Project provide more reliable estimates of extreme precipitation as evidenced by the reduction in uncertainty

bounds by comparison to other methods. The findings from the project provide information necessary for developing watershed precipitation-frequency relationships and employing spatial and temporal storm patterns for conducting hydrologic modeling of floods, particularly extreme floods. These findings may be used in either a standards-based or Risk-Informed Decision framework for assessing spillway adequacy for State Dam Safety programs. Moreover, AEPs of PMP can be estimated, thereby providing State Dam Safety programs with a means of prioritizing projects and assessing risk.

## 2. Overview

The primary application of the findings from Task 2 are in watershed modeling of extreme floods for assessing the adequacy of spillways on existing dams and for sizing spillways for rehabilitation of existing dams or for construction of new dams. The results from watershed modeling of floods may be used within either a standards-based or risk-informed decision making (RIDM) framework. To meet these objectives, the scope and methods of analyses employed in Task 2 were chosen to provide storm-related information in a manner that supports both standards-based and probabilistic watershed modeling.

A variety of storm types can produce floods in Colorado and New Mexico for watersheds of various sizes. These include: Local Storms (LS), Mesoscale Storms with Embedded Convection (MEC), synoptic scale Mid-Latitude Cyclones (MLC) and Tropical Storm Remnants (TSR). Each of these storm types has different precipitation-frequency, spatial, temporal, and seasonal characteristics.

Figure 1 depicts examples of temporal patterns (hyetograph) for rare storm events for the LS storm. The LS storm type is characterized by very short-duration very high precipitation intensities with a very localized spatial footprint (Figure 2) and which occurs predominately in the warm season in the study area. Similarly, an example of the MEC storm type which also occurs predominately in the warm season, is shown in Figure 3. It has mesoscale spatial coverage (Figure 4) with moderate duration and moderate to very high precipitation intensities. The MLC storm type is characterized by long-duration low to moderate precipitation intensities which aggregate to a large total volume. The MLC storm type (Figure 5) produces widespread precipitation with a synoptic scale spatial footprint (Figure 6) and occurs over a wider range of seasons extending primarily from early spring through late-fall in the project area. Particular note should be given to the relative magnitudes of precipitation intensities in Figure 1, Figure 3 and Figure 5 where convective activity produces high precipitation intensities for the LS and MEC storm types and precipitation mechanisms in the frontal systems of the MLC storm type result in low to moderate precipitation intensities.

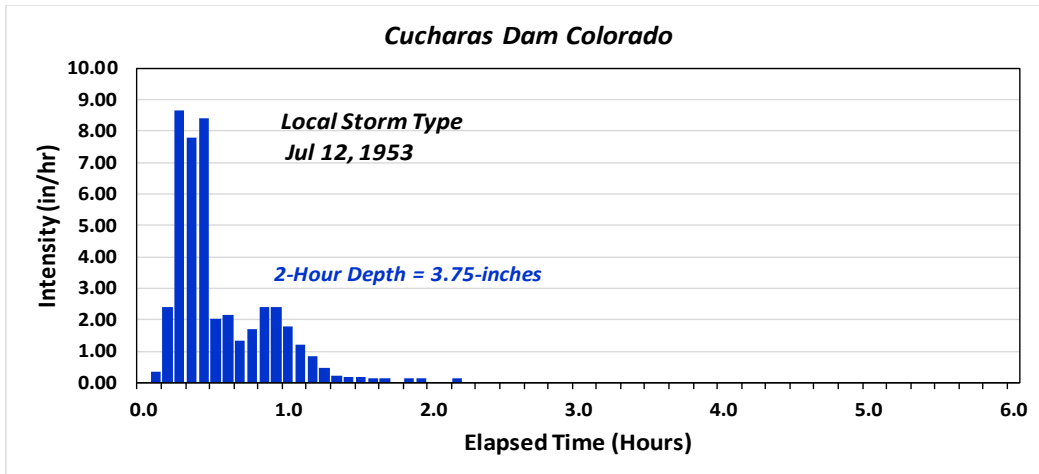


Figure 1. Example of Hyetograph Shape for Local Storm (LS) recorded at Cucharas Dam Colorado on July 12, 1953

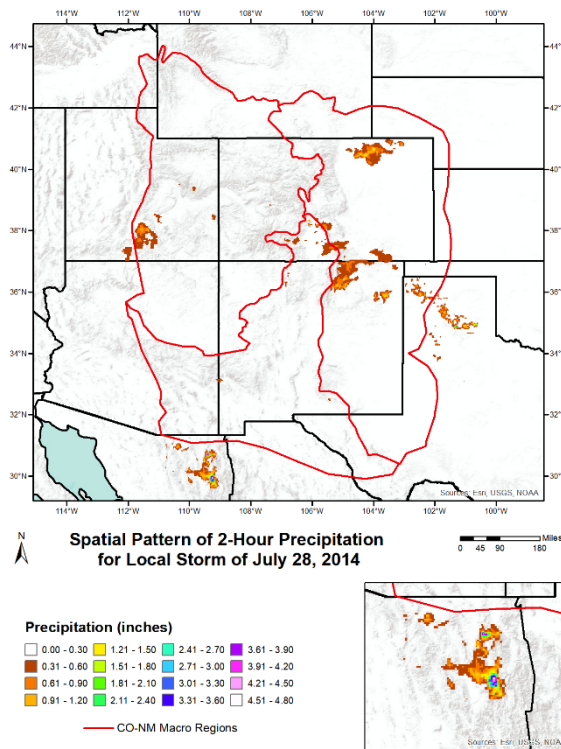


Figure 2. Example of the spatial extent of a Local Storm (LS) on July 28, 2014

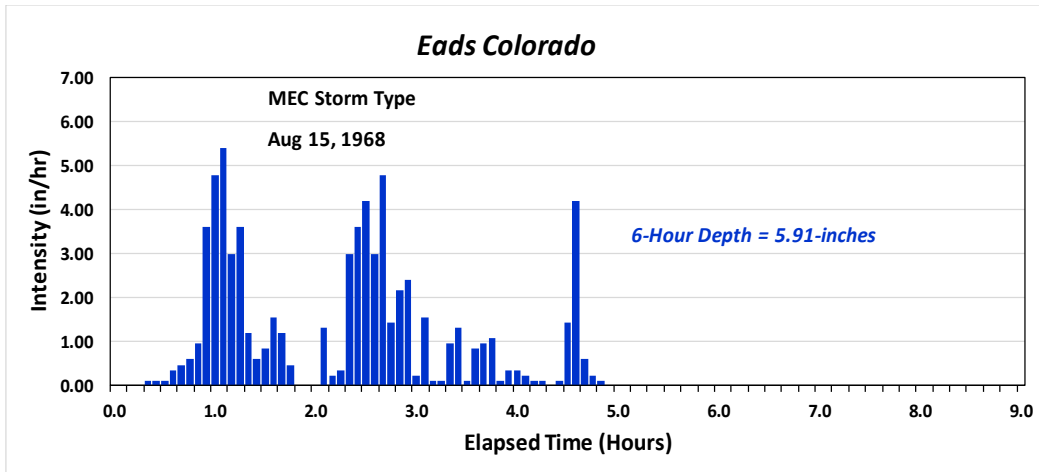


Figure 3. Example of Hyetograph Shape for Mesoscale Storm with Embedded Convection (MEC) recorded at Eads Colorado on August 15, 1968

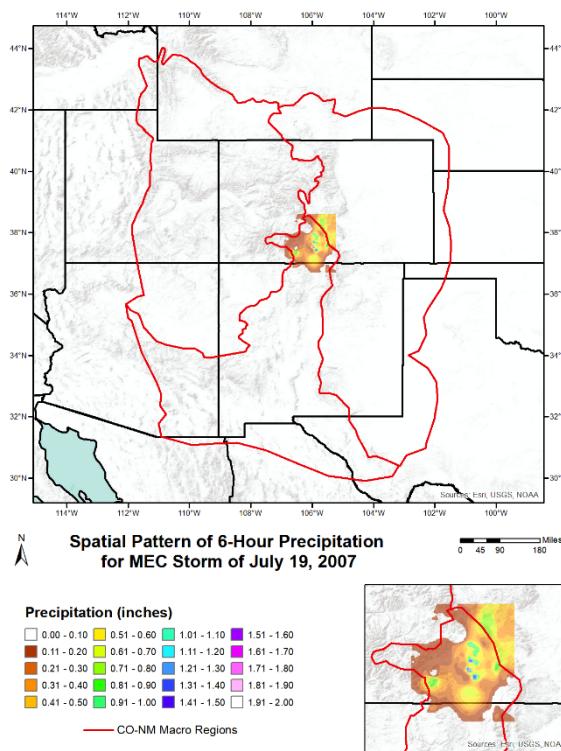


Figure 4. Example of the spatial extent of a Mesoscale Storm with Embedded Convection (MEC) storm on July 19, 2007

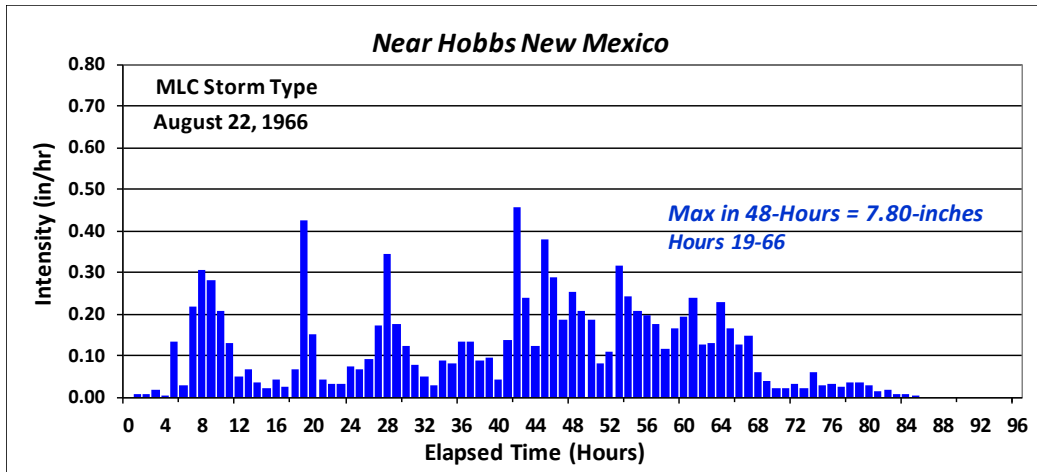


Figure 5. Example of Hyetograph Shape for Mid-Latitude Cyclone (MLC) recorded near Hobbs New Mexico on August 22-23, 1966

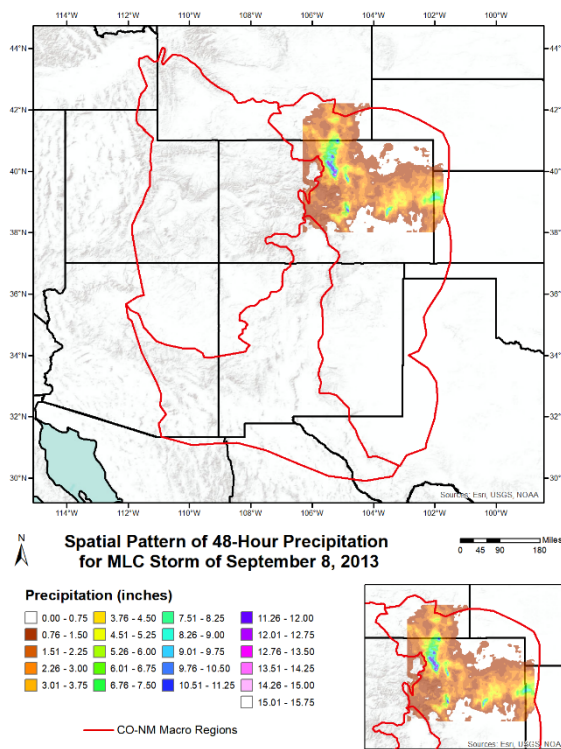


Figure 6. Example of the spatial extent of a Mid-Latitude Cyclone (MLC) storm on September 8, 2013

Antecedent soil moisture, antecedent streamflow, and initial reservoir levels also vary with the season of the year and can be important elements for watershed modeling in setting initial conditions prior to the occurrence of a rare/extreme storm event. Therefore, the precipitation-frequency, spatial, temporal, and seasonal characteristics for each storm type must be maintained as a package for realistic modeling of floods.

In reviewing the many factors discussed above and the Dam Safety Program need to focus on extreme storms/floods, the following methods of analysis were selected and considerations given to provide the storm-related information required for realistic modeling of floods.

1. Use Storm Typing procedures to classify precipitation events by storm type on a daily basis for locations throughout the Colorado - New Mexico project area;
2. Use the results from storm typing for assembling annual maxima data series at precipitation stations for a key duration for each storm type. The key durations of 2-hour (LS), 6-hour (MEC) and 48-hour (MLC-TSR) are representative of the time period during which the majority of precipitation typically occurs for each storm type;
3. Conduct both automated and manual quality-checking to confirm the validity of the data with particular attention given to the largest and smallest annual maxima at a station that have the greatest influence on computed L-Moments and the precipitation-frequency of extreme events;
4. Use Regional L-Moment methodologies [Hosking and Wallis (1997)] for reducing sampling variability and increasing the reliability of point precipitation-frequency estimates of extreme events;
5. Use the Schaefer-Wallis-Taylor (Appendix C) climate region approach to regional L-Moment analysis which was developed specifically for the spatial mapping of L-Moment statistics in mountainous terrain and is focused on reduction of uncertainties for estimation of the at-site mean, regional L-Cv, and regional L-Skewness;
6. Increased attention given to analysis of precipitation at high elevations (above 10,000-feet) and the variation of precipitation with elevation;
7. Particular attention given to spatial mapping of L-Skewness and identification of the regional probability distribution which are the greatest contributors to the total uncertainty (width of uncertainty bounds) for extreme events;
8. Computation of an Equivalent Independent Record Length (EIRL) of the full annual maxima record as a measure of the information contained in the regional dataset to assist in characterizing uncertainties in the regional L-Moment statistics;
9. Use stochastic storm transposition methods along with storm spatial patterns and findings from point precipitation-frequency analyses to develop watershed precipitation-frequency relationships for a range of watershed sizes for each of the three storm types (see Appendix D);
10. Conduct stochastic storm transposition in a manner that accounts for uncertainties for all of the contributing factors to produce a watershed mean precipitation-frequency curve (best-estimate) along with uncertainty bounds;
11. Use the results from stochastic storm transposition for geographically fixed areas (watersheds) to develop precipitation-frequency areal reduction factors (PF-ARF) for developing a watershed precipitation-frequency relationship and uncertainty bounds for any watershed of interest via a PF-ARF scaling procedure;
12. Provide scalable historical storm temporal patterns for each storm type for watershed modeling where the collection of historical patterns constitutes a diverse suite of temporal patterns exhibited by the rarest storm events;
13. Develop a synthetic temporal pattern for each storm type for use in watershed modeling where the temporal pattern contains commonly observed storm characteristics. The synthetic temporal pattern is developed from the findings of probabilistic analysis of important temporal storm characteristics using procedures from the Washington State Dam Safety method (Schaefer 1989);
14. Provide monthly-frequency information on storm seasonality for each storm type based on the rarest storm events for each storm type.

It will be seen later that the complex topography in the Colorado and New Mexico study area results in three distinct areas for storm-related characteristics. These three areas are formed by major mountain barriers and are termed Macro Regions (Figure 7). The three Macro Regions include: The Eastern Macro Region for areas east of the Continental Divide and east of the crestline of the Sangre de Cristo range; the Rio Grande Macro Region for areas between the Continental Divide and Sangre de Cristo range and south of the Mogollon Rim; and Western Macro Region for areas west of the Continental Divide and north of the Mogollon Rim. Each Macro Region has distinct sources of atmospheric moisture and exhibits differences in temporal and spatial storm patterns and storm seasonality.

The three Macro Regions along with the three storm types result in nine separate combinations for development of watershed precipitation scaling procedures, analysis of temporal and spatial patterns, and storm seasonality (items 9 through 14 above).

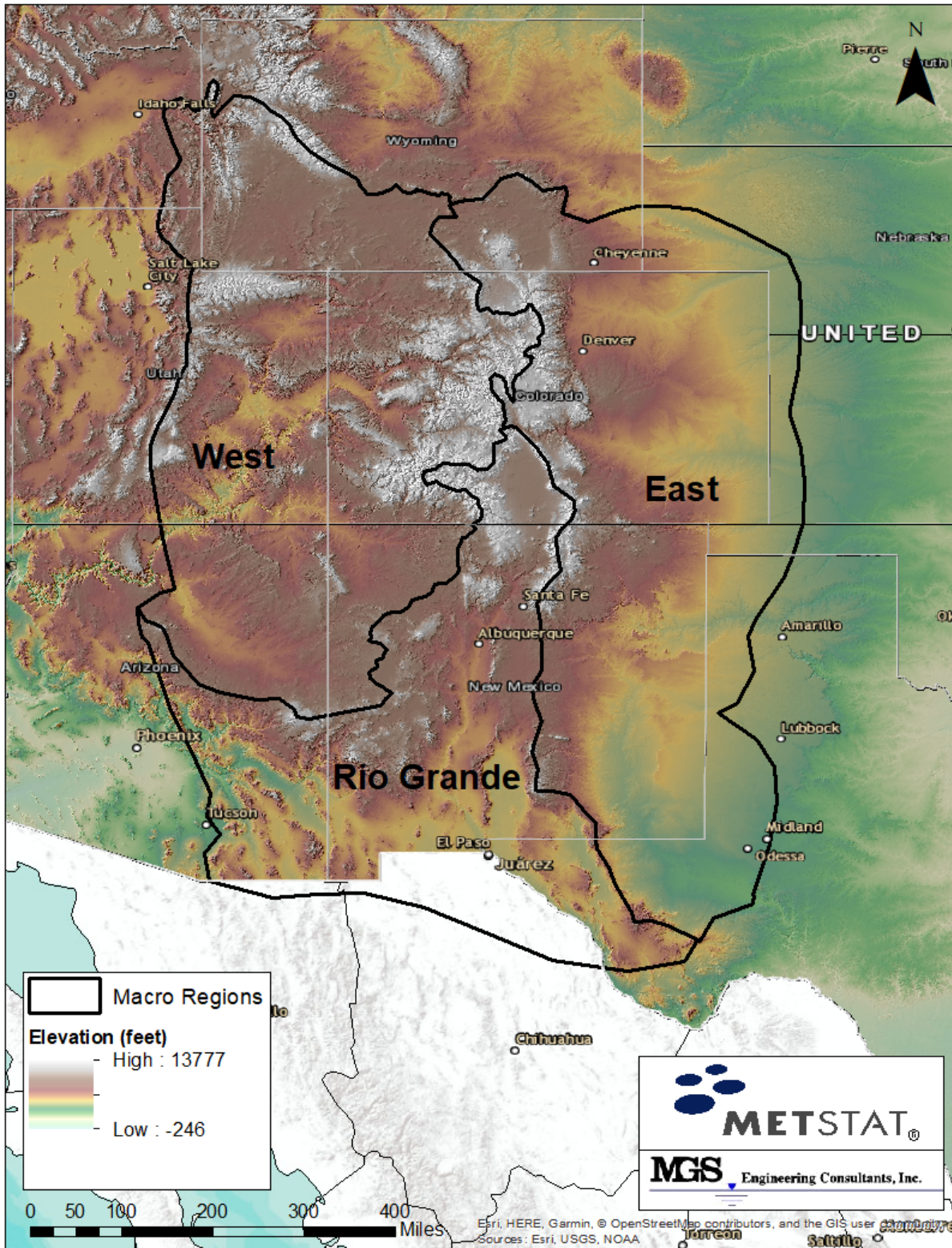


Figure 7. Depiction of three Macro Regions formed by major mountain barriers delineating areas with distinct differences in precipitation-frequency, temporal and spatial characteristics, and storm seasonality

The following sections provide an overview of the methods of analysis and procedures employed in completing the study elements outlined in items 1 through 13 above.

## 2.1. Regional Frequency Analysis and Storm Typing for Data Homogeneity

Regional frequency analysis methods are appropriate whenever data are available for the same phenomena that are measured at multiple sites. For the case of regional precipitation-frequency analysis focused on application of extreme events, it is critically important that the data are homogeneous with regard to the phenomenon of interest. Thus, storm typing is an essential element of this project where precipitation annual maxima datasets are assembled for the same storm type - the same meteorological phenomenon.

The cornerstone of a regional analysis [Hosking and Wallis (1997)] is that data from sites within a homogeneous region can be pooled to improve the reliability of the magnitude-frequency estimates for all sites. The success of a regional precipitation-frequency analysis is determined by the ability to identify homogeneous regions and to spatially map the precipitation-frequency statistical measures. In this project, heterogeneous climate regions of similar meteorological and climate characteristics were first developed to provide a framework for investigating the spatial variability of the L-Moment statistics. Statistically homogeneous sub-regions were formed within these heterogeneous climate regions as collections of observational sites (stations) within a small range of selected climatic and/or location indices. The climatic indices included mean seasonal precipitation for the dominant months of storm occurrence for each of the three storm types in each of the three Macro Regions (Figure 7). The seasonal climatic indices at each station were computed from the Parameter-Elevation Regression on Independent Slopes Model [Daly 1994; Daly et al. (1994)]. Site elevation and latitude were also used as indices to group observational sites into homogeneous sub-regions.

The climatic and meteorological complexity in the Colorado and New Mexico areas required a large number of homogeneous sub-regions to describe the spatial variability of the L-Moment statistics. There were 192 homogeneous sub-regions utilized for the MLC storm type and 31 homogeneous sub-regions used for the MEC and LS storm types.

## 2.2. L-moment Statistics

L-Moment methodologies [Hosking 1990; Hosking and Wallis (1997)] were used for computing sample statistics, conducting tests for heterogeneity, computing regional L-Moment statistics for a collection of sites (stations) within a homogeneous sub-region and identifying a regional best-fit probability distribution. L-moment statistics are a significant improvement over standard product-moment statistics and are particularly well-suited for analyses of environmental data where small sample sizes are common and the data are often highly skewed.

The software program L-RAP [Schaefer and Barker (2009)] was used to conduct the regional precipitation-frequency analyses and support the SWT climate region method. Appendix A is an excerpt of the L-RAP User's Manual [Schaefer and Barker (2009)] and is included to provide additional background information on L-Moment statistics and associated discordancy, homogeneity, and goodness-of-fit measures.

### 2.3. Regional Growth Curve

Implicit in the definition of a homogeneous region (sub-region) is the condition that all sites can be described by one probability distribution having common distribution parameters after the site data are rescaled by their at-site mean. This formulation is termed an Index-Flood approach, originally introduced by Dalrymple (1960) for use in flood-frequency analysis. Thus, all sites within a homogeneous region have a common regional magnitude-frequency curve, termed a Regional Growth Curve (Figure 8), that becomes site-specific after scaling by the at-site mean of the data from the site of interest. Thus,

Equation 1

$$Q_i(F) = \hat{\mu}_i q(F)$$

where:  $Q_i(F)$  is the at-site inverse Cumulative Distribution Function (CDF),  $\hat{\mu}_i$  is the estimate of the population at-site mean, and  $q(F)$  is the regional growth curve (i.e., regional inverse CDF).

Using the regional growth curve format [Hosking and Wallis (1997)], L-Cv is seen to control the slope of the precipitation-frequency relationship (Figure 9) and L-Skewness controls the shape of the upper tail of the precipitation-frequency relationship (Figure 10). L-kurtosis also has an effect on the upper tail, similar to L-Skewness. These figures are helpful in visualizing the effect of changes in the magnitude of L-Cv and L-Skewness on precipitation-frequency relationships across the project area.

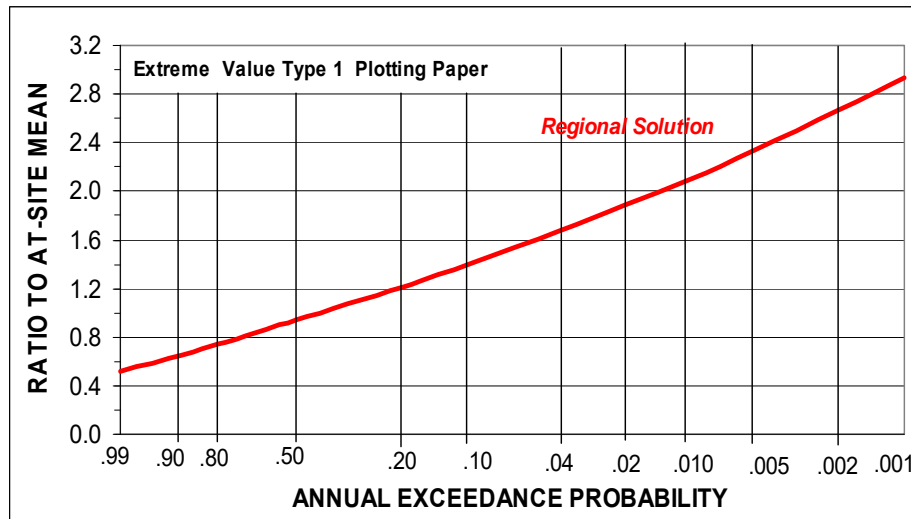


Figure 8. Example of a Regional Growth Curve

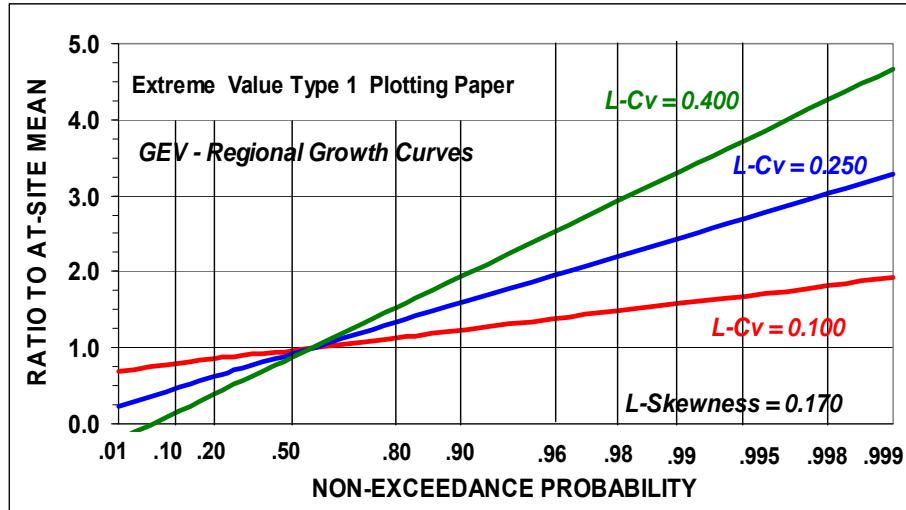


Figure 9. Example of effect of changes in L-Cv on Regional Growth Curve

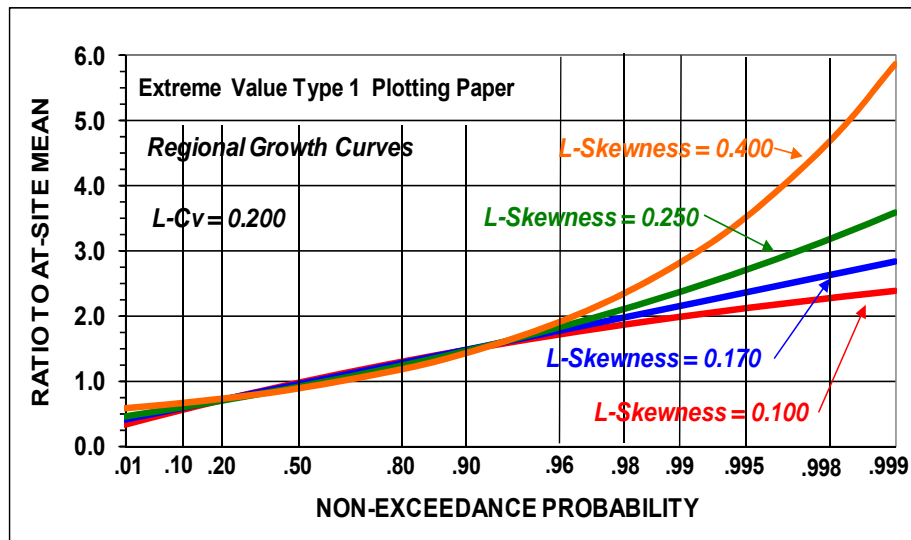


Figure 10. Example of effect of changes in L-Skewness on Regional Growth Curve

The effect of changes in L-Cv and L-Skewness on the shape of the Regional Growth Curve will be helpful in later sections of this report in viewing maps of the spatial variability of L-Cv and L-Skewness across the project area.

## 2.4. Regional Probability Distribution

The L-Moment goodness-of-fit test [Hosking and Wallis (1997)] was used for identifying the best-fit regional probability distribution. Experience in analysis of precipitation annual maxima for durations of several days and shorter in the United States and British Columbia [Schaefer 1997; Schaefer et al. (2002); Schaefer and Barker (2006); Schaefer et al. (2007); MGS et al. (2015)] has shown the best-fit regional probability distribution to often be near the Generalized Extreme Value (GEV) distribution.

The 4-parameter Kappa distribution [Hosking and Wallis (1997), Equation 2] is a very flexible distribution capable of emulating distributions near GEV or any 3-parameter distribution. In

particular, the 4-parameter Kappa distribution with a fixed shape parameter ( $h$ ) has been found to provide a suitable regional probability distribution and has the added advantage of emulating alternative probability distributions near the GEV and including the Generalized Normal (GN) and Gaucho distributions. This capability is useful in uncertainty analyses. In this context, near-GEV refers to the nearness of the L-Skewness and L-Kurtosis pairings for a homogeneous subregion residing near the GEV curve (Figure 11) on the L-moment ratio diagram.

Three-parameter probability distributions, such as the GEV, GN, and Gaucho have a fixed relationship between L-Skewness and L-Kurtosis. L-moment ratio diagrams are useful for depicting the relationship between L-Skewness and L-Kurtosis for a number of 3-parameter probability distributions (Figure 11). In addition, the L-moment ratio diagram provides a graphical depiction of the L-moment goodness-of-fit test by showing the nearness of regional L-Skewness and L-Kurtosis pairings to a specific 3-parameter probability distribution [Hosking and Wallis (1997)]. Figure 11 provides a graphical depiction of the L-moment goodness-of-fit test for 84 homogeneous sub-regions in the Eastern Macro Region of the project area for 48-hour precipitation maxima for the MLC storm type. The centroid of the cluster of L-Skewness and L-Kurtosis pairings is taken as the indicator of the best-estimate 3-parameter probability distribution. The scattering of data in the cluster is due to the natural sampling variability of skewness and kurtosis measures that is inherent in real-world datasets where the sampling distributions for L-Skewness and L-Kurtosis are near Normally Distributed. A review of the scatter pattern in Figure 11 is indicative of a Bi-variate Normal sampling distribution. The quantile function for the 4-parameter Kappa distribution is:

Equation 2

$$q(F) = \xi + \frac{\alpha}{\kappa} \left\{ 1 - \left( \frac{1 - F^h}{h} \right)^\kappa \right\}$$

where:  $\xi$ ,  $\alpha$ ,  $\kappa$ , and  $h$  are location, scale and two shape parameters respectively.

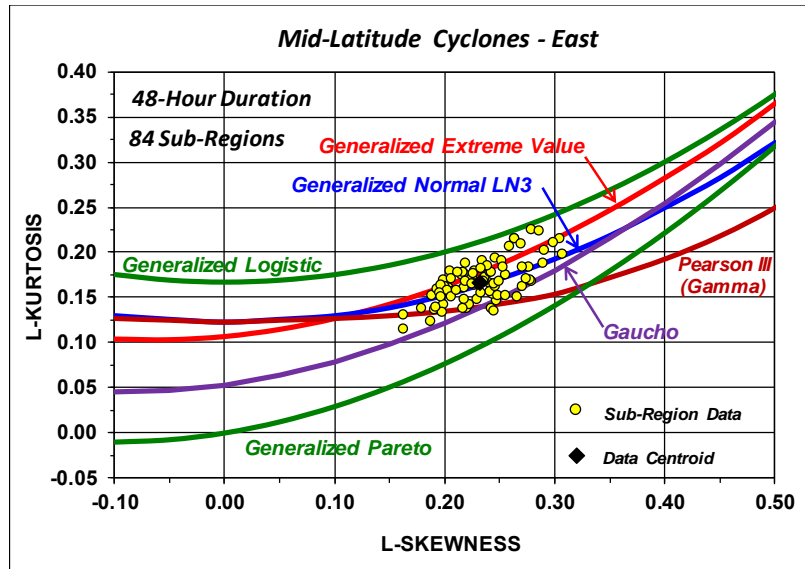


Figure 11. L-Moment ratio diagram depicting regional L-Skewness and L-Kurtosis values for homogeneous sub-regions in the Eastern region of the project area for 48-Hour precipitation maxima for MLCs

The regional L-moment ratio statistic for the 5<sup>th</sup> moment, termed L-Cinco, can also be used to confirm the suitability of the 4-parameter Kappa distribution. The easiest way to present this information is via L-Moment Ratio diagrams. Figure 12 and Figure 13 show the traditional L-Moment diagrams for L-Kurtosis and L-Skewness and also diagrams for L-Cinco for the LS, MEC and MLC storm types, respectively, for the three Macro Regions.

CO-NM Regional Extreme Precipitation Study

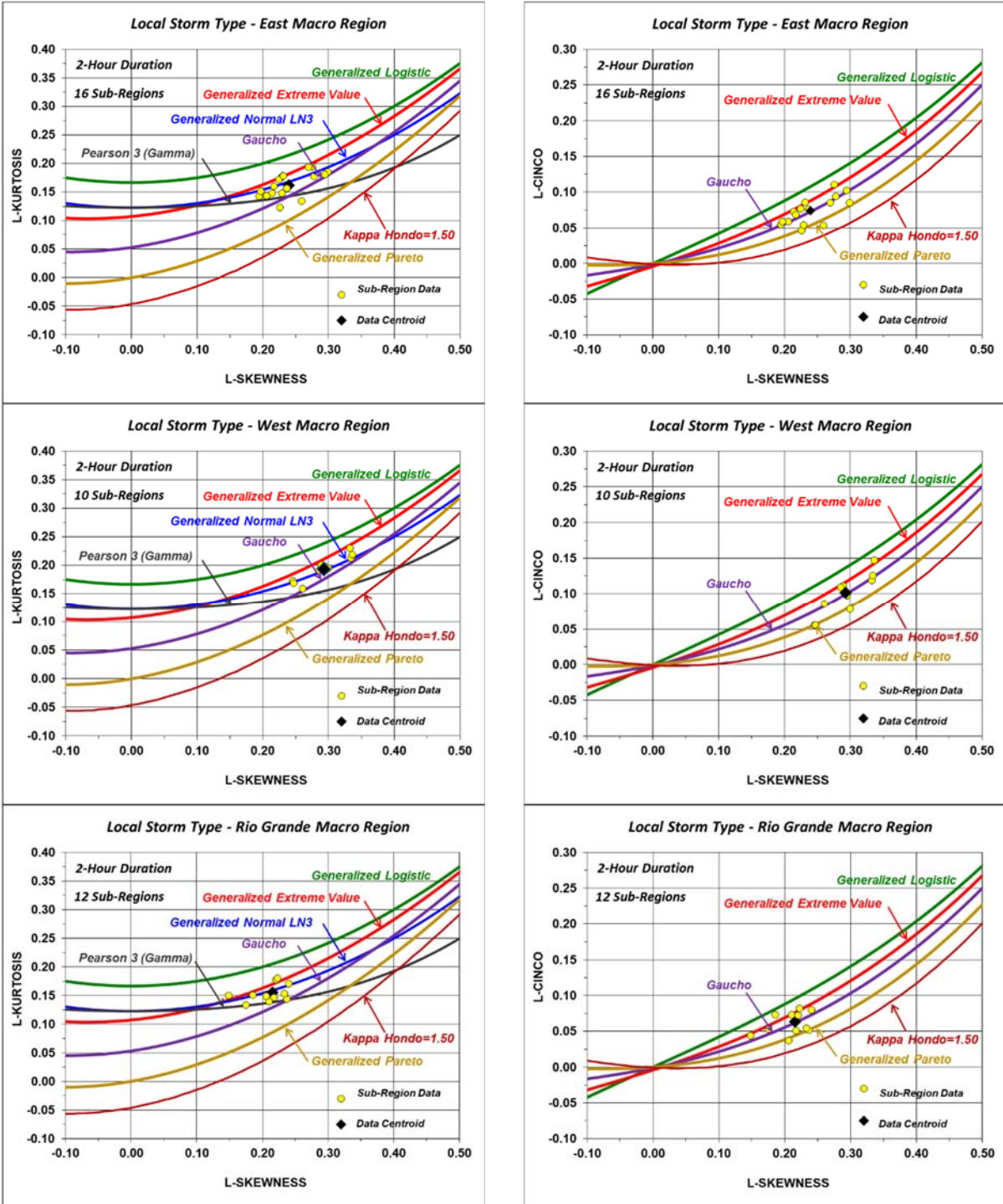


Figure 12. L-Moment Ratio Diagrams for L-Skewness, L-Kurtosis and L-Cinco for the Local Storm type for each Macro Region

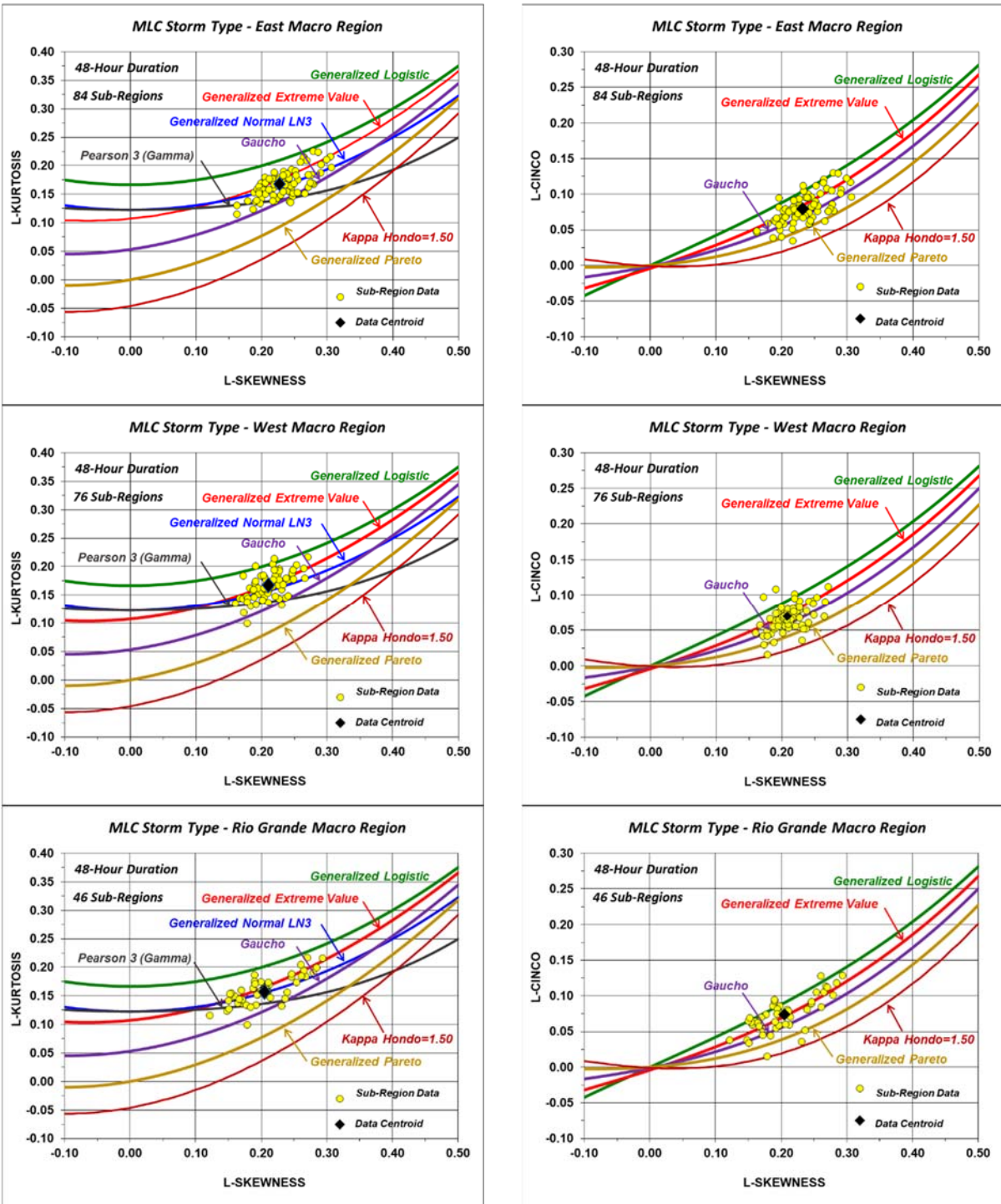


Figure 13. L-Moment Ratio Diagrams for L-Skewness, L-Kurtosis, and L-Cinco for the Mid-Latitude Cyclone (MLC) storm type for each Macro Region

## 2.5. Spatial Mapping of L-Moment Statistics

The primary product from the SWT climate region method of regional analysis is the production of gridded datasets of L-Moment statistics for the at-site mean, regional L-Cv,

regional L-Skewness, and the second shape parameter (Hondo) for the 4-parameter Kappa distribution. A major element of this study is the spatial mapping of the L-Moment statistics for each of the three storm types within the construct of homogeneous sub-regions using predictor equations where similar behavior with explanatory variables was identified.

## 2.6. Point Precipitation-Frequency

Point precipitation-frequency estimates can be obtained for any location in the project area by using the gridded datasets of spatially mapped L-Moment statistics. Specifically, distribution parameters for the 4-parameter Kappa distribution are solved using grid-cell specific values of the spatially mapped at-site mean, regional L-Cv, regional L-Skewness, and regional Hondo. The inverse CDF for the Kappa distribution (Equation 2) is then used to compute quantile estimates for selected Annual Exceedance Probabilities (AEPs). This process is repeated for each grid-cell in the project domain to produce gridded datasets for selected Annual Exceedance Probabilities (AEPs).

Gridded datasets were generated for AEPs of 0.9, 0.5, .05, .02,  $10^{-1}$ ,  $10^{-2}$ ,  $10^{-3}$ ,  $10^{-4}$ ,  $10^{-5}$ ,  $10^{-6}$ , and  $10^{-7}$ . Figure 59 and Figure 60 show example isopluvial maps for AEPs of 1:100 and 1:1,000, respectively.

## 2.7. Watershed Precipitation-Frequency Relationships

Stochastic storm transposition methods were used along with historical storm spatial patterns and findings from point precipitation-frequency analyses to develop watershed precipitation-frequency relationships for a range of watershed sizes for each of the three storm types. The stochastic storm transposition simulations were conducted in a manner that accounts for uncertainties from all contributing components to produce a watershed mean precipitation-frequency curve (best-estimate) and uncertainty bounds.

The results from stochastic storm transposition simulations for geographically fixed areas (watersheds) were used to develop precipitation-frequency areal reduction factors (PF-ARF). The PF-ARF values provide for development of a watershed precipitation-frequency relationship and uncertainty bounds for any watershed of interest via a PF-ARF scaling procedure (Figure 14). A PF-ARF scaling procedure and graphics for storm scaling were developed for each of the three Macro Regions and three storm types for a total of nine separate PF-ARF relationships.

Ten watershed shapes were used in the PF-ARF analysis ranging from point to 8, 13, 18, 40, 77, 85, 139, 318, 459, and 1,017 square miles. The analysis utilized 72 storms from SPAS (Volume 2) and HRRR model (Volume 4) output (Table 1) for quantifying the spatial characteristics of storm precipitation. The focus of this element of the study was on small (<100 mi<sup>2</sup>) watersheds and the Local and MEC storm types given the vast majority of state-regulated dams in Colorado and New Mexico are associated with very small watersheds. The mathematics of computing PF-ARFs results in mostly cancelling the site-specific aspects for small watershed-sizes because there isn't much spatial variability in both the numerator (watershed-average precipitation) and denominator (areal-average point precipitation) for very small watersheds, thus making for small ARFs.

The Stochastic Storm Transposition Method (SSTM) (Appendix D) is intended for application with convective storms and was used for local storms and MECs in all three macro regions. An alternative stochastic storm generation procedure is typically used for synoptic scale storms (MGS et al., 2015). However, this procedure is data and labor intensive and impractical given the number of watershed sizes, three storm types, three macro regions, and relatively few numbers of available storms for analysis. The SSTM was therefore adapted for use with synoptic scale storms to provide a practical approach to developing a watershed PF scaling procedure for the MLC storm type for a range of watershed sizes in all three Macro Regions. This approach was possible because of the primary interest being small watersheds where there is less spatial variability in MLC precipitation due to the small scale of the watersheds of interest. In addition, the process of computing a dimensionless scaling factor for a variety of watershed shapes tends to average out the variability due to watershed shape and orographic influences. This results in generic PF-ARF values representative of typical watershed shapes. Elongated watershed shapes would be expected to have higher attenuation and smaller PF-ARF values compared to the generic PF-ARF values presented in the application graphics. Conversely, compact, near circular, watershed shapes would be expected to have higher PF-ARF values relative to the generic values shown in the application graphics.

Accounting for the spatial variability of orographic precipitation is important for computing watershed-specific PF relationships for larger watersheds subject to MLC events in mountainous terrain. Therefore, the PF-ARFs for synoptic-scale MLC storms should be revisited as more data on spatial patterns become available. In addition, care should be taken in applying the PF-ARF values in larger watersheds with significant orographic diversity. Site-specific detailed studies are often needed in these cases to properly account for orographic precipitation and watershed shape.

Although PF-ARFs vary with AEP (typically smaller ARF values for extreme/rare events and larger ARF values for common events), the limited dataset did not allow for that level of refinement. The PF-ARF values provided as part of this project represent best-estimates for all AEPs for all storm types.

*Table 1. Number of spatial storm patterns used for calculating PF-ARFs*

NUMBER OF SPATIAL STORM PATTERNS FOR CALCULATING PF-ARFS									
MACRO REGION	LOCAL STORM			MEC			MLC/TSR		
	HRRR	SPAS	Total	HRRR	SPAS	Total	HRRR	SPAS	Total
West	15	8	23	16	0	16	0	4	4
Rio Grande	27	3	30	16	6	22	0	3	3
East	15	8	23	21	12	33	0	16	16

ARFs have been used since the 1950s to provide an estimate of watershed precipitation using point precipitation information. However, nearly all applications of ARFs have been for deterministic standards-based storm/flood studies. There are important differences between deterministic storm-based ARFs and frequency-based PF-ARF values for geographically-fixed areas (watersheds). Those differences are briefly discussed below so that users of the findings of these studies have a clear description of PF-ARF values.

As indicated above, there are two types of analyses used to develop ARFs which include storm-based analyses and geographically-fixed analyses. ARFs published in

Hydrometeorological Reports (e.g., HMR 55A [Hansen et al. (1988)] are obtained from storm-based analyses where the spatial characteristics of the storm are analyzed without reference to any specific watershed. In application, storms in deterministic flood analyses are typically centered over the watershed of interest.

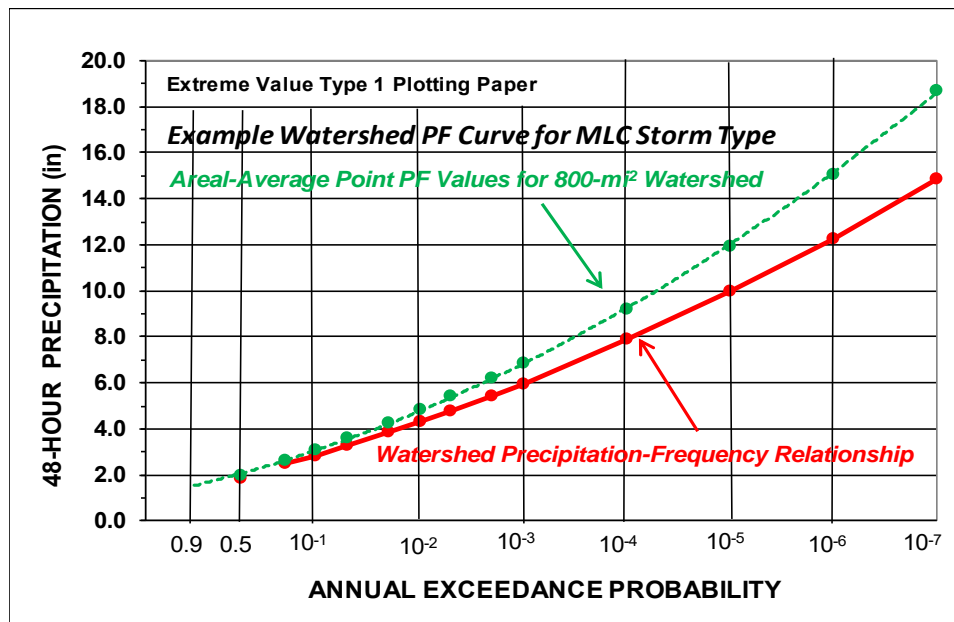


Figure 14. Example Watershed Precipitation-Frequency relationship for an 800-m<sup>2</sup> watershed on the eastern face of the Rocky Mountains near Denver

ARFs obtained from geographically-fixed analyses account for the natural variability of the location of the storm and storm center(s) relative to a fixed location (watershed). Therefore, ARF values from storm-based and geographically-fixed analyses are not interchangeable. This is true for all storm types.

## 2.8. Risk-Informed Decision-Making (RIDM) Framework

One of the objectives of this Volume was to provide storm-related information in a manner that may be used in either a standards-based or Risk-Informed Decision-Making (RIDM) framework.

Most State Dam Safety Programs in the U.S. currently employ deterministic standards-based regulations where the PMP/PMF are the benchmark standards. The States of Washington, Montana and California currently use probabilistic and risk concepts in their regulations. Other State Dam Safety Programs are exploring options for incorporating risk concepts into their programs.

Federal Dam Safety Programs have migrated to a Risk-Informed Decision-Making (RIDM) approach over the past two decades. The U.S. Army Corps of Engineers (USACE), U.S. Bureau of Reclamation (USBR), and Tennessee Valley Authority (TVA) are self-regulating Federal agencies that are using RIDM approaches. RIDM is being used for activities such as: prioritization of detailed probabilistic analyses to a portfolio of dams; decisions on the need for rehabilitation/modification of dams; and allocating financial resources for risk-reduction.

The Federal Energy Regulatory Commission (FERC) is in the early phases of allowing RIDM as an alternative to standards-based regulation of federally-licensed hydropower projects.

Risk, as implemented in the Dam Safety community, can be defined as: “*a measure of the probability and severity of undesirable consequences*” (ICOLD 2005). Risk is a product of two elements, the *probability of failure* and the *consequences of failure* where failure is defined as the uncontrolled release of the reservoir contents. Life-safety risk is quantified on an annualized basis in units of lives lost per year. Economic risk is measured in units of economic expense (dollars) per year. In application, risk is computed as the product of three components: 1) the probability of a given loading condition (hydrologic, seismic, static); 2) the response of the dam/system to the loading condition (conditional probability of failure to loading condition); and 3) if failure occurs the life-safety and economic consequences of failure from a given failure mode. Note that the product of items 1 and 2 equate to the *probability of failure*.

The goal in a Risk-Informed approach is to evaluate the risk associated with the various failure modes at a given dam and use that information to make decisions about a proper course of action. This would include activities such as: prioritizing detailed probabilistic analyses to be conducted for a portfolio of dams; decisions on the need for rehabilitation/modification for specific dams; and allocating financial resources for risk-reduction at specific dams.

The following paragraphs provide a brief description of elements of RIDM which may be implemented using probabilistic information from Volume 3.

The Schaefer-Wallis-Taylor (SWT) approach of the climate region method for regional precipitation-frequency analysis, discussed above and in detail in the Appendix C, provides a probabilistic measure of precipitation, as opposed to a deterministic value of probable maximum precipitation. This probabilistic method could synonymously be referred to as a risk-based method, where the term risk-based was commonly used in the dam safety community in the 1980s and 1990s to distinguish between probabilistic and deterministic methods. However, the term ‘risk-based’ has fallen out of favor because it was too easily inferred that the numerical results from risk-analyses directly determined the decision for action/no-action. Thus, to adhere to current practice, the term ‘probabilistic’ is applied.

The benefit of using a probabilistic approach to quantify extreme precipitation is that an entire suite of storm events, from the common to the very rare, may be identified. This ensemble of events may then be used as input into a hydrologic model to determine a flood-frequency relationship, for the full range of flood possibilities. Furthermore, the probabilistic approach allows for the quantification of flood risk, “*a measure of the probability and severity of undesirable consequences*” (ICOLD 2005) associated with the full range of flood possibilities. This contrasts with the information provided by a deterministic approach, where the theoretical upper limit of precipitation is found without consideration of uncertainty or probability and severity. In the case of Probable Maximum Precipitation (PMP), only the probable maximum flood (PMF) may be modeled, again without consideration of more common events or the probability associated with that theoretical upper limit.

The information obtained from the SWT approach, and subsequent hydrologic modeling, allows for the completion of a hydrologic risk analysis. A risk analysis uses all available information to estimate the risk to individuals, populations, property, or environment from

hazards. Risk analyses generally contain the following steps: scope definition, hazard identification, and risk estimation. Consistent with the common dictionary definition of analysis, viz. “A detailed examination of anything complex made in order to understand its nature or to determine its essential features”, risk analysis involves the disaggregation or decomposition of the dam system and sources of risk into their fundamental parts (ICOLD 2005).

A risk analysis is followed by a risk assessment. A risk assessment is the process of making a decision or recommendation on whether existing risks are tolerable and whether present risk control measures are adequate, and if not, whether alternative risk control measures are justified or will be implemented. Risk assessment incorporates the results from the risk analysis. Consistent with the common dictionary definition of assessment, viz. “To analyze critically and judge definitively the nature, significance, status or merit of...[risk]”, risk assessment is a decision-making process, often sub-optimal between competing interests, that results in a statement that the risks are, or are not, being adequately controlled. Risk assessment involves the analysis, evaluation, and decision about the management of risk; and all parties must recognize that adverse consequences might materialize, and owners will be required to deal effectively with any consequences of the failure event (ICOLD 2005).

The risk analysis and risk assessment falls within the Risk-Informed Decision-Making (RIDM) framework. RIDM is the terminology currently preferred in the dam safety community because it makes a clear distinction between the decision and the findings from the analysis. Risk information is used to inform the decision where other factors may come into play in addition to information on risks. RIDM is defined in ICOLD (2005) as, “Decision-making, which has as a main input the results of risk assessment. It involves a balancing of social and other benefits.”

### 2.8.1 History of Uses and Application by Federal Agencies/Dam Owners

In 1979, the Federal Guidelines for Dam Safety were developed by a committee of Federal agency representatives. At that time, RIDM was a new concept and was not promoted for implementation until additional research could be completed. Additional steps were taken by the USBR to refine and improve risk-based analyses, and a risk-based framework was adopted to meet the Federal Guidelines to assess high and significant hazard Reclamation structures in the mid-1990s (USBR 2011). Currently, the USBR establishes annual exceedance probabilities to flood and earthquake loads to fully understand the likelihood of such an extreme event of occurring. The USBR Dam Safety Public Protection guidelines explicitly state that the “standards-based approaches use established rules for events and loads, structural capacity, safety coefficients, and defensive measures and can result in uneven risk across failure modes and loading types” (USBR 2011), further justifying their shift from deterministic to probabilistic methods. Using this risk-based framework, the USBR is able to identify the largest risks and apply mitigation factors. Specifically, the USBR has used the SWT approach with subsequent hydrologic modeling to determine hydrologic risk at several of their facilities (USBR 2012).

The USACE created the Risk Management Center (RMC) in Lakewood, Colorado following the catastrophic flooding in New Orleans from hurricane Katrina in August 2005. They use risk analyses to evaluate dam safety risks from all hazard sources, primarily: hydrologic; seismic; geotechnical; and structural. The USACE currently uses a RIDM approach for a wide range of actions including: assembling preliminary risk measures for their portfolio of dams;

prioritizing detailed studies; and for making decisions on a course of action. The probabilistic methods of analysis including storm typing, SWT and Stochastic Storm Transposition that are being used for the Colorado and New Mexico study were recently used for stochastic flood analyses on the Trinity River above Dallas Texas.

The Tennessee Valley Authority (TVA) has become a leader in the dam safety community for development of analytical tools for conducting probabilistic flood analyses, implementing risk concepts on complex systems of dams and for RIDM. A major component of their recent work was the development of precipitation data series that were comprised of precipitation maxima produced by specific storm types [MGS et al. (2015)]. This was accomplished by using meteorological criteria to identify the storm type for each rainy day in the period from 1881 through mid-2014 and using this database in assembling precipitation maxima for each of four storm types. The storm types included Local Storms (LSs), Mesoscale Storms with Embedded Convection (MECs), Mid-Latitude Cyclones (MLCs), and Tropical Storm Remnants (TSRs). Separate regional precipitation-frequency analyses were conducted for precipitation maxima data series for each of the four storm types. The TVA study developed precipitation-frequency relationships and scalable storm templates for watersheds in the Tennessee Valley. The results were then used to conduct stochastic modeling for floods generated by the various storm types and to develop hydrologic hazard curves for dams and nuclear plants operated by the TVA.

The Federal Energy Regulatory Commission (FERC) is in the process of implementing a RIDM process for identifying, analyzing, assessing, and managing the risks associated with FERC-regulated dams. A Probabilistic Flood Hazard Analysis (PFHA) is used to estimate the frequency of flooding hazards. Often these hazard curves are presented as graphs/tables of peak flow and volume versus annual exceedance probability (AEP); the AEPs offer sufficient support to FERC for ascertaining acceptable risk. At present, this is an option as an alternative to using a deterministic PMF approach (FERC 2014).

As part of its approach to evaluating natural hazards and potential consequences of its nuclear facilities, the U.S. Nuclear Regulatory Commission (NRC) is in the process of completing a 5-year plan (the NRC Strategic Plan for Fiscal years 2014-2018; Safety Strategy 2) for establishing policies and procedures for future regulatory guidance. This 5-year plan includes a research perspective with the anticipated result of tools and products to assess and evaluate PFHA. The new guidance will replace the deterministic methods currently in use (NRC 2014).

## 2.8.2 Application and Use by State Regulatory Agencies

Washington State was among the first states to utilize risk-based hydrologic study findings for ascertaining spillway adequacy. Washington State Dam Safety Office created regulations in 1993 that implemented criteria for assessing spillway adequacy that included: watershed precipitation-frequency information; probabilistic hyetographs; probabilistic soils and hydrologic modeling parameters; and evaluation of consequences. This approach provided a risk-based framework for assessing hydrologic adequacy of spillways at existing dams and sizing of spillways for new dams.

In Montana, early Dam Safety regulations for spillways were based on the reservoir volume and dam height. The minimum in-flow design flood (IDF) for a dam impounding less than 100 acre-feet and less than 20 feet high was the 100-year flood. For larger dams/reservoirs

impounding 50,000 acre-feet or greater and with heights of 100 feet or higher, the IDF increased by fractions of the PMF up to a maximum of the full PMF for the largest dams. However, in many cases the required spillway size was disproportionate to the level of downstream development, particularly for large dams in rural areas or smaller dams with high-density downstream development. In 1999, new hydrologic standards provided downstream protection by relating the required spillway size to the consequences of a dam failure, or estimated loss of life, rather than to the size of the impoundment or dam. The Montana Dam Safety Office implemented criteria similar to that used by Washington for assessing spillway adequacy and sizing of spillways (Hydrometrics 2010).

The California Dam Safety Office uses consequence-based criteria for dams, which they determine as requiring a PMP/PMF design. The potential consequences resulting from the uncontrolled release of a reservoir determine the hazard classification of a dam. The minimum allowable design required is a 1,000-year storm, which corresponds with the lowest hazard classification. The PMP is required for the highest hazard classification of dams, whereas intermediate classifications and requirements lie between these two limits. Therefore, California dam regulations represent a hybrid of deterministic and probabilistic approaches.

Per personal communication with the Association of State Dam Safety Officials (ASDSO) in February 2018 and examination of the Federal Emergency Management Agency's (FEMA) Summary of Existing Guidelines for Hydrologic Safety of Dams (2012), it would seem that all other states (as of 2013) use the PMP/PMF or some percent of PMP/PMP, depending on the dam hazard classification, for regulation.

There are a number of aspects of risk assessment and risk management from which state dam safety organizations can benefit. Even if regulations are based on PMP/PMF deterministic methods, it's the underlying risk that dam safety offices are looking to minimize, understand and make decisions upon. Risk-based studies empower decision-makers to make well-informed decisions that impact public safety and the economics of waterway projects. Often a percent of PMP (POP) is used as design criteria, which in of itself is a non-deterministic method of ascertaining an acceptable risk. However, the probability of POP of an event (i.e., activation of spillway) is largely unknown. Unless however, a regional precipitation-frequency study has been conducted (as the CO-NM REPS represents), which allows the POP to be put into a probabilistic perspective.

It is important to note that the probabilities for extreme rainfall are calculated by extrapolating the estimates from probability distributions for precipitation observed over the last century using the most current statistical approaches available. It is critically important to understand that these statistical analyses are not an expression of over-confidence in the statistical approach, but rather are needed by the dam safety community to assess the behavior of the frequency curves and assess uncertainty for extreme storm events and to make comparisons with PMP. As RIDM is becoming more commonly applied in assessing the hydrologic performance and operation of critical infrastructure, there is great interest in knowing the likelihood of extreme storm events and PMP. Studies [MGS et al. (2015); Schaefer 1997; Schaefer and Barker (2005); Schaefer et al. (2002, 2006, 2007)] have found the AEPs associated with PMP range from  $10^{-4}$  to  $10^{-10}$ , which represents a very wide range and can result in a wide difference in the level of protection/risk for a PMP/PMF approach across a large area such as a State. The results of this project for Colorado and New Mexico can adequately demonstrate the rarity of PMP, thereby providing regulators a more comfortable,

and objective measure of the likelihood of extreme floods including the Probable Maximum Flood (PMF) at dams and other critical water-related infrastructure.

### 3. Data Description and Sources

The sub-sections of Section 3 provide the source, description, and formatting of data acquired for use in this project. Additional details about the use of the data are provided in Section 4 Methodology.

#### 3.1. Precipitation Gauge Data

Digital precipitation data measured at 1-day and 1-hour intervals were acquired for gauges within the project area from various sources. Annual maxima series (AMS) were extracted for key durations for each storm type that impacts the study area (Table 2).

*Table 2. Storm Types and their key durations for the Colorado-New Mexico area*

Storm Type	Abbreviation	Key Duration
Local Storm	LS	2-hour
Mesoscale Storm with Embedded Convection	MEC	6-hour
Tropical Storm Remnant	TSR	48-hour
Mid-Latitude Cyclone	MLC	48-hour

The primary source of 1-day precipitation gauge data for this project was National Center of Environmental Information's (NCEI) Global Historical Climatology Network (GHCN), and in particular the NWS Cooperative Observer Program's (COOP) station data, which has been operating since the late 1800s. In addition, the National Oceanic and Atmospheric Administration's (NOAA) National Weather Service (NWS) Office of Hydrologic Development's Hydrometeorological Design Studies Center (HDSC) provided their quality-controlled time series data used to develop the AMS for NOAA Atlas 14 [Perica et al. (2013)] Data were also collected from other local and state sources (Table 3). The data collection resulted in a total of 4,638 stations with 1-day data which were then quality controlled and screened (e.g., based on a minimum number of data years, as described in Section 4.3) resulting in 1,052 stations for inclusion into the PF analysis.

Similarly, the primary source of 1-hour precipitation gauge data was NCEI's Hourly Precipitation Data set supplemented by HDSC's quality-controlled data with additional local data sources listed in Table 3. In total, 1,165 stations with 1-hour data were acquired and quality controlled and screened (Section 4.3) resulting in up to 347 stations for inclusion in the PF analysis. Appendix B lists the metadata and sample L-moment statistics for stations used in the analysis after quality screening.

*Table 3. List of data sources and reporting interval for precipitation gauge data. (ALERT data are Automatic Local Evaluation in Real Time rain gauges that do not report at regular intervals but were converted to hourly increments.)*

Data Set	Reporting Intervals
NOAA Atlas 14 (HDSC)	1-Day, 1-Hour
NCEI	1-Day, 1-Hour
National Atmospheric Deposition Program (NADP)	1-Day
Hydromet (U.S. Bureau of Reclamation)	1-Hour
Colorado Agricultural Meteorological Network (CoAgMet)	1-Hour
Northern Colorado Water Conservancy District (NCWCD)	1-Hour
Remote Automated Weather Stations (RAWS)	1-Hour
SNOW TELemetry (SNOTEL; Natural Resources Conservation Service)	1-Day, 1-Hour
Denver Urban Drainage Flood Control District (UDFCD)	ALERT - 1-Hour
Fort Collins Utility	ALERT - 1-Hour
Sevilleta NM Long-Term Ecological Research (LTER)	1-Hour
Jornada NM LTER	1-Day, 1-Hour
Los Alamos National Laboratory (LANL)	1-Day, 1-Hour
U.S. Geological Survey (USGS)	1-Day, 1-Hour
University of Colorado Boulder Mountain Research Stations (MRS)	1-Day
Community Collaborative Rain, Hail and Snow Network (CoCoRaHS)	1-Day

### 3.2. Meteorological Variables for Storm Typing

Along with the station observations, other meteorological data were collected for use in assigning a storm type to each day of the precipitation gauge record. To facilitate the typing of storms as they moved across the area, the project area was divided into seventeen Storm Typing Zones defined as 2-degree latitude by 2-degree longitude zones (Figure 15), coincident with the NOAA-CIRES data described below. The datasets used for storm typing included:

- NOAA's North Atlantic tropical storm-track database from International Best Track Archive for Climate Stewardship (IBTrACS v03rNN) [Knapp et al. (2010); <http://www.ncdc.noaa.gov/ibtracs/>];
- NOAA-CIRES Twentieth Century Global Reanalysis Version II [Compo et al. (2011); [https://www.esrl.noaa.gov/psd/data/gridded/data.20thC\\_Rean.html](https://www.esrl.noaa.gov/psd/data/gridded/data.20thC_Rean.html)], called "Reanalysis Data" herein; and
- Daily precipitation data from the sources listed above in Section 3.1.

## CO-NM Regional Extreme Precipitation Study

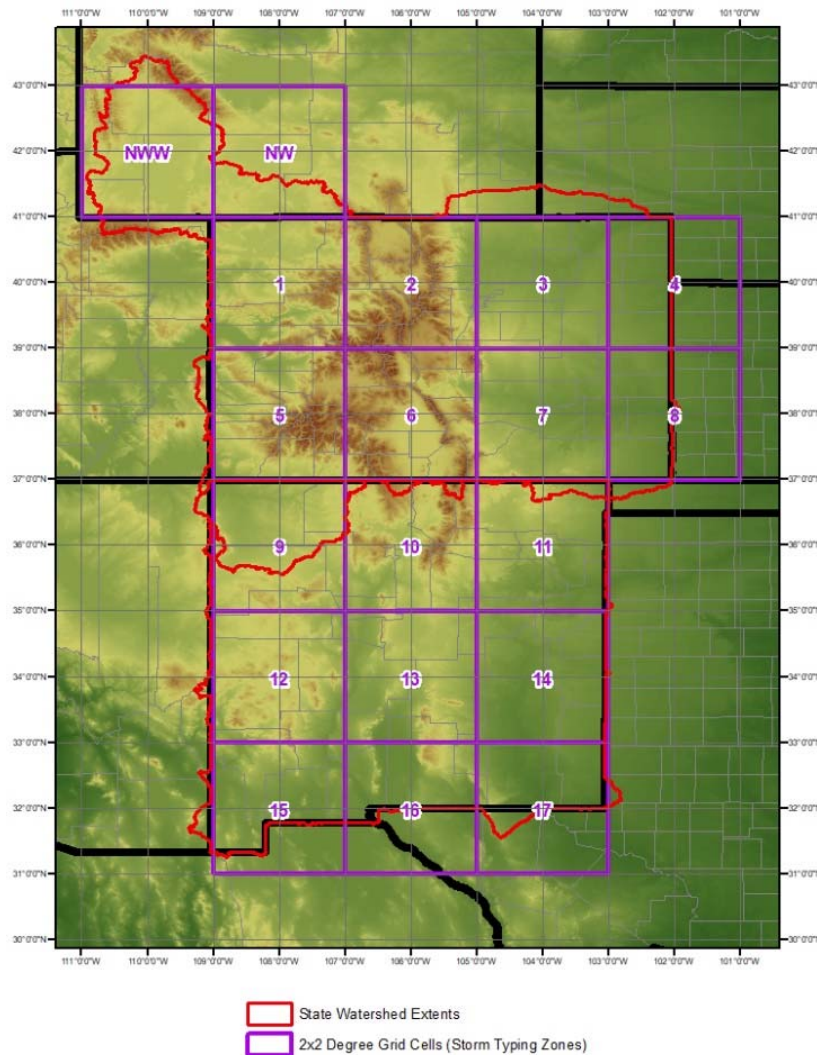


*Figure 15. Project area and the defined Storm Typing Zones. (The NW and NWW Zones were typed based on Zone 1.)*

Storm typing was accomplished for days associated with TSRs by using the IBTrACS data. As described more fully in Section 4.2.1, dates were designated as TSR when a tropical storm track was in or near (within ~250 miles) the project area and could have caused precipitation associated with a tropical storm meteorological environment. The period of record for the IBTrACS data was 1850 through 2014.

Several meteorological parameters available on a daily basis from the Reanalysis Data from 1895 through 2014 were used. These data have a spatial resolution of 2-degrees latitude and 2-degrees longitude (coinciding with our Storm Typing Zones) and a temporal resolution of six hours (at 00Z, 06Z, 12Z, and 18Z). Contoured maps, areal values, and pressure gradients were developed for each Storm Typing Zone. To compute the gradients of these parameters, a matrix of 3x3 Reanalysis Data cells (i.e., Storm Typing Zones) was considered. The maximum 6-hour value over a defined time interval, depending on the duration of interest, was used to

assign a representative value to a given day. The maximum 6-hour value over 24-hours (starting with 12Z) was used to represent the value for each parameter in each Storm Typing Zone for each day for the 6-hour duration of interest (MECs and Local Storms), and over the 48-hour period (starting with 12Z of the start day) for the 48-hour duration of interest (MLCs and TSRs).

The meteorological parameters included:

- geopotential height fields at the 850 millibar and 500 millibar atmospheric pressure levels;
- Precipitable Water (PW); and
- Convective Available Potential Energy (CAPE).

The 850mb gradient identifies low-level jets and mesoscale shortwaves typical of MEC events. The 500mb gradient identifies upper air organization providing a good indicator for large-scale synoptic events. PW represents the depth of water in a column of the atmosphere if it were entirely condensed out. PW provided the manual storm-typing effort auxiliary information but was not used in the automatic storm-typing algorithm (Section 4.2). CAPE is the amount of potential energy available to be released for convection. High values of CAPE are typically associated with higher intensities of precipitation and a good indicator of situations where storms contain convective cells (i.e., Local and MEC storm types).

### 3.3. Mapping Datasets

Continuous gridded spatial data is integral in mapping point precipitation-frequency estimates (Section 4.4.3). Common predictor variables such as elevation and seasonal average precipitation are available as gridded datasets from various sources.

Various pre-existing gridded datasets were used to provide predictor variables in the spatial mapping of the PF estimates and to guide the delineation of Climate Super Regions (Section 4.4.1). The following is a list of the pre-existing gridded datasets used in this project:

- Digital Elevation Model (DEM) [USGS 2017]
- Slope (as derived from DEM)
- Aspect (as derived from DEM)
- PRISM Mean Monthly, Seasonal and Annual Precipitation (Daly 1994)
- NOAA Atlas 14 Precipitation-Frequency Estimates [Bonnin et al. (2011); Perica et al. (2013)]
- HRRR model output precipitation - mean annual maxima (Task 3, Volume 4)
- Grids of latitude and longitude.

Given the dominant impact of the PRISM gridded datasets, the projection and resolution of the final grids associated with this project are consistent with the PRISM grids. The PRISM grids are in a longitude-latitude “geographic” coordinate system based on the WGS84 datum at a spatial resolution of 30-arc seconds, which equates to about 0.33 mi<sup>2</sup>.

Additional pre-existing vector datasets were used to inform delineation of Heterogeneous Climate Regions. These included:

- The extreme storm regions published in the Colorado Extreme Storm Precipitation Data Study [McKee and Doesken (1997)] as shown in Figure 16;

- NOAA's U.S. Climate Regions, which are contiguous regions of similar climatological characteristics; these regions are useful for calculating climate anomalies and other climatological information [Karl and Koss (1984)]; and
- Continental divide shapefile (National Atlas of the United States 2002).



Figure 16. Hydroclimatic regions of Colorado used to describe and characterize extreme precipitation events ([https://ccc.atmos.colostate.edu/pdfs/Climo\\_97-1\\_Extreme\\_ppt.pdf](https://ccc.atmos.colostate.edu/pdfs/Climo_97-1_Extreme_ppt.pdf))

Lastly, to compute Watershed Precipitation-Frequency relationships, shapefiles of Test Basins within the project area were required. The criteria and considerations for selecting the watersheds were:

- 3-6 watersheds per super climate region;
- Geographically spaced apart;
- Represent different climatological and meteorological settings/areas;
- Range in size from 80 mi<sup>2</sup> to 1,000 mi<sup>2</sup> and sub-divided into sub-basins of 5-50 mi<sup>2</sup>;
- Their immediate benefit for the Sponsors or other active stakeholders.

All of the selected watershed shapefiles were provided by the REPS Sponsors, whereas the sub-basins were created using USGS's StreamStats (<https://streamstats.usgs.gov/ss/>). Figure 17 provides a map of the selected watersheds used to compute scalable ARFs for each of the three Macro Regions.



Figure 17. Selected Watersheds for computing scalable ARFs

### 3.4. Storm Data

The development of watershed precipitation-frequency relationships using stochastic storm generation methods requires a suite of storms with their temporal and spatial characteristics. Storm analyses completed by the Deterministic PMP Task (Volume 2) of the REPS project and provided from HRRR model output (Volume 4) were utilized. These data were used to develop scalable spatial and temporal storm patterns for the three dominant storm types (MLC/TSR, MEC, LS) to use in developing watershed precipitation-frequency relationships. This section briefly describes the data received from those Tasks.

Storm data provided by the Deterministic PMP Task (Table 4) consisted of hourly precipitation grids generated from the Storm Precipitation Analysis Software (SPAS). Storms were selected based on classification of storm type from that task with a total of 15 MLC, 13 Local, and 8

MEC storms used. From this set of storms, a total of 22 MLC, 45 Local, and 50 MEC spatial and temporal patterns were developed.

To supplement the sample size of the storm patterns developed from the Volume 2 storm data, specific storm data were also collected from the HRRR model output (Volume 4) (Table 5). Storm dates were selected based on high-ranking annual maxima to obtain a variety of spatial precipitation patterns over the region. Hourly precipitation grids were extracted from the HRRR model output and the same procedure for developing spatial and temporal precipitation patterns was applied to these data. The HRRR model output provided a total of 5 storm dates, from which 56 MEC and 304 Local Storm spatial patterns were developed.

A manual analysis of hourly precipitation grids was performed to determine the spatial and temporal extents of the precipitation. The analyst first determined individual storms from a temporal perspective, finding the maximum core precipitation period (2-, 6-, or 48-hours depending on storm type) for every spatially distinct storm in the original storm analysis domain. The analyst then moved through the storm period to determine if there are additional spatially-distinct storms and repeated the process until the original storm analysis duration was complete. This procedure produced the maximum number possible of spatially- and temporally- distinct storms per storm analysis. Table 4 and Table 5 outline details from each storm source.

*Table 4. List of SPAS storm analyses (Volume 2) which were used to provide storm spatial patterns and their associated Macro Region (Figure 7)*

SPAS Storm Number	Source Storm Type	Macro Region	Number of spatial patterns	Storm Date
1074	MLC	Rio	1	1983-09-27
1075	MLC	West	1	1970-09-03
1241	MLC	West	1	2010-10-25
1251	MLC	East	1	1955-05-19
1253	MLC	East	1	1969-05-04
1295	MLC	East	3	1935-05-30
1302	MLC	East	4	2013-09-08
1486	MLC	East	1	1941-09-20
1529	MLC	Rio	2	2008-07-26
1531	MLC	East	1	2014-09-21
1568	MLC	East	1	1966-08-22
1587	MLC	East	2	1941-05-20
1652	MLC	West	1	1961-09-20
1653	MLC	East	1	1993-08-27
1654	MLC	East	1	1997-06-06
1033	LS	East	3	2002-07-05
1131	LS	West	1	2001-08-14
1230	LS	East	2	1997-07-28
1247	LS	East	4	1981-07-02
1264	LS	West	1	1990-08-15
1487	LS	Rio	3	1978-08-19
1508	LS	West	8	2001-08-08
1509	LS	West	5	1999-07-31

SPAS Storm Number	Source Storm Type	Macro Region	Number of spatial patterns	Storm Date
1510	LS	West	6	2003-08-15
1511	LS	West	3	1976-07-13
1528	LS	Rio	5	2006-08-01
1613	LS	East	2	1948-06-06
1661	LS	East	2	1996-08-01
1231	MEC	East	4	1976-07-31
1293	MEC	East	14	1965-06-16
1294	MEC	East	1	1921-06-02
1529	MEC	Rio	1	2007-07-27
1650	MEC	Rio	21	1915-07-19
1651	MEC	West	1	1927-06-26
1658	MEC	Rio	7	1977-07-08
1663	MEC	Rio	1	2007-07-19

*Table 5. List of storms from HRRR model output (Volume 4) which were used to provide storm patterns and their associated Macro Region (Figure 7)*

Storm ID	Storm Type	Number of spatial patterns East	Number of spatial patterns West	Number of spatial patterns Rio	Storm Date
2013071808	LS	60	43	83	2013-07-18
2014072806	LS	47	33	38	2014-07-28
2013071808	MEC	3	2	3	2013-07-18
2014072806	MEC	4	3	6	2014-07-28
2014092106	MEC	4	4	3	2014-09-21
2013091108	MEC	5	3	1	2013-09-11
2012070506	MEC	8	3	4	2012-07-05

### 3.5. Temporal Distribution Datasets

The probabilistic temporal distribution analysis required hyetographs (time series of precipitation) for a large sample size of each storm type, across each Macro Region. To resolve temporal patterns, hyetographs at a temporal scale of 5-minutes, 15-minutes, and 1-hour were necessary for the LS, MEC, and MLC storm types, respectively. Hyetographs were obtained from four primary sources: SPAS storm analyses (Volume 2) including radar and non-radar storms, weighing-bucket recording rain gauge charts (Kunkel 2018), U.S. 15-Minute Precipitation Data (DSI-3260; NCEI), and Denver's Urban Drainage and Flood Control District (UDFCD) network. See Appendix E for a list of the selected storms for use in developing representative temporal patterns.

To bolster the sample size for MLCs, hyetographs were obtained at both storm center (point of maximum storm rainfall) and manually identified Storm Center Zones associated with less extreme, but still useful, rainfall centers from the SPAS analyses. Local Storm hyetographs were supplemented with six extreme rainfall events at gauges in Denver's Urban Drainage and Flood Control District (UDFCD) network.

The most temporal distribution precipitation data came from the weighing-bucket recording rain gauge charts and the U.S. 15-Minute Precipitation Data from NCEI. The weighing-bucket rain gauge strip charts were requested from NCEI for extreme events identified in the AMS data. NCEI provided scanned images of the 1-day strip charts that were then translated and digitized into 5-minute incremental precipitation amounts. Extreme MEC events that occurred at/near a 15-minute gauging sites were extracted from the 15-minute database. To ensure adequate temporal coverage of the event and potentially important antecedent or post-storm conditions, a +/- 1-day buffer was applied to the data extraction.

### 3.6. Temperature Time Series

Snowpack plays an important role in water resources across Colorado and New Mexico with a large portion of the water supply driven by snowpack at high-elevations. With large snowpack comes the potential for large volumes of snowmelt runoff, sometimes rapidly if warm environmental temperatures occur over prolonged periods and/or rainfall occurs on ripe or near-ripe snowpack. Therefore, it can be important to consider snowmelt in hydrologic modeling efforts related to dam safety.

Temperature time series represent the inputs typically applied in the Stochastic Event Flood Model (SEFM (2015)) or other, high-elevation watershed modeling effort. The temperature time series are derived using the following information:

- (i) A climatology of freezing level (ZL) heights to select a reference value; and
- (ii) A climatology of 1000-mb temperatures (1000T) to select a reference value.

A centroid location was selected for each of the three Macro Regions to represent the climatology for the respective Macro Region. Data were drawn from the model reanalysis products: 20th Century Reanalysis (1850-1947), NCAR-NCEP Reanalysis (1948-1978), Climate Forecast System Reanalysis (1979-2015), and Climate Forecast System Reanalysis Version 2 (2011-2015) data sets. These reanalysis datasets are publicly available from NOAA or NOAA-sponsored agencies.

The precipitation-frequency magnitudes provided in this Report are based total precipitation (i.e., they are not rainfall only). As such, temperature time series are only used for longer duration, cool-season storms (i.e., MLC), as smaller convective events (i.e., MEC and LS) are considered to be warm enough for liquid precipitation due to their convective nature.

## 4. Methodology

### 4.1. Storm Types of Interest

There are four storm types that impact the Colorado and New Mexico watersheds that can produce floods with characteristics that pose a hazard to dams: Mid-Latitude Cyclones (MLC), Tropical Storms and Remnants (TSR), Mesoscale storms with Embedded Convection (MEC), and Local Storms (LS). Each of these storm types exhibits different spatial and temporal characteristics, which, in turn, produce differing flood characteristics, in terms of flood peak discharge, duration, and volume of runoff, and flood hydrograph shapes. Depending on the watershed size and location, one or more storm type may contribute to the flood hazard at a given dam. The precipitation-frequency relationships and spatial and temporal characteristics of each of these storm types are important considerations. Each of the four storm types is described below.

A Database of Daily Storm Types (DDST) developed as a part of this project (Section 4.2) lists the storm type for each day, for each Storm Type Zone (see Figure 15) during the period from 1895-2014. Figure 18 shows the counts of days typed as each storm type in the DDST, where we combine the Storm Typing Zones into three generalized areas West, East, and South for convenience of summarization. Local Storms are not included in this Figure because all days not attributed to other storm types were designated LS to account for any storms missed by our definition of the spatial extent of Local Storms.

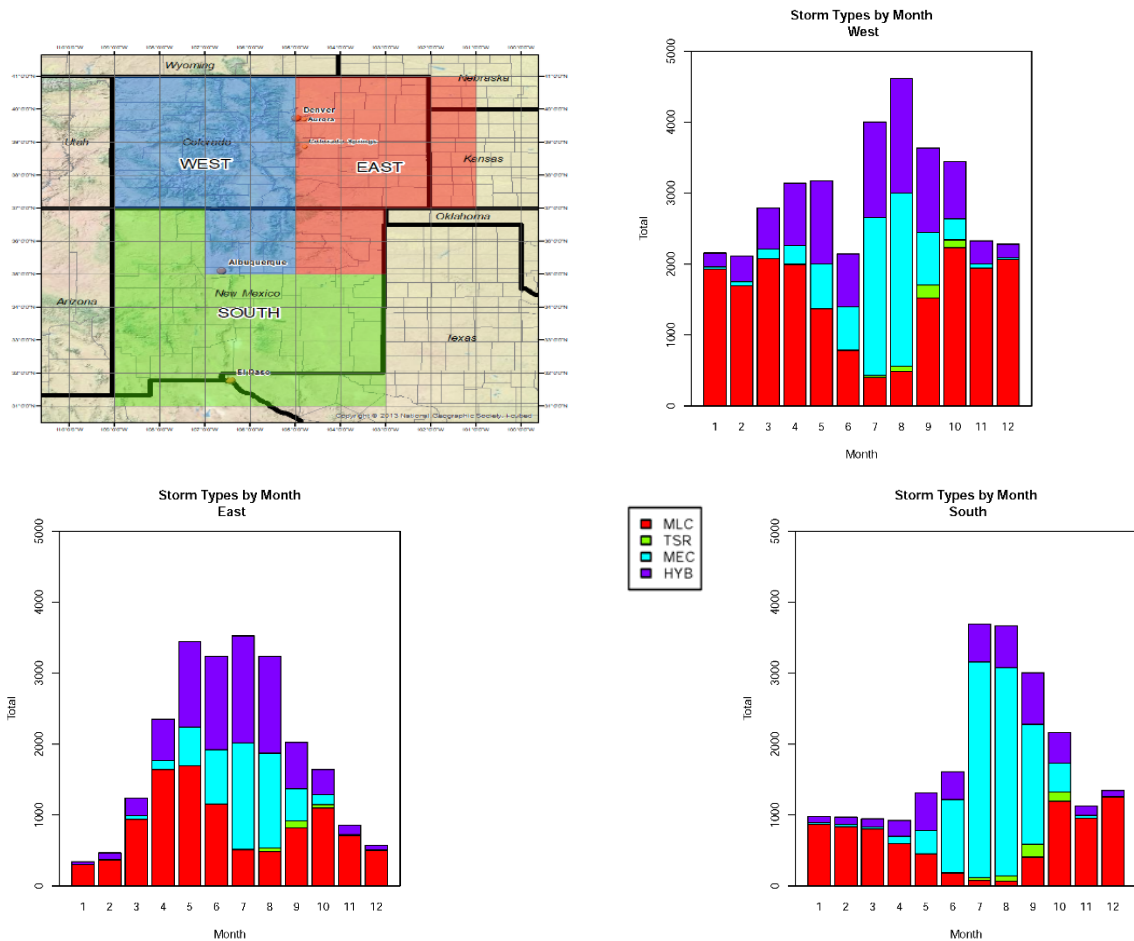


Figure 18. Seasonal Distribution of storm types for 1895-2014 period from DDST where the y-axis is the total number of days across the Storm Typing Zones (Figure 15) for each type

where MLCs are red, TSRs are green, MECs are light blue and hybrid MLC/MEC are purple. The data are grouped into larger general macro-climatic areas- West, East and South

#### 4.1.1 Local Storms (LS)

LS is the term given to relatively small-scale convective events (thunderstorms) which occur in the warm season in the absence of any larger-scale atmospheric circulation. The areal coverage and duration of these storms are limited, typically less than a nominal 100 mi<sup>2</sup> and only one hour in duration. A 2-hour duration was used to account for storms not confined to a single (constrained) reporting period. LSs occur primarily from April through October, with a peak storm season in June, July and August. During the formulation of the DDST, "dry days," those days that our gridded datasets did not indicate any precipitation, were designated as LS to account for any storms missed by the definition of the spatial extent of Local Storms. Because of this, LS are not included in Figure 18.

#### 4.1.2 Mesoscale Storms with Embedded Convection (MEC)

MEC is a generic storm type that is intended to include traditionally-defined Mesoscale Convective Complexes (MCCs) and other organized warm-season mesoscale and sub-synoptic scale storms with embedded convective cells (thunderstorms). These have storm characteristics that can cause both widespread precipitation and locally high precipitation intensities that can generate high rates of runoff. The duration of the storm is generally about 6 hours and can occur within larger synoptic-scale storms if the Convective Available Potential Energy (CAPE) is high. This is a storm type that can produce large floods on intermediate size watersheds, less than about 1,000 mi<sup>2</sup> for the Colorado and New Mexico project area. This is generally a warm season event occurring from April through October, with a peak in June through September. Comparing their seasonal distributions (Figure 18), there is a transition from MLC events to MECs in April and May and then reversing in September and October within all three macro-climate areas.

The Hybrid category in Figure 18 describes cases where MECs transitioned to MLCs or vice versa and could not be clearly defined as one or the other; these cases were included in both the MLC data analysis and MEC data analysis at their respective durations. Cases can exist where precipitation exhibits characteristics of both MLC and MEC systems simultaneously, such as a mesoscale complex of thunderstorms developing ahead of the warm sector of a mid-latitude cyclone. Generally speaking, the Hybrid designation accounts for indirect synoptic-scale organization of convective events, which is distinct from the case of a mid-latitude cyclone with embedded convection (Section 4.1.3).

#### 4.1.3 Mid-Latitude Cyclone (MLC)

MLCs are large, synoptic-scale low-pressure systems with cyclonic circulations that form in the mid-latitudes (i.e., 30°N to 60°N). MLCs and associated frontal systems can produce precipitation for several days over very large areas. Conditions ripe for MLCs are mostly predominant in the cool season over the project area (Figure 18). MLCs and associated fronts are the only synoptic storms occurring in the cool season from November through March. Warm season MLCs occur less frequently as the calendar progresses from May into the warm season.

A sub-type of the MLC storm type was defined when there is embedded convection (EC). This storm type is often applicable to a few of the storm typing zones where an MLC (without

convection) is occurring in other zones. For example, organized convection may occur along a cold front associated with an MLC across the eastern Colorado plains while stratiform MLC precipitation occurs in the mountains to the west, leading to MLC designations for the Storm Typing Zones in the mountains and MLC with embedded convection designations for the plains. Overall, there is clear synoptic definition. For the period from 1895-2014, the number of MLCs with embedded convection (MLC/EC) is small relative to the number of MLCs in the West and South, less than 13 percent. However, the East has flatter terrain where convective cells can originate and has up to 39 percent with embedded convection. MLC/EC cases were included during the extraction of MLC annual maxima and in the extraction of MEC 6-hour annual maxima given the mesoscale nature of the convective element.

#### 4.1.4 Tropical Storms and Remnants (TSR)

TSR is a generic term applicable to precipitation directly associated with a tropical cyclone or hurricane atmospheric environment. This is a synoptic-scale storm type, comparable in size and duration to MLCs, where precipitation is associated with an approaching or departing tropical storm or hurricane that has a storm track within roughly 250 miles of the Project Area. Overall, the number of tropical storms that affected the area is low and variable from year-to-year (Figure 19). The seasonality of TSRs is defined by the hurricane season, June through November, with the most occurring in September (Figure 18). There are relatively few TSR events relative to the number of MLCs or MECs in a given year. In fact, there were so few unique storms (only 65) and even fewer with enough precipitation to be considered representative of the phenomena that the TSRs were combined with MLCs, the other synoptic-scale event, for analysis.

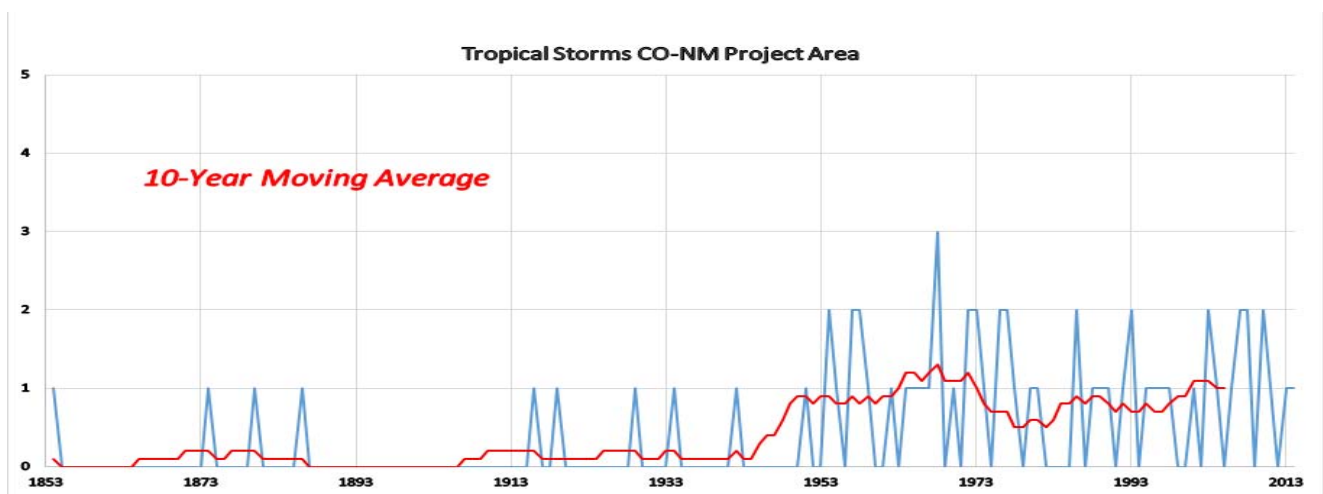


Figure 19. Time series of Tropical Storms and Remnants that affected the Colorado-New Mexico Project Area for 1853-2014 period

## 4.2. Storm Typing Procedures

A major component of this study was the assembly of precipitation annual maxima datasets for each of the three storm types. This required a methodology for identifying the dominant storm type that produced precipitation on any given day for a given station. The Project Area was divided into seventeen 2°x 2° grid cells, known as Storm Typing Zones (Figure 15), consistent with the grid cell size of the Reanalysis Data. The Database of Daily Storm Types

(DDST) contains a listing of the storm type that is applicable for each day in the period from 1895 through 2014 for each Storm Typing Zone.

There are many thousands of rainy days in the period from 1895-2014 across the Storm Typing Zones, so automated procedures for categorizing days into appropriate storm types were developed. This was accomplished in two steps: (1) manually storm typing a selection of storms to establish criteria for an algorithm, and (2) running automated storm typing for each day.

Manual methods were first used to examine the meteorological environment for over 550 storm events representing the different storm types and durations. All-season annual maxima databases that were assembled by the NWS for the NOAA Atlas 14 precipitation-frequency study [Bonnin et al. (2011); Perica et al. (2013)] were initially scanned to identify noteworthy storms to examine at the 2-hour, 6-hour and 2-day durations for storms/dates where precipitation exceeded the 5-year recurrence interval at a station for the 2-hour and 6-hour durations and the 7-year recurrence interval for the 2-day duration. These recurrence interval thresholds provided a reasonably large sample set of storms for local, mesoscale, and synoptic-scale storms. A rarer recurrence interval was used for 2-day given the greater number of daily stations from which to pull storms/dates compared to the hourly durations. Storms from these lists of noteworthy storms were selected based on the ratio of the precipitation total to the median magnitude of that station’s AMS which reflects the rarity of the event.

After the manual storm typing assessment (Section 4.2.1), thresholds for the automated storm typing algorithm were developed after the manual storm typing assessment to assign an appropriate storm type for every day and Storm Center Zone from 1895-2014 (Section 4.2.2). Table 6 lists the various Storm Types and Numerical Codes that were used in the DDST for use in Manual and Automated Storm Typing. Embedded convection, which is the phenomena of LS and MEC storms, was identified within each Storm Type and included in the 2- and 6-hour analyses as well as the dominant large scale storm type (MLC, TSR).

*Table 6. Storm Types and Numerical Codes Used in Storm Typing and DDST*

STORM TYPES AND NUMERICAL CODES		
Storm Type	Acronym	Numerical Code
Mid-Latitude Cyclone	MLC	10
Mid-Latitude Cyclone with Embedded Convection	MLC/EC	13
Tropical Storm and Remnants	TSR	20
Tropical Storm and Remnants with Embedded Convection	TSR/EC	23
Mesoscale Storm	MEC	30

Mesoscale Storm with Embedded Convection	MEC/EC	33
Hybrid - Transition between Mid-Latitude Cyclone and Mesoscale Storms	MLC/MEC	60
Hybrid - Transition between Mid-Latitude Cyclone and Mesoscale Storms with Embedded Convection	MLC/MEC/EC	63
Local Storm (includes Dry Days for potential storms missed by the areal coverage statistic)	LS	40
Local Storm with Enhanced Convection	LS/LEC	43

### 4.2.1 Manual Storm Typing

Several characteristics of the precipitation and meteorological environment on a given day were considered in assigning storm types:

- Seasonality, time of year of storm event;
- Areal coverage of precipitation over each 2° x 2° Storm Typing Zone in the project area;
- Existence of a nearby tropical storm track;
- Spatial gradients in the height of atmospheric pressure fields (500mb and 850mb);
- Magnitudes of Precipitable Water (PW); and
- Convective Available Potential Energy (CAPE).

Each characteristic is described below.

- **Seasonality** - AMS were extracted only from months during which the storm type was dominant and including shoulder months where a given Storm Type is possible but less likely to be dominant (e.g., significant LSs and MECs are warm season phenomena so AMS were extracted from March through November).
- **Areal Coverage of Precipitation** - A measure of the areal coverage of precipitation was needed to differentiate between synoptic-scale storms with wide-spread precipitation, mesoscale storms with moderate coverage, and local storms with very limited coverage. A collection of high-quality precipitation measurement stations, termed the Storm Detection Network (SDN), were assembled in each Storm Typing Zones (Figure 20) for calculation of the areal extent of precipitation. To indicate precipitation sufficiently heavy enough to be considered as part of a “storm,” a threshold of 20 percent of a Storm Center Zone’s average 2-year 24-hour precipitation frequency estimate from NOAA Atlas 14 was used. On a given day, counts were made of the number of stations where the daily precipitation exceeded this threshold and a count was also made for the number of stations that were active (operational) on a given day. Any stations with missing and/or accumulated precipitation values were not counted in the summary statistics for the day. The “percentage of active stations over the threshold” was the indicator for the scale of the areal coverage of precipitation. A separate measure was computed for each Storm Center Zone plus a 1° buffer. The

maximum SDN statistic over a 2-day duration was used to account for storms spanning multiple days.

Plots of gridded daily precipitation [Livneh et al. (2015)] were used during manual storm typing to visualize the spatial extents of daily precipitation for the event of interest and validate the SDN results.

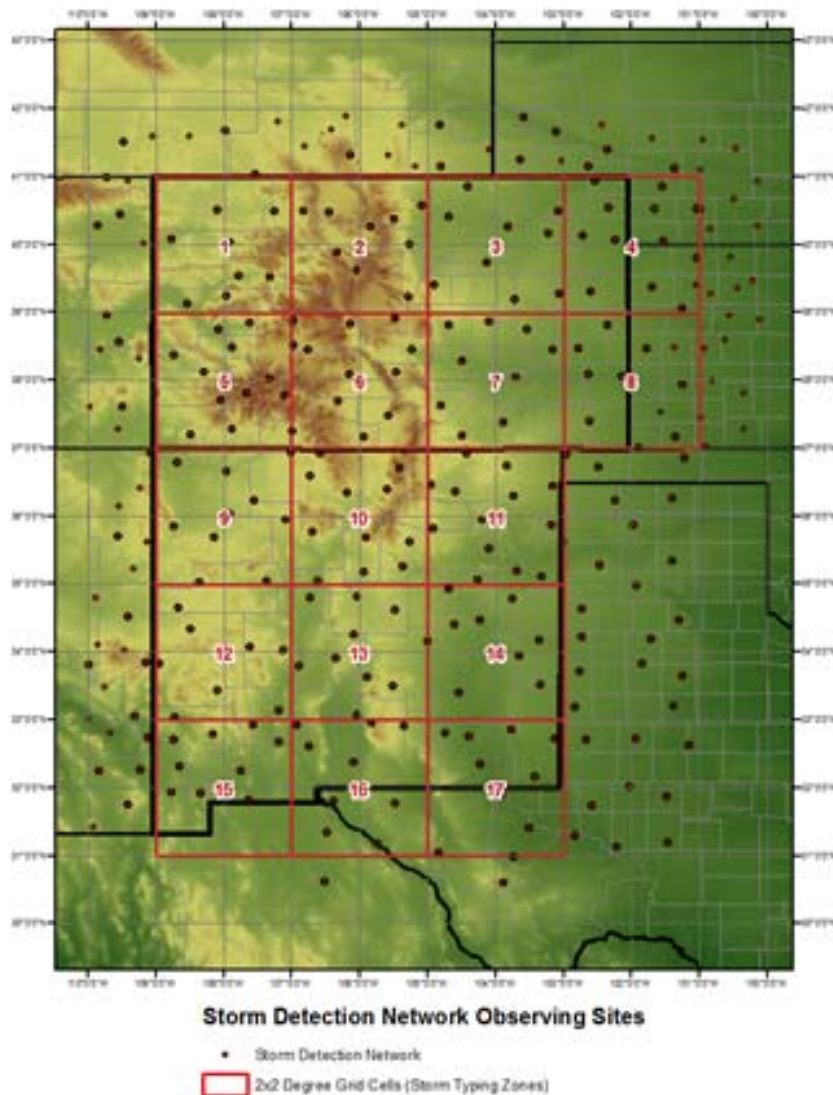


Figure 20. Project Area depicting Storm Detection Network of daily precipitation stations (black dots) and 17 Storm Typing Zones (red boxes)

- **Existence of a Nearby Tropical Storm Track** - The NOAA North Atlantic tropical storm-track database [Knapp et al. (2010)] was used to storm type days associated with TSRs. Specifically, a TSR was assigned to a date when a tropical storm track was in or near (within ~250 miles) the project area (Figure 21) and could have caused precipitation associated with the tropical storm meteorological environment. A rectangular area bounded by the coordinates 43°N, -117.5°W, 26°N, and -101.2°W with a bias towards the west was defined to capture any moisture from Pacific Storms.

Selected tracks were excluded along the southern and western borders of the defined area that were not tracking towards the project area. A buffer of plus 3 days was used to capture approaching moisture from tropical storms that terminated to the south based on the characteristics of several case studies across the project area.

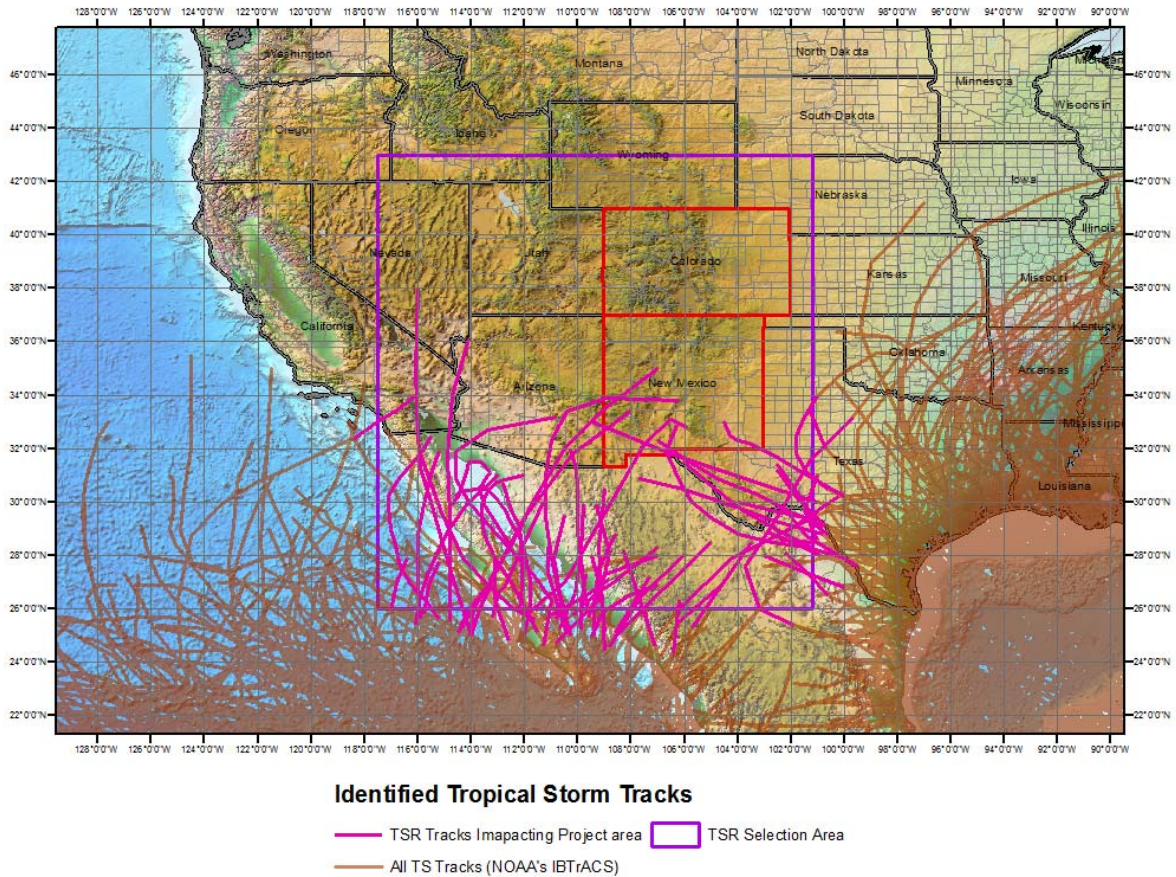


Figure 21. Selected tropical storm tracks (from IBTrACS database) used to define days with TSR influence over the CO-NM Project Area

This process identified a total of 302 days (including buffer), from 65 unique storms, as TSR-influenced from the 1850 through 2014 time period of the available IBTrACS data record. However, not all of these storms produced significant precipitation to be representative of an annual maximum from a TSR phenomenon. As such, there was an insufficient number of data to conduct a precipitation-frequency analysis on the TSR storm type alone. Given the synoptic scale of these storms, TSRs were grouped with MLCs for analysis.

- Gradient in Height of Atmospheric Pressure Fields (500mb and 850mb)** - Measures of atmospheric pressure as geopotential height from the Reanalysis Data can be used to portray the meteorological characteristics for a storm type. The pressure fields were examined as contoured maps and as magnitudes and gradients in each Storm Tying Zone during the manual storm typing process. The 850mb gradient identified low-level jets and mesoscale shortwaves typical of MEC events. The 500mb gradient provided an indicator for large-scale synoptic, MLC organization.

- **Precipitable Water (PW)** - Precipitable Water (PW) represents the depth of water in a column of the atmosphere if it were entirely condensed out. As such, it indicates the amount of moisture in the air that is available for a storm to translate into precipitation on the ground. PW measures lacked correlation with individual storm types as differentiators and were therefore not applied to distinguish between storm types in the automated algorithm, but maps of contoured PW were used to inform the manual storm typing procedure to identify low-level jets and atmospheric river events from the Gulf of Mexico.
- **Convective Available Potential Energy (CAPE)** - Convective Available Potential Energy (CAPE) is the amount of potential energy available to be released for convection. High values of CAPE are typically associated with higher intensities of precipitation. The measure, obtained from the Reanalysis Data, was examined as contoured maps and as magnitudes and gradients within each Storm Typing Zone. The measure of CAPE was found to be a good indicator of situations where storms contained convective cells (thunderstorms).

Some 550 noteworthy storm events were manually examined and assigned storm type numeric codes (Table 6) to each Storm Typing Zone using a Storm Typing Application (or graphical user interface). The Storm Typing Application displayed panels of the SDN statistics, gradients of 500mb and 850mb pressure, and magnitudes/gradients of PW and CAPE for each day for each storm typing grid-cell (Figure 22). To help inform the manual storm typing, the Application also showed contoured maps of 500-mb and 850-mb heights and PW and CAPE for associated days (Figure 23). These data frames along with daily precipitation fields from the Livneh grids provided insight into the spatial nature of the event, its general meteorological characteristics across the grid-cell zones, and ultimately a dominate storm type.

CO-NM Regional Extreme Precipitation Study

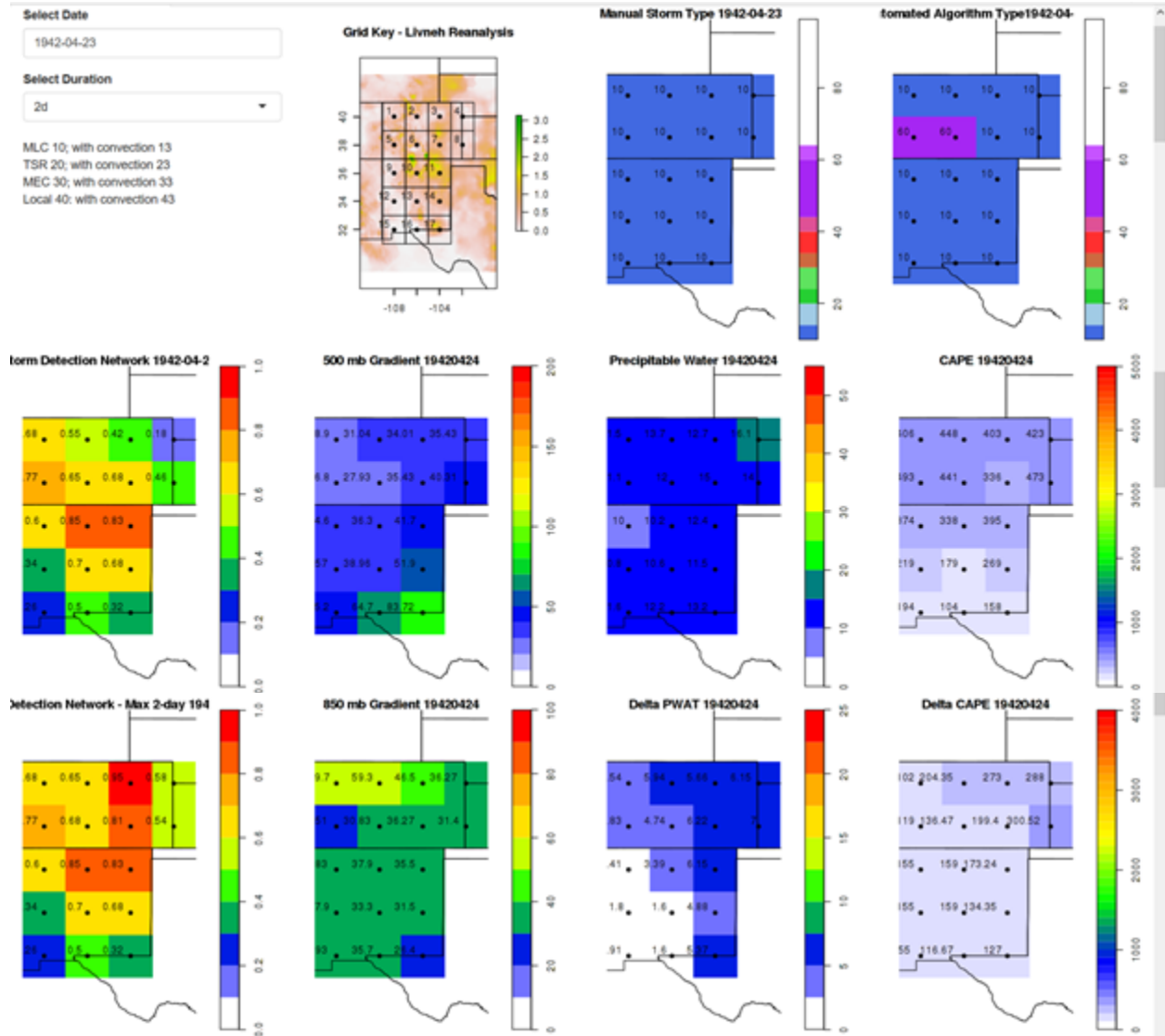


Figure 22. Excerpt of Storm Typing Application panels

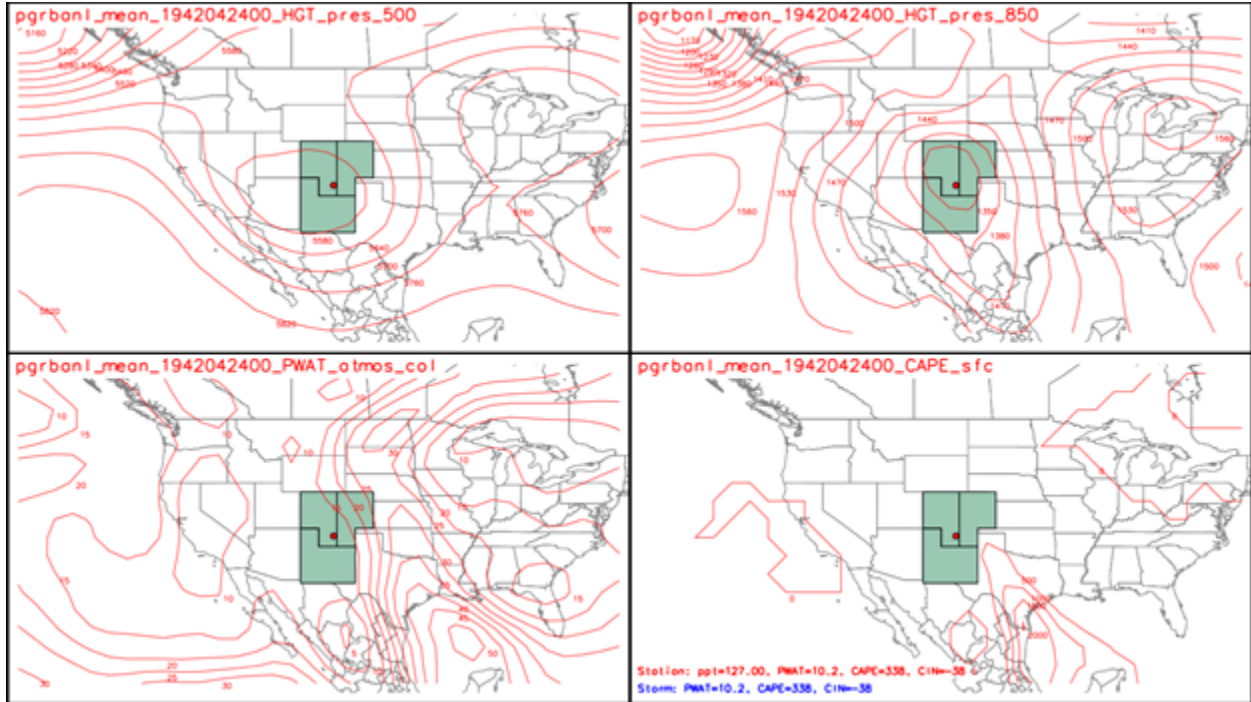


Figure 23. Example of four panel display of 500-mb (upper left) and 850-mb (upper right) Height Contour Maps, Pw (lower left) and CAPE (lower right) used during manual storm typing

#### 4.2.1.1. Manual Storm Tying Examples

As an example, Figure 24 shows the storm measures for a 2-day MLC event on May 26th, 1996. A large but fairly weak upper-level trough was present over the entire Project Area, drawing moisture northwest from the Gulf of Mexico. Instability was minimal, as indicated by the small values of CAPE over the domain. This event was therefore predominantly typed as MLC without convection (10). The event produced widespread heavy precipitation and flooding in Southern Colorado and Northern New Mexico. A large number of daily gauges observed 2-day precipitation during this event that exceeded the 7-year recurrence interval threshold. Note the high percentages in the Storm Detection Network and high gradients in pressure indicative of a synoptic-scale organized system.

An MEC event occurred on July 21, 1972 (Figure 25) in northern New Mexico ahead of a front causing heaving rains of short duration. An upper-level low-pressure center was present over the Pacific Northwest region, but this was too far removed from the Project Area to exert an immediate synoptic influence. However, south and southeasterly flow over Colorado and New Mexico ahead of the low transported moist, unstable air into the region, causing scattered thunderstorms to break out, mainly along and east of the Rockies.

CO-NM Regional Extreme Precipitation Study

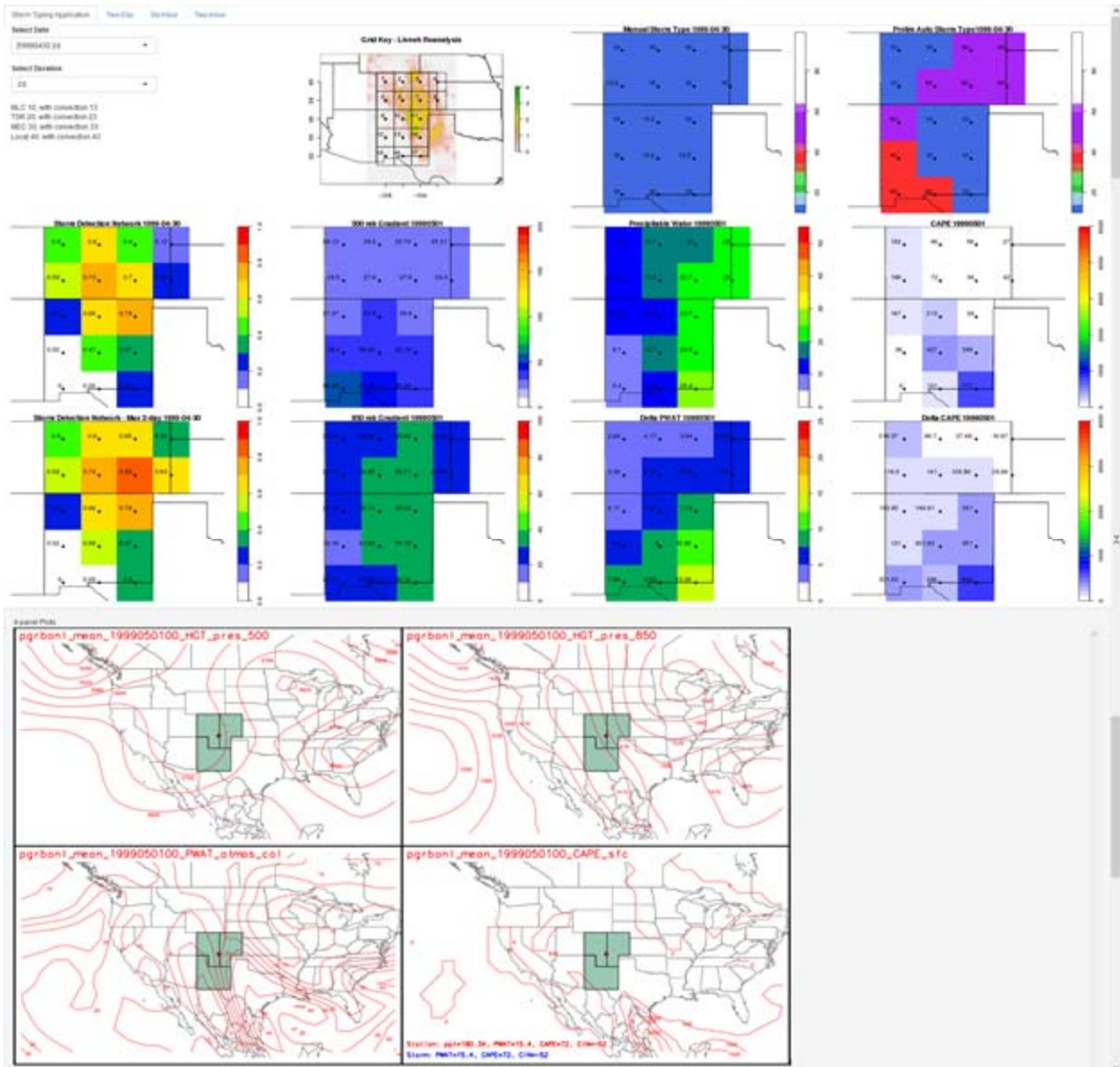


Figure 24. Storm Tying Application panels for May 26th, 1996 MLC event

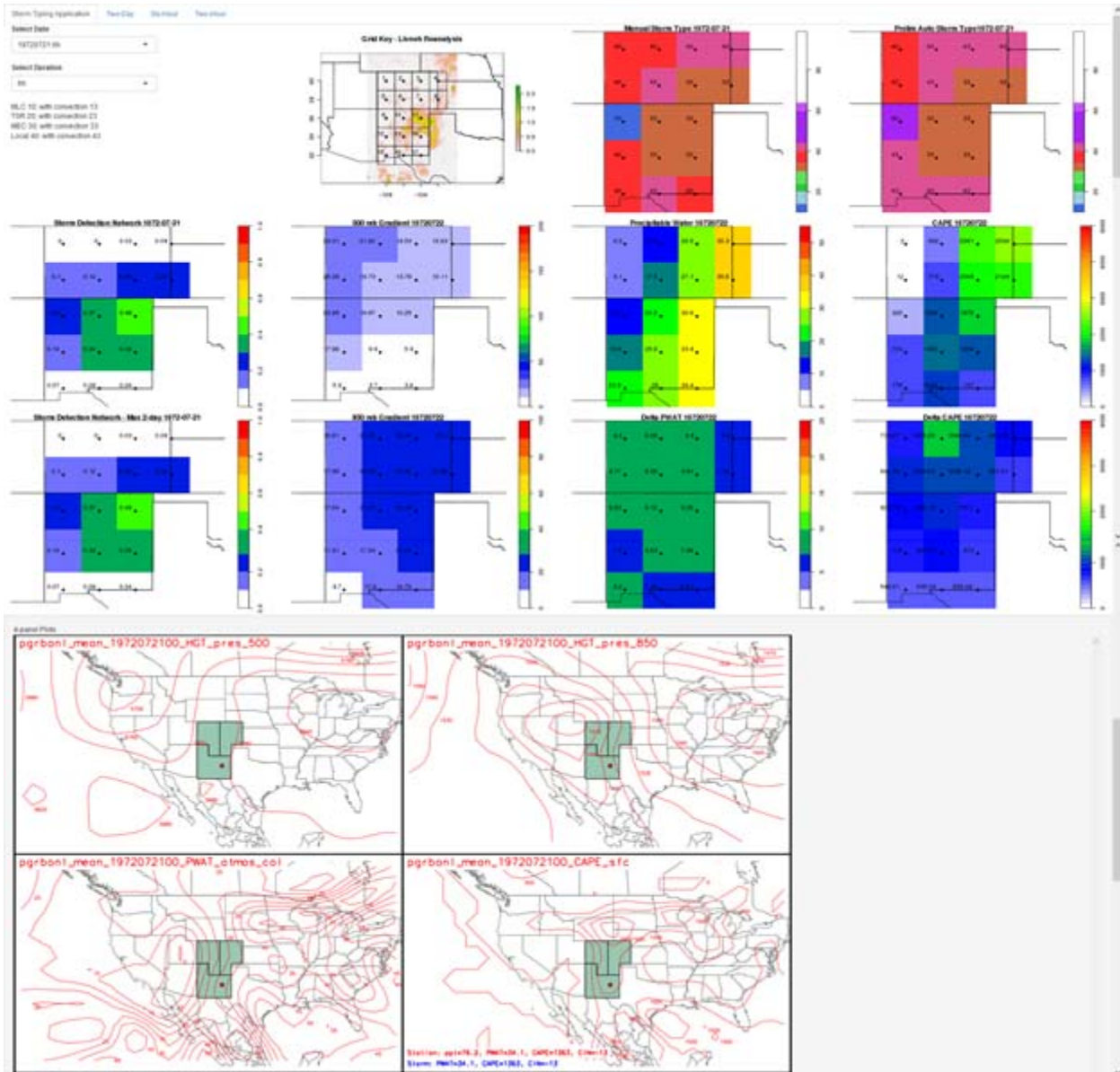


Figure 25. Storm Tying Application panels for July 21st, 1972 MEC event

Experience gained from the Manual Storm Tying was used to set criteria and establish procedures for automated storm typing. A description of criteria and procedures for automated storm typing are presented in section 4.2.2.

### 4.2.2 Automated Storm Tying

Task 2 meteorologists manually evaluated and typed the list of 550 storms to determine thresholds that define the characteristics for each storm type. The measure of the 500mb height gradient across a given Storm Tying Zone was a good indicator of storms with larger synoptic organization versus smaller mesoscale events. CAPE indicated situations where storms contained convective thunderstorm cells.

Established thresholds informed an algorithm to automatically type each day and Storm Tying Zone in the domain (Figure 26).

The final thresholds for the key variables (500mb height gradient, SDN areal percent coverage, and CAPE) were defined as follows:

- **Areal coverage statistic** - Local Storms (LS) were identified for cases where less than 20 percent of the SDN showed daily precipitation magnitudes over the defined precipitation threshold within a Storm Typing Zone. Conversely, mesoscale storms (MECs) and synoptic-scale storms (MLCs and TSRs) were identified when 20 percent or more of the grid cells reported daily precipitation exceeding the threshold.
- **Gradient in Atmospheric Pressure (500mb)** - A strong gradient (greater than or equal to 28 meters per 2 degrees) indicated the synoptic-scale organization of MLCs and a weak gradient (less than 18 meters per 2 degrees) of mesoscale organization and MECs. Moderate gradients in between indicated transitional hybrid cases and were extracted as both MLC and MEC.
- **Convective Atmospheric Potential Energy (CAPE)** - An examination of CAPE measures from previous studies, situations where the CAPE average measure exceeded 500 Joules/kilogram was indicative of conditions for enhanced convective activity naturally associated with MEC and LS storm types. Convective sub-types of MLC and TSR storm types were also identified where values of CAPE exceeded the threshold, indicative of embedded convective activity so that they could appropriately be included in the extraction of 6-hour MEC and 2-hour LS storms.

These thresholds were applied to assign a Storm Type to each day of record from 1895-2014 for each Storm Typing Zone, the DDST. The DDST was then used during the extraction of precipitation annual maxima for each storm type from gauged data.

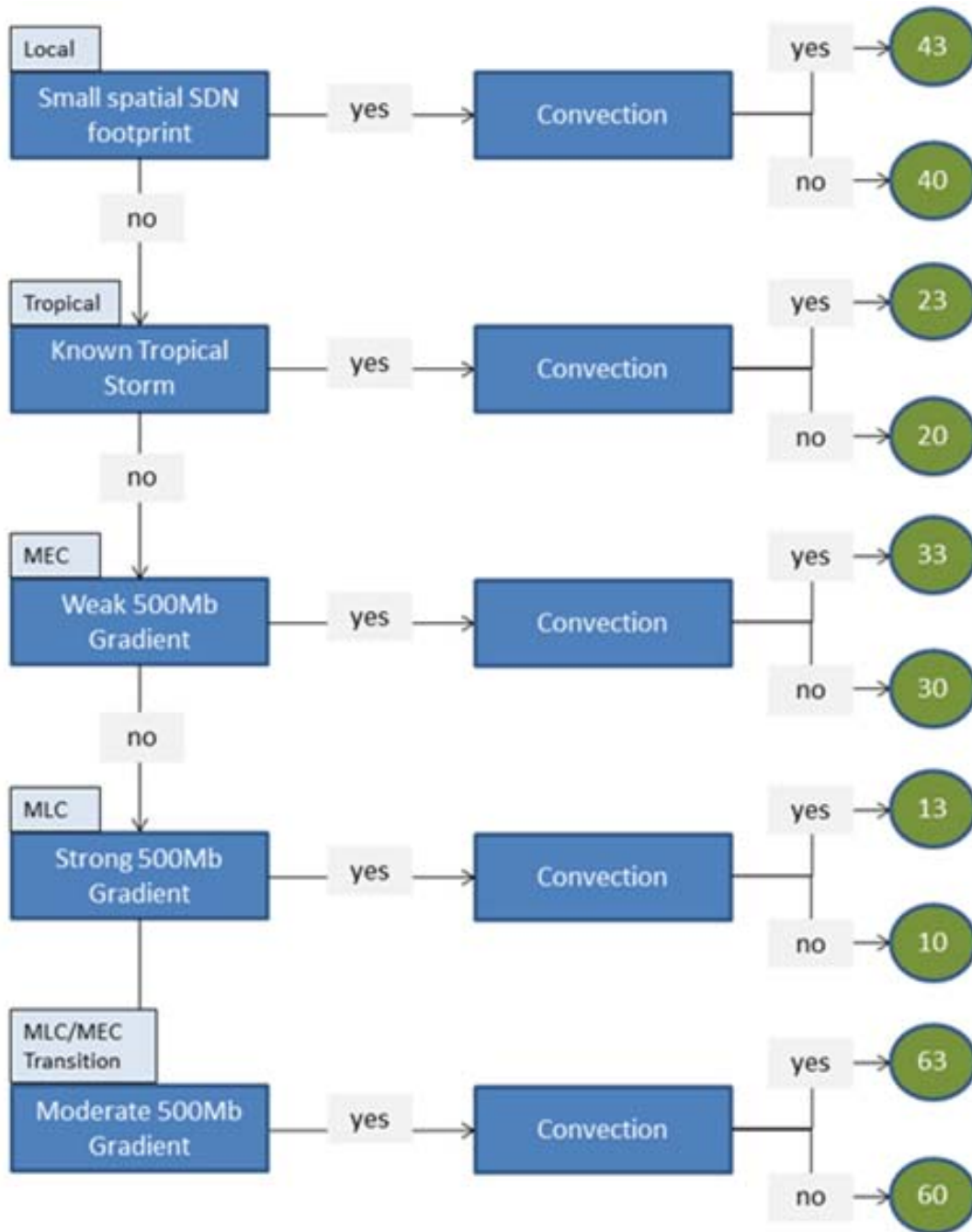


Figure 26. Flowchart of Automated Storm Typing Algorithm

### 4.3. Annual Maximum Series Assembly and Quality Control

#### 4.3.1 Key Durations for Storm Types

The temporal characteristics of the various storm types are such that a key duration can be identified that is representative of the time during which the majority of precipitation typically occurs. Synoptic-scale storms such as MLCs and TSRs are characterized by long-

duration low to moderate-intensity precipitation, which can accumulate to large totals over one or more days. The key duration for these synoptic-scale storms is 48 hours where daily and hourly gauges are suitable for measurement of precipitation for these storm types. Additionally, a 48-hour duration largely avoids issues that arise from constrained 1-day precipitation measurements taken in the middle of a storm.

MEC storms typically occur in the afternoon through late evening hours, have a short life-cycle and are characterized by precipitation with moderate to high intensities over several hours. Therefore, the key duration for MEC storms is 6 hours, where hourly gauges are suitable for measurement of precipitation.

The Local Storm, as the name implies, is more localized in areal coverage and is characterized by short-duration, high-intensity precipitation. The key duration for LSs is 1 hour, where only gauges reporting on an hourly (or shorter) interval are suitable for measurement of precipitation for the LS storm type. A 2-hour duration was used to capture unconstrained precipitation that does not adhere to the clock-hour reporting interval.

The nature of MECs was found to be quite similar to Local Storms in terms of their temporal distribution being front-loaded convective events. Particularly in western Colorado, they also have smaller spatial footprints due to terrain. Therefore, local convective events were included with MEC storms to capture comparable convective phenomena at the 2-hour and 6-hour durations. The differences between Local versus MEC storms can be addressed on the hydrology side using spatial and temporal patterns.

#### 4.3.2 Assembly of Precipitation AMS

Separate precipitation annual maxima datasets were assembled for each storm type and associated duration of interest: 2-day MLCs and TSRs, 6-hour MECs and other convective events, and 2-hour Local Storms. In this context, the term “annual maxima” refers to a single precipitation maximum being selected for each precipitation gauge/storm type/duration for each “climatic year” of record. The climatic year was selected with consideration of the seasonal timing of that storm type so that the start and end of the climatic year occur at a time that is relatively dormant for that particular storm type. It should be noted that while the terminology indicates annual maxima, each storm type has limited seasonality that does not extend to a full 12-month annual period.

All precipitation annual maxima datasets are stored in the L-RAP [Schaefer and Barker (2009)] ASCII Text format and are provided as deliverables for this project.

A number of procedures were required for assembly of precipitation annual maxima datasets for the different storm types:

- **Daily Data Extraction** - Precipitation data from daily gauges were applicable to the 48-hour durations for MLC and TSR storm types. Precipitation annual maxima for daily gauges for these two storm types were identified in two steps. First, each day in the daily time series at a given daily gauge was marked with the applicable storm type from the DDST. Next, the precipitation maximum for each climatic year was determined from those days marked with the storm type of interest. In the case of the 48-hour duration, each 2-day window was examined and precipitation for the given 2-day period was considered as a candidate annual maximum if either one, or both days, had the storm type of interest. For the 72-hour

duration (used to develop relationships to scale from the 48-hour results), each 3-day window was examined and precipitation for a given 3-day period was considered as a candidate annual maximum if either two or all three days were marked with the storm type of interest.

- **Hourly Data Extraction** - Precipitation data from hourly gauges were applicable to all durations for all four storm types. Precipitation annual maxima for hourly gauges were determined in a manner similar to that for daily gauges. First, each hourly precipitation value in the hourly time series at a given hourly gauge was marked with the applicable storm type with consideration given to the date and timing characteristics of the daily gauges used in the Storm Detection Network. Candidate precipitation maxima for a given climatic year were computed if 50 percent or more of the hours in the duration of interest were marked with the storm type of interest. Next, the precipitation annual maximum for each climatic year was determined from the candidate annual maxima.
- **Identification of Duplicate Gauges** - “Duplicate” gauge is the term given to the situation where two or more gauges are either co-located at a given site or closely located and have overlapping years of record. Closely located gauges were considered to be gauges within about 5 miles of each other and within a few hundred feet of elevation. The AMS of candidate pairs were scrutinized for having duplicate data before determining which gauge to exclude as duplicate. Generally, the longer record was retained for analysis as appropriate. Duplicate gauges were marked and documented in the L-RAP files; they were not considered in regional frequency analysis to avoid double-counting.
- **Merging of Data from Nearby Gauges** - It is common for precipitation gauges to be moved short distances from time to time, primarily to accommodate a change in operators/observers and to provide for a continuous long-term record. Some precipitation annual maxima datasets were formed using data from two or more gauges when short distance changes in location were made. Gauges less than 5 miles apart, within a few hundred feet of elevation, and having segments of non-overlapping records were considered in merging of data. All gauges involved in a data merge were marked and documented in the L-RAP files.
- **Observational Period Adjustments** - Precipitation annual maxima for continuous durations are desired for regional precipitation-frequency analysis. This can be visualized as having continuous precipitation measurements and sliding a window of time for the desired duration through the continuous data to determine the precipitation maximum for the climatic year. However, precipitation is reported on fixed time intervals and not on a continuous basis. For example, at a daily gauge where measurements are taken each day at 8 AM, it is easy to imagine situations where part of a continuous 24-hour precipitation event is reported on day 1 and the remainder on day 2. The maximum 1-day measurement underestimates the continuous 24-hour measurement. Standard practice is to use an Observational Period Adjustment [Weiss 1964] to adjust the sample statistics for the mean and standard deviation from fixed interval measurements to be representative of continuous measurements (Table 7).
- Table 8 lists the observational period adjustments that were applied to sample at-site mean values for various precipitation gauges and durations. No adjustments are needed for dimensionless sample L-Moment ratio statistics for L-Cv, L-Skewness and L-Kurtosis.

*Table 7. Observational period adjustments for number of observational periods*

OBSERVATIONAL PERIOD ADJUSTMENTS						
Number of Observational Periods						
1	2	3	4	5	6	7 or more
1.13	1.04	1.03	1.02	1.01	1.01	1.00

Table 8. Observational period adjustments for gauge types and durations

OBSERVATIONAL PERIOD ADJUSTMENTS					
Duration (Hours)					
Gauge Type	2	6	24	48	72
Daily Gauge	n/a	n/a	1.13	1.04	1.03
Hourly Gauge	1.04	1.01	1.00	1.00	1.00

- **Listing of Storm Type in L-RAP Databases** - The L-RAP files include a field listing the storm type for each annual precipitation maximum. For the case of precipitation annual maxima for durations of multiple days, the storm type for each day of the multi-day event is listed. The time-of-day of the end of precipitation is also listed for precipitation annual maxima recorded at hourly gauges.

### 4.3.3 Data Quality Checking

Extensive data quality checking was conducted to eliminate false annual maxima associated with a variety of data measurement and reporting issues/errors. In particular, incomplete reporting (missing data) and accumulations over multiple days are commonly encountered in precipitation records. Data quality-checking was accomplished by examining the completeness of the record during each climatic year and scanning records to locate anomalously small or large precipitation amounts using data quality-checking software previously developed by MGS Engineering Consultants (Schaefer 1997). The software flagged large magnitudes that were not sufficiently corroborated by annual maxima at other stations for manual review. It identified and then accepted or rejected candidate low precipitation annual maxima for years where data were missing for days, weeks or months using a Bayesian-type approach.

The Bayesian approach provides an estimate of the probability of a candidate low annual maximum being the true annual maxima using conditional probabilities. The two inputs are: (1) completeness of the record, which can be viewed directly as the probability that the true annual maximum was observed during the periods when measurements were taken/recorded; (2) non-exceedance probability of the candidate annual maxima computed using the ranked order of the candidate annual maxima within the dataset; computed as  $i/N$  where  $i$  is rank based on ordering from smallest to largest and  $N$  is total number of data. Heuristically, data near the upper end of observations are likely to be true annual maxima and data ranked near the smaller end of observations are more suspect.

The Bayesian Probability of a candidate annual maximum being a true annual maximum listed in Equation 3:

Equation 3

$$(Pc*Pr)/( Pc*Pr + (1-Pc)*(1-Pr))$$

Where,

$P_c$  = probability (evidence) of being true annual maximum based on completeness of record,

$P_r$  = probability of being true annual maximum based on ranking, computed as  $(i/N)$  and ordered from smallest to largest.

Bayesian probability computed as evidence for being a true annual maximum divided by combined probability of being true plus probability of being false. In short, if there is a lot of record missing and the candidate ranks near the low end of the dataset, it is likely a false annual maximum and should be rejected. Conversely, if the candidate is among the largest annual maxima, it should be accepted even if 50 percent of the record is missing.

Additionally, maxima were automatically accepted if the completeness was greater than a given threshold (85 percent in this project). This avoids too frequent rejections for the smallest values in the dataset, which are true annual maxima that would otherwise need a very high level of completeness to avoid rejection from the Bayesian computation.

In summary, the Bayesian computation brings a more quantitative and objective approach to quality control. It is followed by additional quality control during the PF Analysis such as a measure of discordancy [Hosking and Wallis (1997)] which can identify stations whose sample statistics were markedly different from the other stations in a given climatic region. Suspicious data and stations were examined to validate the record. In general, about 6 percent of the candidate annual maxima were rejected and not included in the analyses, primarily because of missing records during the climatic year.

The largest annual maxima in the datasets for each storm type were validated by corroboration with precipitation amounts and timing from nearby stations (Figure 27) or by reviewing published data records, such as the original daily Observation Forms (e.g., Figure 28), Storm Data reports, Monthly Climatological Data publications, and other documents. Changes made to the precipitation annual maxima datasets to address data quality are documented in database records and/or in the L-RAP files.

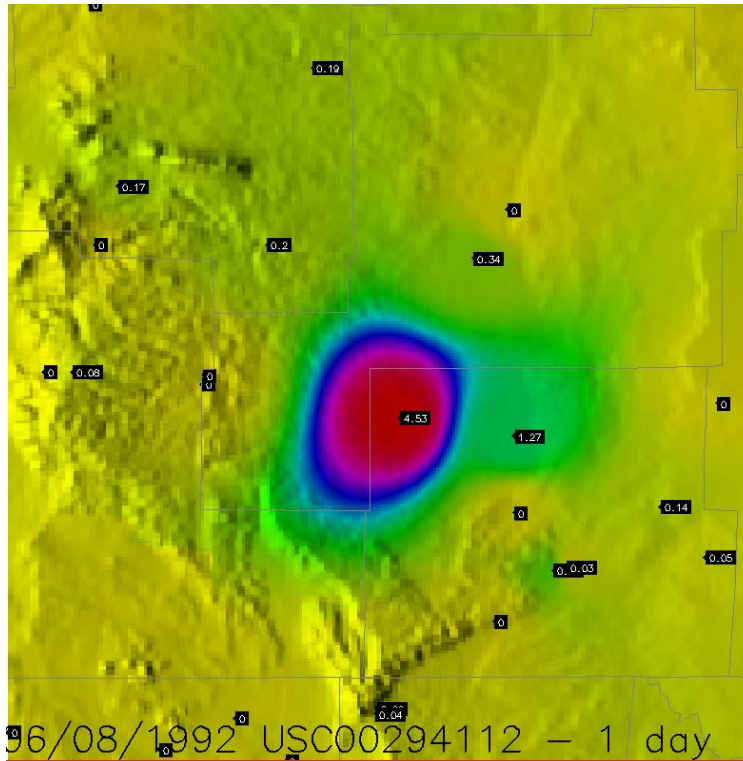


Figure 27. Spatial plot of 1-day observations showing 4.53" at Hope, NM (294112) and some corroborating rain, up to 1.27", nearby on June 8th, 1992

CO-NM Regional Extreme Precipitation Study

STATION (Climatological) <i>Hope NM</i>		(River Station, if different)		MONTH <i>June 1992</i>	WS FORM B-91 (7-89)	NATIONAL OCEANIC AND ATMOSPHERIC ADMINISTRATION U.S. DEPARTMENT OF COMMERCE	
ELEVATION OF GAGE ZERO <i>5700</i>		ELEVATION OF RIVER GAGE ZERO <i>5700</i>		PRECIPITATION STANDARD TIME IN USE <i>MDT</i>		RECORD OF RIVER AND CLIMATOLOGICAL OBSERVATIONS <i>Carbon entered in SOD 7-31-92</i> <i>Original NC'd 8-12-92 SN</i>	
TEMPERATURE F.		PRECIPITATION		WEATHER (Calendar Day)		RIVER STAGE	
24 HRS. ENDING AT OBSERVATION		24-HR AMOUNTS		Draw a straight line (—) through hours precipitation was observed, and a wavy line (~~~~) through hours precipitation probably occurred unobserved.		Mark "X" for all types occurring each day.	
DATE	MAX.	MIN.	AT OBSN.	INCHES	A.M.	NOON	P.M.
1	77	47	61	0			
2	80	46	73	0			
3	83	31	88	0			
4	89	36	76	0			
5	80	36	72	0			
6	82	58	60	0			
7	81	57	68	0			
8	—	45	69	4.53			
9	83	33	77	0			
10	87	35	75	0			
11	83	35	76	0			
12	83	61	78	0			
13	—	52	—	0			
14	92	—	73	0			
15	87	39	82	0			
16	83	49	82	0			
17	83	33	82	0			
18	97	37	76	0			
19	88	60	76	0			
20	88	67	68	0			
21	89	63	73	0			
22	89	39	79	0			
23	87	57	80	0			
24	—	—	—	0			
25	94	—	—	0			
26	—	41	74	10.3			
27	86	37	85	0			
28	80	60	87	0			
29	—	36	—	0			
30	98	—	96	0			
31	—	—	—	0			
SUM		504		15.0	CHECK BAR (For w/weight gage) NORMAL CK. BAR		
CONDITION OF RIVER AT GAGE		HEADING		DATE		OBSERVER	
A. Obscured by rough ice.		75-46-65		5-31-92		<i>Hope NM</i>	
B. Frozen, but open at gage.		91-59-82		6-15-92		<i>Albuquerque</i>	
C. Upper surface of smooth ice.		98		6-30-92			
D. Ice gorge above gage.							
		4.53		15.0		STATION INDEX NO. 29-4112 7	

Figure 28. Original COOP Observation Form showing 4.53" recorded on June 8th, 1992 at Hope, NM (294112) with comments related to severe thunderstorms

### 4.4. Regional Point Precipitation Frequency (PF) Analysis

An L-Moment regional point PF analysis was performed using the Schaefer-Wallis-Taylor (SWT) version of the Climate Region Method (Appendix C) for the specific purpose of providing PF information for extreme storms for use in conducting probabilistic and risk-based analyses of extreme floods for low Annual Exceedance Probabilities (AEPs). A number of significant improvements have been made over the years to the basic Index Flood Method [Hosking and Wallis (1997)] particularly related to reducing aleatoric and epistemic uncertainties in quantile estimates for extreme precipitation magnitudes for specific storm types. The SWT method is described briefly here but fully in Appendix C, Regional Precipitation-Frequency Analysis Using the Climate Region Method for Application in Analyses of Extreme Precipitation and Floods.

Separate regional point precipitation-frequency analyses were conducted using precipitation annual maxima data series for key durations for each of the three storm types. Quantile estimates for selected AEPs were computed ranging from 10<sup>-1</sup> to 10<sup>-7</sup> for each. The general steps are as follows:

1. Delineate climatic regions based on similar climate and topographic characteristics as a starting point to group stations for statistical analysis;
2. Develop a predictor equation(s) for describing the spatial behavior of at-site mean values using some combination of climatic and location indices as explanatory variables. Spatially map the at-site mean values;
3. Form proposed homogeneous sub-regions by assigning stations within a heterogeneous super region or several super regions based on a small range of the climatic and/or location indices;
4. Compute L-moment sample statistics and L-moment heterogeneity measures H1 and H2 [Hosking and Wallis (1997)] for the collection of stations within the proposed homogeneous sub-region;
5. Use L-moment heterogeneity criteria to assess the heterogeneity of the proposed homogeneous sub-region and accept/reject the proposed homogeneous sub-region;
6. Repeat Steps 1 through 3 for all stations within the study area until homogeneous sub-regions have been identified for all locations. Record the regional L-Cv and L-Skewness values for each of the homogeneous sub-regions;
7. Conduct L-moment goodness-of-fit tests to identify a suitable probability distribution for the regional growth curve based on the collective behavior in the homogeneous sub-regions and spatially map established values of Hondo;
8. Develop a predictor equation(s) for describing the spatial behavior of the regional values of L-Cv and L-Skewness for the collection of sub-regions using some combination of climatic and location indices. Spatially map regional L-Cv and regional L-Skewness; and
9. Use the gridded values of the at-site mean, regional L-Cv, regional L-Skewness, and Hondo (Steps 6 through 8) to solve for the distribution parameters for the regional growth curve for each grid-cell in the project area. Use Equation 1 and Equation 2 to compute quantile estimates for each grid-cell and create grids for selected annual exceedance probabilities.

The following sections provide a summary of several of the procedures listed above using some examples from the analysis of 48-hour MLC storms. A more thorough depicting of all results is found in Section 5.

#### 4.4.1 Heterogeneous Super Regions

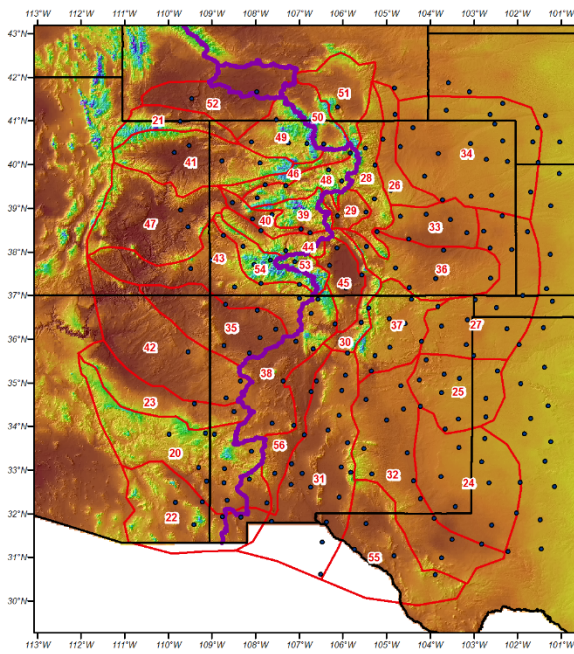
Experience has shown that it is easiest to identify homogeneous regions for precipitation-frequency analysis in complex terrain by starting with heterogeneous Super Regions [Schaefer 1997; Schaefer et al. (2002); Schaefer and Barker (2005); Schaefer et al. (2007)]. In this context, heterogeneous Super Regions (i.e., climatic regions) are locations/areas with similar climatic and topographic characteristics where similarities would be expected in the precipitation-frequency characteristics, although the region may not be statistically homogeneous. It is expected that the similarity of the sources and tracks of atmospheric moisture to a geographic area and the predominant meteorological process will result in similarity in the behavior of at-site means, L-Cv, and L-Skewness within a Heterogeneous Super Region.

Heterogeneous Super Regions are geographically contiguous climate areas that were delineated based on meteorological and climatological considerations using the following parameters and datasets (described in Section 3.3):

## CO-NM Regional Extreme Precipitation Study

- PRISM mean annual precipitation and PRISM multi-month (seasonal) precipitation
- Major mountain barriers such as the Continental Divide, Sangre De Cristo Range and Mogollon Rim
- Elevation (DEM)
- Slope (derived from DEM)
- Aspect (derived from DEM)
- Hydroclimatic Regions of Colorado used to describe and characterize extreme precipitation events
- NOAA's U.S. Climate Regions.

The most influential datasets were the PRISM, slope, and aspect gridded datasets (Figure 29). In Colorado, the Hydroclimatic Regions were heavily relied upon as well. Using the DEM, slopes and aspects were created to clearly identify facets of topography facing the same direction and with similar orographic characteristics (Figure 30). Super Regions were constrained from crossing the Continental Divide, given its prominent impact on moisture available to storms. In fact, many of the regions represent areas of similar windward, leeward, and transitional areas.



**Legend**

- CONM\_Century\_Network\_Final
- Cont. Divide
- climate\_regs\_refined

**PRISM MAP**

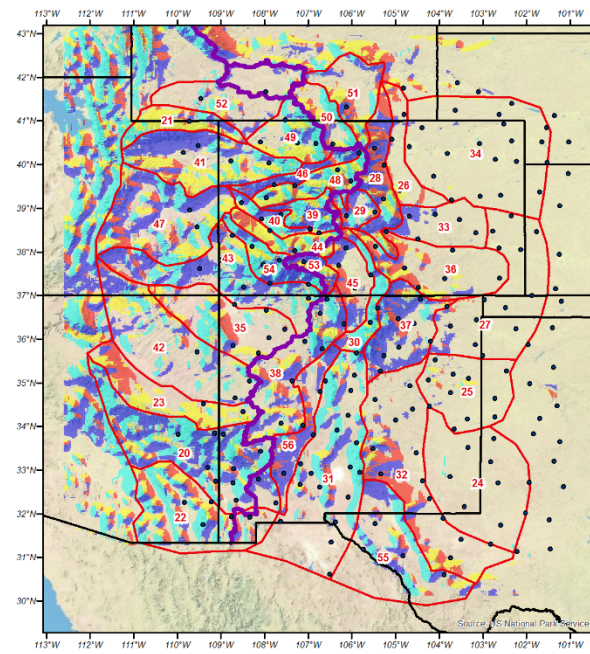
High : 710807  
Low : 4759

**Climatic Regions**

0 37.5 75 150 Miles

AMDSM

*Figure 29. Heterogeneous Climatic Super Regions and PRISM Mean Annual Precipitation*



**Legend**

- CONM\_Century\_Network\_Final
- Cont. Divide
- climate\_regs\_refined

**Slope Facing with >2deg slope**

- NE
- NW
- SW
- SE

**Climatic Regions**

0 37.5 75 150 Miles

AMDSM

*Figure 30. Heterogeneous Climatic Regions with aspects associated with slopes >2 degrees*

In the end, a total of 41 Heterogeneous Super Regions (Figure 31) were identified in the project area. The regions encompassed the states of Colorado, New Mexico, and areas

associated with drainage basins flowing into the states and/or to logical extents of the regions.

Each station was assigned into its respective heterogeneous Super Region to provide an initial construct to begin analyzing the data. These regions preserve the behavior of L-moment statistics at important topographic features such as near the crest of major mountain barriers, at major escarpments, and for sheltered valleys that have rain-shadow effects. QC analysts could then evaluate the annual maximum series of stations with similar climatological, meteorological, and topographical characteristics. These 41 Heterogeneous Super Regions were used to explore the behavior of at-site means, L-Cv, and L-Skewness of the data and begin delineating smaller homogeneous sub-regions for analysis. Later, the heterogeneous Super Regions were assembled into mapping areas (Section 4.4.2) culminating in three Macro Regions: West, East and Rio Grande (Section 5.1.1.2). Each of these mapping regions exhibited markedly different precipitation regimes from one another.

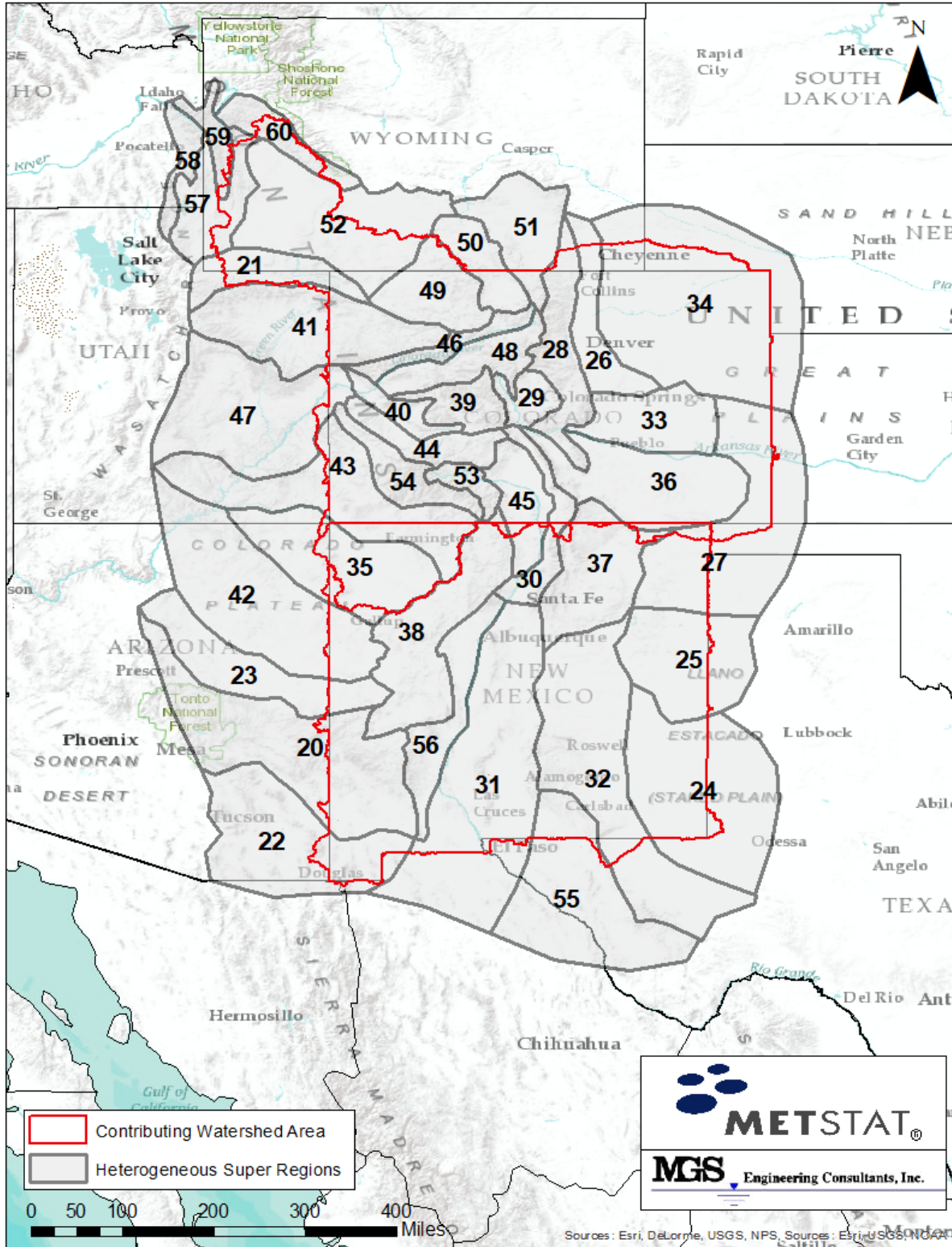


Figure 31. Final Heterogeneous (Climatic) Super Regions

#### 4.4.2 Homogeneous Sub-Regions

The cornerstone of a regional analysis [Hosking and Wallis (1997)] is that data from sites within a homogeneous region can be pooled to improve the reliability of the magnitude-frequency estimates for all sites. This occurs because of the significant reduction in sampling variability of the statistical measures offered by a larger sample of the same phenomenon compared to the sampling variability for a single site. The regional approach works well for regional estimates of L-Cv typically resulting in only minor levels of uncertainty. The regional approach is particularly important for regional estimates of L-Skewness which have inherently high levels of sampling variability.

The success of a regional precipitation-frequency analysis is determined by the ability to identify homogeneous sub-regions and to spatially map the L-moment statistical measures. The term homogeneous sub-region is used here to distinguish them from heterogeneous super-regions.

In this project, the heterogeneous climate super-regions provided a framework for investigating the spatial variability of the L-Moment statistics. Statistically homogeneous sub-regions were formed within these heterogeneous climate regions as collections of observational sites (stations) within a small range of selected climatic and/or location indices. Typically, 12 to 15 stations were grouped together as a candidate homogeneous sub-region for the MLC storm type. Since a smaller dataset was available for the LS and MEC storm types, 8 to 12 stations were typically grouped together as candidate homogeneous regions.

The climatic indices included mean seasonal precipitation for the dominant months of storm occurrence for each of the three storm types in the three Macro Regions (Figure 8). The seasonal climatic indices at each station were computed from the Parameter-Elevation Regression on Independent Slopes Model (Daly 1994). Site elevation and latitude were also used as indices to group observational sites into homogeneous sub-regions.

The climatic and meteorological complexity in the Colorado and New Mexico areas required a large number of homogeneous sub-regions to describe the spatial variability of the L-Moment statistics. There were 192 homogeneous sub-regions utilized for the MLC storm type and 31 homogeneous sub-regions used for the MEC and LS storm types.

L-moment heterogeneity measures H1 and H2 were used to assess the homogeneity of candidate homogeneous sub-regions. An H1 value of 1.0 was originally proposed by [Hosking and Wallis (1997)] for determining if a proposed region/sub-region was acceptably homogeneous. That criterion was based solely on statistical considerations of the sampling characteristics for L-Cv and L-Skewness. H1 and H2 values of 2.0 were used in this study for distinguishing between likely homogeneous and likely heterogeneous regions. These threshold values were adopted to account for additional variability that arises from difficulties in accurate measurement and recording of data and from data quality control issues associated with human intervention in collecting and managing the data [Schaefer and Barker (2009)].

#### 4.4.3 Spatial Mapping of L-Moment Statistics

Spatial mapping was conducted for L-moment statistics for: at-site mean; regional values of L-moment ratios L-Cv and L-Skewness; and Hondo. Hondo is the second shape parameter of the 4-parameter Kappa probability distribution (Equation 2). Predictor equations for the at-site means were developed for stations within one or more heterogeneous super-regions where similar behavior with explanatory variables was identified. Predictor equations for L-

Moment ratios L-Cv and L-Skewness were developed based on the behavior of the regional L-Moment ratios obtained from homogeneous sub-regions. The predictor equations for the at-site means and regional L-Moment ratios were established using concepts from generalized additive modeling which included combinations of polynomials, linear, and logarithmic regression involving one or more explanatory variables.

Explanatory variables were selected which could be described with existing gridded datasets to facilitate spatial mapping on a continuous basis. Explanatory variables included climatic and location indices such as PRISM mean seasonal precipitation, high-resolution DEM elevation, and latitude.

The procedures for spatial mapping of the at-site means and regional L-Cv and L-Skewness are described in detail in L-RAP (Schaefer and Barker 2009) and MGS (Schaefer 2015).

#### 4.4.3.1. Spatial Mapping of At-Site Means

Spatial mapping of at-site means for the key durations and storm types (48-hour MLCs and TSRs, 6-hour MECs, and 2-hour Local Storms) is needed for developing point precipitation-frequency estimates and for producing isopluvial maps for selected annual exceedance probabilities.

Spatial mapping of at-site means involved a three-step process:

1. Determine a predictor equation that describes the regional behavior of the at-site means for a given heterogeneous super-region or grouping of heterogeneous super-regions.
2. Compute a best-estimate of the at-site mean at a given station using a weighted average of the regionally-predicted at-site mean (step 1 above) and the sample at-site mean.
3. Adjust the resulting at-site means to account for spatial coherence of the error residuals (observed-predicted values) in a given locality.

Predictor equations for the at-site means were developed, in a manner similar to that for regional L-Cv and regional L-Skewness, by grouping of stations that exhibited similar behavior with the explanatory variables. At-site means have been found to be well-predicted by climatic indicators such as PRISM mean monthly precipitation for the months when the storm type of interest is dominant.

For example, Figure 32 depicts a scatterplot of sample values of 48-hour at-site means for MLCs for stations with 20 years or more of record against their seasonal means. Review of the behavior of at-site means for selected climatic regions allowed for the grouping of at-site mean data from adjacent climatic regions to develop regression relationships for the prediction of at-site means for spatial mapping. In this way Mapping Areas were delineated for the development of predictor equations. Mapping Areas are groupings of stations/regions that have similar characteristics leading to a single predictive equation.

The concepts of generalized additive models along with combining of Super Regions into so-called "Mapping Areas" significantly reduced the predictive error relative to that for the general relationship seen in Figure 32. Figure 33 depicts a comparison of predicted and observed 48-hour at-site mean values based on that relationship.

Best estimates of the 48-hour at-sites means at the stations were obtained using an Empirical Bayes Approach (Kuczera 1982) as a weighted average of the values predicted from the regression relationship and the sample value of the station at-site mean. Greater weight was given to the sample value of the at-site mean as the record length at a station increased. Residuals were defined as the difference between the weighted-average at-site mean and the regression-predicted at-site mean. Adjustments were then made to the predicted estimates of the at-site means to account for coherence in the spatial distribution of residuals, where the residuals in some geographic areas were not random, but rather systematically over-estimated or under-estimated the at-site mean relative to the regression prediction.

The final mapped values of the MLC 48-hour at-site means for Super Regions 30, 31, 45 and 55, which were combined into Mapping Area A, are depicted in Figure 34. A comparison of Figure 33 with Figure 34 shows a noticeable reduction in the predictive error for the mapped values of the at-site means. This is a result of accounting for both regional information (regional predictive equation) and local information (station at-site mean) and accounting for the spatial coherence of residuals. The final (mapped) values of the at-site mean are judged to be the best-estimates achievable from the collection of regional and at-site information. Figure 34 depicts the final mapped values of the MLC 48-hour at-site mean for Mapping Area A and the results for all storm types are shown in Section 5.

Experience has shown that it is common to achieve a relative RMSE of estimate in real space of less than 6 percent for prediction of at-site means. In some cases, particularly for complex terrain, a second explanatory variable was needed to reduce the unexplained variance in the predicted at-site mean values. Section 5 describes the specific results for this project.

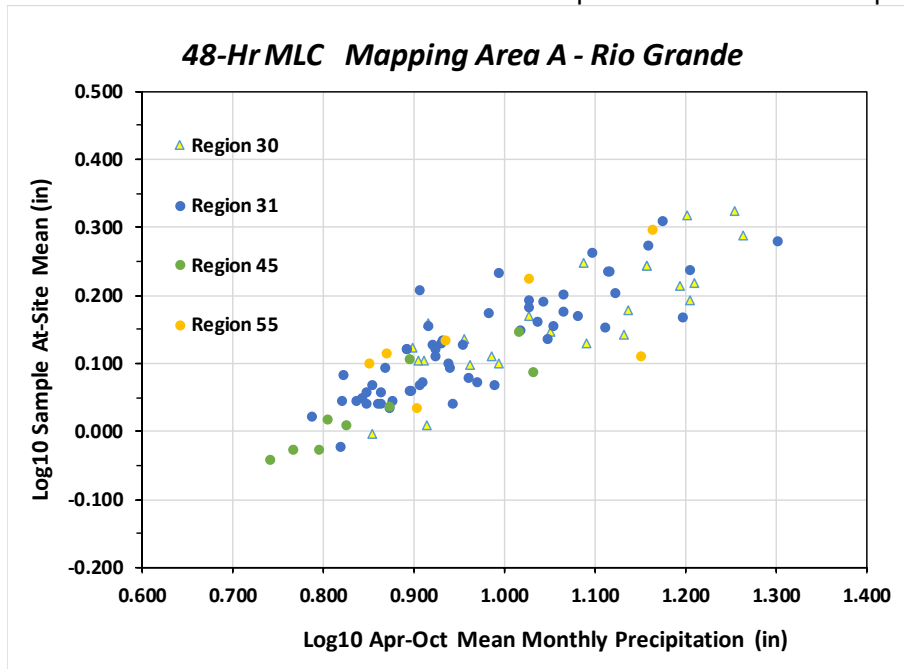


Figure 32. Scatterplot of sample 48-Hour at-site means for MLCs for Super Regions in Mapping Area A in New Mexico for stations with record lengths of 20-years or more

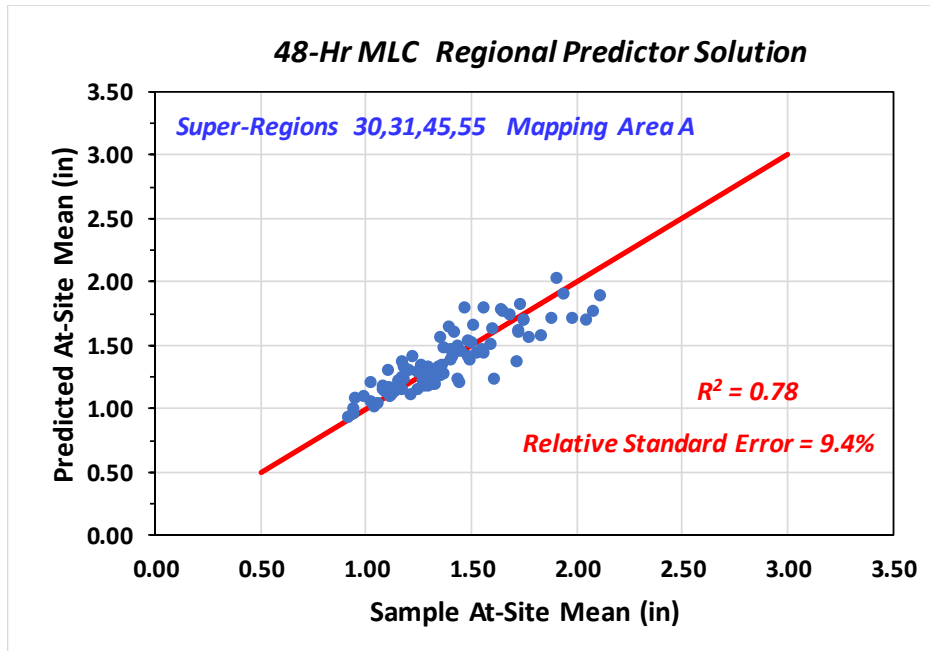


Figure 33. Comparison of regression-predicted 48-hour at-site means and sample 48-hour at-site means for Super Regions 30, 31, 45 and 55 for MLCs

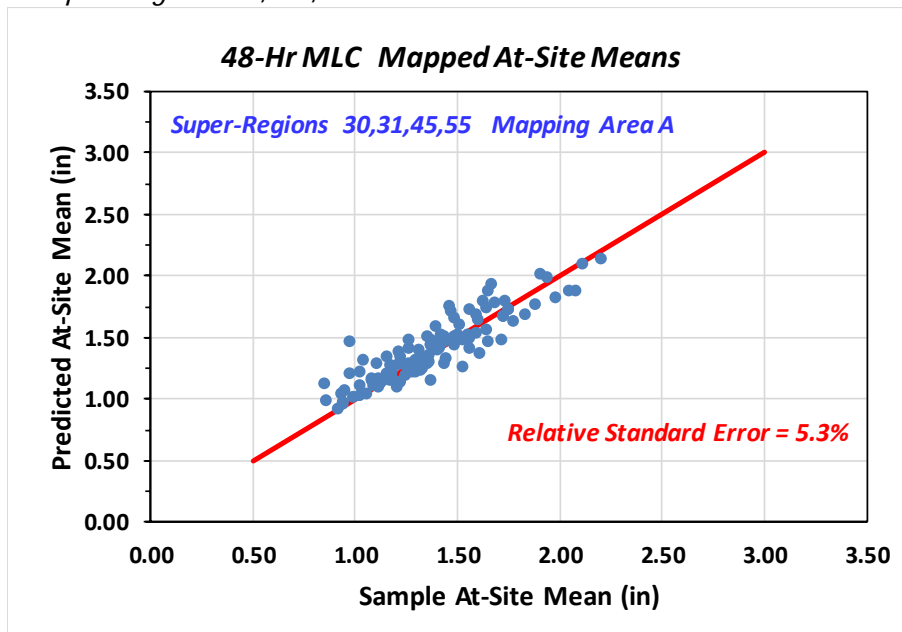


Figure 34. Comparison of spatially mapped 48-hour at-site means and sample 48-hour at-site means for Super Regions 30, 31, 45, 55 in mapping Area A for MLCs

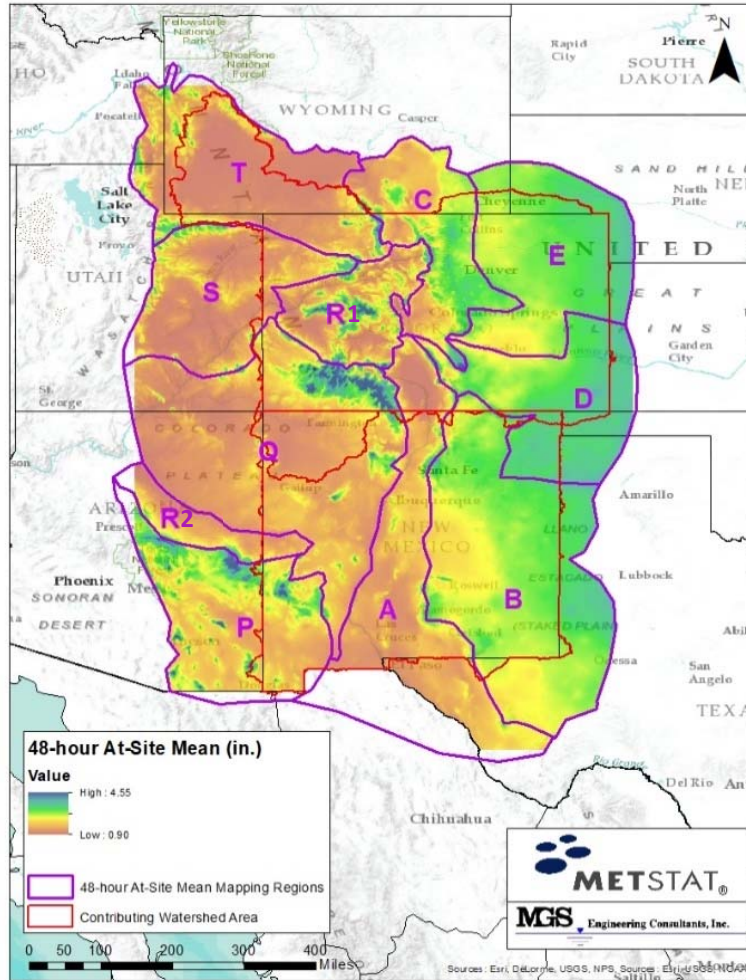


Figure 35. Map of 48-hour at-site means for the MLC storm type showing where Super Regions were combined into Mapping Areas

#### 4.4.3.2. Spatial Mapping of Regional L-Moment Ratios L-Cv and L-Skewness

Regional L-Moment statistics for L-Cv and L-Skewness are computed as a weighted-average of the sample L-Moments for each station within a homogeneous sub-region where the regional L-Moments are weighted by record length. Homogeneous sub-regions are obtained as a collection of stations (sites) within one or more heterogeneous Super Regions. This is typically 8 to 12 stations selected from a small range of climatic and/or location indices of an explanatory variable (e.g., mean monthly precipitation, elevation, and latitude) where the stations are not necessarily geographically contiguous. This sample size is sufficiently large to reduce sampling variability and yet sufficiently small to detect heterogeneity of the data from one or more heterogeneous stations.

Predictor equations for regional L-Cv and regional L-Skewness were obtained using regional values of L-Cv and L-Skewness obtained from the homogeneous sub-regions. For example, each data value in Figure 36 is a regional L-Cv value for a grouping of 12 stations that satisfy homogeneity criteria. An additive regression model was used with various explanatory variables with the forms such as linear, power function (linear in log-space), and 2nd order polynomial.

The resulting predictor equations were used to estimate the regional values of L-Cv and L-Skewness at any location and to allow for spatial mapping of L-Cv and L-Skewness throughout the project area. An example of the systematic variation of regional L-Cv with elevation for 48-hour precipitation maxima for MLCs is shown in Figure 36 for homogeneous sub-regions in the Rio Grande Macro Region. Particular care was taken in developing predictor equations to provide reasonable extrapolations for values of the explanatory variable beyond the range of observed data. These extrapolations were made based on available data in the locality of interest and for climatologically similar locations in the project area. Reasonableness of extrapolations for high elevation areas was of particular importance for this project. Equation 4, Equation 5 and Equation 6 depict examples of the type of forms of predictor equations for regional L-moment ratios, L-Cv and L-Skewness:

Equation 4

$$L-Cv = \alpha_0 + f_1(MonthlyPrecip_{Apr-Oct}) + f_2(Latitude)$$

Equation 5

$$L-Cv = \alpha_1 + f_3(Latitude) + f_4(Elevation)$$

Equation 6

$$L-Skewness = \alpha_2 + \alpha_3 L-Cv$$

where: alpha ( $\alpha_0$ ,  $\alpha_1$ ,  $\alpha_2$ , and  $\alpha_3$ ) are coefficients;  $f_1$ ,  $f_2$ ,  $f_3$  and  $f_4$  are functions such as linear, logarithmic and polynomials;  $MonthlyPrecip_{Apr-Oct}$  and Latitude are example climatic and location indices, respectively;  $L-Cv$  is the second regional L-moment ratio; and  $L-Skewness$  is the third regional L-moment ratio.

It should be noted that much of the apparent scatter in the regional L-moment ratio relationships is often due to sampling variability rather than real differences in systematic behavior. This is particularly true for measures of L-Skewness and L-Kurtosis, which have inherently high sampling variability. Thus, very large datasets are needed to distinguish the signal (systematic trend) from the noise (sampling variability). This situation is partially addressed by using datasets with long records for computing regional L-Cv and L-Skewness. A minimum record length of 20 years was used for determining regional L-Cv, L-Skewness and L-Kurtosis for the MLC, MEC, and LS storm types.

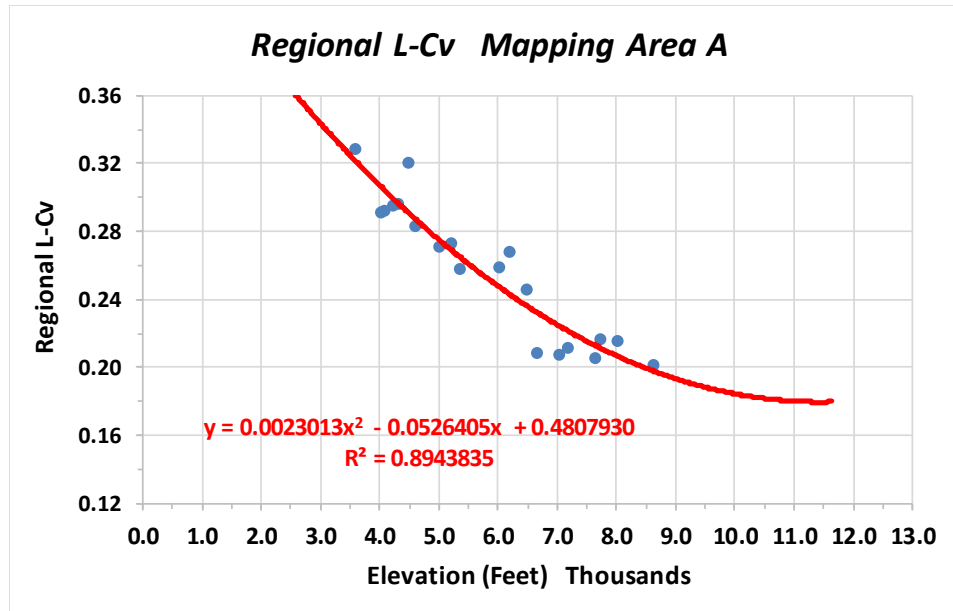


Figure 36. Second order polynomial fitted to regional L-Cv values for homogeneous sub-regions (groupings of stations shown as blue dots) in Mapping Area A in Rio Grande Macro Region

Homogeneous sub-regions are grouped into Mapping Areas based on results during the development of the predictor equations and groupings may vary depending on storm type. Figure 37 shows the Mapping Areas used for the predictor equations for regional L-Cv and L-Skewness. The same regions as L-Skewness were used for Hondo. Given the inherent variability in L-Cv and L-Skewness, Mapping Areas are larger to pool an increasing number of sub-regions, thereby stabilizing the resulting relationships and reducing uncertainty.

It is inevitable there will be some level of discontinuity at the boundaries between mapped areas. In fact, the boundary exists because the differences in L-moment behavior between two areas were large enough to use two Mapping Areas rather than combine them into one mapped area. To the extent practicable, boundaries between Mapping Areas were selected along major mountain barriers and/or locations where there were highly-localized gradients in the mapped L-Moments that were naturally justified. Spatial smoothing could then more accurately describe the transition and spatial variation of high gradients at the boundary between mapped areas.

As such, minor smoothing occurred along the boundary of Mapping Areas where high gradients were present due to the existence of major topographic barriers such as the Continental Divide. The smoothing consisted of using a weight matrix (either 15x19 grid cells, nominally 15km, for L-moment ratios; or 60x76 grid cells, nominally 60km, for Hondo) to determine the percent of each Mapping Area that contributes to a given grid cell. Contributing regional predictor equations were then applied to each grid cell, weighted by the percent contributed from each region.

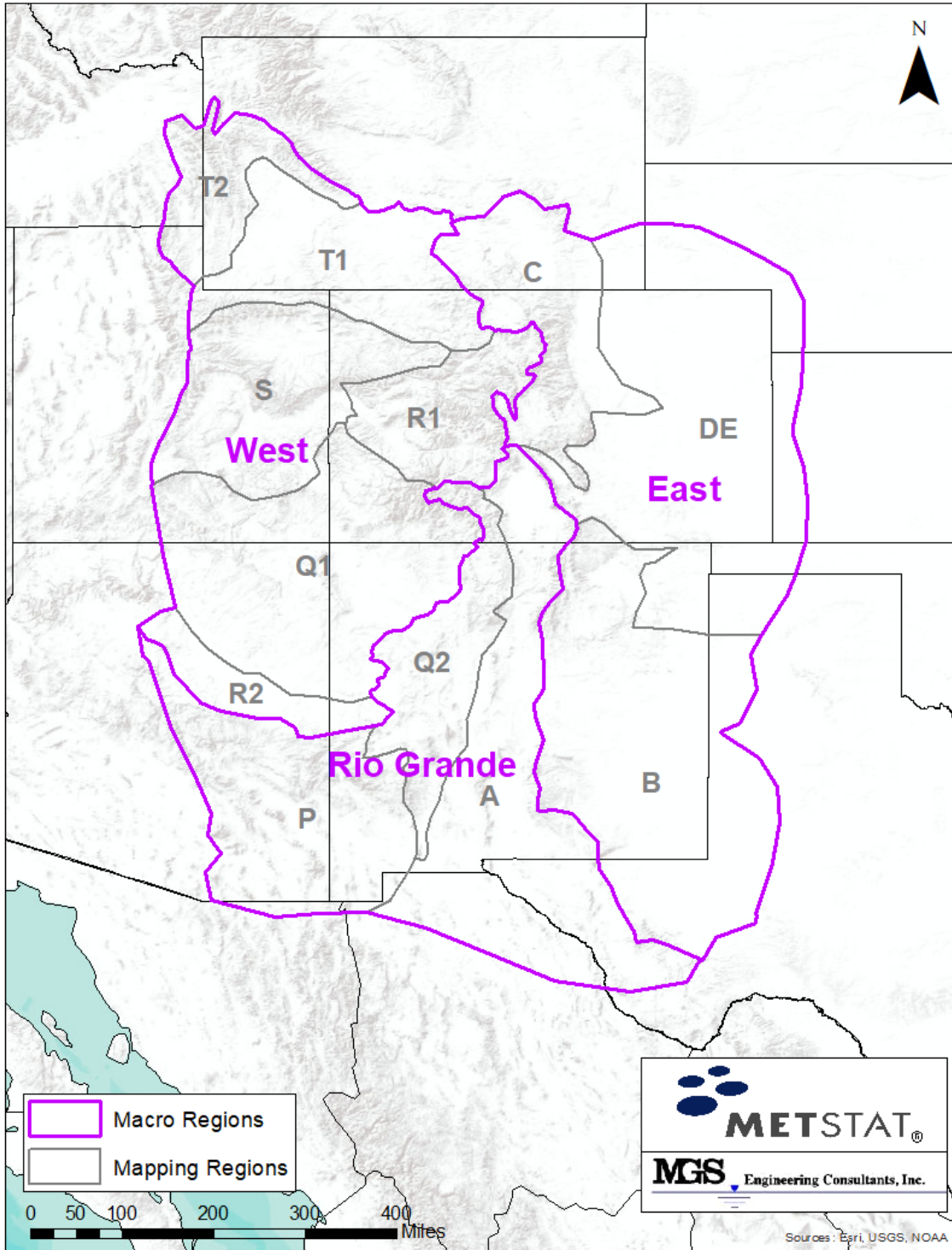


Figure 37. Mapping Areas used for mapping L-Cv and L-Skewness throughout the project area

#### 4.4.4 Identification of the Regional Probability Distribution

L-moment goodness-of-fit tests [Hosking and Wallis (1997)] were used to identify a suitable probability distribution for each of the three storm types. This was accomplished using L-Skewness and L-Kurtosis pairings for the homogeneous sub-regions previously discussed in Section 4.4.2.

The L-Moment goodness-of-fit test [Hosking and Wallis (1997)] was used for identifying the best-fit regional probability distribution. Experience in analysis of precipitation annual maxima for durations of several days and shorter in the United States and British Columbia [Schaefer 1997; Schaefer et al. (2002); Schaefer and Barker (2006); Schaefer et al. (2007)] has shown the best-fit regional probability distribution to be near the Generalized Extreme Value (GEV) distribution. The 4-parameter Kappa distribution [Hosking and Wallis (1997)] is a very flexible distribution capable of emulating distributions near the GEV (Equation 7). In particular, the 4-parameter Kappa distribution with a fixed shape parameter ( $h$ ), Hondo, has been found to provide a suitable regional probability distribution and has the added advantage of emulating alternative probability distributions, which is needed in uncertainty analyses.

The quantile function for the 4-parameter Kappa distribution is:

Equation 7

$$q(F) = \xi + \frac{\alpha}{\kappa} \left\{ 1 - \left( \frac{1 - F^h}{h} \right)^\kappa \right\}$$

where:  $\xi$ ,  $\alpha$ ,  $\kappa$ , and  $h$  are location, scale, and two shape parameters, kappa and Hondo, respectively.

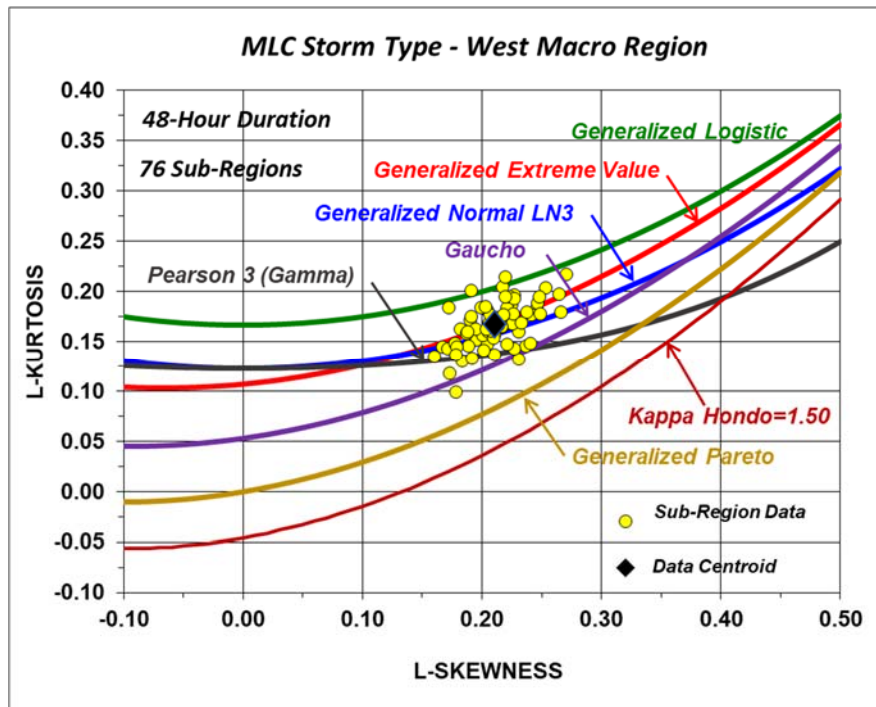


Figure 38. L-Moment ratio diagram depicting regional L-Skewness and L-Kurtosis values for homogeneous sub-regions for 48-hour precipitation maxima for MLCs in the West Macro Region

Three-parameter probability distributions, such as the GEV, have a fixed relationship between L-Skewness and L-Kurtosis. L-moment ratio diagrams are useful for depicting the relationship between L-Skewness and L-Kurtosis for a number of 3-parameter probability distributions (Figure 38). In addition, the L-moment ratio diagram provides a graphical depiction of the L-moment goodness-of-fit test by showing the nearness of regional L-Skewness and L-Kurtosis pairings to a specific 3-parameter probability distribution. Figure 38 provides a graphical depiction of the L-moment goodness-of-fit test for 76 homogeneous sub-regions in the West Macro Region for 48-hour precipitation maxima for MLCs. The centroid of the cluster of L-Skewness and L-Kurtosis pairings is taken as the indicator of the best-estimate 3-parameter probability distribution. The scattering of data in the cluster is due to the natural sampling variability of skewness and kurtosis measures that is inherent in real-world datasets.

The four-parameter Kappa distribution was identified as the best-fit regional probability distribution for all storm types for the Colorado-New Mexico project area where the distribution parameters ( $\xi$ ,  $\alpha$ ,  $\kappa$ , and  $h$ ; Equation 7) are estimated by the Method of L-Moments [Hosking and Wallis (1997)]. Hondo is the second shape parameter for the 4-parameter Kappa distribution and is useful in that it describes the position of the Kappa distribution on the L-Moment Ratio Diagram relative to the Generalized Extreme Value (GEV, Hondo=0) and Generalized Pareto (GP, Hondo=1) distributions. The four distribution parameters for the Kappa distribution, including Hondo, are solved for using the method of L-Moments [Hosking and Wallis (1997)]. Hondo is often a fixed value for a given Macro Region and storm type. However, the Hondo value was not fixed but varied with L-Skewness in the arid and semi-arid West Macro Region for the LS and MEC storm types. Hondo values were obtained for the West Macro Region using homogeneous sub-regions based on L-Skewness and

L-Kurtosis pairings. Gridded datasets for Hondo were prepared for all storm types based on the findings for the regional probability distribution.

#### 4.4.5 Equivalent Independent Record Length (EIRL)

Equivalent Independent Record Length (EIRL) is a measure of the independent information contained in a regional dataset. EIRL is a function of the size of the project area, the typical areal coverage of storms, and the density of precipitation measurement stations. EIRL is expressed in years of record which can be compared to the total station-years of record for the regional dataset.

If the storms of interest have large areal coverage relative to the density of the station network, then the EIRL will be a small fraction of the station-years of record. This occurs because the large areal coverage of the storm produces annual maxima at many stations and results in greater correlation (statistical dependence) amongst the gauge records. This is the typical situation for synoptic scale MLC and TSR storm types. Conversely, if the areal coverage of storms is small and the density of the station network is low, then the EIRL will be a large fraction of the station-years of record. The latter case is the situation for MEC and LS storm types where these storms produce only one or a few annual maxima in a low-density station network and thus the cross-correlation between precipitation annual maxima at stations is low.

EIRL analyses were conducted for each storm type to provide a measure of the effective record length of the statistical information for the storms contained in the regional datasets. The analysis was conducted by counting of independent storm dates for all storm events of a given type. A buffer of 2 dry days between storm events was used for the synoptic scale MLC and TSR storm types.

For the case of LS and MEC storm types, it is common for independent outbreaks of convective activity to occur on the same day. Independent events for these storm types were defined as annual maxima separated by sufficient distance to be considered separate realizations of convective activity. Storm events within a 2° by 2° zone (Figure 15) were considered the same storm event and/or convective system. Storms in adjacent 2° by 2° storm typing grid-cells are separated, on-average, by over 150-km which is generally sufficient for consideration as physically separate events. The use of counting by grid-cell provided a simple and practical approach for obtaining a measure of EIRL.

The EIRL information is used as a demonstration of the trading space-for-time concepts in the regional approach. The practical application is for characterizing uncertainties in L-moment statistics in uncertainty analyses for point precipitation and watershed precipitation. Representative uncertainty bounds for watershed PF curves for each Macro Region (East, West, Rio Grande) are provided for each storm type in later sections of this report.

#### 4.4.6 Spatial Mapping of Point Precipitation-Frequency Estimates

The gridded datasets for the L-moment statistics (Section 4.4.3) were then used to solve for the distribution parameters for the four-parameter Kappa distribution on a grid-cell by grid-cell basis. This allowed spatial mapping of precipitation-frequency estimates for selected AEPs for each storm type for the key durations of 2-hour (LS), 6-hour (MEC), and 48-hour (MLC/TSR).

Twenty-four-hour and 72-hour gridded datasets were also developed to provide reference estimates of the AEP of 24-hour and 72-hour PMP developed in Volume 2, but are not intended for use in design. Precipitation annual maxima datasets for the 24-hour and 72-hour durations for MLCs/TSRs were assembled at a group of high-quality index stations with record lengths near 100-years. These data were used to develop scaling factors for the at-site means comparing 24-hour and 72-hour, each, to 48-hour at-site means for each Macro Region. The PF estimates for 24-hour and 72-hour MLC/TSR data were then mapped using the scaled at-site mean grids with the 48-hour gridded datasets for L-moment statistics as described above.

#### 4.4.7 Uncertainties in Point Precipitation-Frequency Estimates

Uncertainty bounds for point precipitation-frequency estimates were obtained as part of the Stochastic Storm Transposition (SST) simulations [Schaefer 2015; Appendix D] for developing watershed precipitation-frequency relationships for selected watersheds in the three Macro Regions. It should be noted that uncertainties in point precipitation-frequency estimation are the dominant contributors to the total uncertainty for a watershed precipitation-frequency relationship.

The uncertainty analyses for watershed precipitation-frequency required characterizing uncertainties for all contributing factors to the total uncertainty in the watershed PF relationship. This included developing probability distributions or resampling schemes for characterizing uncertainty in the regional L-Moment statistics, the regional probability distribution, and the spatial patterns used in the SST simulations. Table 9 lists an example of the magnitudes of uncertainties and probability distributions in analyzing uncertainties for point precipitation-frequency for a site in the East Macro Region for the MLC storm type as part of the SST simulations.

Dimensionless uncertainty bounds that are applicable to point precipitation-frequency for each storm type and Macro Region were produced as part of the development of the scaling procedure for watershed PF relationships (Sections 4.5 and 4.6). Dimensionless uncertainty bounds are depicted in Section 5.

*Table 9. Uncertainty Characteristics for Point Precipitation-Frequency Estimates for a site in the East Macro Region for the MLC storm type*

Component	Probability Model	Mean	Standard Deviation		
At-Site Mean	Normal	1.360 in	0.069 in		
L-Cv	Normal	0.2010	0.0042		
L-Skewness	Normal	0.2145	0.0070		
Component	Probability Model			Residuals	
L-Kurtosis	L-Kurtosis functionally related to L-Skewness for regional Kappa Distribution			Model	Standard Deviation
				Normal	0.0055

### 4.5. Watershed Precipitation Frequency Relationships

The approach to develop Watershed Precipitation-Frequency relationships is briefly described here and more fully described in Appendix D (Schaefer 2015). Stochastic Storm Transposition (SST) methods were used in combination with point precipitation-frequency information and

spatial patterns from historical storms to develop watershed precipitation-frequency relationships for geographically-fixed areas (i.e., watersheds) for synoptic-scale, mesoscale, and local storms.

The SST method simulates the natural meteorological processes where many storm events occur in a given year to produce precipitation at a given location in the project area. The location where heavy precipitation occurs from a storm event is random relative to the location of the precipitation stations in a network of stations. The precipitation annual maxima at a given station can be produced by a wide range of situations based on the storm magnitude, the nearness of the storm/storm center to the station and the spatial pattern of precipitation. This would include situations such as annual maxima being produced by a small event occurring nearby, or a larger event occurring more distant from the station.

This spatially-random storm behavior is simulated using precipitation fields (raster fields) obtained from spatial analyses of historical storms where the precipitation fields are used for describing the spatial distribution of precipitation within and near the watershed of interest. Figure 39 depicts a precipitation field with a complex pattern of convective storm activity with separate storm centers. The rectangular area encompassing a specific storm center (Figure 39) has been given the name *storm center zone*. Separate storm center zones are spatially distinct and likely have timing differences for the precipitation maxima at the key duration as well.

Watersheds were selected to include a variety of sizes and shapes for each of the three Macro Regions (East, West and Rio Grande). Ten watershed shapes were used in the PF-ARF analysis ranging from point to 8, 13, 18, 40, 77, 85, 139, 318, 459, and 1,017 square miles. A virtual key station is positioned at the watershed centroid and is used for random placement of the watershed relative to a precipitation field. The watershed centroid is a logical choice for the spatial reference-point because the subject of interest is areal-average precipitation for the watershed, which is best represented by the centrally-located watershed centroid. The virtual key station is used for generating precipitation annual maxima at the watershed centroid and for scaling of the precipitation field as part of the stochastic storm generation process. Stochastically-generated precipitation annual maxima at surrounding substations are later used for verification of the storm generating process. The areal-average watershed precipitation is computed from simple arithmetic accounting of the precipitation at each grid-cell in the watershed raster field.

The procedure for random placement of the storm relative to the watershed is to set limits on the location of the virtual key station relative to the storm center (maximum point precipitation). This is accomplished by setting a lower bound on the ratio of the precipitation at the virtual key station relative to the maximum point precipitation at the storm center.

Since there were an inadequate number of spatial storm patterns available for synoptic scale MLCs in the Rio Grande and West Macro regions, watershed PF-ARFS for these Macro Regions were obtained by utilizing the findings for the East Macro region. The PF-ARF values for the Rio Grande Macro region were adopted as equal to those for the East Macro region based on similarity of the limited PF-ARF data in both Macro Regions and the similarity in moisture availability (summer monsoon season for the Rio Grande, and moisture from Gulf of Mexico for the Eastern Macro Region in the spring and fall). The watershed PF-ARF values for the West macro region were obtained by reducing the PF-ARF values from the East Macro region

by 10 percent (greater spatial attenuation) and generally reduced moisture availability in the West macro region.

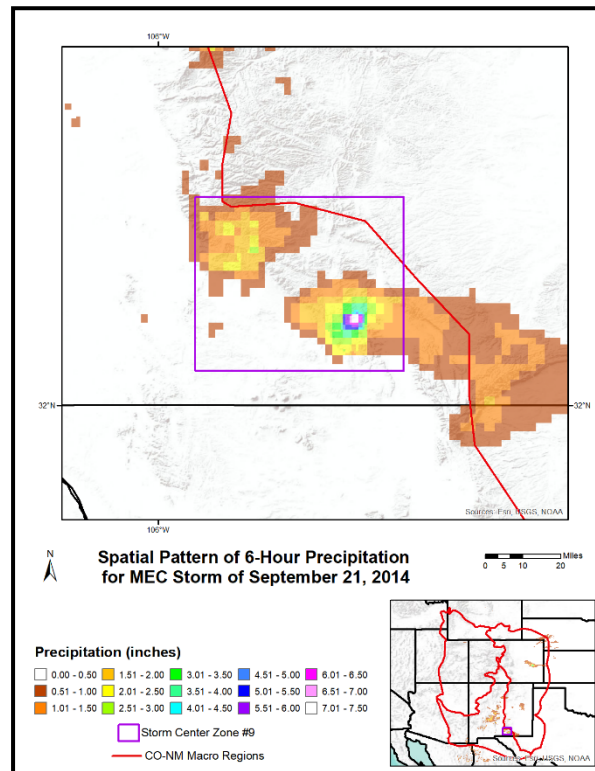


Figure 39. Precipitation field for MEC storm of September 21, 2014 showing separate storm center zones and spatial precipitation patterns for the 6-hour duration

Several probabilistic concepts and Monte Carlo sampling methods as defined in Appendix D were used in the development of a watershed PF relationship and uncertainty bounds using this stochastic storm generation approach. These included:

1. Application of the Total Probability Theorem using precipitation for the key duration at the virtual key station as the independent variable (Benjamin and Cornell 1970; Kuczera 1982; Nathan et al. [2003])
2. Stratified sampling of precipitation annual maxima series data (AMS) from the virtual key station for the key duration
3. Generation of multiple storms per year with precipitation less than the annual maxima at the virtual key station using standard Monte Carlo methods and the point PF relationship from a peaks-over-threshold analysis
4. Latin-hypercube sampling (McKay et al. [1979]) of L-moment parameters for the virtual key station to account for epistemic uncertainties in the estimation of the at-site mean, regional L-Cv, regional L-Skewness and the regional probability distribution
5. Resampling (Efron [1979]) to produce a subset of possible spatial precipitation patterns for storm center zones selected from the full sample of storm center zones
6. Characterization of uncertainties in alternative sampling limits for placement of the virtual key station (watershed) relative to the location of the storm center.

Watershed PF relationships were computed for over 6,000 sample years using plausible scenarios of inputs and probabilistic model parameters with the number of storms simulated

per sample year based on the historical record which typically varied between 1 to 8 storms per sample year.

### 4.5.1 Uncertainties in Watershed Precipitation-Frequency Estimates

Uncertainty analyses were conducted as part of the development of watershed PF relationships for a range of watershed sizes and shapes. This was accomplished by simulation of alternative plausible watershed PF relationships that account for epistemic uncertainties through different scenarios of plausible inputs and probabilistic model parameters. Typically, 200 simulation scenarios were computed to capture the effects of uncertainties which provides for computation of a mean watershed PF relationship and 90 percent uncertainty bounds (Figure 40). An example of uncertainty characterizations for point precipitation were presented previously (Table 9) and an example of uncertainty characterizations for spatial precipitation are listed in Table 10. The uncertainty simulations typically result in stochastic generation of about 6 million separate storms with three storms on-average generated each sample year for watershed and storm type.

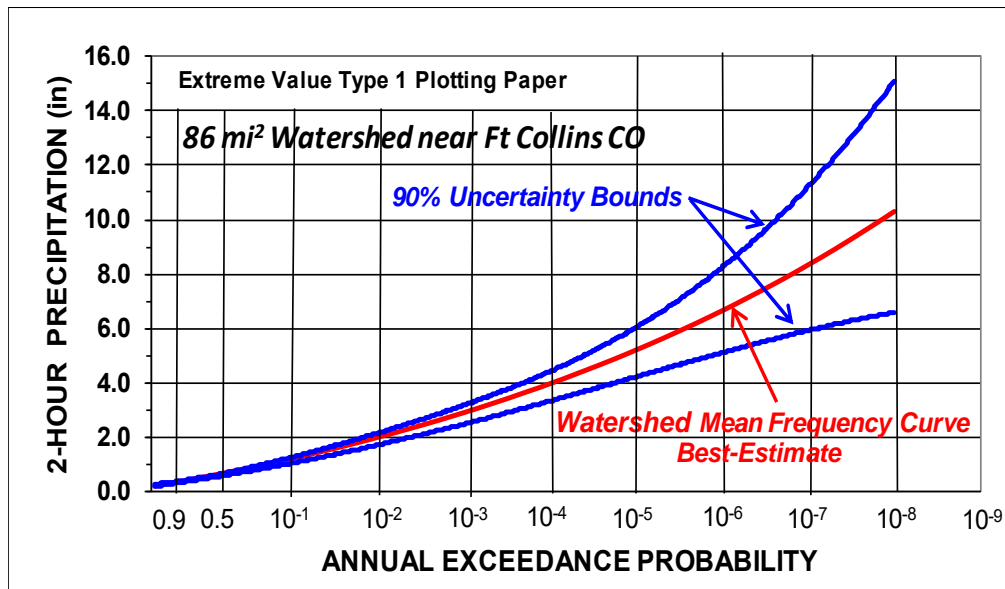


Figure 40. Watershed precipitation-frequency relationship and 90 percent uncertainty bounds for 86-mi<sup>2</sup> watershed near Ft Collins for LS storm type

Table 10. Additional uncertainty characteristics for Watershed Precipitation-Frequency for the LS and MEC storm types

Component	Probability Model	Details
Number of storms per year	Truncated Poisson, minimum of 1 storm per year	Mean of 3 storms/yr
Storm Centering	Uniform Distribution with lower and upper bounds based on storm centering relative to a given location based on historical storm characteristics	Precipitation magnitude for given location (grid-cell) relative to storm center
Storm Spatial Patterns	Resampling from storm spatial patterns	Stratified resampling of spatial patterns rarest storms and storm

		spatial patterns used for estimating extreme precipitation events
--	--	---

As noted in Section 4.4.7, uncertainties in point precipitation-frequency estimation are the dominant contributors to the total uncertainty for a watershed precipitation-frequency relationship. Figure 41 depicts the typical relative contributions to the total uncertainty from the various sources of uncertainty for the MEC storm type for a watershed in the East Macro Region.

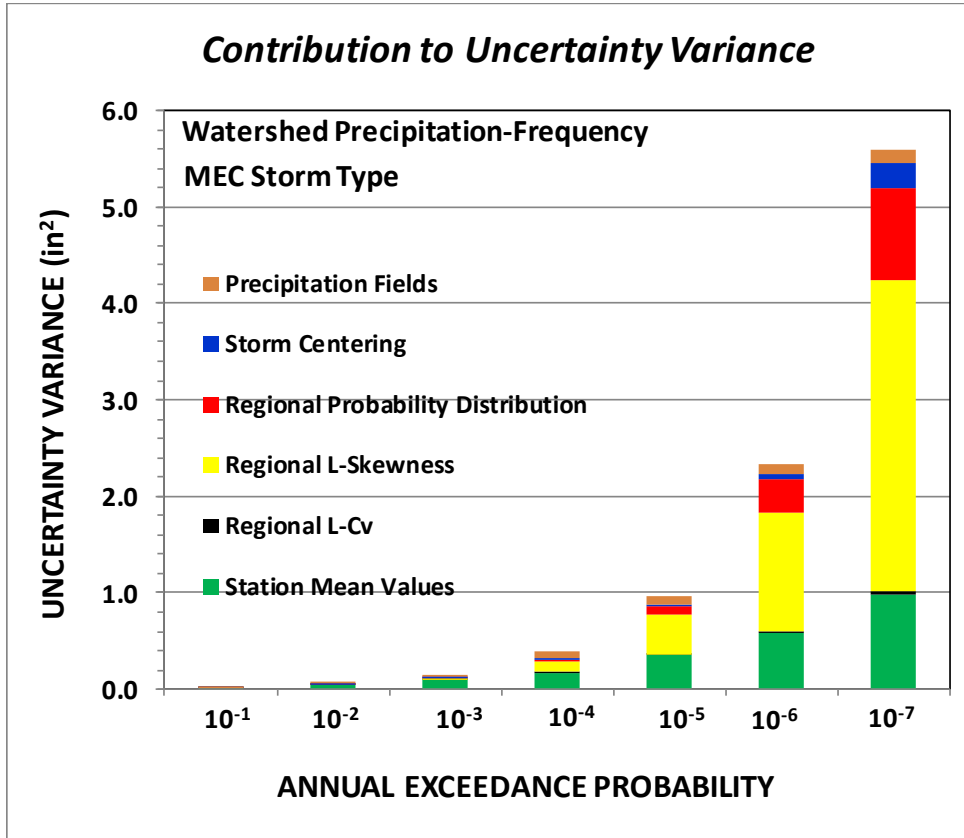


Figure 41. Example of relative contribution to total uncertainty from various sources of uncertainty in developing Watershed Precipitation-Frequency Relationship for the MEC Storm Type in the East Macro Region

### 4.6. Development of Watershed PF Relationships via a Scaling Procedure

Watershed PF relationships and uncertainty bounds are needed for application on selected watersheds throughout Colorado and New Mexico. This is accomplished by utilizing the findings for selected watersheds (Section 4.5) for a range of watershed sizes to develop Precipitation-Frequency Areal-Reduction Factors (PF-ARFs) for each storm type and Macro Region. A watershed PF curve was computed in the conventional manner as the product of the PF-ARF value for a given watershed size and the point-PF values for a centrally-located site (centroid) within the watershed of interest. Figure 42 depicts an example of the

precipitation-frequency areal-reduction factors (PF-ARFs) used to compute watershed precipitation-frequency based on point-precipitation-frequency values for the watershed centroid. Watershed PF-ARF curves will be presented later in this report for each of the Macro Regions.

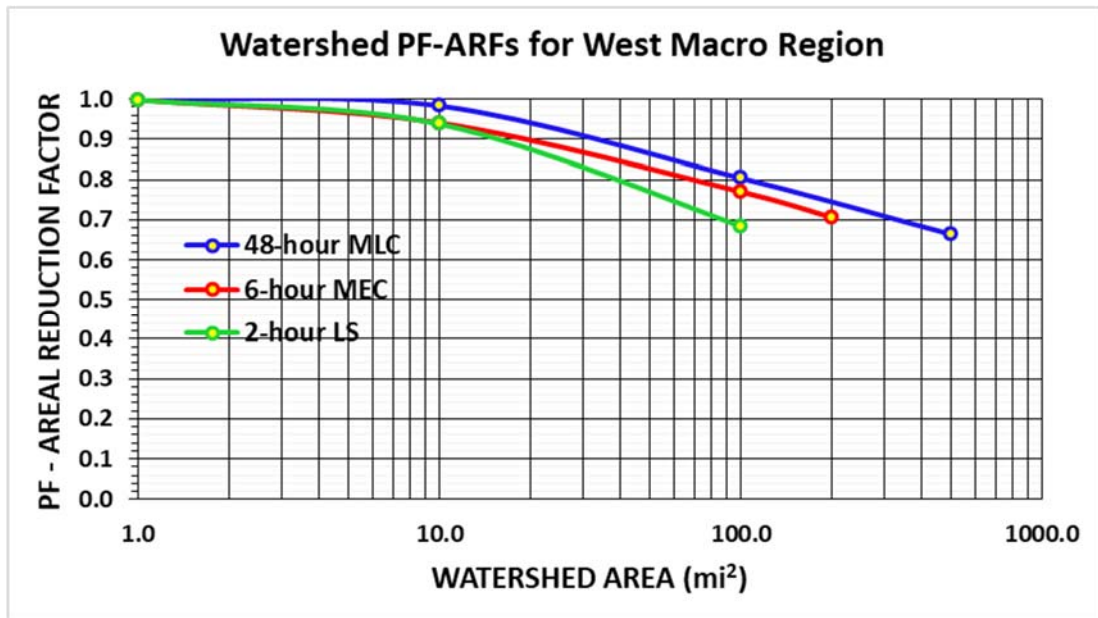


Figure 42. Example of Watershed Precipitation-Frequency Areal Reduction Factors for the three storm types for the West Macro Region

## 4.7. Spatial and Temporal Distributions for Each Storm Type

Scalable temporal and spatial storm templates are needed in conjunction with watershed precipitation-frequency (PF) relationships to conduct watershed modeling of floods for assessing spillway adequacy at existing dams and for sizing spillways at proposed dams. Scalable temporal patterns are provided for each of the three Macro Regions (East, West, and Rio Grande) and each of the three storm types for scaling at the key durations of 2-hours (LS), 6-hours (MEC), and 48-hours (MLC). The key durations were chosen at the beginning of this project as representative of the storm duration during which the majority of precipitation occurs for a given storm type. The storm temporal templates are presented as dimensionless temporal mass-curves (hyetographs) using the precipitation at the key duration as the indexing value and where the total duration of precipitation may differ from the key duration. This approach was taken to both preserve the PF relationship at the key duration and to allow the total storm duration to reflect historical storm behavior.

Storm spatial patterns can be obtained based on scaling of the monthly mean precipitation grids from the 1981-2010 PRISM data. Lastly, for cool season MLC events, climatologies of 1000-mb temperature and freezing level heights were developed from Reanalysis Data.

### 4.7.1 Temporal Precipitation

Two types of temporal scalable storms are provided for each storm type and Macro Region: a suite of scalable historical storms, comprising a representative sample of the characteristics of historical storms; and a synthetic storm assembled from storm characteristics that are

typically observed for the given storm type. Unlike the “critically stacked method” or other fully fabricated temporal patterns, the synthetic patterns in this study are based on statistics of temporal characteristics from actual storms. The suite of historical storms is intended for use by consultants and dam safety staff for detailed flood analyses where greater scrutiny of spillway adequacy is warranted. The synthetic temporal patterns contain depth-duration values and temporal patterns typically observed in historical storms and are anticipated to be used by the Dam Safety Program engineers for developing unbiased estimates of spillway performance. Dam Safety programs can adopt one or more representative historical patterns in a given macro region to augment the synthetic pattern(s). This decision could be made after hydrologic pilot tests are conducted to examine typical flood responses for the various synthetic and historical temporal patterns.

The suite of historical storm templates (Appendix E) was assembled directly from storms with large magnitudes of precipitation for a given storm type that occurred within each of the three Macro Regions. The synthetic storm patterns were assembled using procedures developed by the Washington State Dam Safety Program (Schaefer 1989) for probabilistic analyses of important temporal characteristics. This included characteristics such as: elapsed time to peak intensity; magnitude of peak intensity; arrangement of high intensity increments near the peak intensity; depth-duration statistics for inter-duration incremental precipitation amounts; intermittent or non-intermittent patterns (i.e., the macro shape of storm temporal pattern). Specifically, mean values for each of these characteristics were computed from a sample set of historical storms and incorporated into the synthetic temporal patterns in a manner representative of typical storm behavior. These two types of scalable storm templates provide for both a practical and flexible approach to conducting flood modeling in administration of the Dam Safety Programs.

Precipitation time-series data were collected for the largest magnitude storms in each Macro Region. A time-step of 5-minutes was used for the LS storm type, 15-minutes for the MEC storm type, and 1-hour for the MLC-TSR storm type. A simple type of clustering analysis was used to group macro temporal patterns for hyetograph shapes. When there was a dominant single macro temporal pattern, as was common for the LS storm type, then a single synthetic pattern using the depth-duration, timing and sequencing statistics was created. For each storm, several storm characteristics were measured that are important for watershed modeling of floods using procedures described in Schaefer (1989). The storm temporal characteristics included:

- Elapsed time from start of precipitation to occurrence of peak intensity
- Total duration of precipitation
- Sequencing of three highest precipitation increments that contain peak intensity
- Sequencing of three major segments of precipitation including segment that contains peak intensity
- Depth-duration statistics are computed for precipitation maxima for selected inter-durations and durations greater than the key duration. Precipitation maxima for selected inter-durations are indexed by the maximum precipitation for the key duration. For the Local Storm Type, for example, inter-durations would include 5, 10, 15, 20, 30, 45, 60, 75 and 90-minutes for the 2-hour key duration, plus depth-duration statistics for durations greater than the key duration.
- Tercile of the key duration that has the maximum precipitation total. This helps define front-loaded, middle-loaded and back-load temporal patterns and the fraction of intermittent and continuous patterns.

Mean values were computed for each of the storm characteristics and used to assemble a synthetic storm temporal pattern for each storm type in each of the three Macro Regions. These synthetic temporal patterns are considered the typical manner in which storms occur and should be useful in watershed modeling of floods for approximating best-estimate (unbiased) flood-frequency relationships.

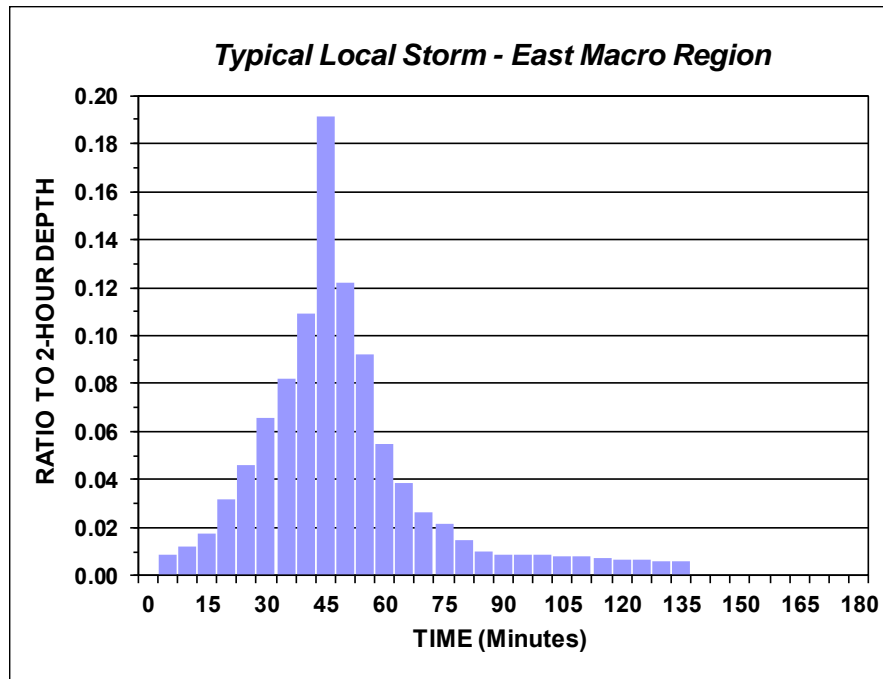


Figure 43. Example of synthetic temporal pattern for Local Storm type for East Macro Region

Convective events (LS and MEC) tend to be single pulse events with similar behavior in temporal patterns where the majority of precipitation is concentrated around a major burst. For these events, front-loaded versus back-loaded is not as significant because the majority of precipitation is concentrated around the major burst. So small amounts of precipitation may precede or follow the major burst. In contrast, MLC events have a diversity of temporal patterns including single and multiple pulse events where front-loaded versus back-loaded can be important for hydrologic modeling and reservoir response.

When there were two prevalent macro temporal patterns, two synthetic patterns were provided based on the depth-duration, timing and sequencing statistics for those groupings of macro temporal patterns. In the case of the MLC storm type, there were an insufficient number of noteworthy historical storms in the West and Rio Grande (West 9, Rio 13, East 21) to provide a good sample size for each of the macro patterns identified from clustering. The available data suggested similarity in patterns between macro regions which is consistent with the idea of similarity in synoptic forcing for the MLC events. It was considered prudent to provide some diversity in temporal patterns for the West and Rio Grande by adopting the temporal patterns from the East macro region.

#### 4.7.2 Spatial Precipitation

The vast majority of dams regulated by the Colorado and New Mexico Dam Safety Programs are on small watersheds, less than 20 square miles. A uniform spatial pattern of precipitation is often adequate on very small watersheds. There are several options available for those cases where a spatial pattern is desired. For the case of the MLC storm type over larger watersheds, the spatial pattern of the PRISM gridded data set for the month of storm occurrence normalized by the watershed mean may be used for distributing the areal average precipitation (Figure 44 - top). Each grid cell within the watershed would then be multiplied by the magnitude of precipitation for a selected AEP (i.e., scaled to the selected AEP) (Figure 44 - bottom). Representative storm spatial patterns are based on the monthly mean precipitation grids from the 1981-2010 PRISM data.

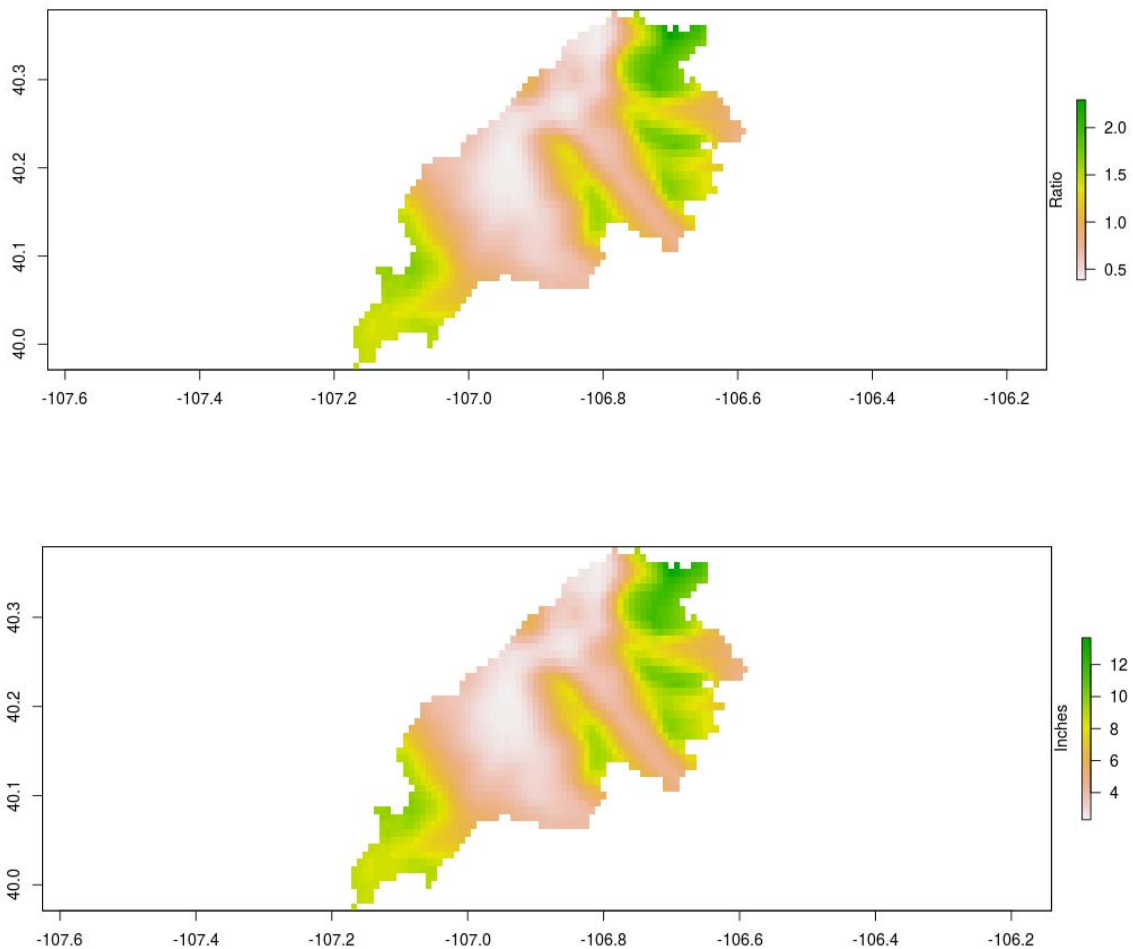


Figure 44. The ratio of the PRISM precipitation relative to the watershed mean clipped to the watershed (top) and precipitation amounts scaled to a selected AEP (bottom)

### 4.7.3 Temperature Time Series

Freezing levels and 1000-mb temperatures are used to identify phase changes from liquid to solid precipitation. Representative time series of freezing levels and 1000-mb temperatures for selected storms (from the list in Section 4.7.1) were developed from the 20<sup>th</sup> Century

Reanalysis Dataset to produce representative patterns of freezing level heights and 1000-mb time series for MLCs for each region (e.g., Figure 45 shows the plots for the Rio Grande Macro Region). No freezing level patterns were developed for MEC and LS events due to their warm season nature.

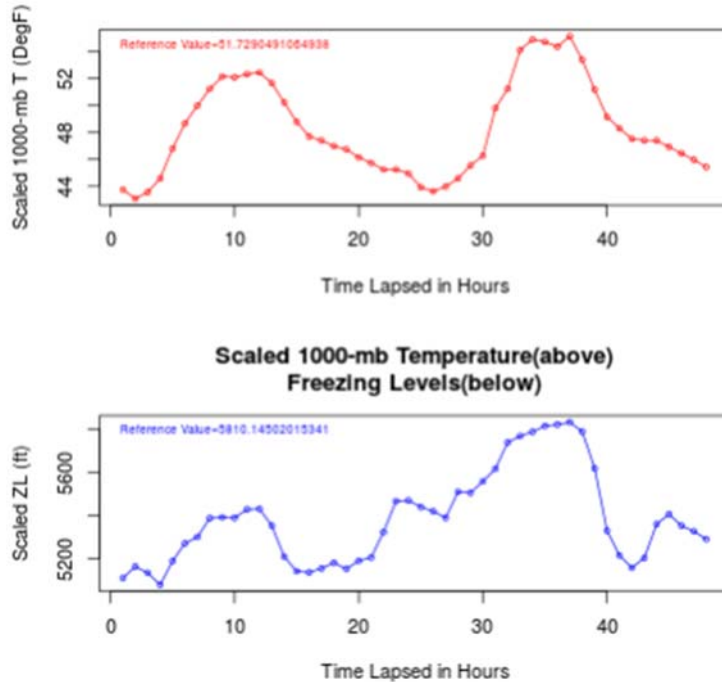


Figure 45. Example time series of freezing-level height (ZL) and 1000-mb temperatures (1000T) for the Rio Grande Macro Region

For both freezing-level heights and 1000-mb temperatures, a climatology for each month that provides the 5<sup>th</sup>, 10<sup>th</sup>, 25<sup>th</sup>, 50<sup>th</sup>, 75<sup>th</sup>, 90<sup>th</sup>, and 95<sup>th</sup> percentile values of each variable were produced from reanalysis data sets (Section 3.6). The climatological values for a selected month and percentile value serve as the index values to scale the freezing-level heights and 1000-mb temperature patterns for hydrologic modeling. Information on combining the index value with the reference value and dimensionless time series to generate lapse rates and, hence, the elevation level of rain-snow transition is available in the User Guide for the CO-NM MetPortal. Output from MetPortal provides an indication of rain or snow depending on the user-input elevation for each time step.

## 4.8. Storm Seasonality

The storm seasonality of interest for watershed flood modeling is the seasonality when the rarest (largest) storm events of a given storm type have occurred in the historical record. An initial perspective on the seasonality of the three storm types was previously obtained by using the DDST to develop a frequency histogram of days when the various storm types occurred (Figure 18). However, those histograms include many days with small precipitation totals which are smaller than the precipitation annual maxima. Therefore, those histograms are representative of the full range of precipitation rather than seasonality of the rarest storm events.

The seasonality analysis for the LS, MEC and MLC-TSR storm types was conducted using precipitation annual maxima for the key durations for the rarest storm events of a given storm type. An initial examination of storm seasonality for the rarest events showed significant variation in seasonality from north to south in both the East and West Macro Regions. The East and West Macro regions were therefore sub-divided into north and south areas to better describe the spatial variation of storm seasonality. This resulted in five Seasonality Sub-areas (Figure 46). A dataset of about 50 of the rarest storms was assembled for each storm type for the five sub-areas where storm rarity was measured by the ratio of the precipitation magnitude to the median value of annual maxima precipitation for the key-duration at each station. All storms used in the seasonality analysis had a ratio to median value exceeding 2.4, exceeding about a 1:50 AEP. The histograms developed for each of the five Seasonality Sub-areas are shown in the Results sections for each storm type.

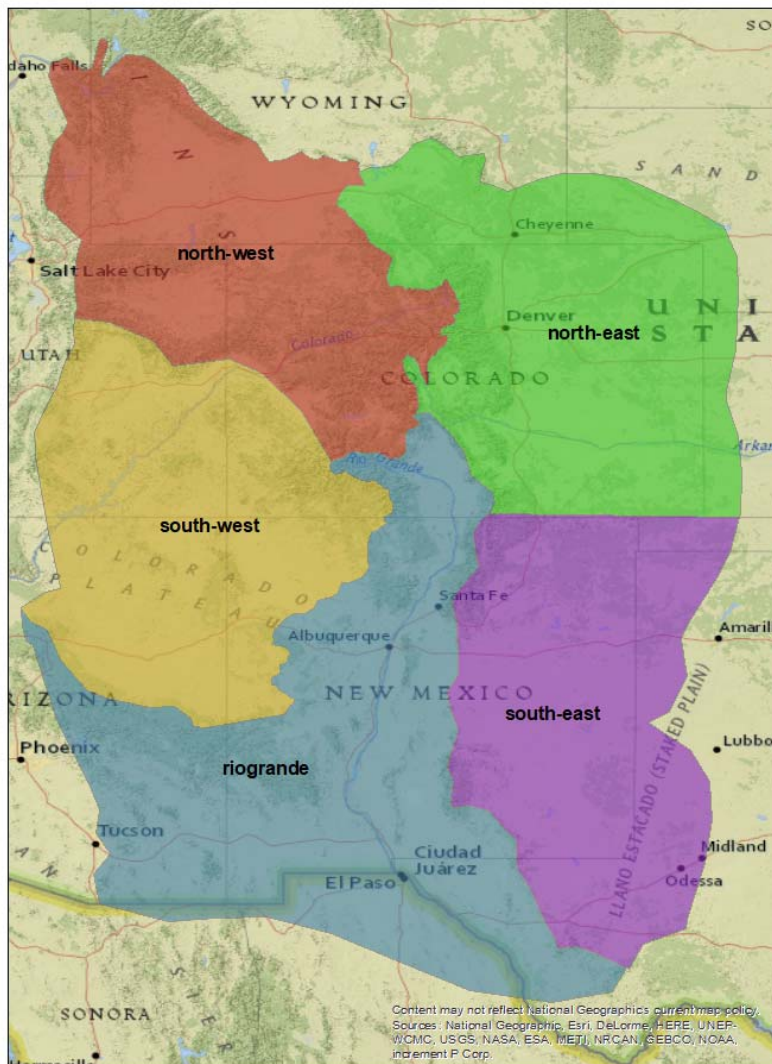


Figure 46. Seasonality Sub-areas used to provide seasonal information for extreme storms of each Storm Type

## 5. Results

The following sections provide findings for each storm type including spatially-mapped L-moment statistics; sample maps of point precipitation frequency estimates for selected AEPs ranging from  $10^{-1}$  to  $10^{-7}$ ; and seasonality histograms. Results for each storm type show distinctive differences with regard to magnitude and spatial patterns.

### 5.1. Point Precipitation-Frequency

#### 5.1.1 48-Hour Mid-Latitude Cyclones

Daily and hourly stations were used in the regional analyses for 48-hour precipitation annual maxima for MLCs where stations with 20 years or more of record were included in the analyses (Figure 47). Table 11 provides a listing of the number of stations and total number of data years used in the analysis of MLCs; and Figure 48 depicts a histogram of the number of data years. Hourly stations were selectively included in areas not already populated by daily stations.

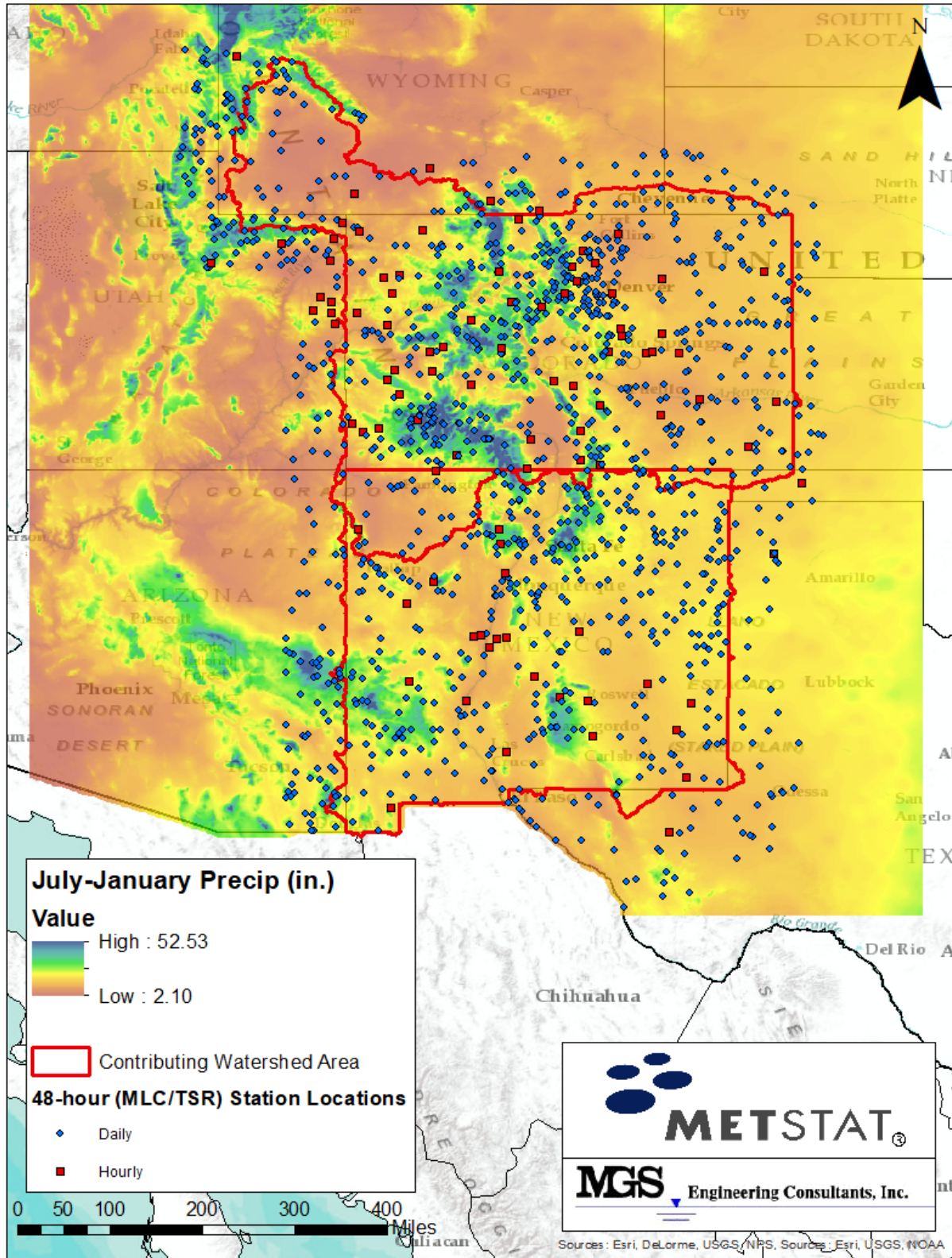


Figure 47. Location of daily and hourly precipitation stations used in the precipitation-frequency analysis for MLCs and the seasonal mean precipitation used in the predictor equations for the West Macro Region

Table 11. Number of Stations and data years for stations with 20 or more data years used in the precipitation-frequency analysis for MLCs

PRECIPITATION GAUGE TYPE	NUMBER OF STATIONS/GAUGES	TOTAL STATION DATA YEARS	AVERAGE STATION-YEARS
Daily Stations	1,052	60,019	57
Hourly Stations	91	3,373	37
TOTAL	1,143	63,392	55

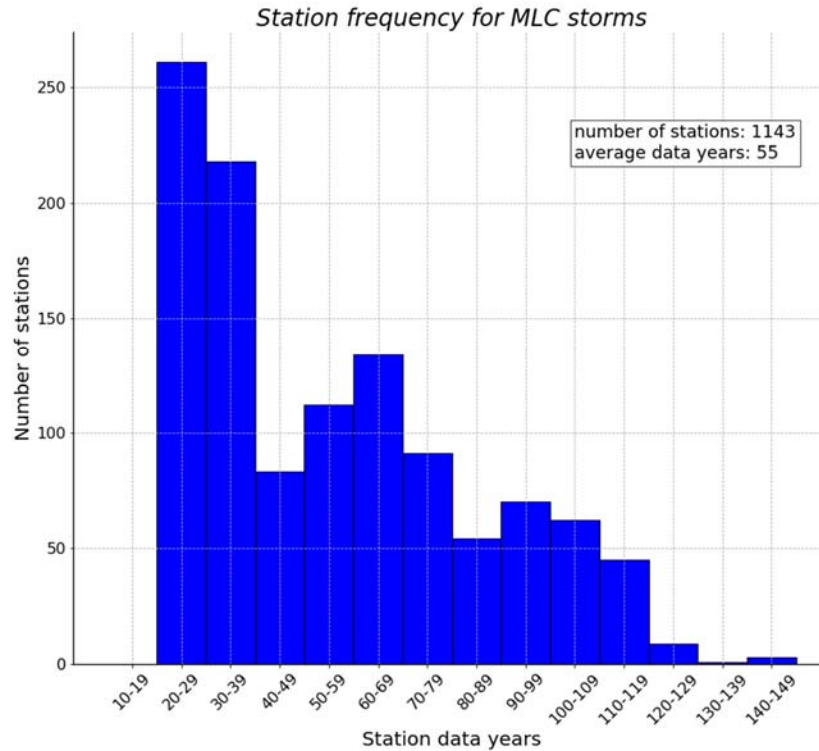


Figure 48. Histogram of data years for stations used in the precipitation-frequency analysis for MLCs

5.1.1.1. At-Site Means - MLC

Spatial mapping of 48-hour at-site means for MLCs was conducted using DEM elevation and gridded values of mean monthly precipitation (Daly 1994) as explanatory variables. PRISM mean monthly precipitation (1981 through 2010) for April through October was used for the East and Rio Grande Macro Regions and PRISM mean monthly precipitation for July through January was used for the West Macro Region. These choices were made after reviewing the behavior of the relationship of at-site means with mean monthly precipitation in different groupings of Heterogeneous Super Regions (Figure 49) for the months when MLCs were most common.

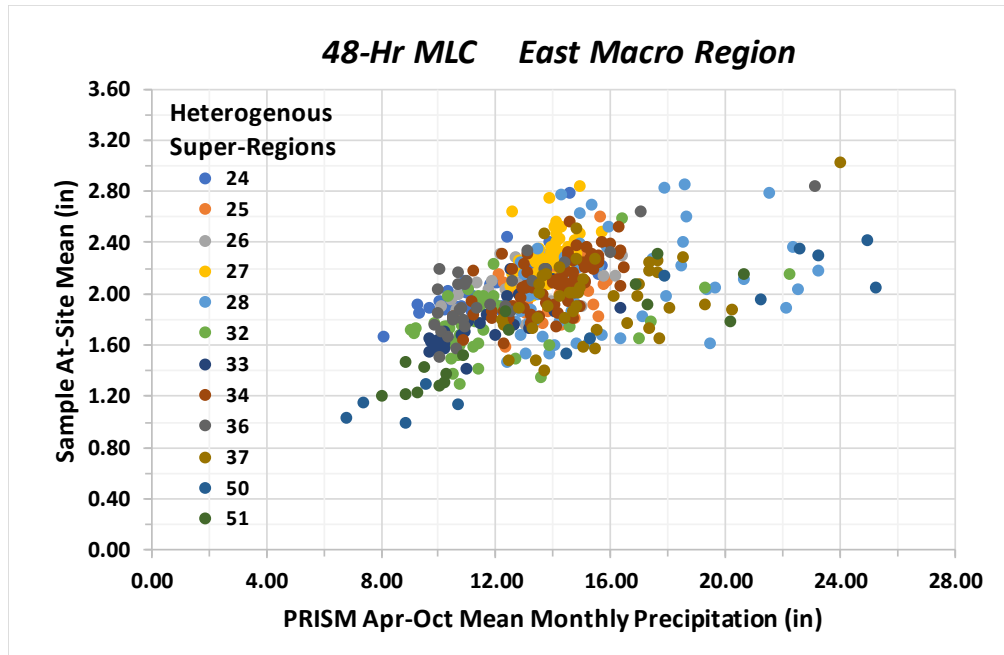


Figure 49. Scatterplot of station sample values of 48-Hour at-site means for MLCs against seasonal mean precipitation for East Macro Region

Collections of stations from adjacent Super Regions were grouped where they exhibited similar behavior. Generalized additive modeling methods were used for the sample at-site means for the collections of stations, which resulted in a variety of mathematical relationships with the explanatory variables. The predictor variables for each mapping area are shown in Table 12 along with the resultant relative root-mean-square-error (RMSE). Best estimates of the at-site means were computed as a weighted-average of the station-sample values and regression-predicted values, as discussed in Section 4.4.3. Figure 50 depicts an example of comparisons of station sample values and mapped values of the 48-hour at-site means. The observed station at-site mean values that are most distant from the red line of equality are mostly associated with stations with short record lengths (generally less than 20-years). Overall, the mapped values of the 48-hour at-site means are nearly unbiased and have a relative RMSE of 7.8 percent which drops to a relative RMSE of 6.6 percent for stations with more than 25-years of record. The spatial map of 48-hour at-site means for MLCs is shown in Figure 51.

*Table 12. Listing of explanatory variables for 48-Hour at-site means for MLCs and Relative RMSE for predictive equations*

Mapping Area	Explanatory Variables	Relative RMSE
A	Apr-Oct Mean Monthly Precipitation; Elevation	9.2%
B	Apr-Oct Mean Monthly Precipitation; Elevation	10.6%
C	Apr-Oct Mean Monthly Precipitation; Elevation	10.9%
D	Apr-Oct Mean Monthly Precipitation; Elevation	7.9%
E	Apr-Oct Mean Monthly Precipitation; Elevation	7.5%
P	Jul-Jan Mean Monthly Precipitation	11.2%
Q	Jul-Jan Mean Monthly Precipitation	10.1%
R	Jul-Jan Mean Monthly Precipitation	11.4%
S	Jul-Jan Mean Monthly Precipitation	8.2%
T	Jul-Jan Mean Monthly Precipitation	9.9%

CO-NM Regional Extreme Precipitation Study

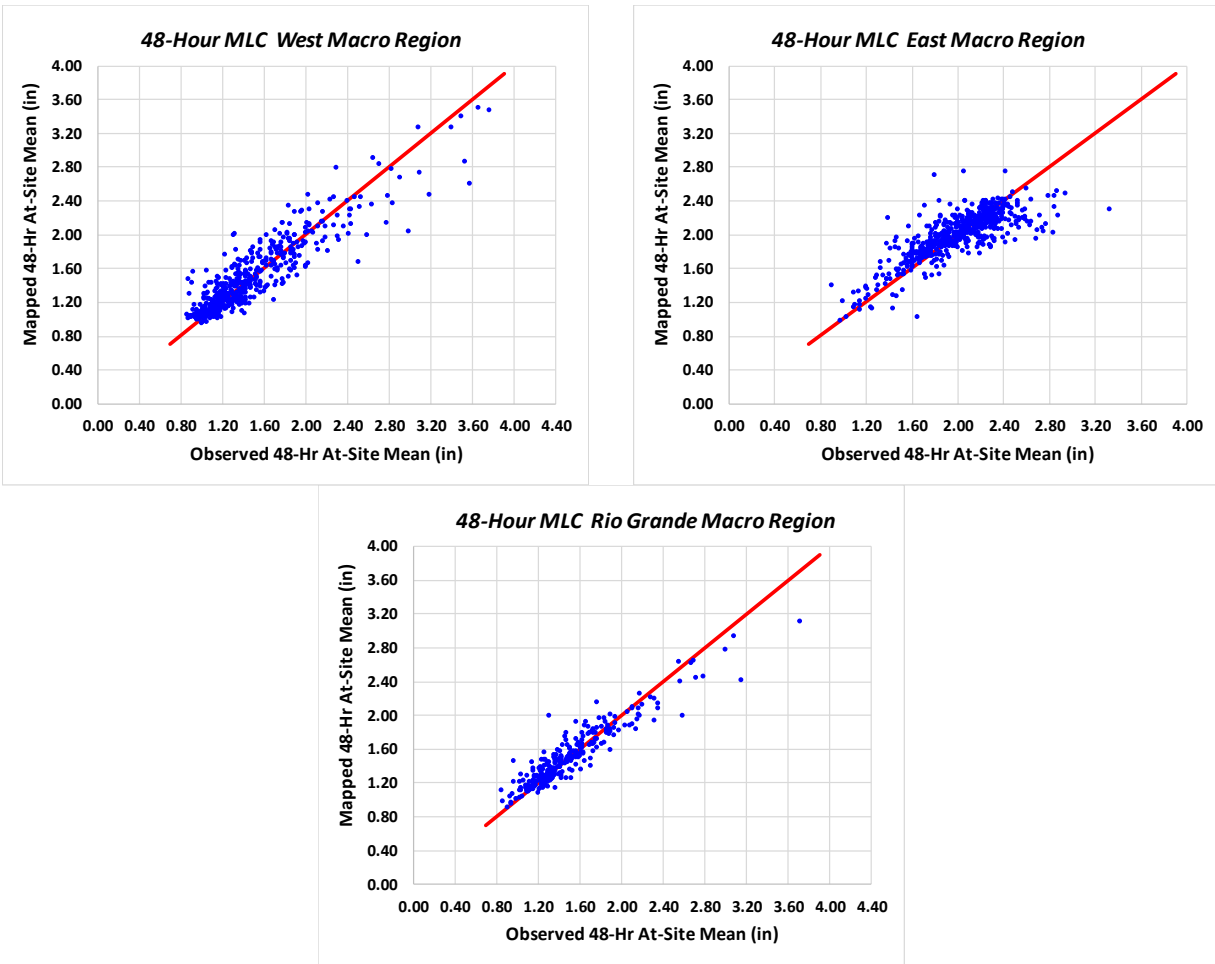


Figure 50. Comparison of observed and mapped 48-Hour at-site means for MLC storm type for three Macro Regions

CO-NM Regional Extreme Precipitation Study

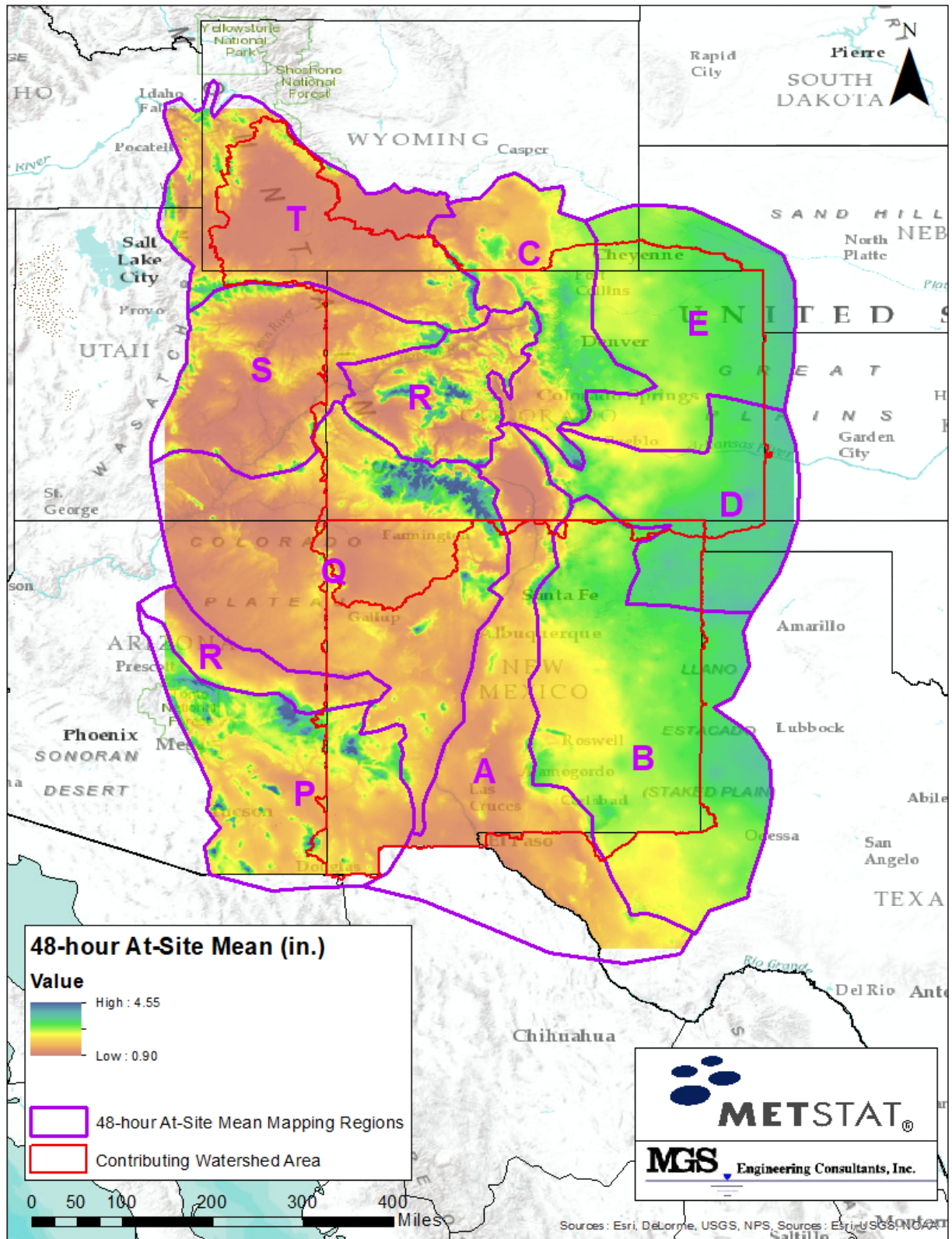


Figure 51. Map of at-site means for 48-Hour duration for MLCs

### 5.1.1.2. Regional L-Cv and L-Skewness - MLC

Homogeneous sub-regions were formed as groupings of stations within a limited range of latitude and elevation for each Super Region. Stations were included that had a record length of 20 years or more. There were 192 sub-regions formed in this manner, where each sub-region produced a regional L-Cv and L-Skewness value associated with a group-average latitude and group-average elevation weighted by station record length. Of the 192 sub-regions, 136 were found to be acceptably homogeneous based on L-moment heterogeneity test measures H1 and H2. The majority of sub-regions that exceeded the H1 and H2 thresholds were moderately heterogeneous with H1 and H2 values below 3.0. A modest amount of heterogeneity was not unexpected given the topographic and climatic complexity of the Colorado and New Mexico project area. The collection of 192 sub-regions was judged more than adequate for spatial mapping of regional L-Cv and L-Skewness.

A review of the regional L-Cv values showed a systematic variation with elevation and latitude (Figure 52). The regional values of L-Cv were used in multiple regression analyses for each mapping area with elevation and latitude as explanatory variables. Table 13 lists the number of homogeneous sub-regions used to form the multiple regressions for regional L-Cv for each designated mapping area, and Figure 53 depicts a comparison of observed and mapped values of regional L-Cv for 48-hour precipitation annual maxima, where the RMSE for prediction of regional L-Cv was 4.9 percent (Table 15). The spatial mapping of regional L-Cv for the 48-hour duration is shown in Figure 54, where regional L-Cv is seen to vary over a relatively narrow range.

*Table 13. Listing of number of homogeneous sub-regions for each mapping area for 48-hour L-Cv for MLCs and RMSE for regional prediction equations*

Mapping Area	Number of Homogeneous Sub-Regions	Relative RMSE
A	20	5.1%
B	28	5.1%
C	22	3.8%
D + E	34	5.0%
P	14	2.9%
Q1 + R2	18	5.1%
Q2	12	4.3%
R1 + S + T1	35	4.8%
T2	9	2.9%

Development of a predictor equation for L-Skewness is more difficult than for L-Cv because of the naturally high sampling variability for skewness measures. The prediction of regional L-Skewness was accomplished using linear regression with regional L-Cv for the 192 homogeneous sub-regions as the explanatory variable. The homogeneous sub-regions were grouped into three mapping areas (the three Macro Regions) as described in Table 14 and Figure 7. Table 24 lists the summary statistics for mapping of regional L-Skewness, where the RMSE is 9.8 percent. Figure 55 shows the spatial mapping of regional L-Skewness, which is seen to have moderate variation across the project area but increased variation in the Rio Grande Macro Region.

*Table 14. Listing of number of homogeneous sub-regions for each mapping area for 48-hour L-Skewness for MLCs and RMSE for regional prediction equations*

CO-NM Regional Extreme Precipitation Study

Mapping Area	Description of Macro Region	Number of Homogeneous Sub-Regions	Relative RMSE
B, C, D, E = East	East of Continental Divide and Sangre De Cristo Mountains	84	11.2%
A, P, Q2 = Rio Grande	Rio Grande Drainage and Southwestern Mountains in New Mexico west of Continental Divide	46	11.5%
Q1, R1, R2, S, T1, T2 = West	West of Continental Divide and North of Southwestern Mountains in New Mexico	62	11.1%

Table 15. Summary statistics for spatial mapping of 48-hour duration regional L-Cv and L-Skewness for MLCs within contributing watershed area

L-MOMENT RATIO	RANGE OF MAPPED L-MOMENT RATIO	STANDARD DEVIATION RESIDUALS	RELATIVE RMSE
Regional L-Cv	$0.1588 \leq L-Cv \leq 0.3153$	0.0062	4.9%
Regional L-Skewness	$0.1622 \leq L-Skewness \leq 0.2728$	0.0184	9.8%

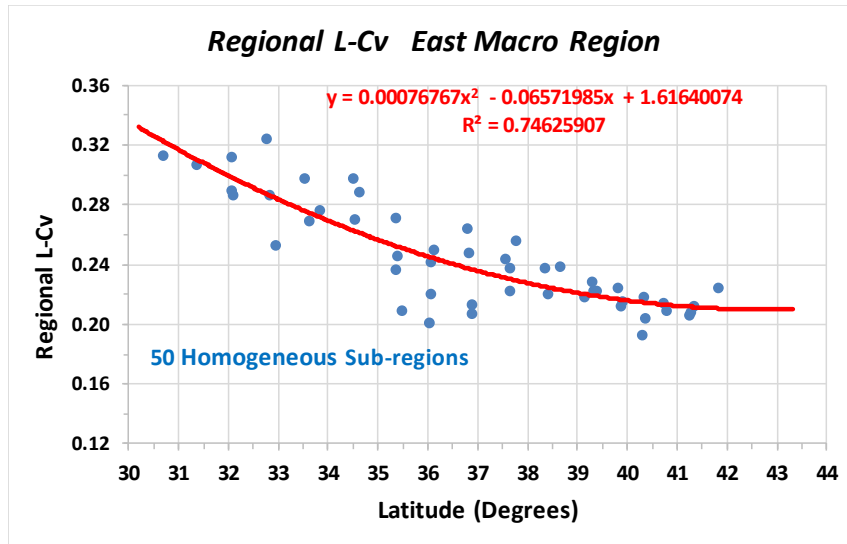


Figure 52. Example of variation of regional L-Cv with latitude for 48-hour MLCs in the East Macro Region

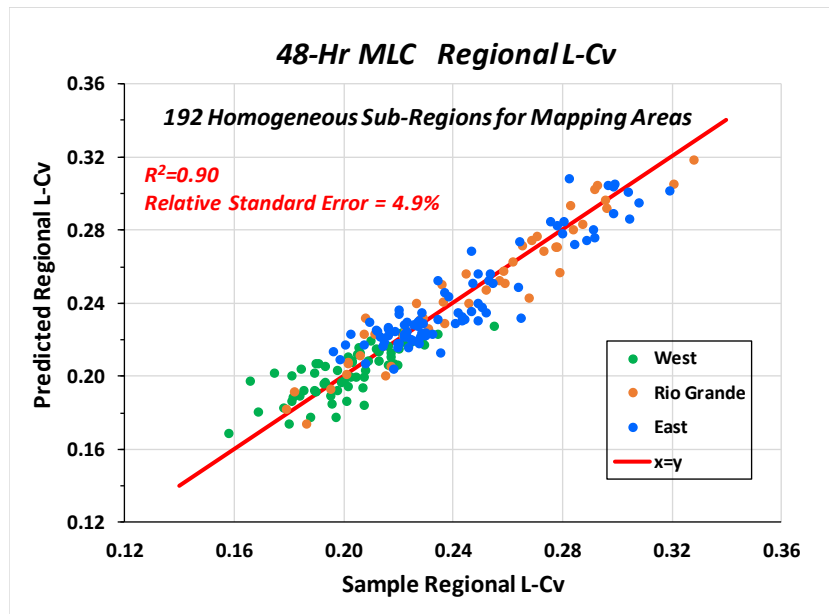


Figure 53. Comparison of observed regional L-Cv and mapped regional L-Cv for 192 homogeneous sub-regions for 48-Hour MLCs using latitude and DEM elevation as explanatory variables

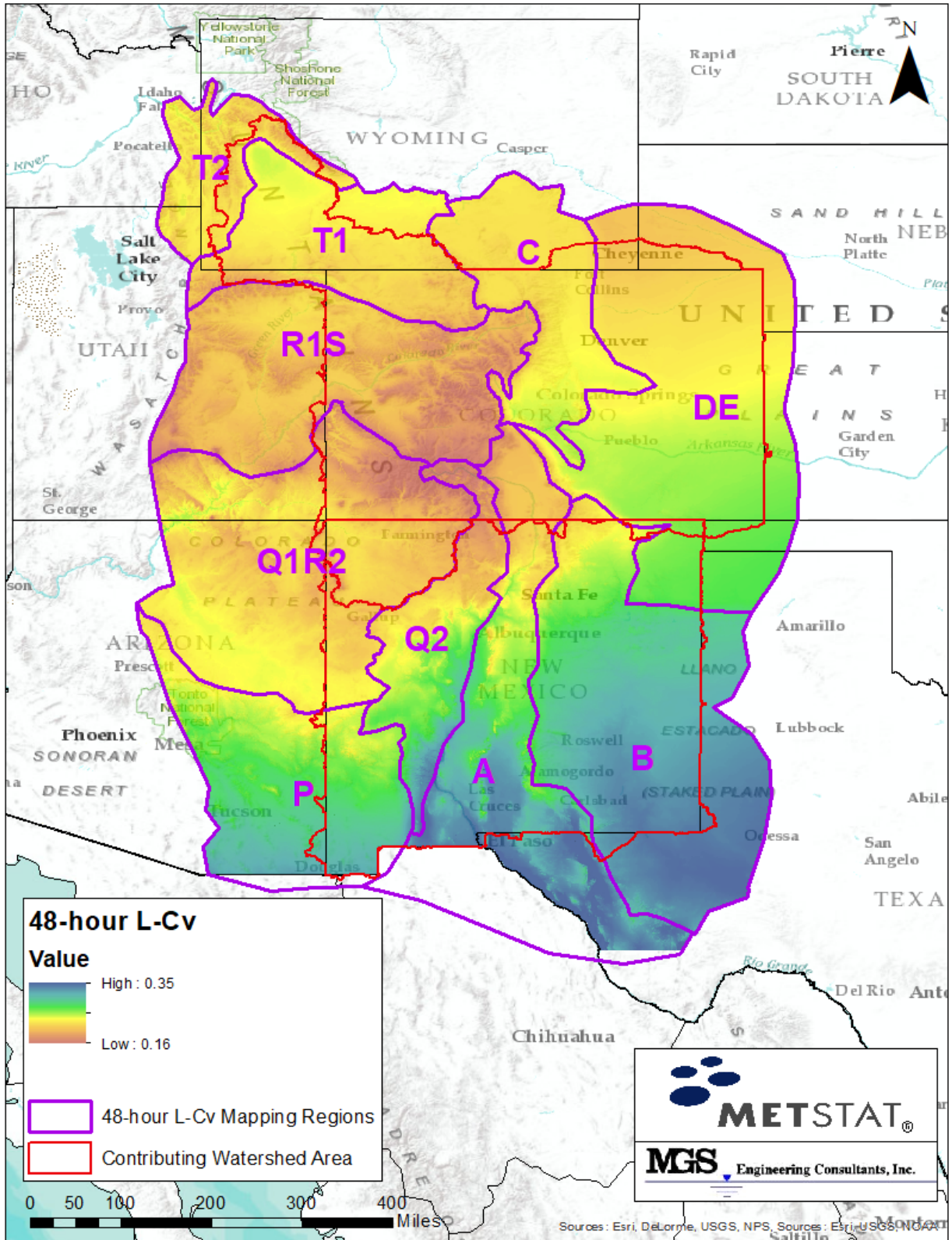


Figure 54. Map of regional L-Cv for 48-hour duration for MLCs

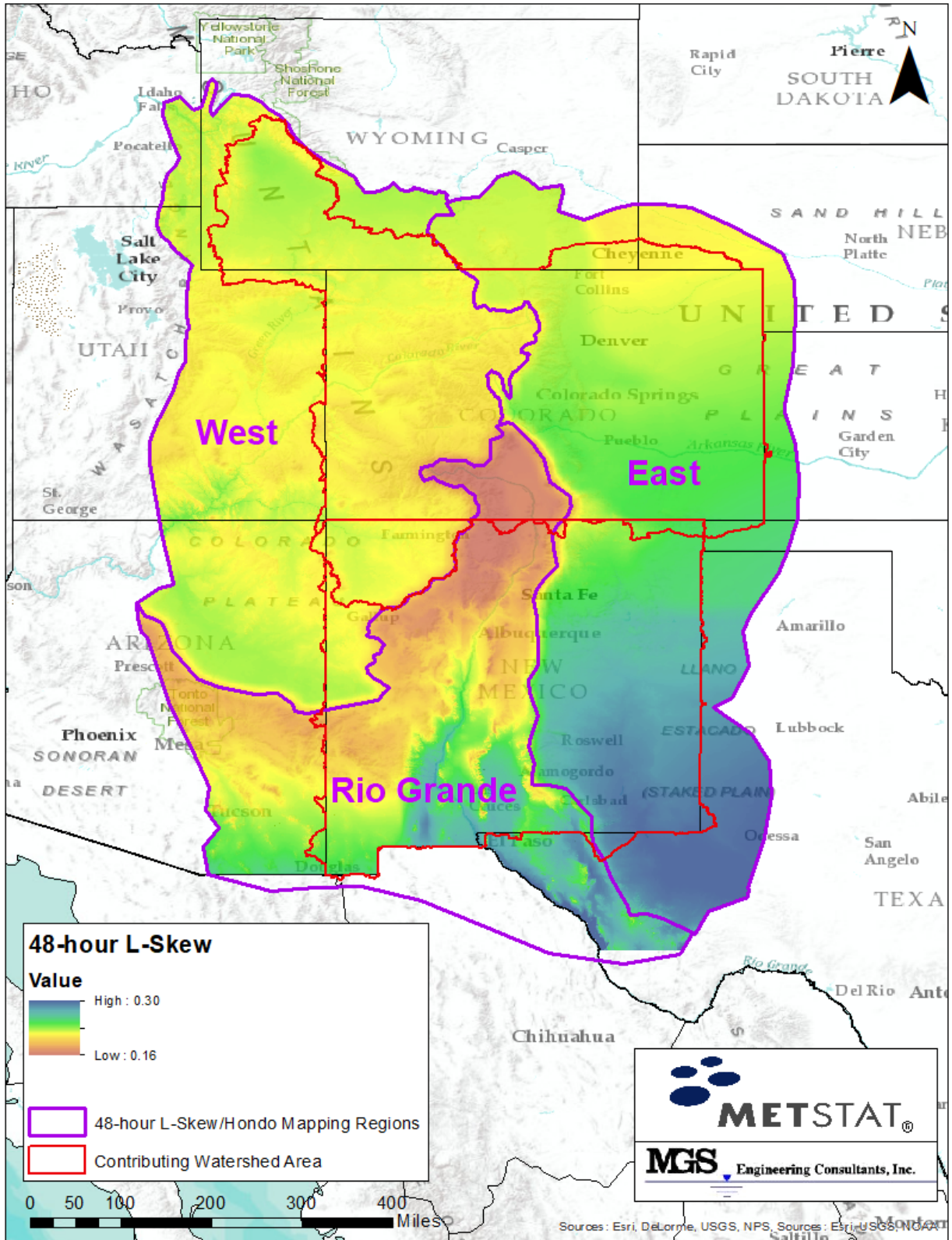


Figure 55. Map of regional L-Skewness for 48-hour precipitation annual maxima for MLCs

5.1.1.3. Identification of Regional Probability Distribution - MLC

L-moment goodness-of-fit tests were conducted for each of the 192 homogeneous sub-regions for each Macro Region (East, West, and Rio Grande) and the GEV distribution was identified as the best-fit 3-parameter probability distribution for the collection of sub-regions. A review of Figure 56 shows the centroid of the cluster of regional L-Skewness and L-Kurtosis pairs for the sub-regions within each Macro Region to be very near the GEV distribution. As discussed previously, the 4-parameter Kappa distribution with a fixed shape parameter ( $h$ , Hondo) emulates the GEV and near-GEV distributions and was selected for describing the point precipitation-frequency relationships for MLCs. Each of the three Macro Regions were found to have slightly different Hondo values (Figure 57). These minor differences only become important for extreme (very low AEP) precipitation estimates. Spatial smoothing of the Hondo values was conducted in the vicinity of the boundaries between the three Macro Regions where the boundaries align along major mountain barriers (Figure 7) to provide a transition between the Macro Regions.

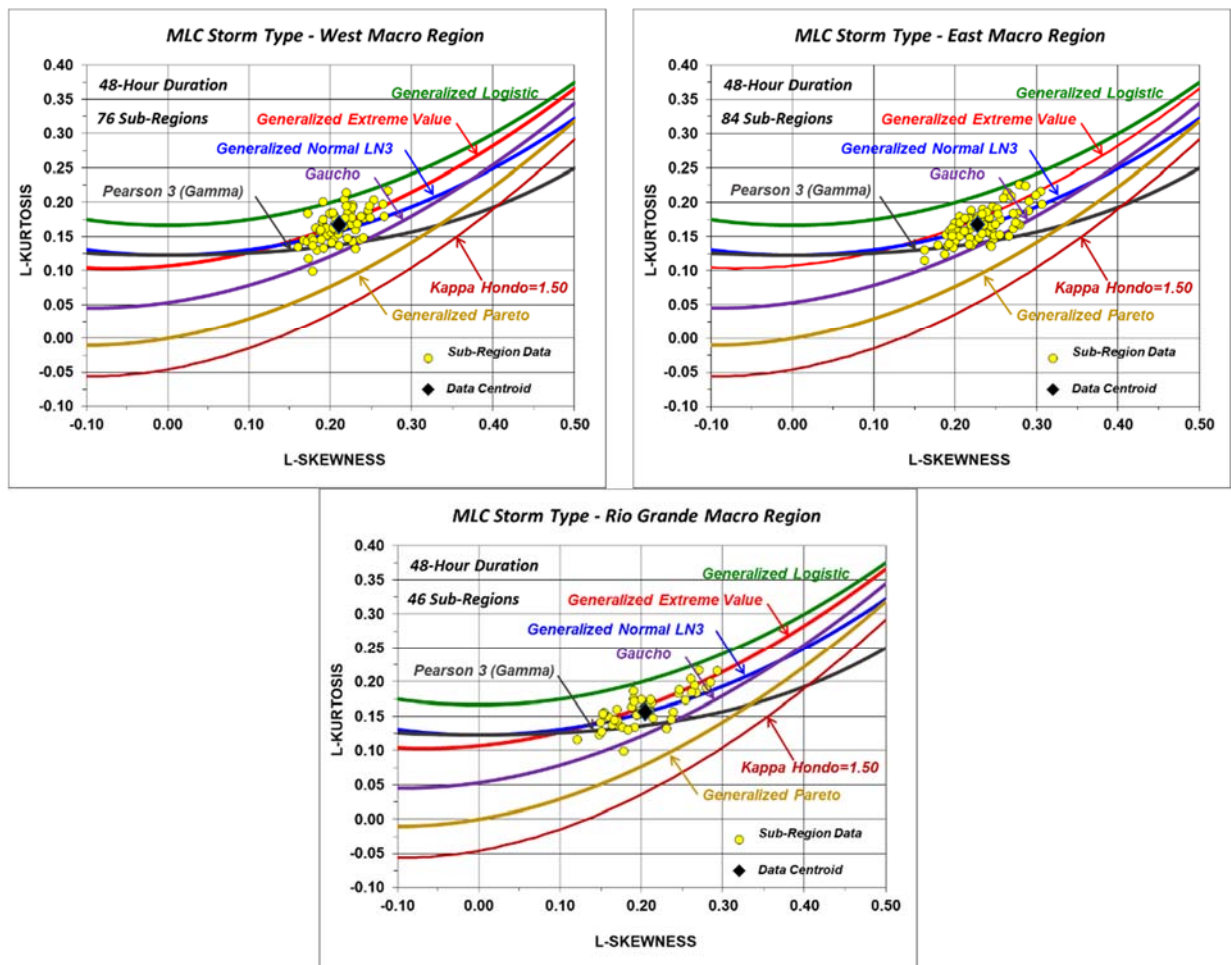


Figure 56. L-Moment ratio diagrams depicting regional L-Skewness and L-Kurtosis pairings for homogeneous sub-regions for 48-Hour duration for MLCs for each of the Macro Regions

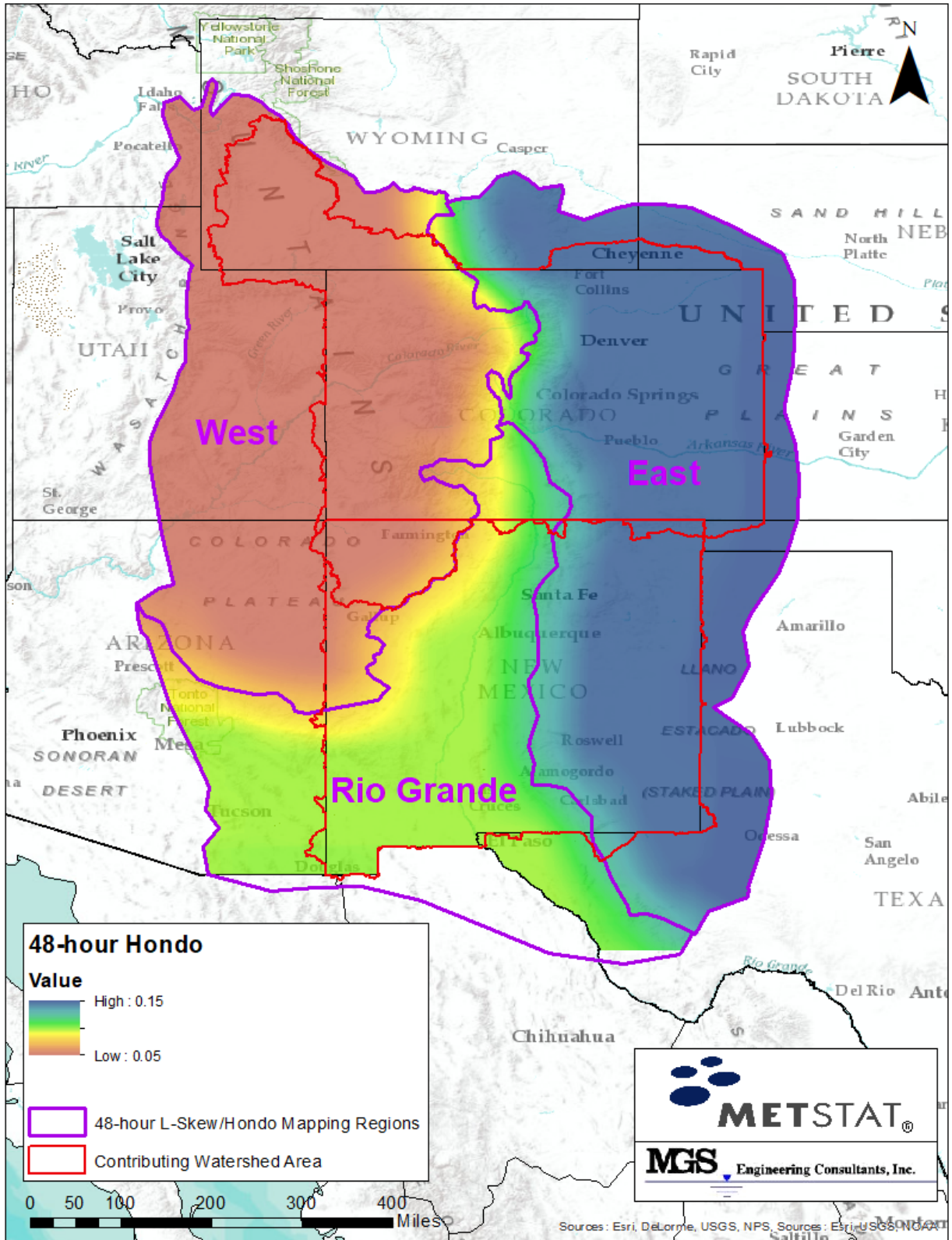


Figure 57. Map of regional Hondo for 48-hour precipitation annual maxima for MLCs

#### 5.1.1.4. Point Precipitation-Frequency Estimates for MLC Storm Type

Point precipitation-frequency estimates at any location in the project area can be obtained from the gridded datasets of spatially mapped L-Moment statistics. Specifically, distribution parameters for the Kappa distribution are solved using grid-cell specific values of the 48-hour at-site mean (Figure 51), regional L-Cv (Figure 54), regional L-Skewness (Figure 55), and regional Hondo (Figure 57). This process is repeated for each grid-cell and the inverse CDF for the Kappa distribution (Equation 2) is used to compute quantile estimates for selected Annual Exceedance Probabilities (AEPs).

For the purposes of illustration, a precipitation-frequency curve has been developed for a station in each Macro Region in the manner described above and compared with a probability plot of historical data (Figure 58). These comparisons provide an example of the general shape of the precipitation-frequency relationship for MLC storm types and the general goodness-of-fit to stations with long-term records.

Isopluvial gridded datasets were generated for AEPs of 0.9, 0.5, .05, .02,  $10^{-1}$ ,  $10^{-2}$ ,  $10^{-3}$ ,  $10^{-4}$ ,  $10^{-5}$ ,  $10^{-6}$ , and  $10^{-7}$ . Figure 59 and Figure 60 show example isopluvial maps for AEPs of 1:100 and 1:1,000, respectively.

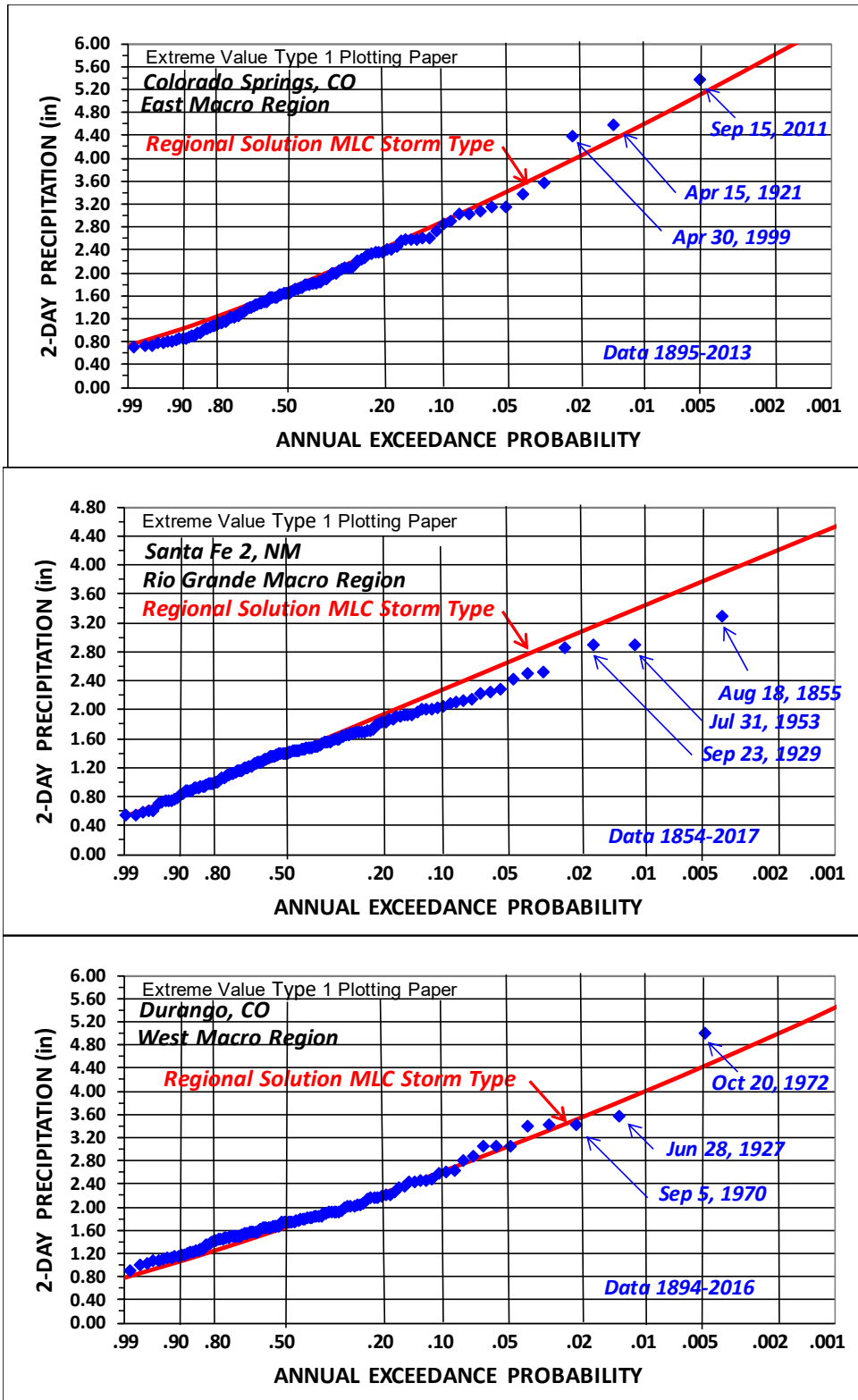


Figure 58. Probability plots of historical 2-day precipitation annual maxima for MLC storm type for stations located in the three Macro Regions and comparison with regional precipitation-frequency relationship for those locations

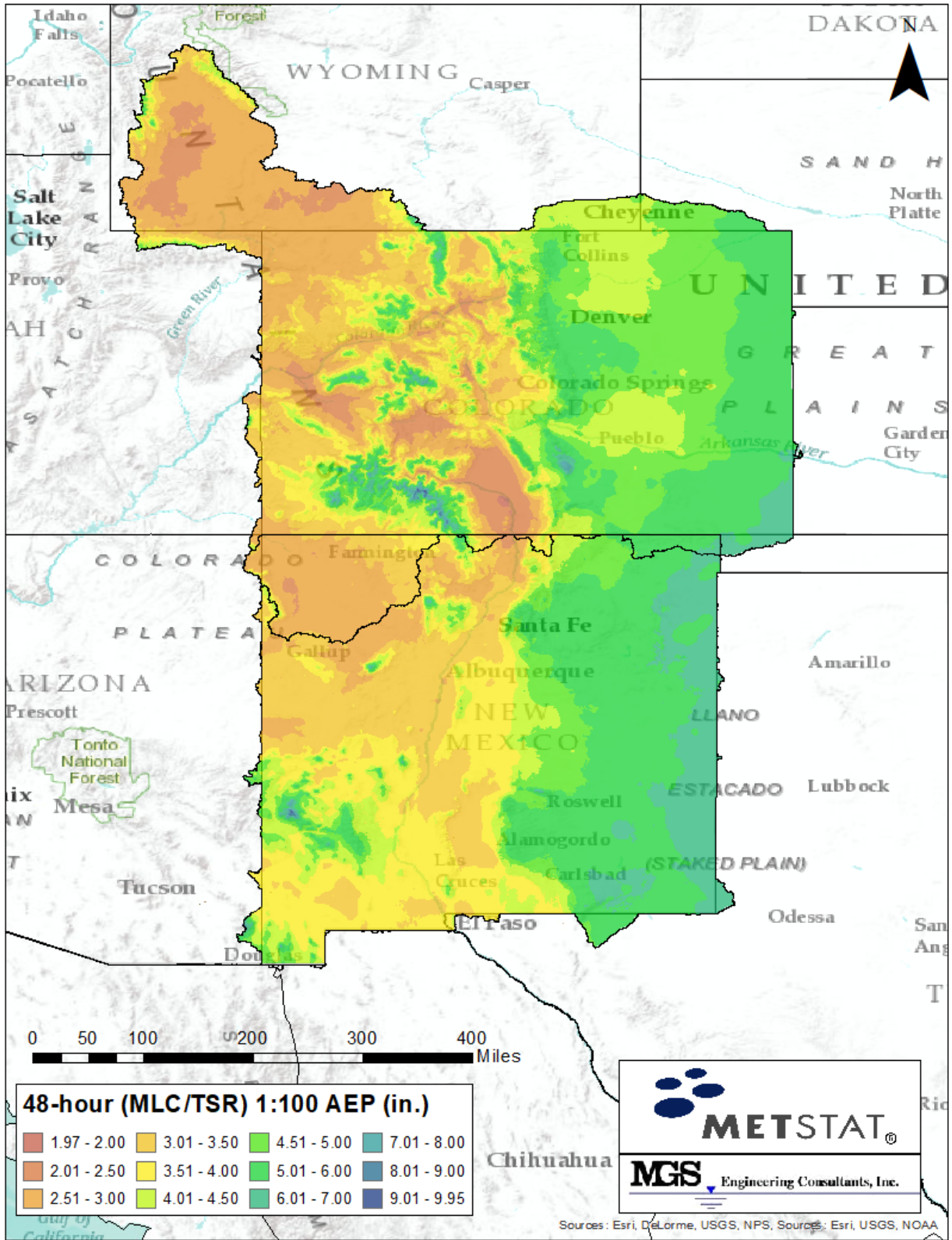


Figure 59. Isopluvial map of 48-hour precipitation maxima for an AEP of 1:100 for MLCs

CO-NM Regional Extreme Precipitation Study

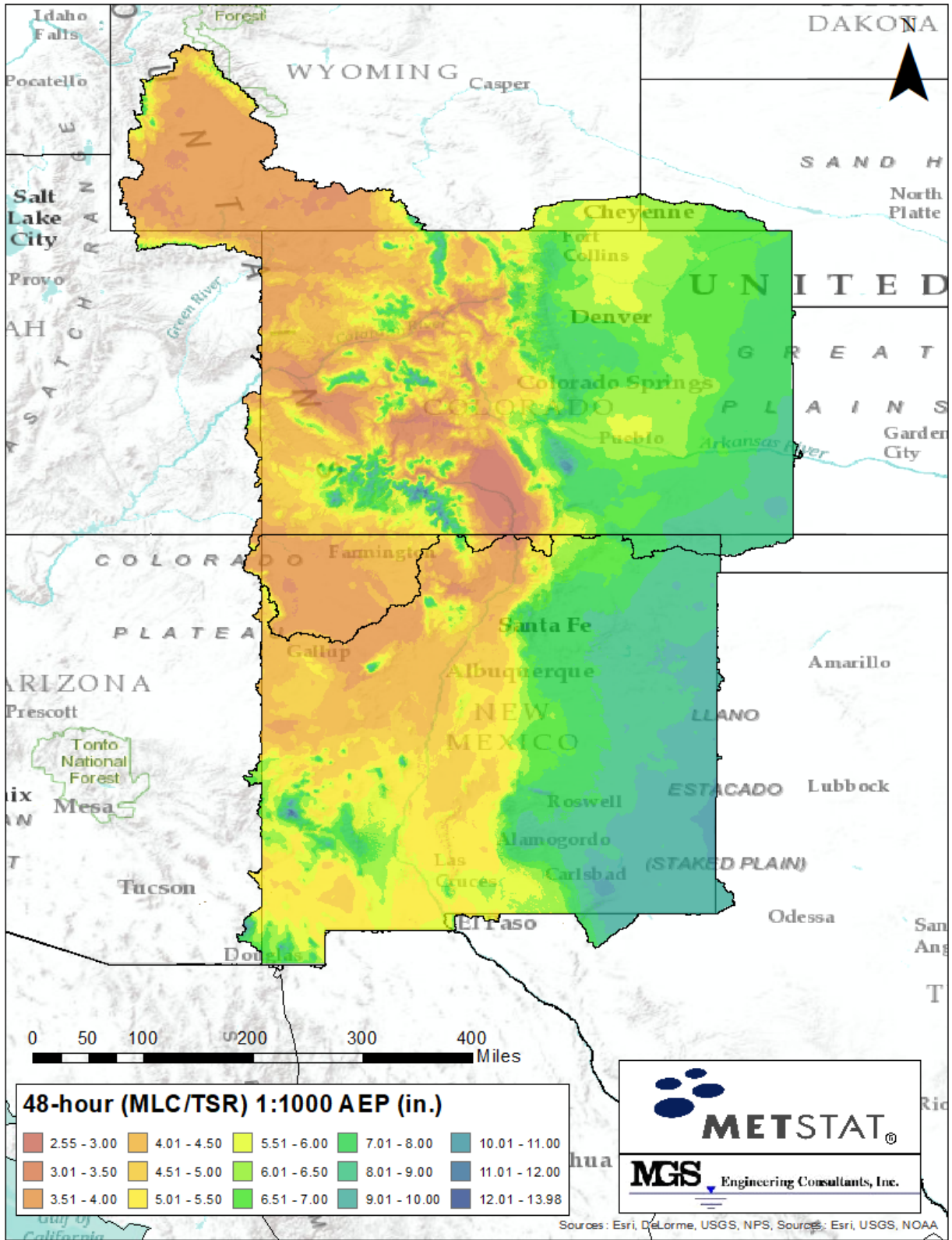


Figure 60. Isopluvial map of 48-hour precipitation maxima for an AEP of 1:1,000 for MLCs

5.1.1.5. Seasonality of Extreme Storms for Mid-Latitude Cyclones

The storm seasonality analyses for the MLC storm type was conducted using the 50 rarest storm events for each of the five Seasonality sub-areas as described in Section 4.8. Frequency histograms representing the seasonality of extreme 48-hour duration MLCs in each of the five Seasonality Sub-areas are shown in Figure 61.

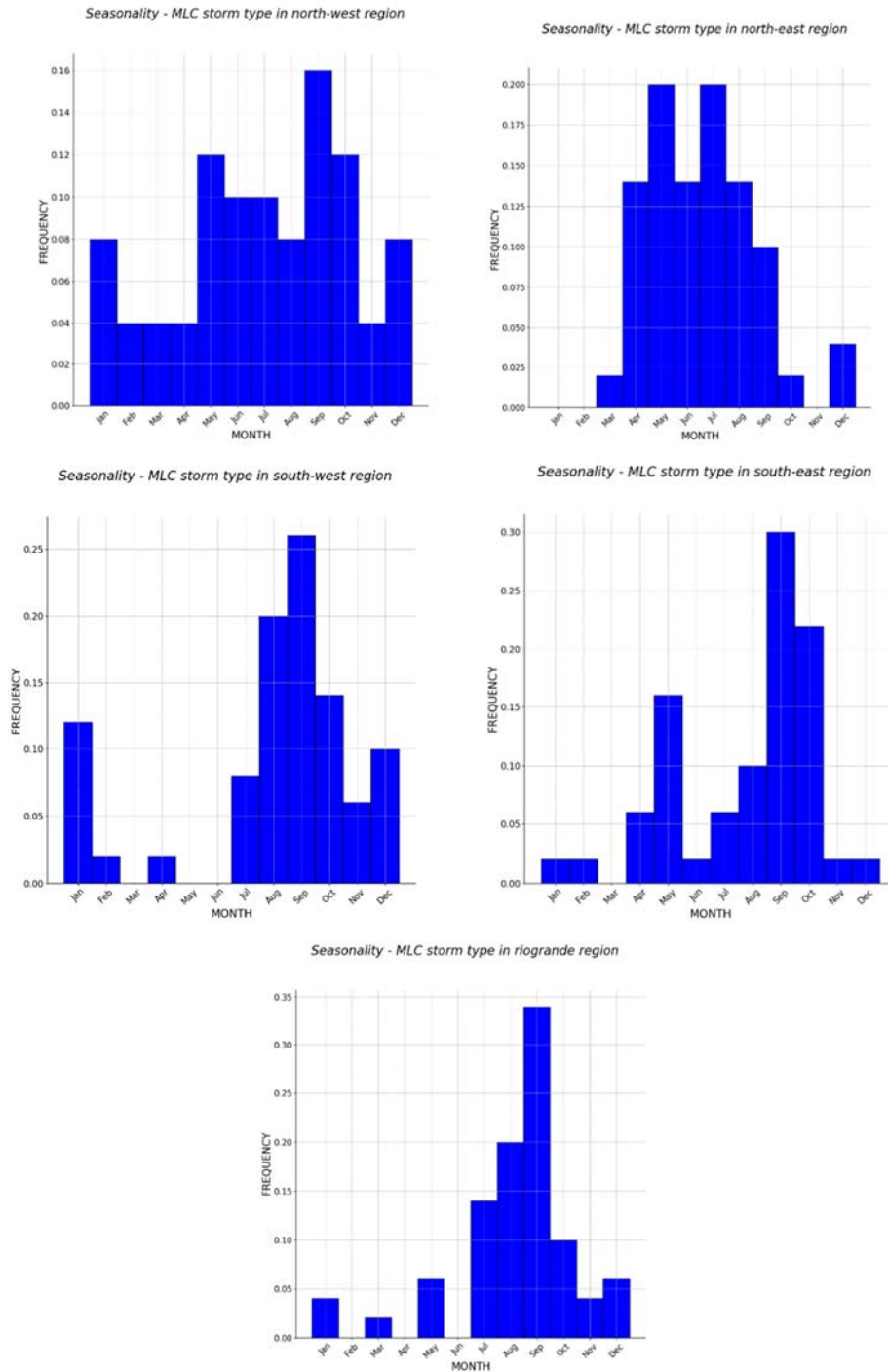


Figure 61. Frequency histograms for seasonality of extreme 48-hour duration MLCs

5.1.1.6. Validation of Findings and Equivalent Independent Record Length (EIRL) for Mid-Latitude Cyclone Storms

EIRL was estimated by counting the number of *independent* storm dates from all precipitation annual maxima for stations with record lengths of 20 years or more as described in section 4.4.7. Counting of independent storm dates, dates separated by 2 or more non-MLC storm days, resulted in an EIRL estimate of 5,035 years (Table 16). The widespread areal coverage of synoptic scale MLCs results in the EIRL being only 8.3 percent of the station-years of record of the regional annual maxima dataset. This estimate of EIRL is likely an underestimate as it is possible for multiple widely separated storm centers to occur on separate days within a given MLC 2-day to 3-day period. Nonetheless, the EIRL provides a useful demonstration of the statistical information in a regional dataset relative to the chronological period of record.

Table 16. Estimate of EIRL for 48-Hour duration for MLCs

Station-Years of Record	EIRL Estimates (Years) as Storm Count	EIRL Percent of Station-Years
60,734	5,035	8.3%

The Binomial Distribution (Equation 8), can be used as a statistical check for comparing the actual number of exceedances versus the predicted number of exceedances to demonstrate the reasonableness of quantile estimates obtained from the regional PF analysis. Table 17, Table 18, and Table 19 show the results for the expected number of exceedances for the 1:100 and 1:1,000 AEPs for the MLC storm type for the three Macro Regions. Comparisons of the number of predicted exceedances and that expected from the Binomial distribution show the number of exceedances from the quantile estimates are typically near expected values and within the 5<sup>th</sup> and 95<sup>th</sup> percentiles from the Binomial distribution. These results support the reasonableness of the solutions from the regional PF analysis.

Equation 8

$$\Pr(x = k) = \binom{n}{k} p^k q^{n-k}$$

$p$  – probability that event occurs ( $p=1/T$ )

$q=1-p$

$n$  – period of record

$k$  – number of times event occurs in  $n$  trials

$x$  – Bernoulli random variable

Table 17. Comparison of actual number of exceedances for selected AEPs with expected number from binomial distribution for Mid-Latitude Cyclone (MLC) storm type for West Macro Region

Record Length	# Stations	Station-Years	1:100 AEP Actual (Expected)	1:1,000 AEP Actual (Expected)
31-50	105	3,819	30 (38)	0 (3)
51-70	64	3,836	33 (38)	2 (4)
71-90	39	3,091	28 (31)	2 (3)
> 90	46	4,844	46 (48)	6 (5)
ALL	254	15,590	137 (156)	10 (16)
			135 - 156 - 177	9 - 16 - 22
			5 <sup>th</sup> Percentile - Mean - 95 <sup>th</sup> Percentile	

Table 18. Comparison of actual number of exceedances for selected AEPs with expected number from binomial distribution for Mid-Latitude Cyclone (MLC) storm type for Rio Grande Macro Region

Record Length	# Stations	Station-Years	1:100 AEP Actual (Expected)	1:1,000 AEP Actual (Expected)
31-50	71	2,736	22 (27)	2 (3)
51-70	56	3,417	26 (34)	1 (3)
71-90	32	2,529	28 (25)	3 (3)
> 90	45	4,658	47 (47)	6 (5)
ALL	204	13,340	123 (133)	12 (13)
			114 - 133 - 153	7 - 13 - 19
			5 <sup>th</sup> Percentile - Mean - 95 <sup>th</sup> Percentile	

Table 19. Comparison of actual number of exceedances for selected with expected number from binomial distribution for Mid-Latitude Cyclone (MLC) storm type for East Macro Region

Record Length	# Stations	Station-Years	1:100 AEP Actual (Expected)	1:1,000 AEP Actual (Expected)
31-50	99	3,773	42 (38)	5 (4)
51-70	129	7,936	73 (79)	10 (8)
71-90	69	5,404	49 (54)	3 (5)
> 90	92	9,788	100 (98)	11 (10)
ALL	388	26,901	264 (269)	29 (27)
			242 - 269 - 297	18 - 27 - 35
			5 <sup>th</sup> Percentile - Mean - 95 <sup>th</sup> Percentile	

#### 5.1.1.7. Dimensionless Uncertainty Bounds for MLC Storm Type

Uncertainty analyses were conducted as part of the Stochastic Storm Transposition (SST) simulations (Schaefer 2015; Appendix D) for developing watershed precipitation-frequency relationships for selected watersheds in the three Macro Regions. The uncertainty analyses required characterizing uncertainties for all of the contributing factors to the total uncertainty in the watershed PF relationship. This included developing probability distributions or resampling schemes for characterizing uncertainty in the regional L-Moment statistics, the regional probability distribution, and the spatial patterns used in the SST simulations. Table 9 and Table 10 list examples of the magnitudes of uncertainties and the probability distributions employed in conducting the uncertainty analysis.

Dimensionless 90 percent uncertainty bounds for the point MLC estimates are depicted in Figure 62 for each of the Macro Regions. Polynomial equations are contained in the graphics where  $x$  is equal to  $\log_{10}(1/AEP)$ , and  $y$  is a dimensionless ratio to the best estimate. To compute the AEP of the 90 percent upper (or lower bound), compute the ratio to the best-estimate, then multiply it by the best-estimate of the precipitation for a given AEP.

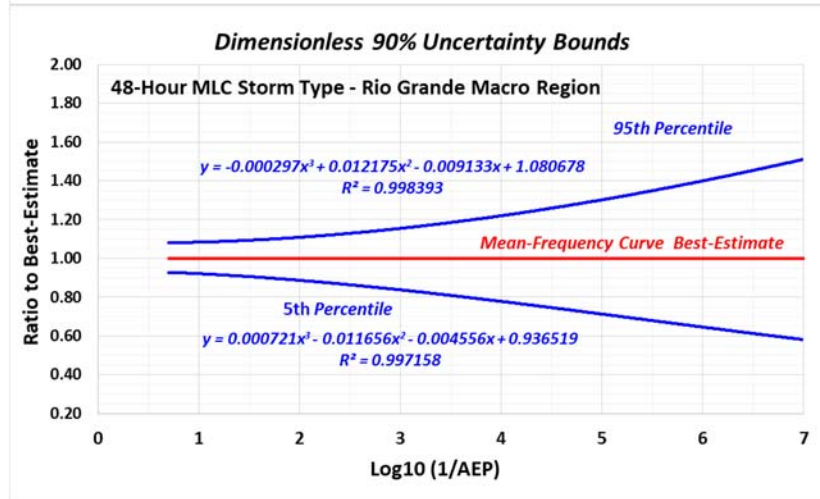
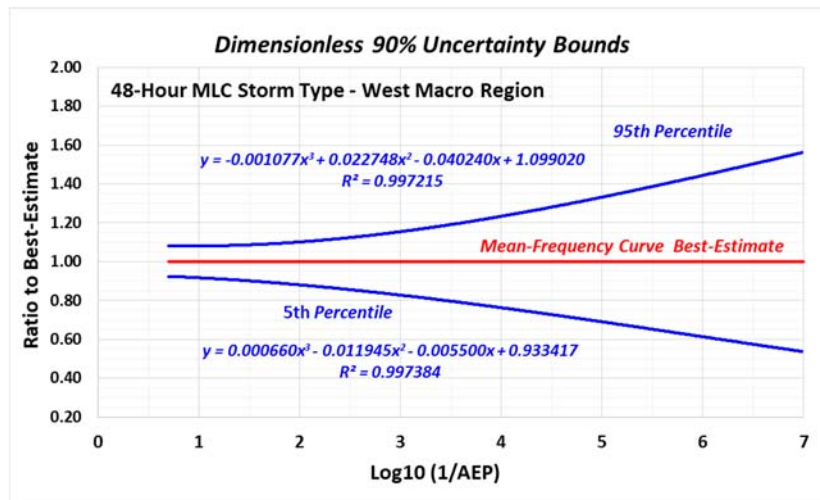
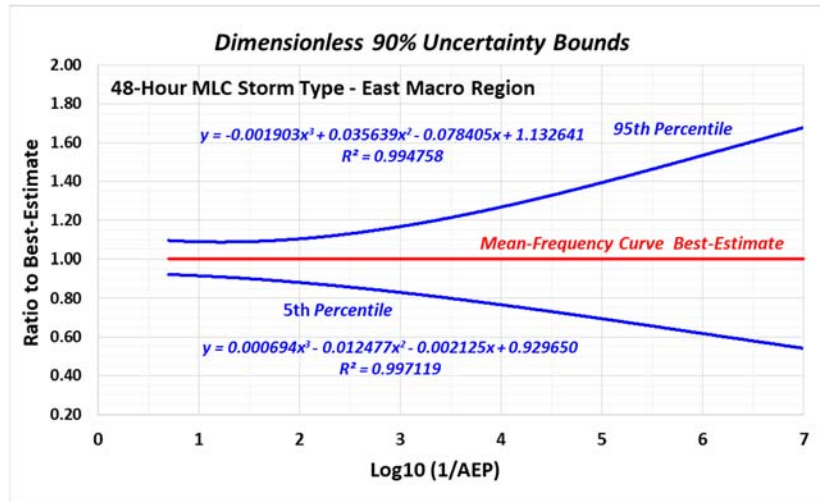


Figure 62. Probability graphics depicting magnitude of dimensionless uncertainty bounds for point MLC precipitation-frequency estimates

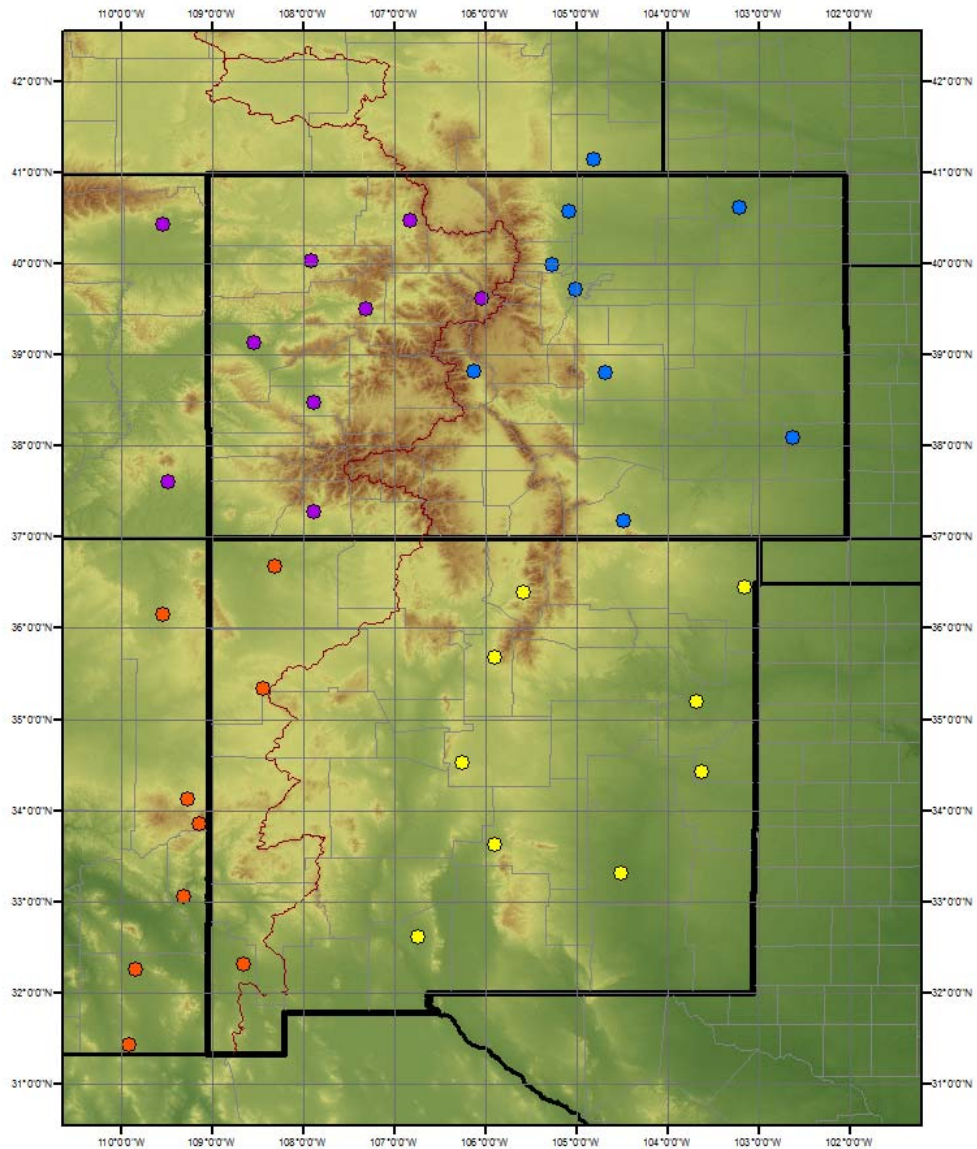
**5.1.1.8. 24-Hour and 72-Hour Mapping**

The project sponsors were interested in examining PF estimates for the 24-hour and 72-hour durations for the MLC storm type in addition to the key duration of 48-hours. These PF estimates were intended to be used for informational purposes and not for design applications. Accordingly, PF estimates for the 24-hour and 72-hour durations were developed using a simplified approach using scaling procedures that were based on the findings for the 48-hour key duration but are not recommended for direct use.

Precipitation annual maxima datasets were also assembled for the 24-hour and 72-hour durations for MLCs for 36 long-term index stations located in the eastern and western sections of Colorado and New Mexico (Figure 63). These datasets were assembled to provide scaling factors for 24-hour and 72-hour at-site means relative to at-site means for the 48-hour duration. PRISM July-January mean monthly precipitation was an adequate explanatory variable for the 24hr/48hr and 72hr/48hr depth-duration ratios. This allowed mapping for the 24-hour and 72-hour at-site means to be a simple grid-cell calculation using the gridded dataset for 48-hour at-site means.

The 72hr/24hr ratios were smallest (1.25 range) for low-orographic areas/arid climates and larger ratios (1.50 range) were seen for mountain areas with greater orography. This is the same behavior seen for the MLC storm type along the west coast of the US where mean annual precipitation was used as the explanatory variable [Schaefer et al. (2002, 2006, 2007)].

The gridded at-site means were applied with the L-moment ratios from the 48-hour analysis to develop grids of AEPs for the 24-hour and 72-hour durations for the MLC storm type. Figure 64 shows the resulting estimates for the 1:1,000 AEP comparing all three durations.



**Long Term Index Stations  
in Four Quadrants of Colorado-New Mexico Project Area**

- Colorado East
- Colorado West
- New Mexico East
- New Mexico West

*Figure 63. Long-term index stations used to develop 24-hour and 72-hour relationships to apply to 48-hour MLC AEP*

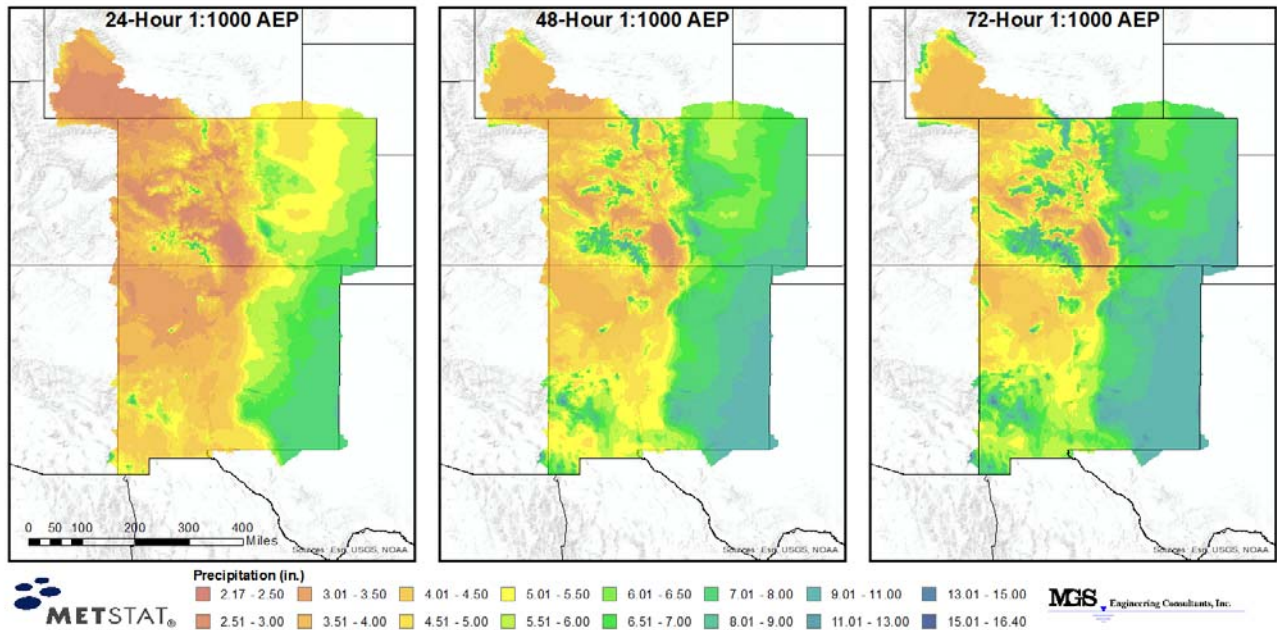


Figure 64. Comparison of 24-hour, 48-hour and 72-hour precipitation-frequency estimates for 1:1000 AEP for 48-hour MLCs

#### 5.1.1.9. Tropical Storm Remnants in 48-Hour Storms

Due to the limited number of impactful TSR events in the historical record across the Colorado-New Mexico project area, a separate TSR-only precipitation-frequency analysis was not feasible. Only 13 of 100 years were identified with tropical storm influence (Section 4.2.1). TSR storms were found to have similar temporal and spatial characteristics as MLCs, therefore, TSR events were included with the MLC analysis. In fact, it is common to have TSR-related moisture interacting with synoptic or MLC features to produce extreme precipitation events across Colorado-New Mexico.

Days with tropical storm influence were identified as described in Section 4.2 using the IBTrACS dataset (Figure 21). There was a total of 301 days identified from only 65 different storms from the 1850 through 2014 time period of the available data record. Not all storms produced significant precipitation, but closer examination suggested that a higher percentage of tropical influence occurred in southeastern New Mexico and eastern Colorado, which is meteorologically expected.

Figure 65 demonstrates no statistical difference in the magnitudes of TSRs compared to MLCs. The first plot compares the magnitudes of the MLC events in the 48-hour annual maximum series to the magnitudes of the TSR events. The second plot normalizes those values by the at-site mean of 48-hour annual maximum series for the stations. Median values and 1<sup>st</sup> and 3<sup>rd</sup> Quartiles are comparable. Most notably, TSRs were dispersed throughout the distribution of the 48-hour annual maxima, but only 4 percent of all extracted 48-hour annual maxima were TSR related.

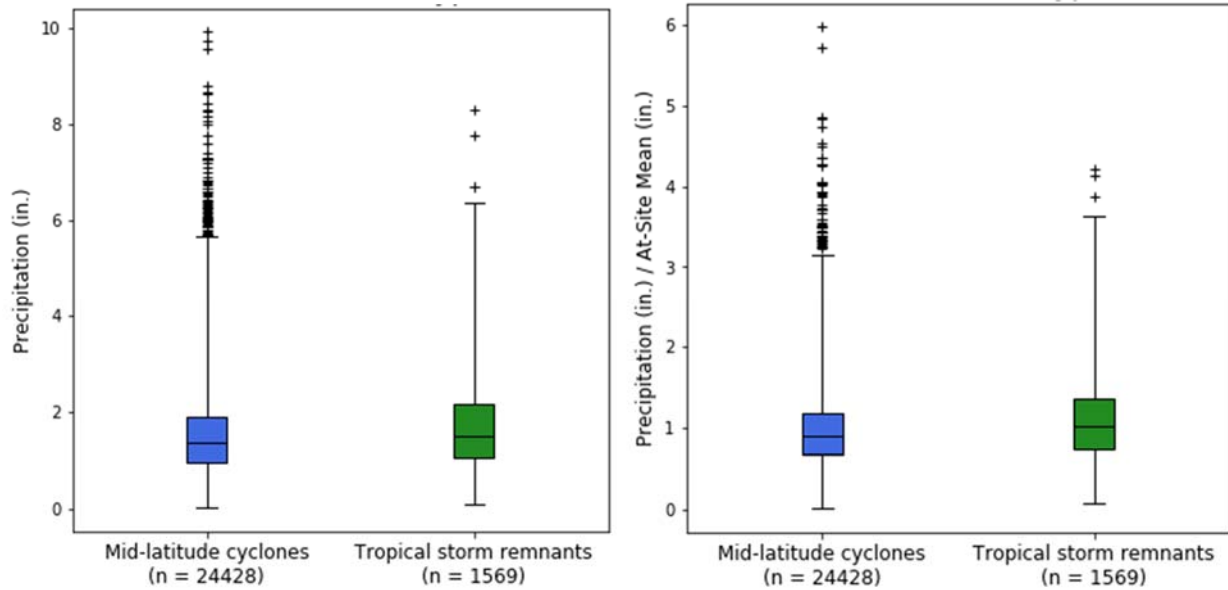


Figure 65. Comparison of the magnitudes of TSR and MLC 48-hour annual maxima and a comparison of TSR and MLC annual maximum precipitation magnitudes relative to the at-site mean at stations in the CO-NM project area where the whiskers extend four times the Interquartile Range

### 5.1.2 2-hour Local Storms

Thunderstorm cells and associated convective storm activity can occur in a variety of meteorological environments. This situation was addressed by allowing all storm-types that have convective elements to provide candidates for 2-hour precipitation annual maxima. Specifically, 2-hour annual maxima were obtained from the greatest precipitation amounts produced in the April 1st through October 31st time frame by any of the storm types where storm typing had indicated high levels of CAPE (Section 4.2) for the given date and station location.

Hourly stations were used in the regional analyses for 2-hour precipitation annual maxima for Local Storms where stations with 20 years or more of record were included in the analyses (Figure 66). Table 20 provides a listing of the number of stations and total number of data years used in the analysis of Local Storms (LS), and Figure 67 depicts a histogram of the number of data years.

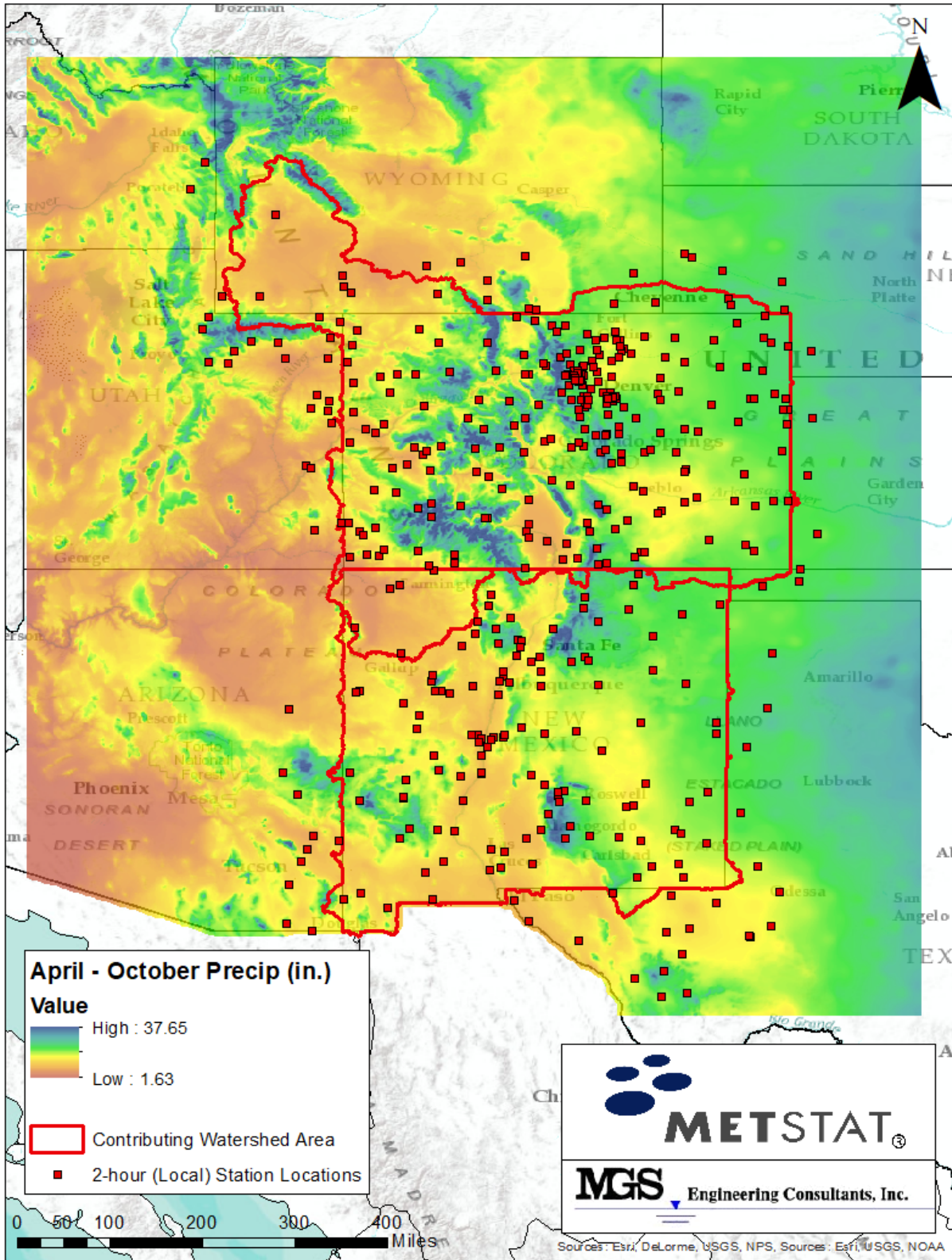


Figure 66. Location of hourly precipitation stations used in the precipitation-frequency analysis for Local Storms (LS) and the seasonal mean precipitation used in the predictor equations

Table 20. Number of Stations and data years for stations with 20 or more data years used in the precipitation-frequency analysis for Local Storms

PRECIPITATION GAUGE TYPE	NUMBER OF STATIONS/GAUGES	TOTAL STATION DATA YEARS	AVERAGE STATION DATA YEARS
Hourly Stations	341	15,527	41

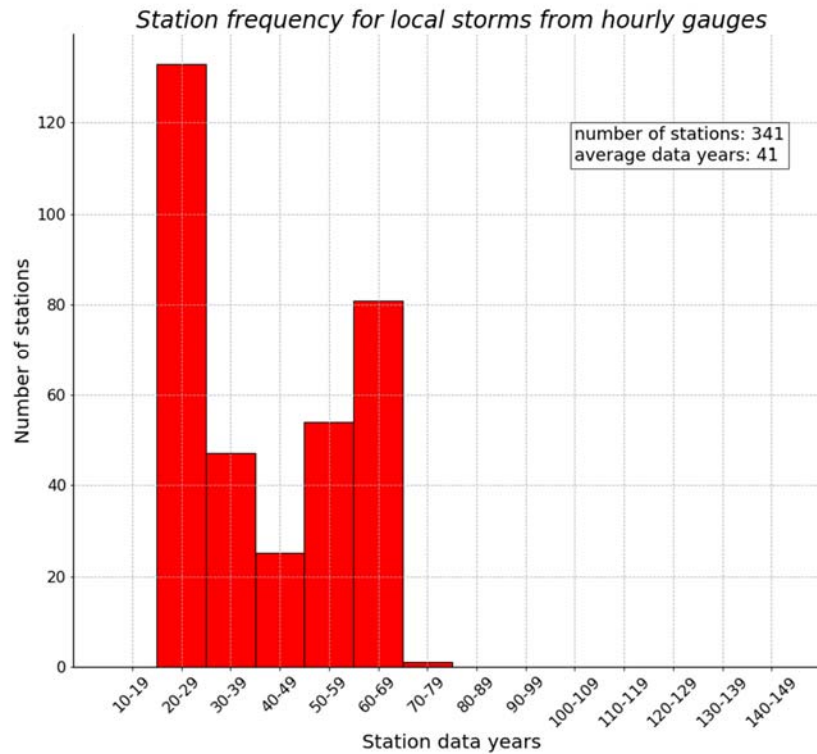


Figure 67. Histogram of data years for stations used in the precipitation-frequency analysis for Local Storms

5.1.2.1. At-Site Means - LS

Spatial mapping of 2-hour at-site means for Local Storms was conducted using elevation, latitude, and gridded values of April through October mean monthly precipitation (Daly 1994) as explanatory variables. This choice was made after reviewing the behavior of the relationship of at-site means with the mean monthly precipitation. The mean monthly precipitation for April through October primarily includes the warmer months when Local Storms (i.e., convection) are more likely plus the shoulder months where fewer convective storms occur.

Collections of stations from adjacent Super Regions were grouped where they exhibited similar behavior. Multiple linear regression methods were used for the collections of stations, which resulted in various mathematical relationships between explanatory variables and predicted values. The explanatory variables for each Mapping Area are shown in Table 21 along with the resultant root-mean-square-error (RMSE). Resultant multiple linear regression equations were used to generate regression-predicted values of 2-hour at-site means. Best estimates of the at-site means were computed as a weighted-average of the station-sample

values and regression-predicted values, as discussed in Section 4.4.3. Figure 68 depicts an example of comparisons of station sample values and mapped values of the 2-hour at-site means. The spatial map of 2-hour at-site means for Local Storms is shown in Figure 69.

Table 21. Listing of explanatory variables for 2-hour at-site means for Local Storms and RMSE for regional prediction equations

Mapping Area	Explanatory Variables	RMSE
A + P + Q2 (i.e., Rio Grande Macro Region)	Apr-Oct Mean Monthly Precipitation; Latitude	10.8%
B	Latitude; Elevation	10.1%
C + D + E	Apr-Oct Mean Monthly Precipitation; Elevation; Latitude	12.9%
C	Apr-Oct Mean Monthly Precipitation; Elevation; Latitude	13.8%
R1	Apr-Oct Mean Monthly Precipitation; Latitude	10.6%
Q1 + R2 + S + T1 + T2	Apr-Oct Mean Monthly Precipitation; Latitude	13.6%

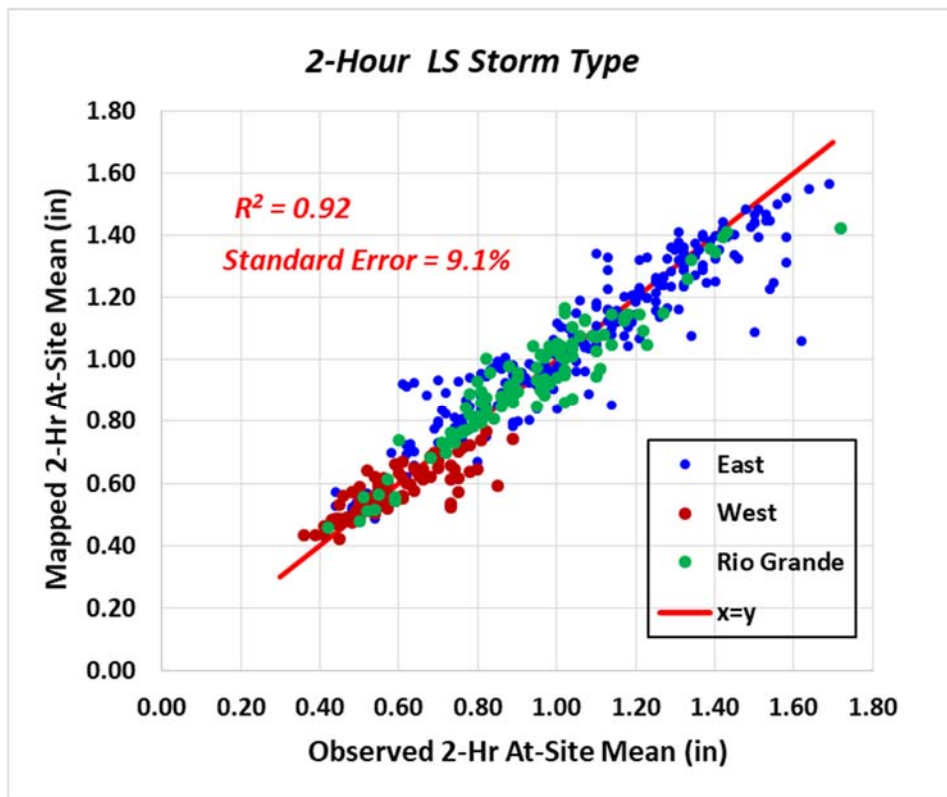


Figure 68. Comparison of station values and mapped values of 2-Hour at-site means for all Mapping Areas for Local Storms

CO-NM Regional Extreme Precipitation Study

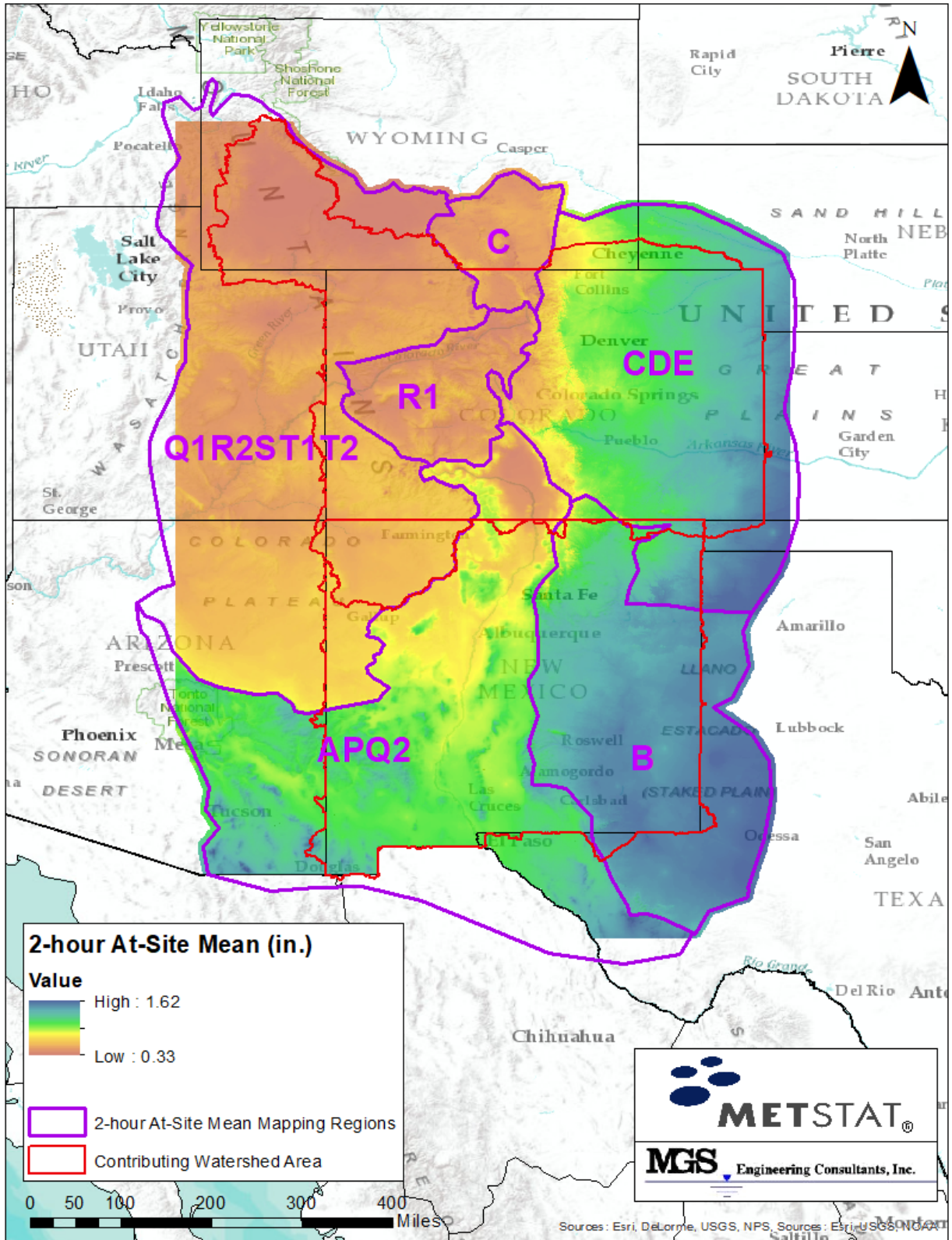


Figure 69. Map of at-site means for 2-hour duration for Local Storms

**5.1.2.2. Regional L-Cv and L-Skewness - LS**

Homogeneous sub-regions were formed as groupings of stations within a limited range of latitude and March to November mean monthly precipitation for each Super Region. March through November was a broader season than the April through October that was used in the predictor equations for at-site means. Stations were included that had a record length of 20 years or more. Thirty-one sub-regions were formed in this manner, where each sub-region produced a regional L-Cv and L-Skewness value associated with a group-average latitude and mean monthly precipitation.

A review of the regional L-Cv values showed a systematic variation with latitude and elevation. Regional values of L-Cv were used in multiple regressions for each Mapping Area with latitude and elevation as explanatory variables. Table 22 lists the number of homogeneous sub-regions used to form of the multiple regressions for regional L-Cv for each designated Mapping Area and resultant RMSE values; and Figure 70 and Figure 71 depict a comparison of observed and mapped values of regional L-Cv and L-skewness, respectively, for 2-hour precipitation annual maxima. A spatial map of regional L-Cv for the 2-hour duration is shown in Figure 72, where regional L-Cv is seen to vary over a relatively narrow range. In assessing homogeneity of the candidate sub-regions (dots on Figure 70), 24 of the 31 sub-regions were acceptably homogeneous based on the Hosking and Wallis (1996) L-Moment heterogeneity test. Of the 7 sub-regions that exceeded the H1 and H2 heterogeneity thresholds, 6 of the 7 sub-regions had modest heterogeneity with H1 and H2 values below 3.0. The benefits from reduction of sampling variability by regionalization far outweighed the effects of modest heterogeneity and all sub-regions were acceptable for spatial mapping of regional L-Cv.

*Table 22. Listing of number of homogeneous sub-regions for each mapping area for 2-hour L-Cv for Local Storms and RMSE for predictive equations*

Mapping Area	Number of Homogeneous Sub-Regions	RMSE
East	16	3.7%
West	7	3.2%
Rio Grande	8	2.5%

Development of predictor equations for L-Skewness is more difficult than for L-Cv because of the naturally high sampling variability for skewness measures. The prediction of regional L-Skewness was accomplished using linear regression with L-Cv for 31 homogeneous sub-regions grouped into three Mapping Areas, the Macro Regions, as described in Table 23. Table 15 lists the summary statistics for mapping of regional L-Skewness, where the RMSE for the watershed area is 9.8 percent and Figure 73 shows the spatial mapping of regional L-Skewness.

Table 23. Listing of number of homogeneous sub-regions for each mapping area for 2-hour L-Skewness for Local Storms and RMSE for regional prediction equations

Mapping Area	Description of Macro Region	Number of Homogeneous Sub-Regions	RMSE
B, C, D, E = East	East of Continental Divide and Sangre De Cristo Mountains	16	11.8%
A, P, Q2 = Rio Grande	Rio Grande Drainage and Southwestern Mountains in New Mexico west of Continental Divide	12	10.1%
Q1, R1, R2, S, T1, T2 = West	West of Continental Divide and North of Southwestern Mountains in New Mexico	10	8.5%

Table 24. Summary statistics for spatial mapping of 2-hour duration regional L-Cv and L-Skewness for Local Storms within contributing watershed area

L-MOMENT RATIO	RANGE OF MAPPED L-MOMENT RATIO	STANDARD DEVIATION OF RESIDUALS	RMSE
Regional L-Cv	$0.2000 \leq L-Cv \leq 0.2651$	0.0062	3.3%
Regional L-Skewness	$0.1750 \leq L-Skewness \leq 0.3311$	0.0184	9.8%

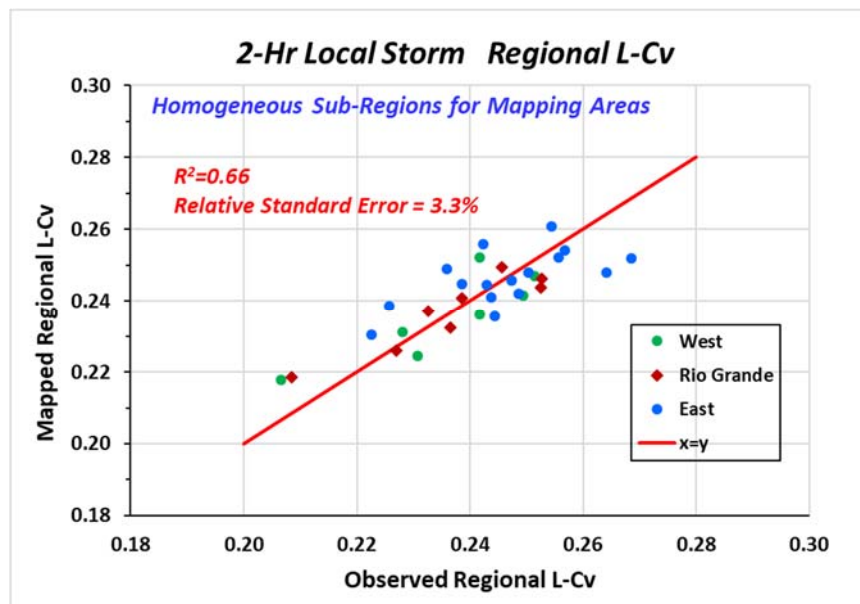


Figure 70. Comparison of observed regional L-Cv and mapped regional L-Cv for 2-hour duration for homogeneous sub-regions for Local Storms

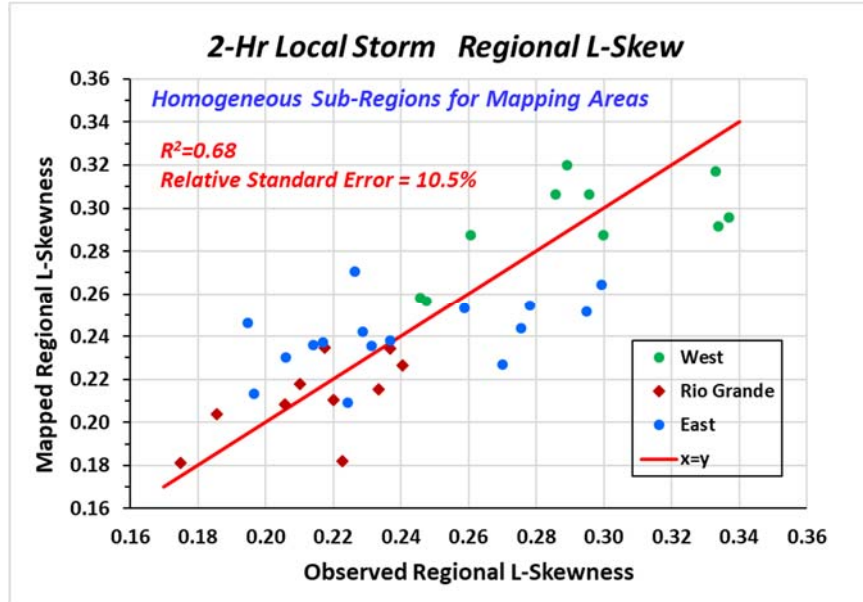


Figure 71. Comparison of observed regional L-Skew and mapped regional L-Skew for 2-hour duration for homogeneous sub-regions for Local Storms

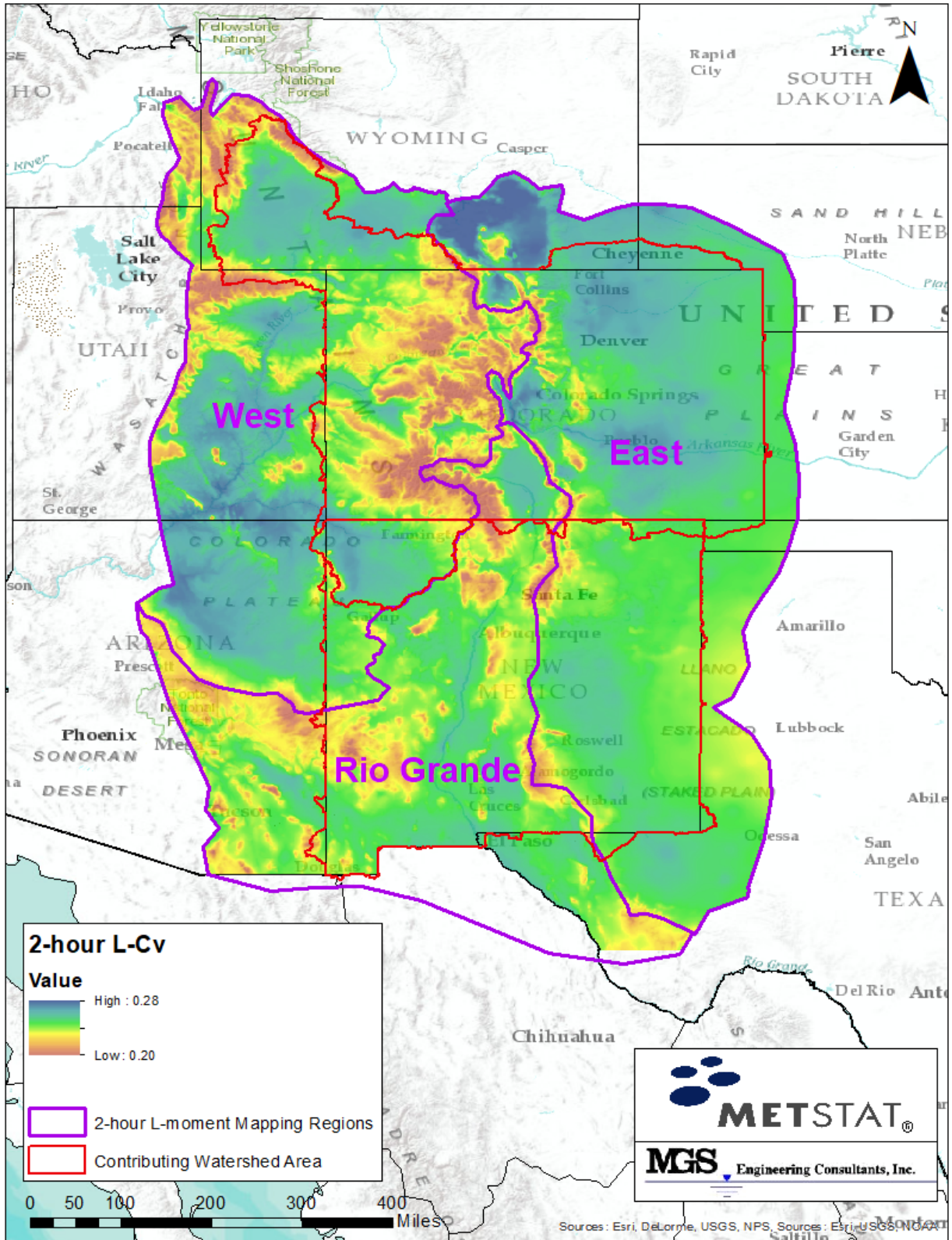


Figure 72. Map of regional L-Cv for 2-hour duration for Local Storms

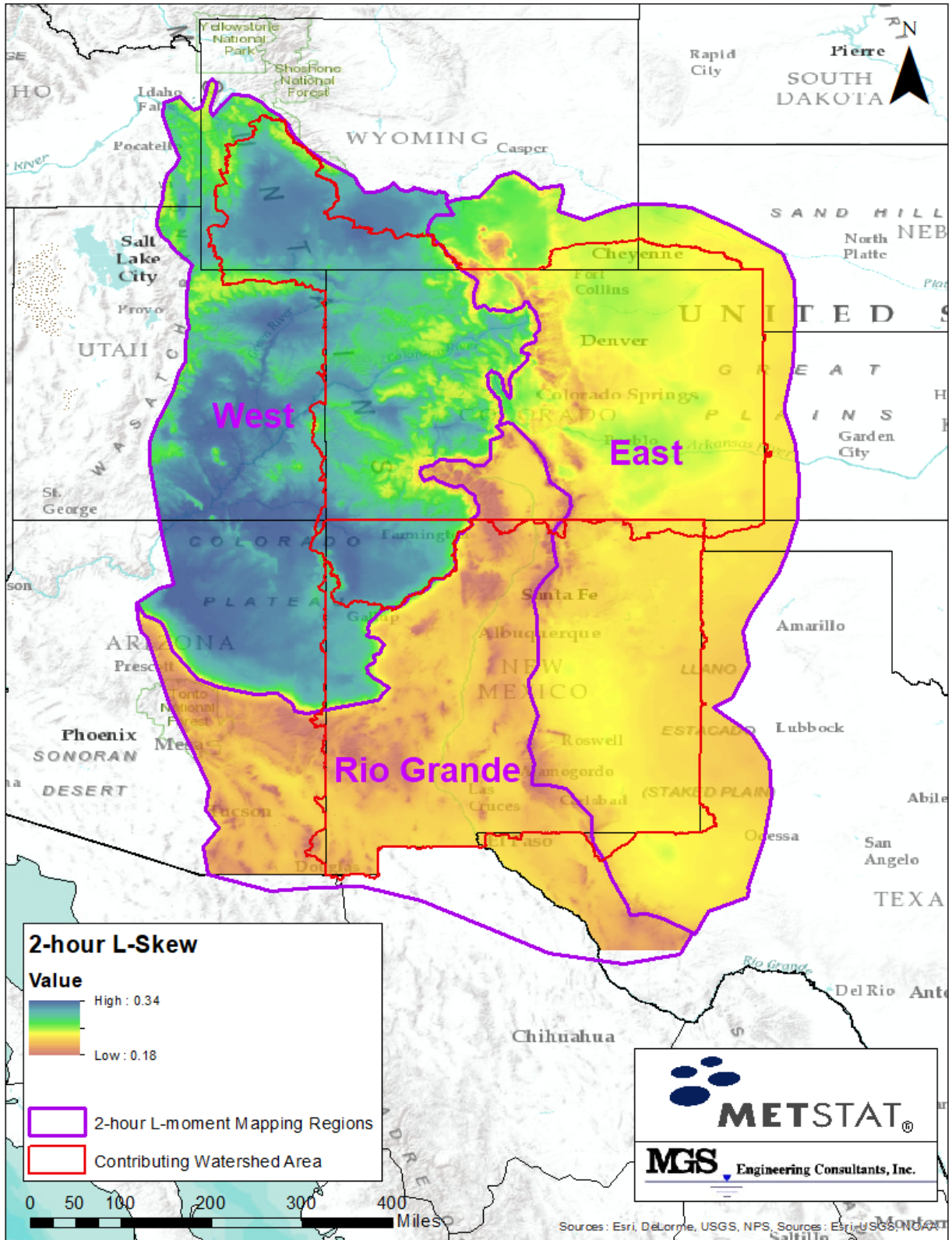


Figure 73. Map of regional L-Skewness for 2-hour precipitation annual maxima for Local Storms

5.1.2.3. Identification of Regional Probability Distribution - LS

L-moment goodness-of-fit tests were conducted for each of the 38 homogeneous sub-regions and the GEV distribution was identified as the best-fit 3-parameter probability distribution for the collection of sub-regions. A review of Figure 74 shows the centroid of the cluster of regional L-Skewness and L-Kurtosis pairs for the 31 sub-regions to be below the GEV distribution and near the Generalized Normal (LN3) distribution. As discussed previously, the 4-parameter Kappa distribution with a fixed shape parameter ( $h$ , Hondo) is capable of emulating the GEV, near-GEV, and LN3 distributions. In addition, varying the Hondo parameter for the 4-parameter Kappa distribution offers the important ability to account for uncertainty in identification of the regional probability distribution which is needed as part of uncertainty analyses for developing watershed PF relationships. For these reasons, the 4-parameter kappa distribution and was selected for describing the point precipitation-frequency relationships for Local Storms.

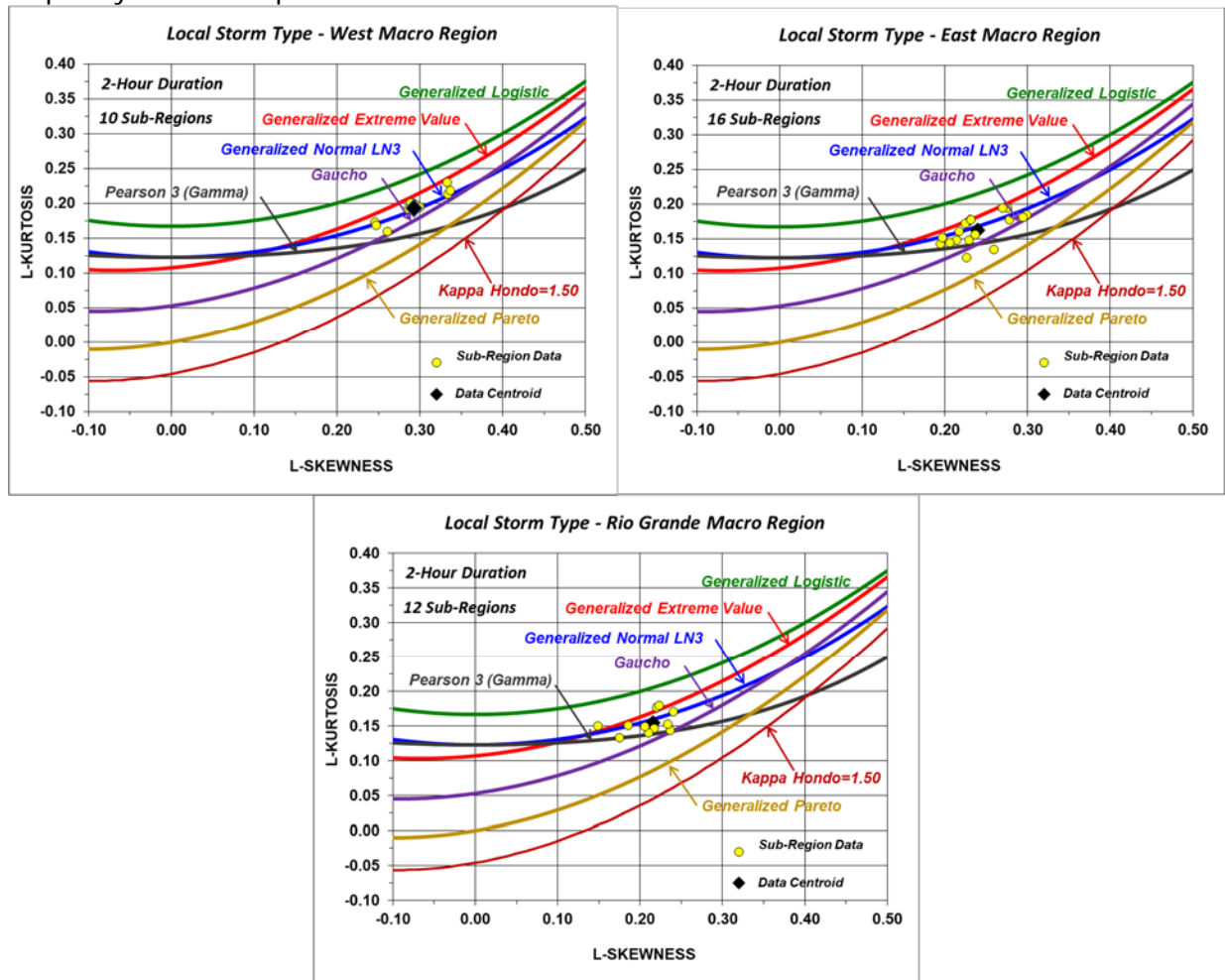


Figure 74. L-Moment ratio diagrams depicting regional L-Skewness and L-Kurtosis values for homogeneous sub-regions for 2-Hour duration for Local Storms for each of the Macro Regions

Similar to the MLC storm type, fixed Hondo values were also found for East and Rio Grande Macro Regions for Local Storms. However, Hondo values were found to spatially vary in the West Macro Region for large values of L-Skewness. This behavior is related to the situation where in some years there are very few local storms of significance in arid and semi-arid climates from which the annual maxima are selected. This results in increases in L-Cv and L-

Skewness without significant changes to the shape of the upper portion of the point PF relationship. This behavior arises as a result of Hondo becoming increasingly positive as L-Skewness increases in arid and semi-arid climates. Accordingly, a predictor equation for Hondo was developed for the West Macro Region using L-Skewness as the explanatory variable. Figure 75 depicts the spatial variability of Hondo for the LS storm type.

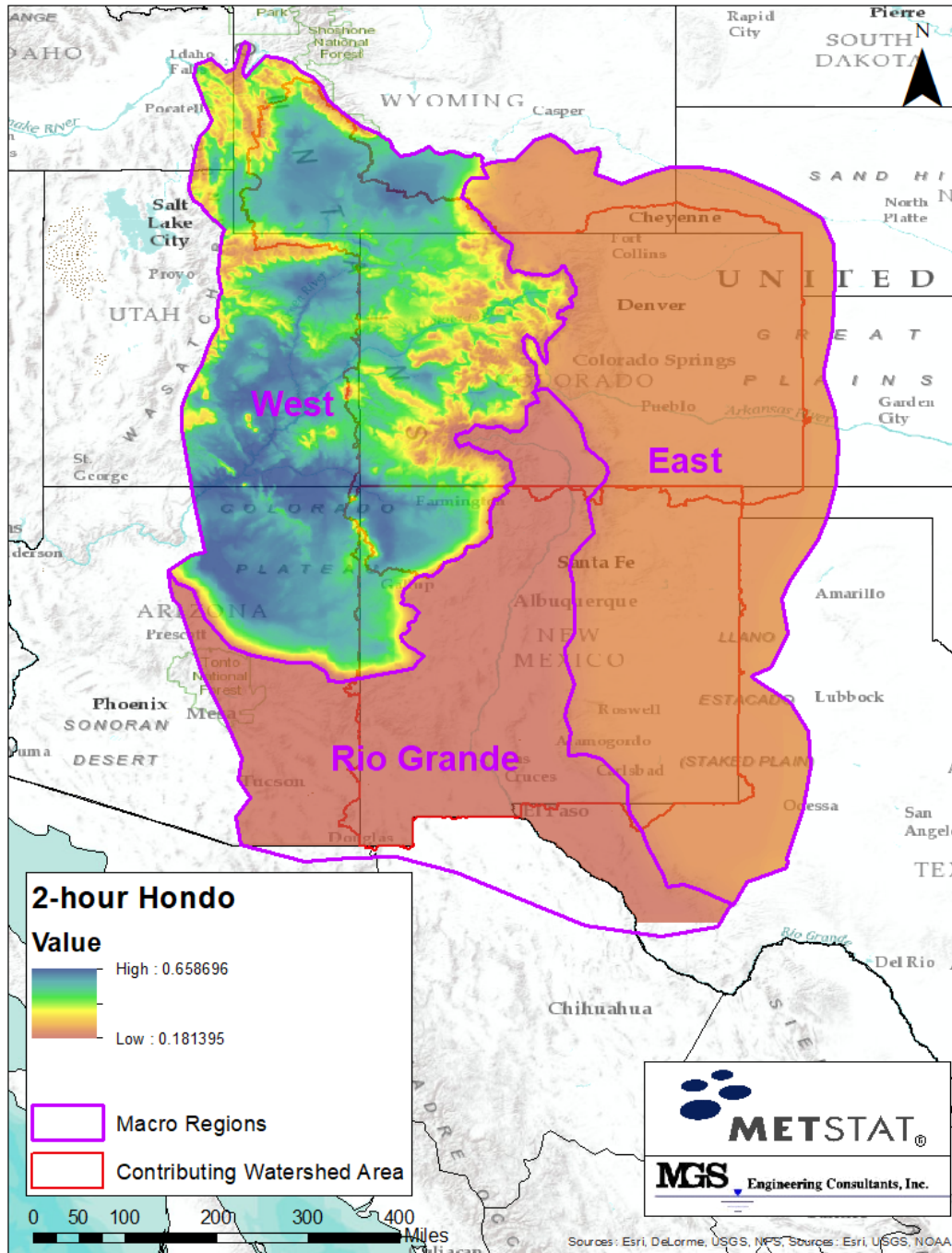


Figure 75. Map of regional Hondo for 2-hour precipitation annual maxima for Local Storms

#### 5.1.2.4. Point Precipitation-Frequency LS Storm Type

Point precipitation-frequency estimates for the LS storm type can be obtained for any location in the project area using the gridded datasets of spatially mapped L-Moment statistics. Specifically, distribution parameters for the Kappa distribution are solved using grid-cell specific values of the 2-hour at-site mean (Figure 51), regional L-Cv (Figure 72), regional L-Skewness (Figure 73), and regional Hondo (Figure 75). This process is repeated for each grid-cell and the inverse CDF for the Kappa distribution (Equation 2) is used to compute quantile estimates for selected Annual Exceedance Probabilities (AEPs).

A precipitation-frequency curve has been developed for a station in each Macro Region in the manner described above and compared with a probability plot of historical data (Figure 76). These comparisons provide an example of the general shape of the precipitation-frequency relationship for LS storm types and the general goodness-of-fit to stations with long-term records.

Isopluvial gridded datasets were generated for AEPs of 0.9, 0.5, .05, .02,  $10^{-1}$ ,  $10^{-2}$ ,  $10^{-3}$ ,  $10^{-4}$ ,  $10^{-5}$ ,  $10^{-6}$ , and  $10^{-7}$ . Figure 77 and Figure 78 show example isopluvial maps for AEPs of 1:100 and 1:1,000, respectively.

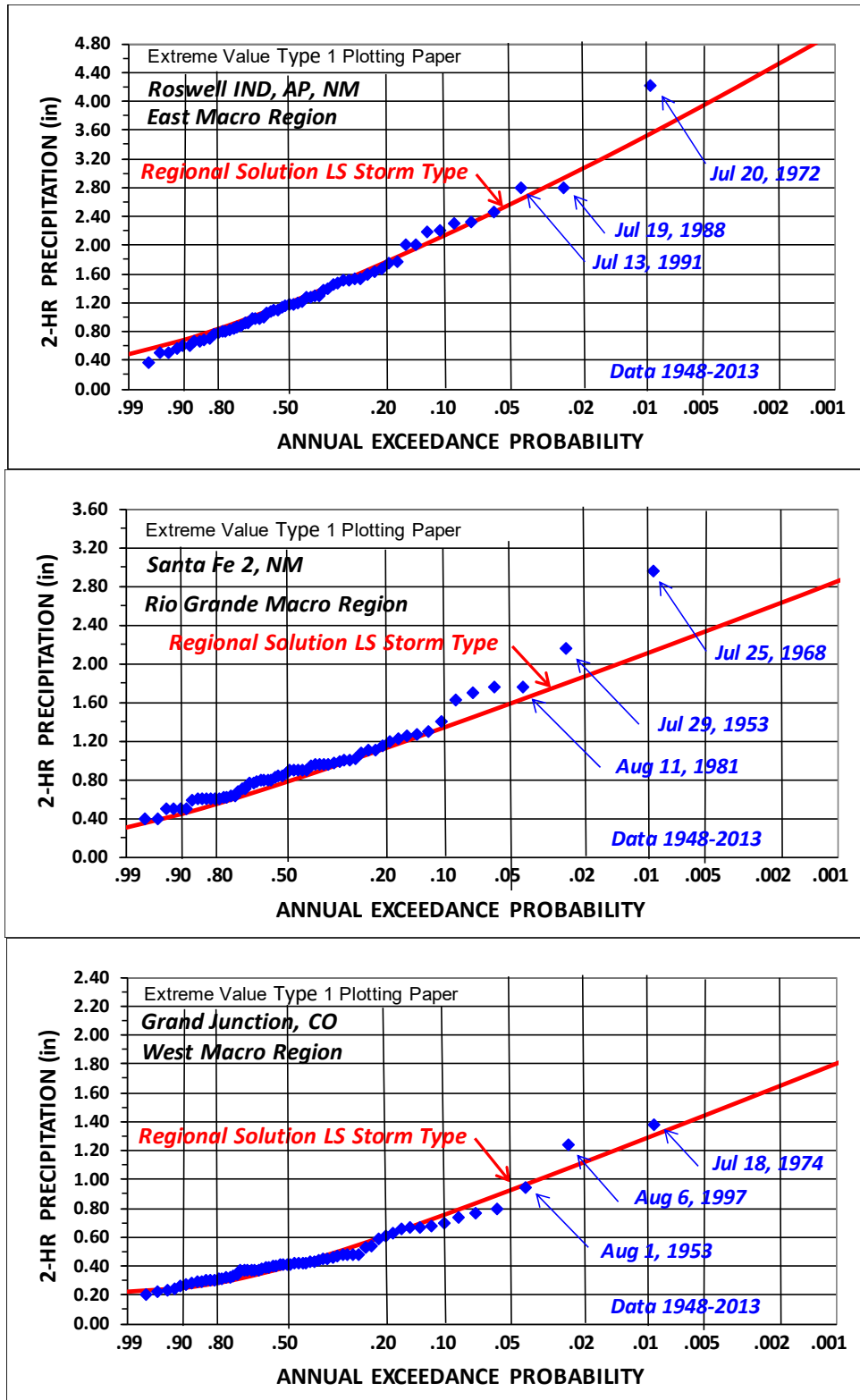


Figure 76. Probability plots of historical 2-hour precipitation annual maxima for Local Storm type for stations located in the three Macro Regions and comparison with regional precipitation-frequency relationship for those locations

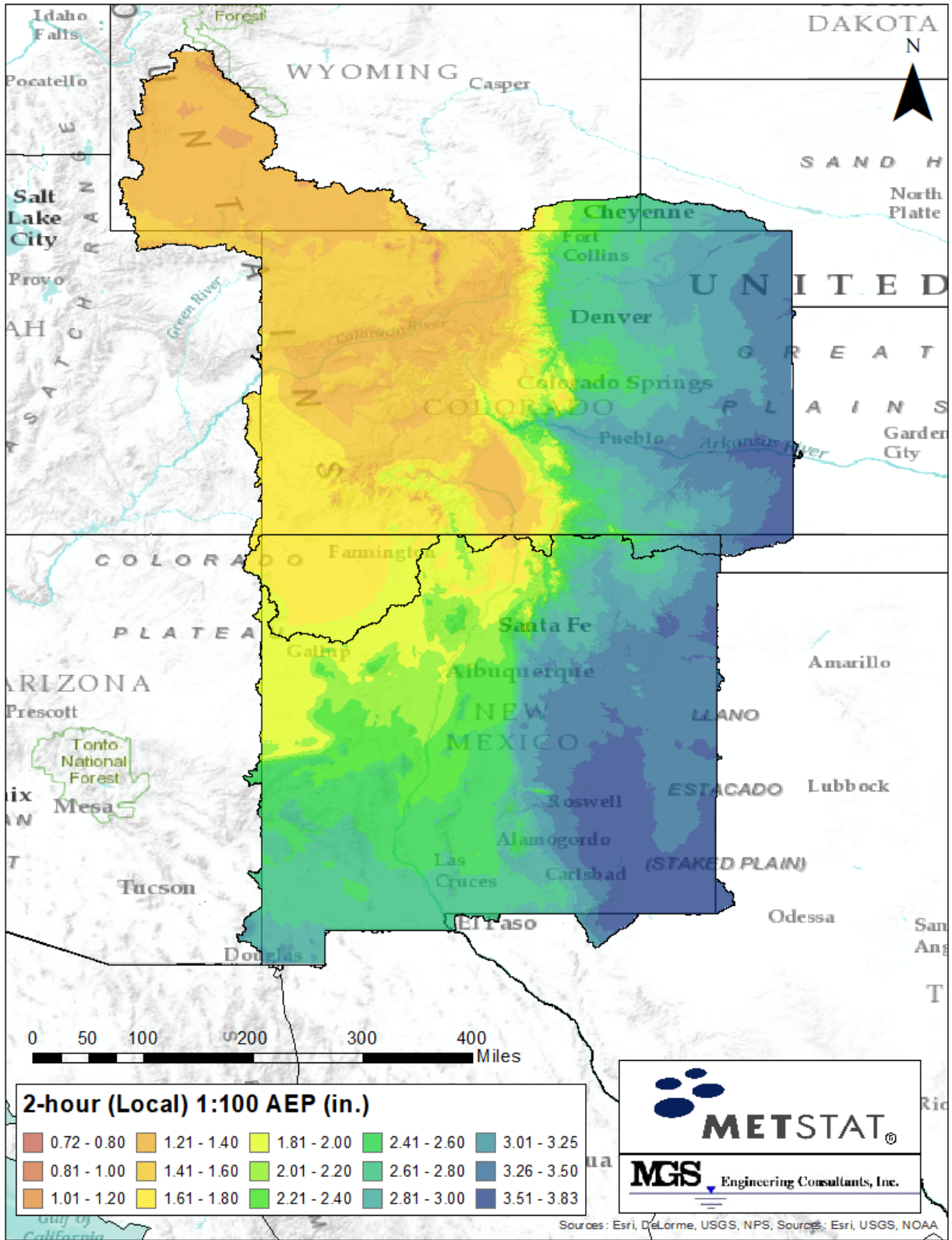


Figure 77. Isopluvial map of 2-hour precipitation maxima for an AEP of 1:100 for Local Storms

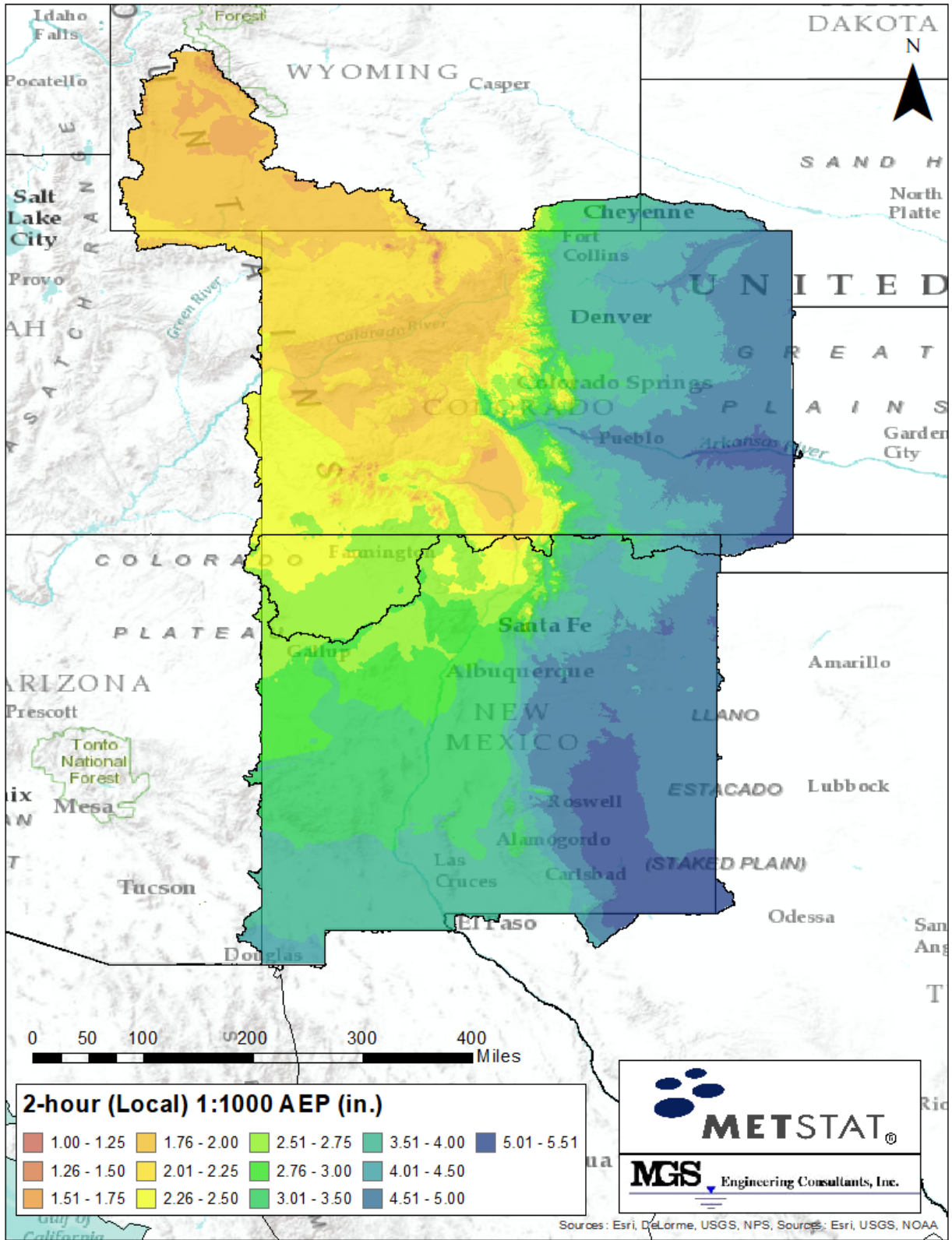


Figure 78. Isopluvial map of 2-hour precipitation maxima for an AEP of 1:1000 for Local Storms

**5.1.2.5. Seasonality of Extreme Storms for Local Storms**

The storm seasonality analyses for the LS storm type was conducted using the 50 rarest storm events for each of the five Seasonality Sub-areas as described in Section 4.8. The South-West Seasonality Sub-area had only 35 storms due to the relative low station density in that sub-area. Frequency histograms representing the seasonality of the rarest 2-hour duration Local Storms in each of the five Seasonality Sub-areas are shown in Figure 79.

# CO-NM Regional Extreme Precipitation Study

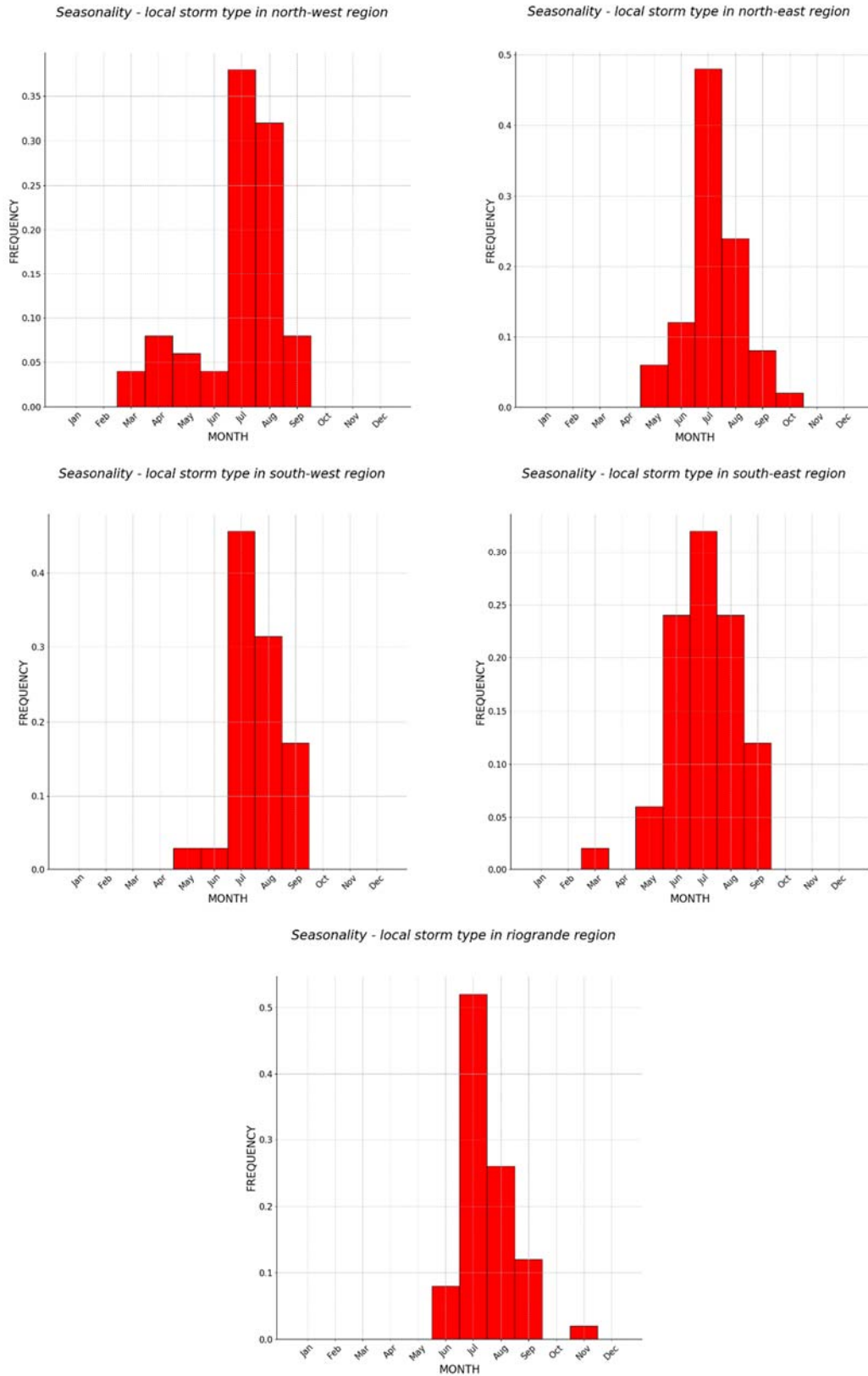


Figure 79. Frequency histograms for seasonality of extreme 2-hour duration Local Storms

**5.1.2.6. Validation of Findings and Equivalent Independent Record Length (EIRL) for Local Storms**

EIRL was estimated by counting the number of physically independent storm events as described in Section 4.4.5. This resulted in an EIRL estimate of 11,462 years (Table 25). The high fraction of EIRL to the station-years of record is attributable to the localized areal coverage of local storms and the low density of automated stations.

*Table 25. Estimate of EIRL for 2-Hour duration for Local Storms*

Station-Years of Record	EIRL Estimates (Years) as Storm Count	EIRL Percent of Station-Years
15,527	11,462	73.8%

The Binomial Distribution (Equation 8), can be used as a statistical check for comparing the actual number of exceedances versus the predicted number of exceedances to demonstrate the reasonableness of quantile estimates obtained from the regional PF analysis. Table 26, Table 27, and Table 28 show the results for the expected number of exceedances for the 1:100 and 1:1,000 AEPs for the LS storm type for the three Macro Regions. Comparisons of the number of predicted exceedances and that expected from the Binomial distribution show the number of exceedances from the quantile estimates are typically near expected values and within the 5<sup>th</sup> and 95<sup>th</sup> percentiles from the Binomial distribution. These results support the reasonableness of the solutions from the regional PF analysis.

*Table 26. Comparison of actual number of exceedances for selected with expected number from binomial distribution for Local Storm (LS) storm type for West Macro Region*

Record Length	# Stations	Station-Years	1:100 AEP Actual (Expected)	1:1,000 AEP Actual (Expected)
< 30	46	1,157	12 (12)	1 (1)
31-50	15	558	5 (6)	2 (1)
51-70	22	1,299	14 (13)	1 (1)
ALL	83	3,014	31 (30)	4 (3)
			21 - 30 - 40	0 - 3 - 6
			5 <sup>th</sup> Percentile - Mean - 95 <sup>th</sup> Percentile	

Table 27. Comparison of actual number of exceedances for selected AEPs with expected number from binomial distribution for Local Storm (LS) storm type for Rio Grande Macro Region

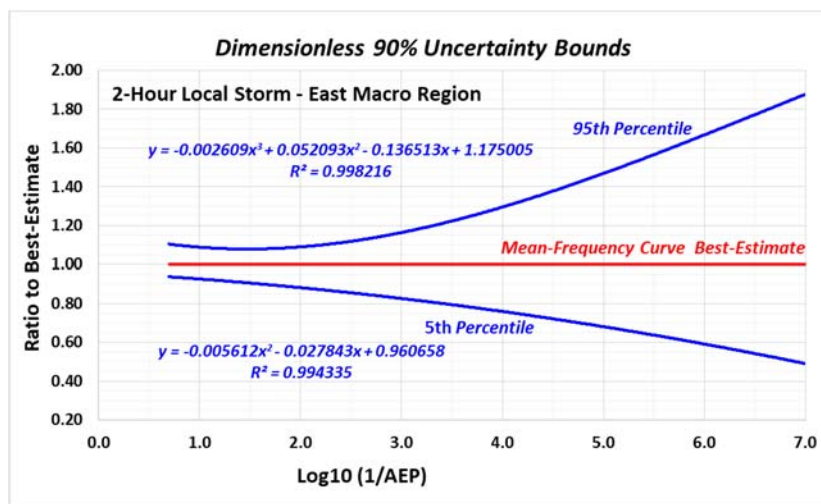
Record Length	# Stations	Station-Years	1:100 AEP Actual (Expected)	1:1,000 AEP Actual (Expected)
< 30	33	808	6 (8)	1 (1)
31-50	19	731	7 (7)	0 (1)
51-70	30	1,776	17 (18)	0 (1)
ALL	82	3,315	30 (33)	1 (3)
			23 - 33 - 43	0 - 3 - 6
			5 <sup>th</sup> Percentile - Mean - 95 <sup>th</sup> Percentile	

Table 28. Comparison of actual number of exceedances for selected AEPs with expected number from binomial distribution for Local Storm (LS) storm type for East Macro Region

Record Length	# Stations	Station-Years	1:100 AEP Actual (Expected)	1:1,000 AEP Actual (Expected)
< 30	58	1,410	12 (14)	1 (1)
31-50	31	1,207	15 (12)	0 (1)
51-70	83	5,031	47 (50)	4 (5)
ALL	172	7,648	74 (76)	5 (8)
			58 - 76 - 87	3 - 8 - 11
			5 <sup>th</sup> Percentile - Mean - 95 <sup>th</sup> Percentile	

5.1.2.7. Dimensionless Uncertainty Bounds for LS Storm Type

Dimensionless 90 percent uncertainty bounds for the point LS estimates are depicted in Figure 80 for each Macro Region. Polynomial equations were fitted to the uncertainty bounds for use in the MetPortal tool where x is equal to log<sub>10</sub>(1/AEP), and y is a dimensionless ratio to the best estimate. To compute the AEP of the 90 percent upper (or lower bound), compute the ratio to the best-estimate, then multiply it by the best estimate for a selected AEP.



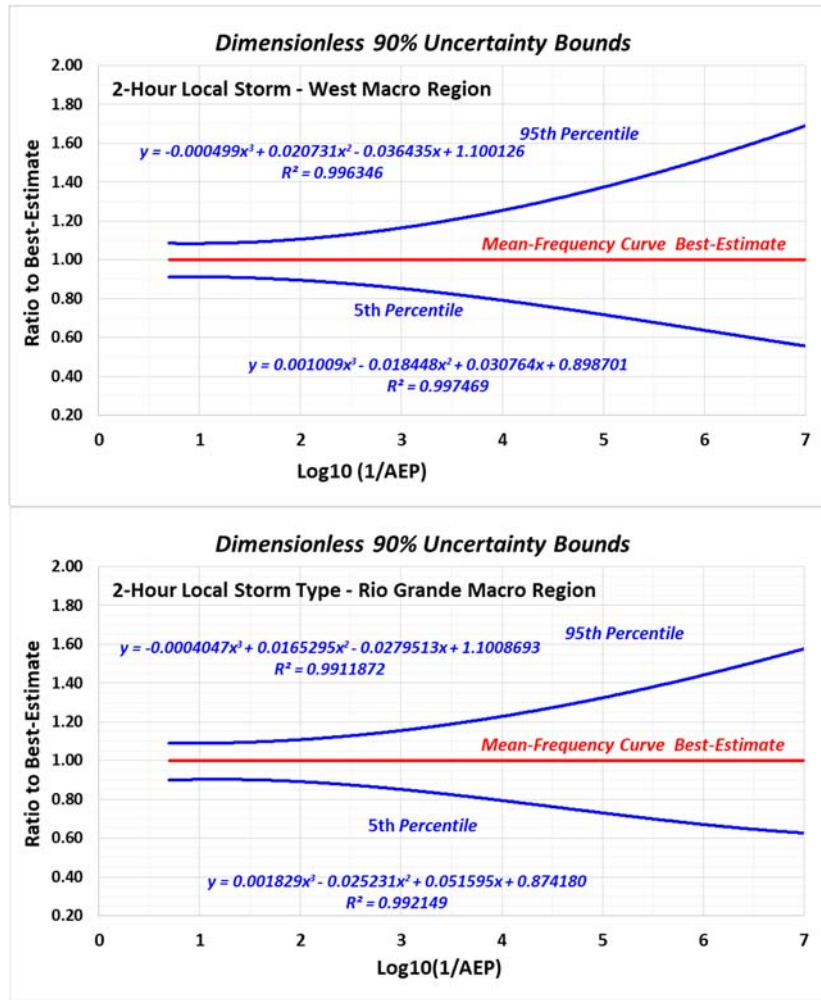


Figure 80. Probability graphics depicting magnitude of dimensionless uncertainty bounds for point LS precipitation-frequency estimates

### 5.1.3 6-hour Mesoscale Storms with Embedded Convection

Hourly stations were used in the regional analyses for 6-hour precipitation annual maxima for MEC Storms where stations with 20 years or more of record were included in the analyses (Figure 81). Table 29 provides a listing of the number of stations and total number of data years used in the analysis of MEC Storms, and Figure 82 depicts a histogram of the number of data years.

Given the nature of convective events in the project area, it was reasonable to anticipate there would be similarity in the behavior of L-moment statistics for the 6-hour MEC and 2-hour LS storm types, particularly in the intermountain areas. Predictor equations for the MEC storm type in the West and Rio Grande Macro Regions were developed based upon the findings for the 2-hour Local Storm analysis. MEC development over the foothills and plains of the East Macro Region, however, is more pronounced and required careful scrutiny.

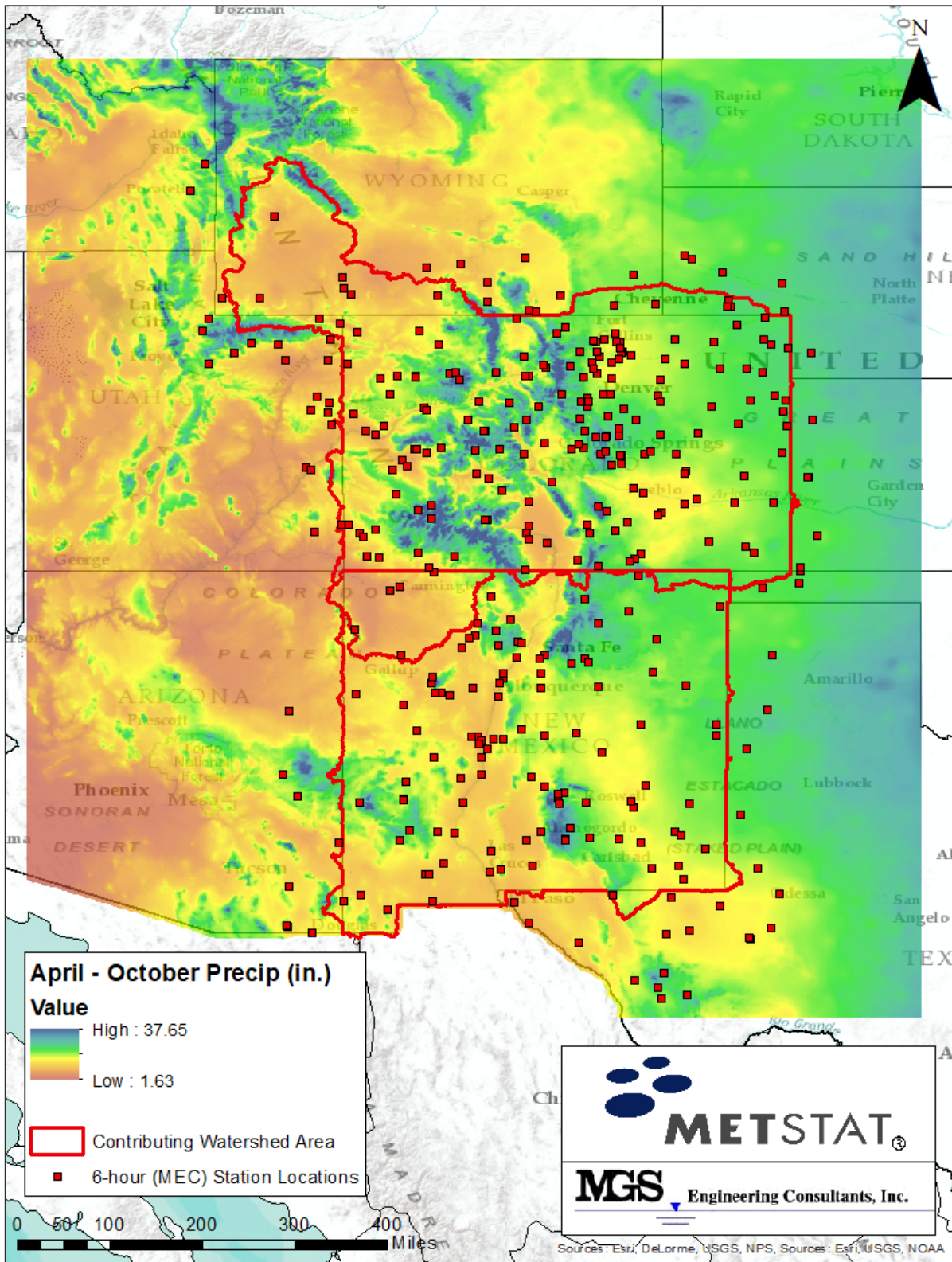


Figure 81. Location of hourly precipitation stations used in the precipitation-frequency analysis for MECs and the seasonal mean precipitation used in the predictor equations

Table 29. Number of Stations and data years for stations with 20 or more data years used in the precipitation-frequency analysis for MECs

PRECIPITATION GAUGE TYPE	NUMBER OF STATIONS/GAUGES	TOTAL STATION DATA YEARS	AVERAGE STATION DATA YEARS
Hourly Stations	347	15,731	39

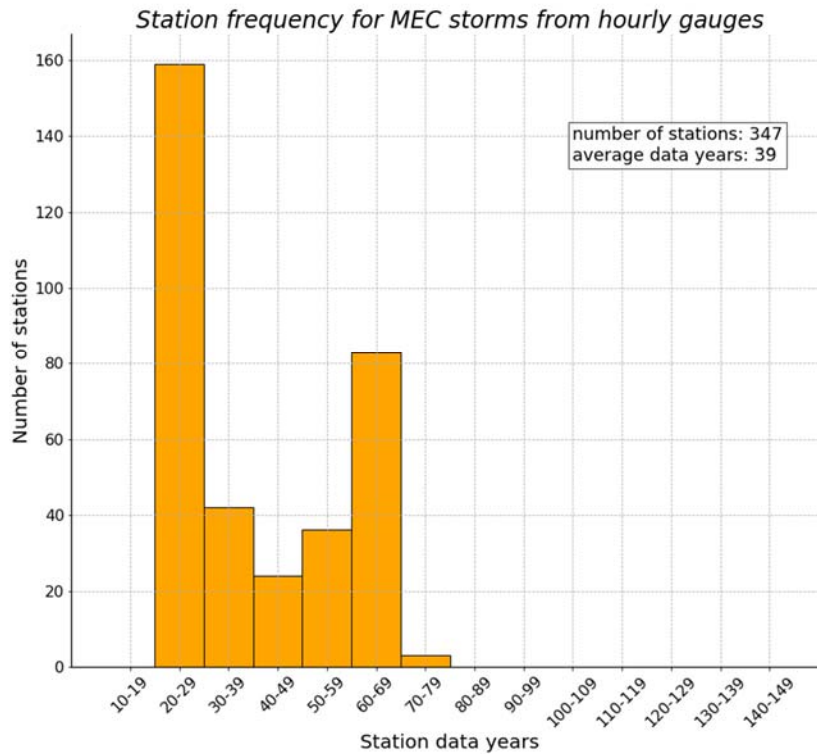


Figure 82. Histogram of data years for stations used in the precipitation-frequency analysis for MECs

5.1.3.1. At-Site Means - MEC

Over the Colorado-New Mexico domain, it was found that the 2-hour at-site mean ranges from approximately 70 percent of the 6-hour at-site mean values in the east to over 90 percent in the west, indicating a strong correlation between the 2-hour and 6-hour annual maxima time series. In addition, comparison of temporal patterns for MEC suggested that the majority of precipitation for MEC events falls within a 2-hour timeframe.

As such, spatial mapping of 6-hour at-site means for MEC Storms was conducted using gridded values of 2-hour Local Storm means as the explanatory variable. The explanatory variables for the 2-hour at-site means for Local Storms were elevation, latitude, and gridded values of April through October mean monthly precipitation (Daly 1994). This choice was made after reviewing the behavior of the relationship of at-site 6-hour MEC means with at-site 2-hour LS means. The mean monthly precipitation for April through October is shown in Figure 81 and includes the warmer months when MEC Storms Types are more likely. Figure 83 depicts the scatter plot of the observed 6-hour at-site means with the mapped means; stations with the widest scatter from the line of equality are stations with short periods of record.

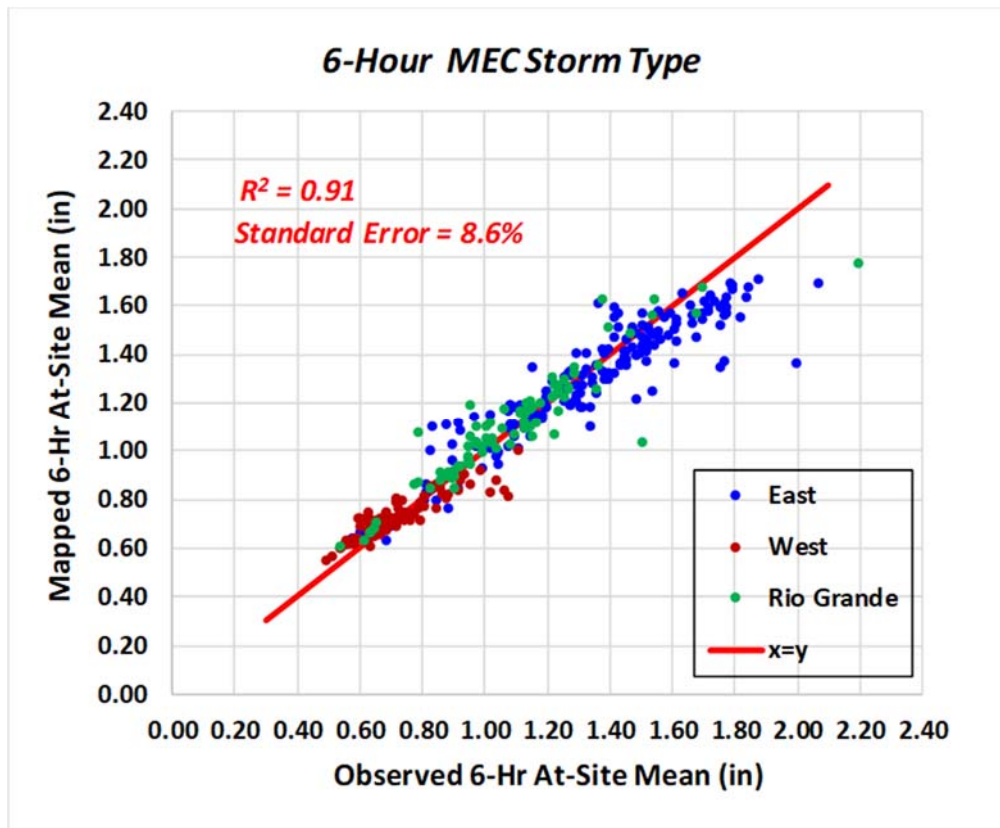


Figure 83. Scatter plot of the observed 6-hour MEC at-site means with the mapped at-site means

Stations were grouped using the previously delineated Macro Regions (East, West, and Rio Grande) for analysis. Generalized additive model concepts were used in developing predictor equations for the at-site mean at the collection of stations. The resulting root-mean-square-error (RMSE) for the predictor equations are shown in Table 30. Resultant multiple linear regression equations were then used to generate the mapped values of 6-hour at-site means. Best estimates of the at-site means were computed as a weighted-average of the station-sample values and regression-predicted values, as discussed in Section 4.4.3. The relative RMSE drops from 8.6 percent to 7.0 percent for the more reliable station sample mean values with more than 25-years of record.

Table 30. Listing of explanatory variables for 6-hour at-site means for MECs and RMSE for predictive equations

Mapping Area	Explanatory Variables	RMSE
East Macro Region	2-hour at-Site Local Storms Mean	9.1%
West Macro Region	2-hour at-Site Local Storms Mean	8.2%
Rio Grande Macro Region	2-hour at-Site Local Storms Mean	8.0%

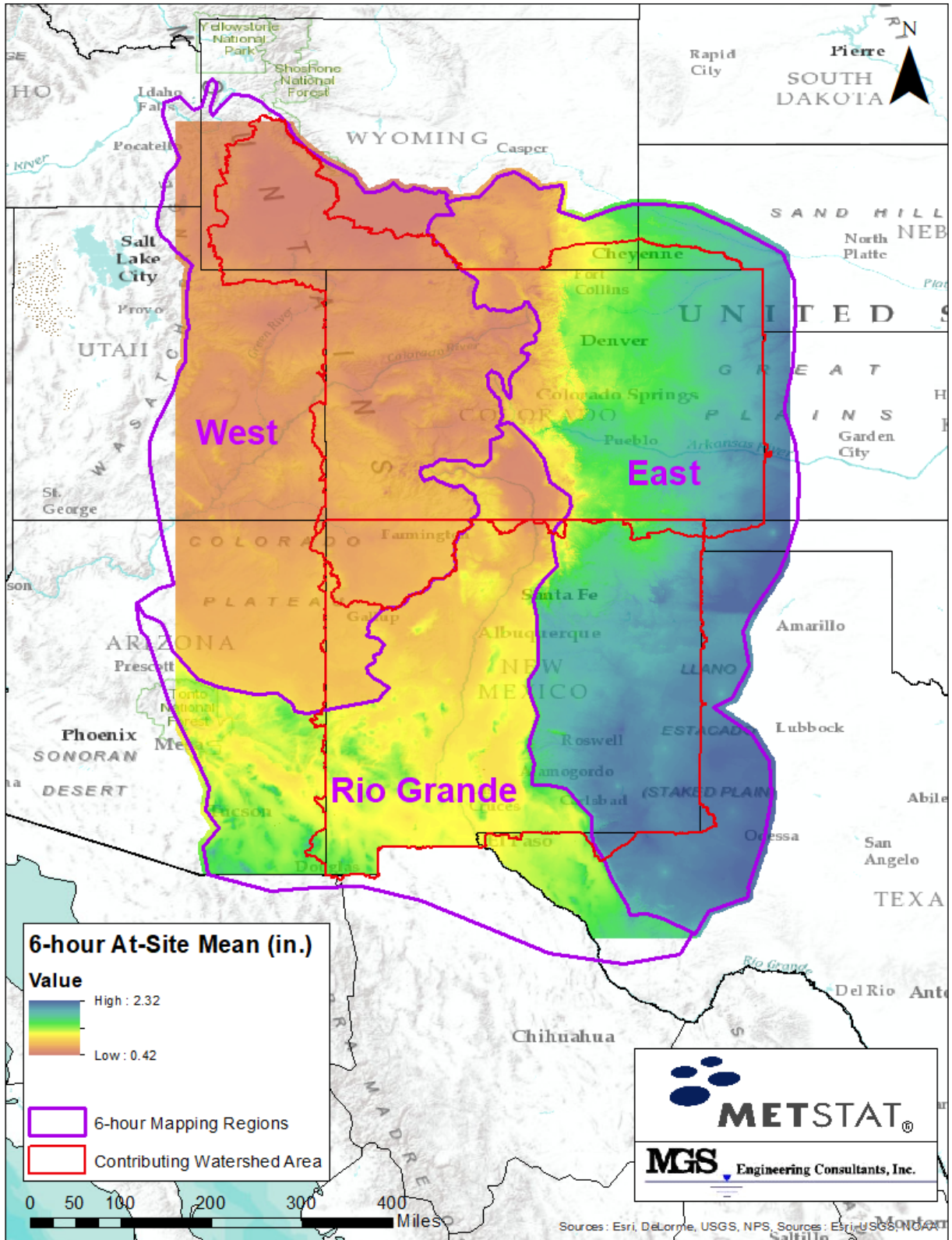


Figure 84. Map of at-site means for 6-hour duration for MECs

**5.1.3.2. Regional L-Cv and L-Skewness - MEC**

As described earlier, the predictor equations for the 6-hour MEC L-Cv and L-Skewness in the West and Rio Grande Macro Regions were based on the 2-hour Local Storm analysis. For those two Macro Regions the predictor variable was the 2-hour LS L-Cv and L-Skewness.

The East Macro Region, however, required closer inspection because MEC storms can meteorologically develop over the plains. For this Macro Region, a review of the regional L-Cv values showed a systematic variation with latitude and mean seasonal March through November precipitation. Table 31 lists the number of homogeneous sub-regions used to form of the multiple regressions for regional L-Cv for each designated Mapping Area (the Macro Regions in this case) and resultant RMSE values. Figure 85 depicts a comparison of observed and mapped values of regional L-Cv for the 6-hour precipitation annual maxima.

*Table 31. Listing of number of homogeneous sub-regions for each mapping area (the Macro Regions in this case) for 6-hour L-Cv for MEC Storms and RMSE for predictive equations*

Mapping Area	Number of Homogeneous Sub-Regions	RMSE
East	16	4.8%
West	7	3.5%
Rio Grande	8	3.0%

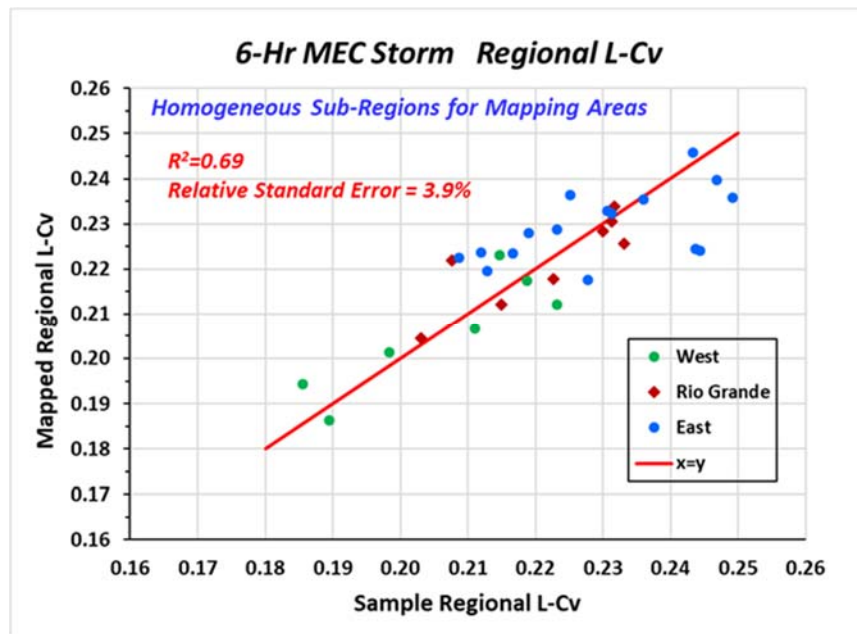


*Figure 85. Comparison of observed regional L-Cv and mapped regional L-Cv for 6-hour duration for homogeneous sub-regions for MEC Storms*

Development of predictor equations for L-Skewness is more difficult than for L-Cv because of the naturally high sampling variability for skewness measures. The prediction of regional L-Skewness was accomplished using linear regression with LS (2-hour) L-Skewness for 31 homogeneous sub-regions grouped into the three Macro Regions, as described in Table 32. The spatial mapping of regional L-Cv used for the 6-hour duration is shown in Figure 86 and Figure 87 shows the spatial mapping of regional L-Skewness.

Summary statistics for both L-Cv and L-Skewness are shown in Table 33.

*Table 32. Listing of number of homogeneous sub-regions for each mapping area (the Macro Regions in this case) for 6-hour L-Skewness for MEC Storms and RMSE for predictive equations*

Mapping Area	Number of Homogeneous Sub-Regions	RMSE
East	16	14.6%
West	7	11.6%
Rio Grande	8	6.4%

*Table 33. Summary statistics for spatial mapping of 6-hour duration regional L-Cv and L-Skewness for MECs within contributing watershed area*

L-MOMENT RATIO	RANGE OF MAPPED L-MOMENT RATIO	STANDARD DEVIATION OF RESIDUALS	RMSE
Regional L-Cv	$0.1690 \leq L-Cv \leq 0.2523$	0.0062	3.3%
Regional L-Skewness	$0.1932 \leq L-Skewness \leq 0.2937$	0.0184	9.8%

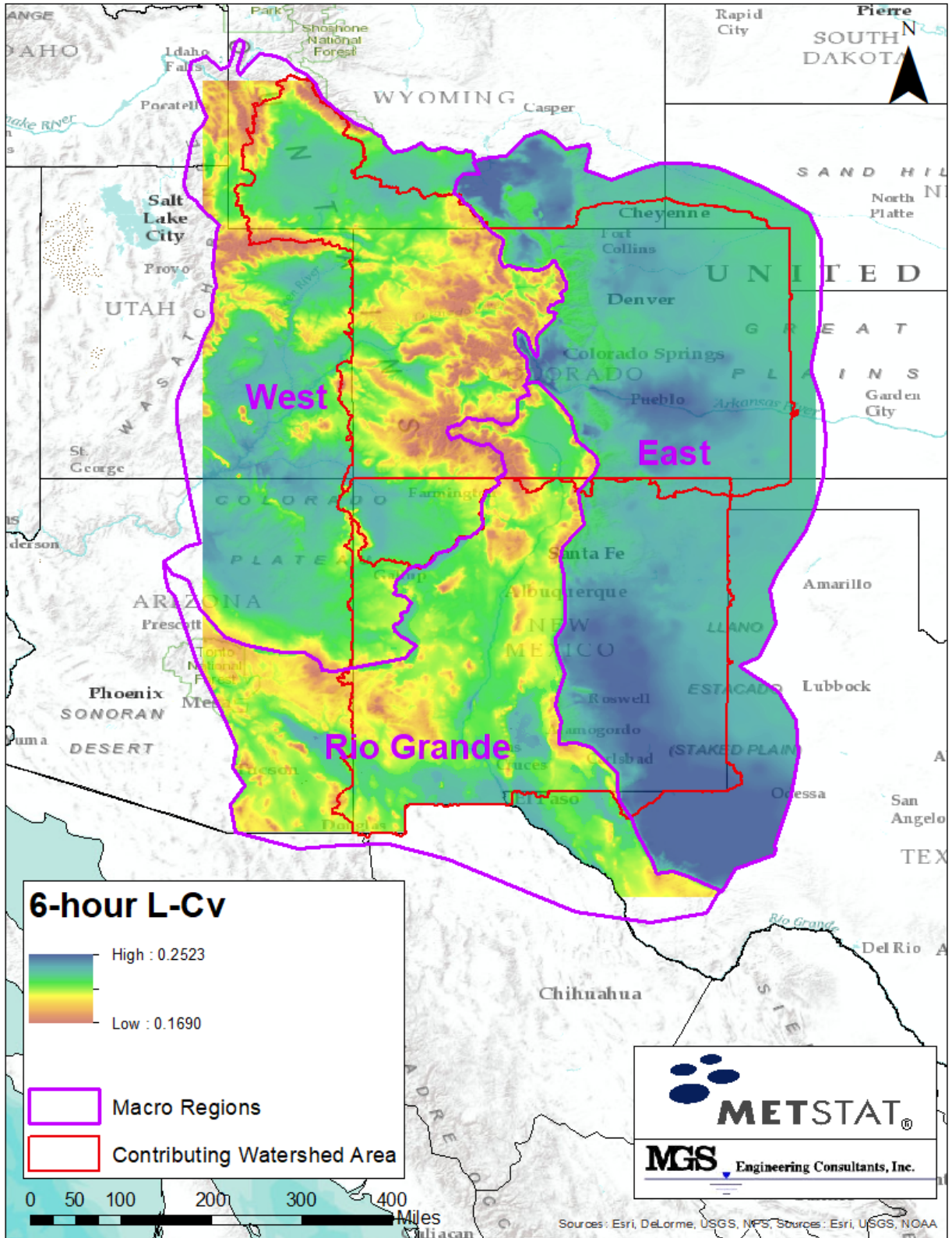


Figure 86. Map of regional L-Cv for 6-hour duration for MECs

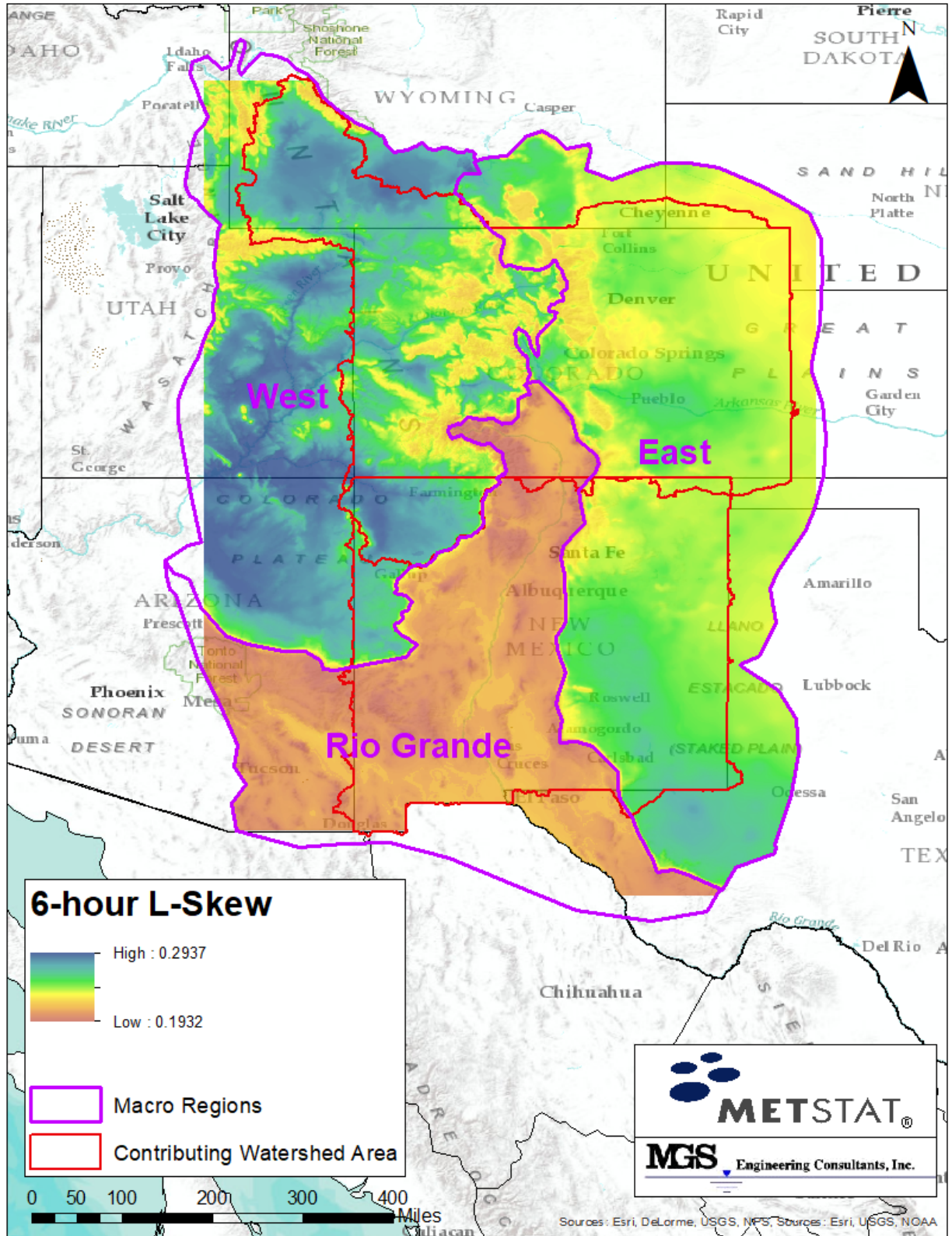


Figure 87. Map of regional L-Skewness for 6-hour precipitation annual maxima for MECs

#### 5.1.3.3. Identification of Regional Probability Distribution - MEC

The 2-hour Local Storm analysis identified the GEV distribution as the best-fit 3-parameter probability distribution for the collection of 37 homogeneous sub-regions using L-moment goodness-of-fit tests; this was also applied for the MEC storm type. The 4-parameter Kappa distribution with a fixed shape parameter ( $h$ , *Hondo*) emulates the GEV and near-GEV distributions and was selected for describing the point precipitation-frequency relationships for MECs. Varying the Hondo parameter for the 4-parameter Kappa distribution offers the important ability to account for uncertainty in identification of the regional probability distribution which is needed as part of uncertainty analyses for developing watershed PF relationships. For these reasons, the 4-parameter kappa distribution was selected for describing the point precipitation-frequency relationships for MEC storms.

Similar to the Local Storm findings, Hondo values were found to spatially vary for large values of L-Skewness. This behavior is related to the situation where in some years there are very few MEC storms of significance in arid and semi-arid climates from which the annual maxima are selected. This results in increases in L-Cv and L-Skewness without significant changes to the shape of the upper portion of the point PF relationship. This behavior arises as a result of Hondo becoming increasingly positive as L-Skewness increases in arid and semi-arid climates. Accordingly, a predictor equation for Hondo was developed for all three Macro Region using L-Skewness as the explanatory variable. Figure 88 depicts the spatial variability of Hondo for the MEC storm type.

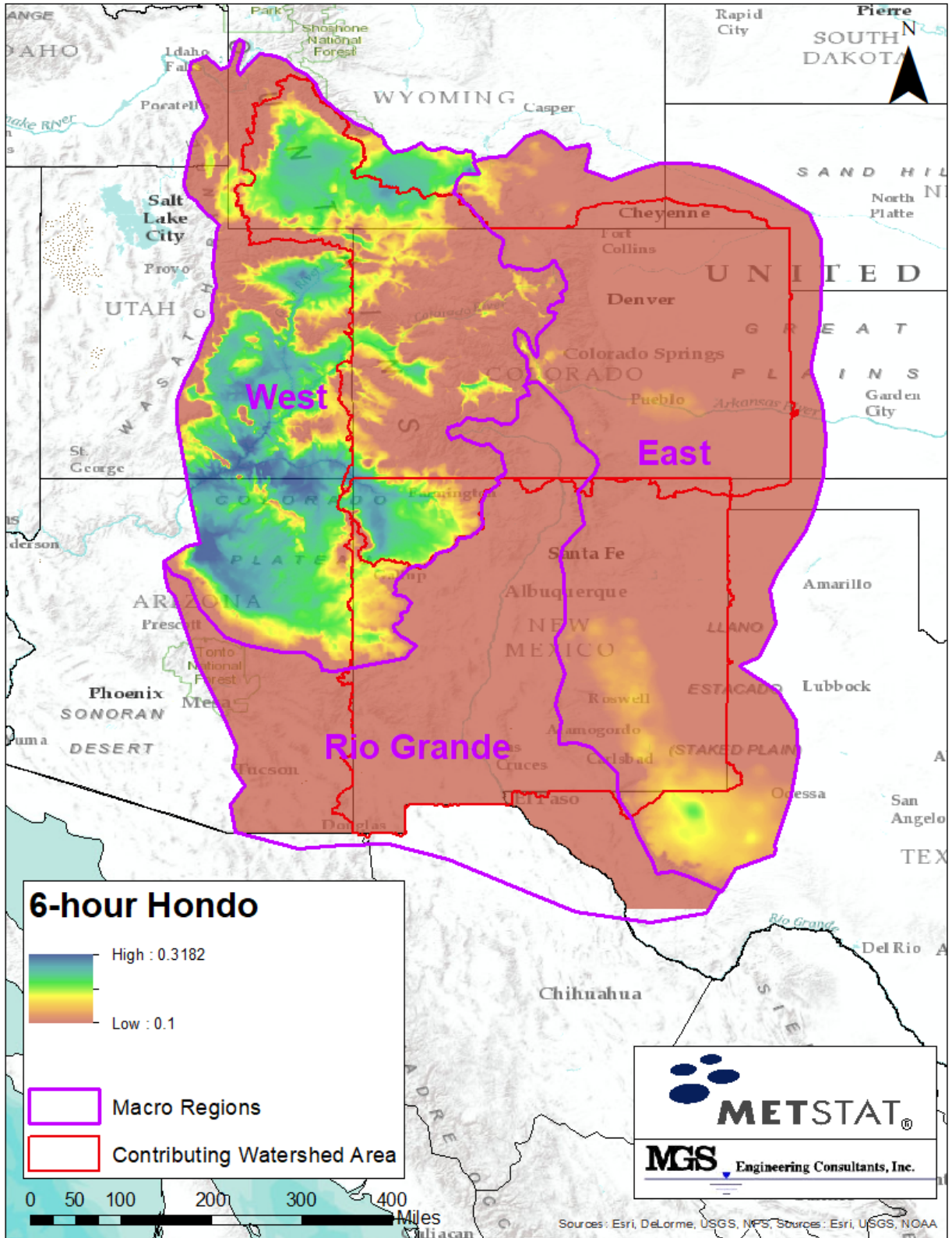


Figure 88. Map of regional Hondo for 6-hour precipitation annual maxima for MECs

#### 5.1.3.4. Point Precipitation-Frequency MEC Storm Type

Point precipitation-frequency estimates for the MEC storm type can be obtained for any location in the study area using the gridded datasets of spatially mapped L-Moment statistics. Specifically, distribution parameters for the Kappa distribution are solved using grid-cell specific values of the 6-hour at-site mean (Figure 84), regional L-Cv (Figure 86), regional L-Skewness (Figure 87), and regional Hondo (Figure 88). This process is repeated for each grid-cell and the inverse CDF for the Kappa distribution (Equation 2) is used to compute quantile estimates for selected Annual Exceedance Probabilities (AEPs).

The 2-hour LS and 6-hour MEC convective storms are similar in nature and their precipitation-frequency estimates were developed independently. Inconsistencies can arise in spatial mapping where estimated 2-hour magnitudes can be greater than 6-hour magnitudes for rare AEPs in some grid-cells due to sampling variability associated with both datasets. This situation did occur in some transition areas between Mapping Areas and in some sparsely gaged mountainous terrain. Minor adjustments were made to L-Cv and L-Skewness grid-cell values to provide consistency in quantile estimates for rare AEPs across the project area. Specifically, adjustments were made in grid-cells where the 6-hour/2-hour values for a given AEP were less than 1.02. Iterations were conducted by incrementing L-Cv and L-Skewness on those grid-cells to yield consistency where the 6-hour precipitation value exceed the 2-hour value. This was done primarily in transition areas between the West and Rio Grande Macro Regions and represented less than 2% of the project area.

A precipitation-frequency curve has been developed for a station in each Macro Region in the manner described above and compared with a probability plot of historical data (Figure 89). These comparisons provide an example of the general shape of the precipitation-frequency relationship for MEC storm types and the general goodness-of-fit to stations with long-term records.

Isopluvial gridded datasets were generated for AEPs of 0.9, 0.5, .05, .02,  $10^{-1}$ ,  $10^{-2}$ ,  $10^{-3}$ ,  $10^{-4}$ ,  $10^{-5}$ ,  $10^{-6}$ , and  $10^{-7}$ . Figure 90 and Figure 91 show example isopluvial maps for AEPs of 1:100 and 1:1,000, respectively.

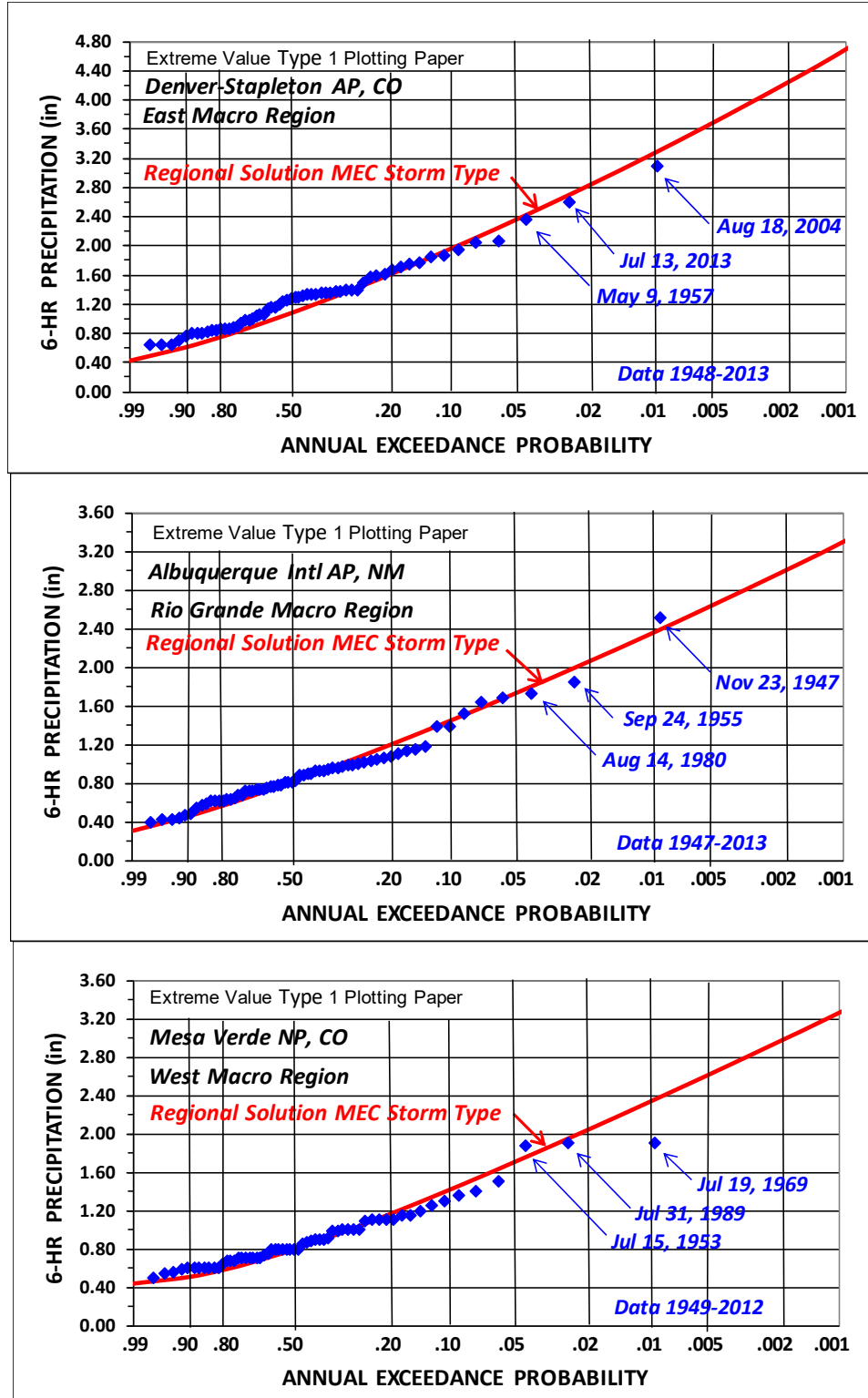


Figure 89. Probability plots of historical 6-hour precipitation annual maxima for MEC storm type for stations located in the three Macro Regions and comparison with regional precipitation-frequency relationship for those locations

CO-NM Regional Extreme Precipitation Study

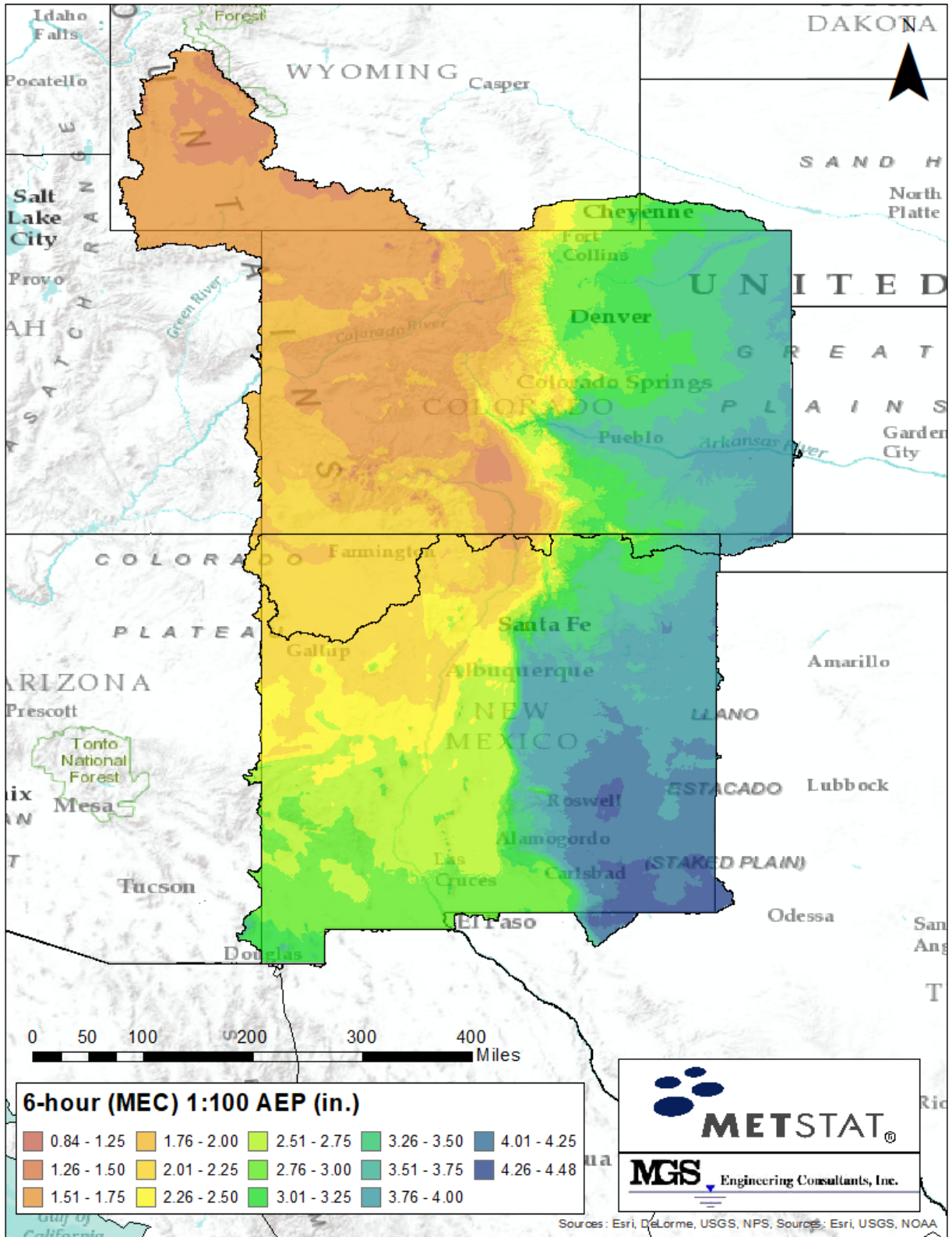


Figure 90. Isopluvial map of 6-hour precipitation maxima for an AEP of 1:100 for MECs

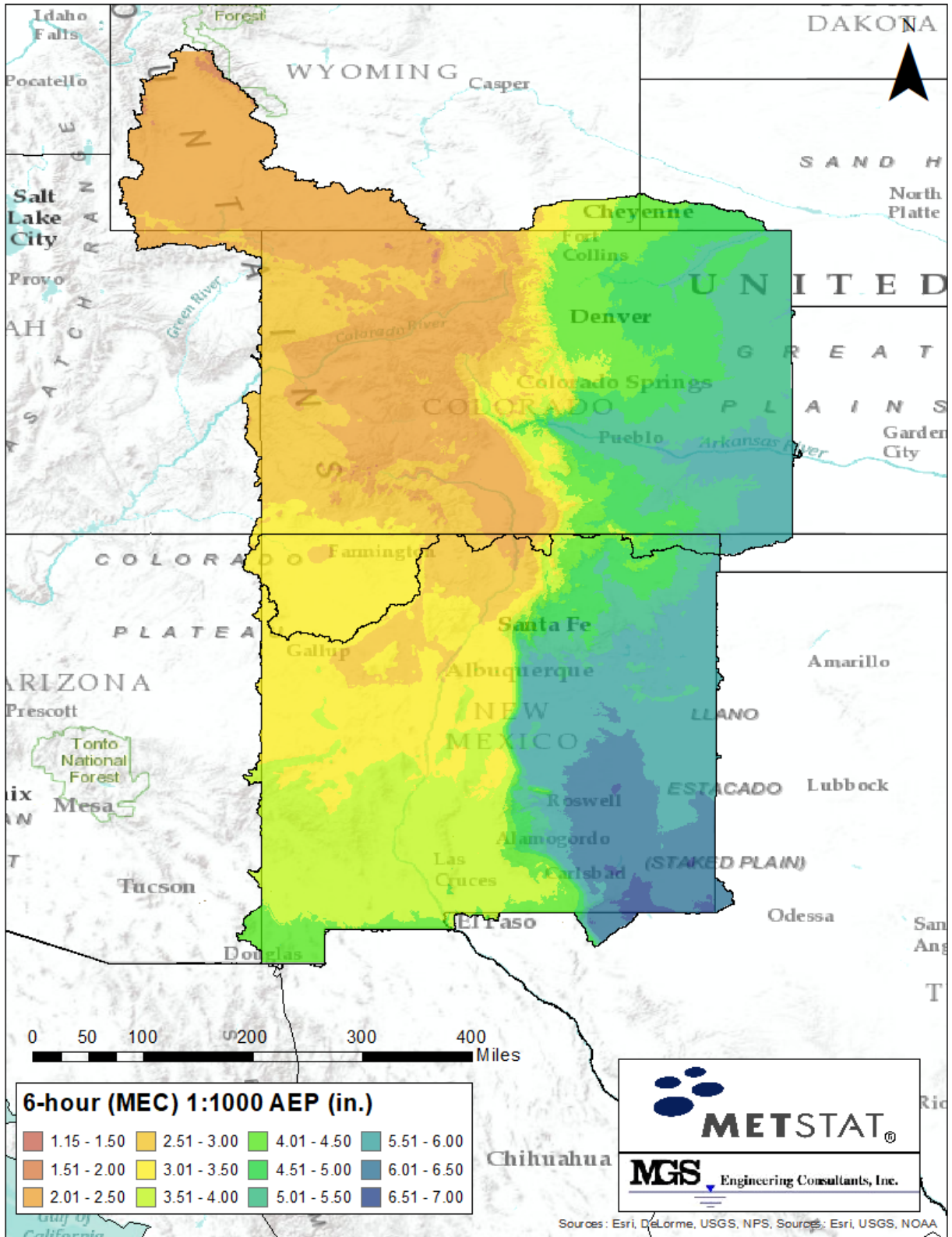


Figure 91. Isopluvial map of 6-hour precipitation maxima for an AEP of 1:1000 for MECs

**5.1.3.5. Seasonality of Extreme Storms for Mesoscale Storms with Embedded Convection**

The storm seasonality analyses for the MEC storm type was conducted using the 50 rarest storm events for each of the five Seasonality Sub-areas as described in Section 4.8. The South-West and North-West Seasonality Sub-areas had a sample size of 23 and 46 storms, respectively, where the small sample size was due to the low station density in those sub-areas.

Frequency histograms for the seasonality of extreme 6-hour duration MEC storms in each of the five Seasonality Sub-areas are shown in Figure 92.

# CO-NM Regional Extreme Precipitation Study

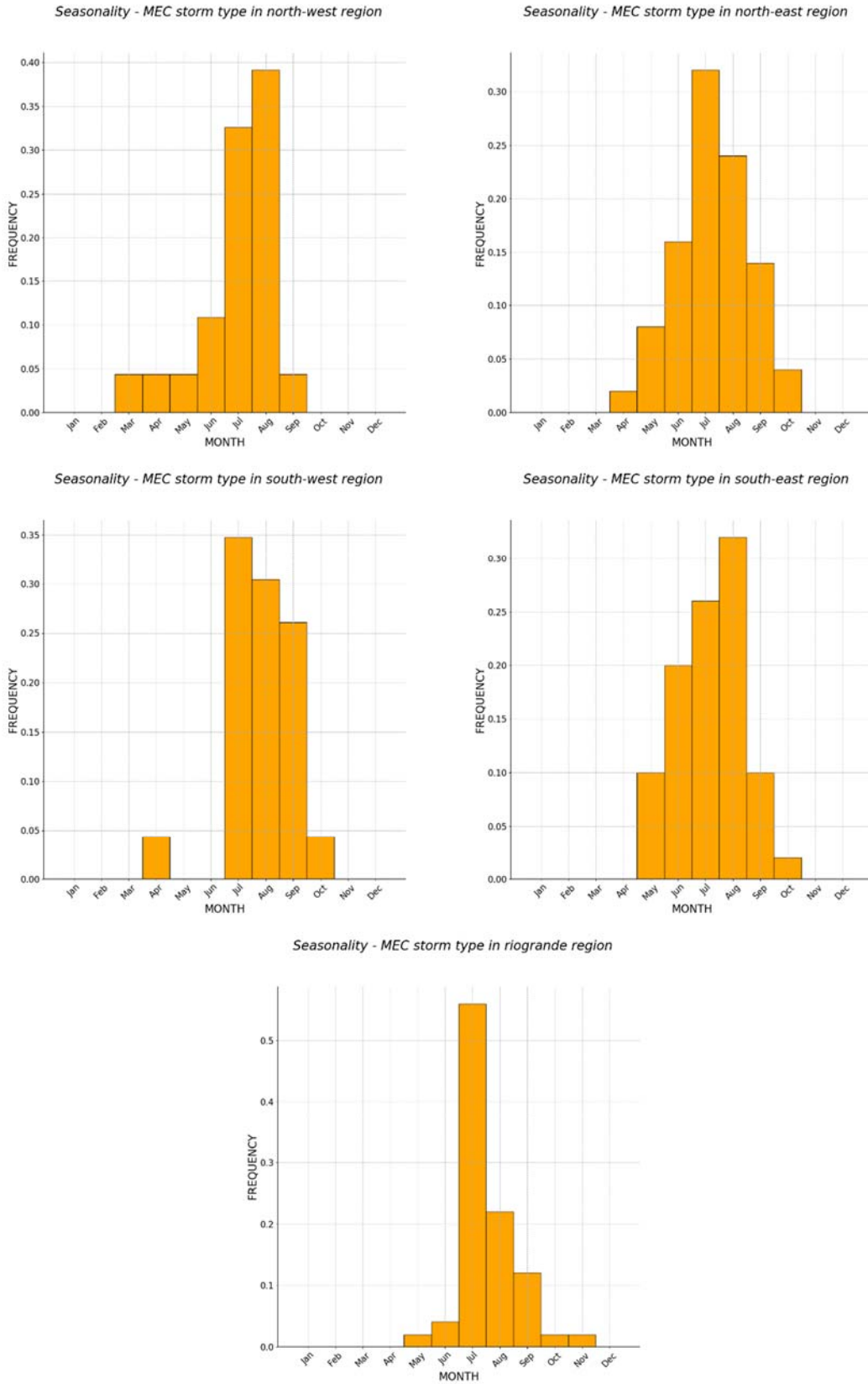


Figure 92. Frequency histograms for seasonality of extreme 6-hour duration MECs

**5.1.3.6. Validation of Findings and Equivalent Independent Record Length (EIRL) for Mesoscale Storms with Embedded Convection**

EIRL was estimated by counting the number of physically independent storm events as described in Section 4.4.5. This resulted in an EIRL estimate of 12,517 years (Table 34). As was the case for Local Storms, the high fraction of EIRL to the station-years of record is attributable to the generally localized areal coverage of the high intensity area of MEC storms and the low density of automated stations.

*Table 34. Estimate of EIRL for 6-Hour duration for MECs*

Station-Years of Record	EIRL Estimates (Years) as Storm Count	EIRL Percent of Station-Years
15,731	12,517	79.6%

The Binomial Distribution (Equation 8), can be used as a statistical check for comparing the actual number of exceedances versus the predicted number of exceedances to demonstrate the reasonableness of quantile estimates obtained from the regional PF analysis. Table 35, Table 36, and Table 37 show the results for the expected number of exceedances for the 1:100 and 1:1,000 AEPs for the MEC storm type for the three Macro Regions. Comparisons of the number of predicted exceedances and that expected from the Binomial distribution show the number of exceedances from the quantile estimates are typically near expected values and within the 5<sup>th</sup> and 95<sup>th</sup> percentiles from the Binomial distribution. These results support the reasonableness of the solutions for the MEC storm type obtained from the regional PF analysis.

*Table 35. Comparison of actual number of exceedances for selected AEPs with expected number from binomial distribution for Mesoscale Storm with Embedded Convection (MEC) storm type for West Macro Region*

Record Length	# Stations	Station-Years	1:100 AEP Actual (Expected)	1:1,000 AEP Actual (Expected)
< 30	50	1,264	11 (13)	1 (1)
31-50	14	523	4 (5)	1 (1)
51-70	22	1,331	14 (13)	2 (1)
ALL	86	3,118	29 (31)	4 (3)
			22 - 31 - 41	0 - 3 - 6
			5 <sup>th</sup> Percentile - Mean - 95 <sup>th</sup> Percentile	

Table 36. Comparison of actual number of exceedances for selected AEPs with expected number from binomial distribution for Mesoscale Storm with Embedded Convection (MEC) storm type for Rio Grande Macro Region

Record Length	# Stations	Station-Years	1:100 AEP Actual (Expected)	1:1,000 AEP Actual (Expected)
< 30	37	903	12 (9)	2 (1)
31-50	19	758	7 (8)	0 (1)
51-70	29	1,743	19 (17)	1 (2)
ALL	85	3,404	38 (34)	3 (3)
			24 - 34 - 44	0 - 3 - 6
			5 <sup>th</sup> Percentile - Mean - 95 <sup>th</sup> Percentile	

Table 37. Comparison of actual number of exceedances for selected AEPs with expected number from binomial distribution for Mesoscale Storm with Embedded Convection (MEC) storm type for East Macro Region

Record Length	# Stations	Station-Years	1:100 AEP Actual (Expected)	1:1,000 AEP Actual (Expected)
< 30	62	1,498	16 (15)	1 (1)
31-50	31	1,230	12 (12)	2 (1)
51-70	83	5,044	42 (50)	3 (5)
ALL	176	7,772	70 (78)	6 (8)
			63 - 78 - 93	3 - 8 - 12
			5 <sup>th</sup> Percentile - Mean - 95 <sup>th</sup> Percentile	

5.1.3.7. Dimensionless Uncertainty Bounds for MEC Storm Type

Dimensionless 90 percent uncertainty bounds for the point MEC estimates are depicted in Figure 93. Probability graphics depicting magnitude of dimensionless uncertainty bounds for point MEC precipitation-frequency estimates for each Macro Region. Polynomial equations were developed for the 90 percent uncertainty bounds for the MetPortal tool where x is equal to  $\log_{10}(1/AEP)$ , and y is a dimensionless ratio to the best estimate. To compute the AEP of the 90 percent upper (or lower bound), compute the ratio to the best-estimate, then multiply it by the best estimate for a selected AEP.

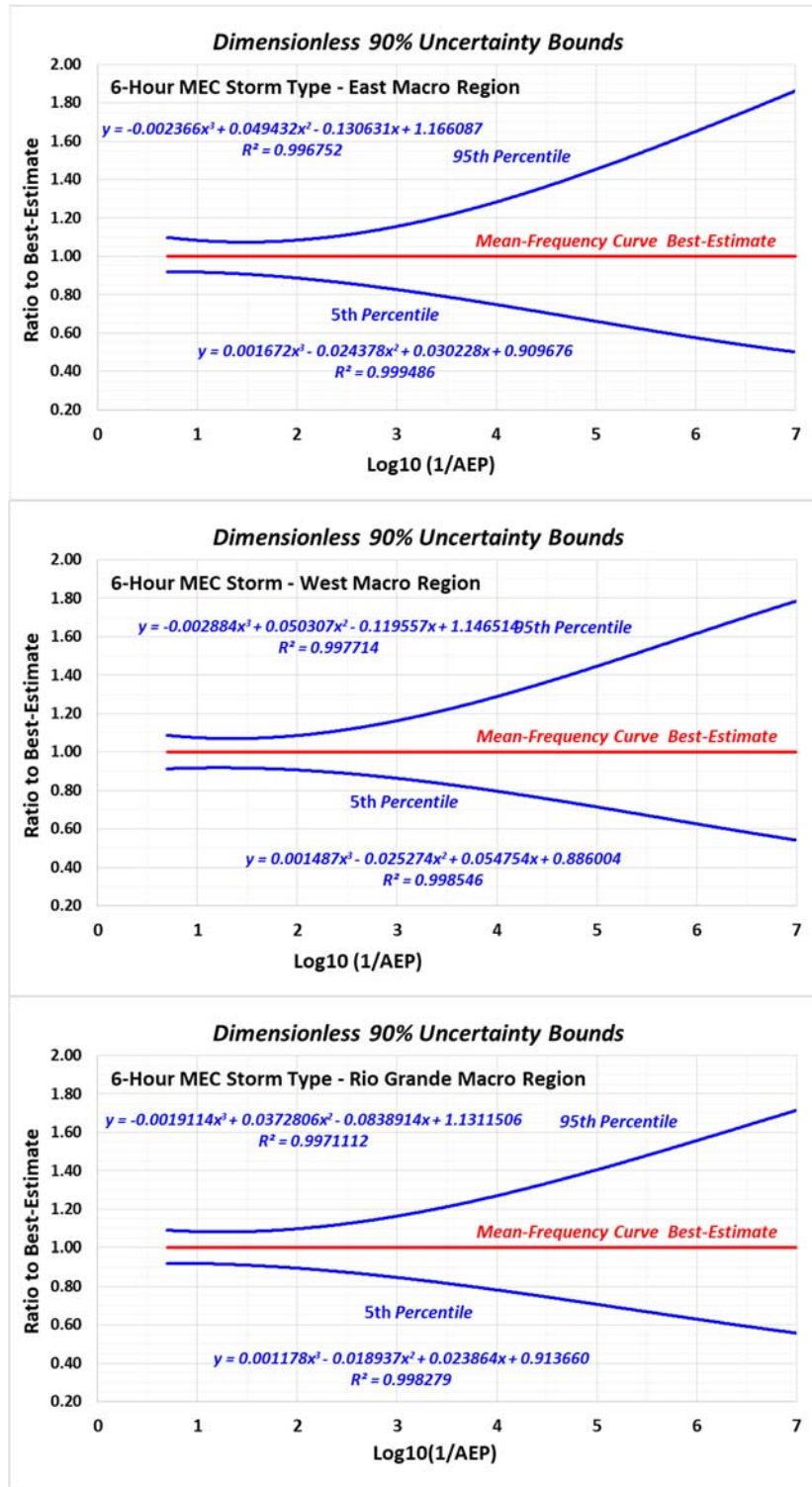


Figure 93. Probability graphics depicting magnitude of dimensionless uncertainty bounds for point MEC precipitation-frequency estimates

## 5.2. Watershed Precipitation Frequency Scaling

It is not practical to provide detailed analyses of watershed PF relationships for the many thousands of dams/watersheds regulated by Colorado and New Mexico. Scaling procedures were therefore developed for producing watershed-specific PF relationships among each of the three Macro Regions for each of the three storm types (MLC, MEC, and LS). These procedures were developed by conducting detailed stochastic storm generation analyses, as described in Sections 2.7 and 4.5, of selected watersheds over a wide range of watershed sizes in each Macro Region.

Watershed PF relationships are shown as Areal Reduction Factors (ARFs) for synoptic-scale, mesoscale, and local storms for each of the Macro Regions - East, West, and Rio Grande in Figure 94, Figure 95, and Figure 96, respectively. Watershed area sizes beyond the end-points of the curves for each storm type in each region have greater uncertainty and the curves should not be extrapolated.

The area size limits (Table 38) are based on the size of test watersheds that were used for calculating the PF-ARFs and not a representation of storm footprint size. For watersheds larger than 1,000 mi<sup>2</sup>, a detailed site-specific watershed precipitation frequency analysis is required; users of the MetPortal deliverable will be alerted to this when operating with a large (>1,000 mi<sup>2</sup>) watershed size.

Table 38. Watershed size limits for application of PF-ARFs

MACRO REGION	LS (2-HOUR)	MEC (6-HOUR)	MLC (48-HOUR)
East	Up to 200 mi <sup>2</sup>	Up to 500 mi <sup>2</sup>	Up to 1,000 mi <sup>2</sup>
Rio Grande	Up to 200 mi <sup>2</sup>	Up to 500 mi <sup>2</sup>	Up to 500 mi <sup>2</sup>
West	Up to 100 mi <sup>2</sup>	Up to 200 mi <sup>2</sup>	Up to 500 mi <sup>2</sup>

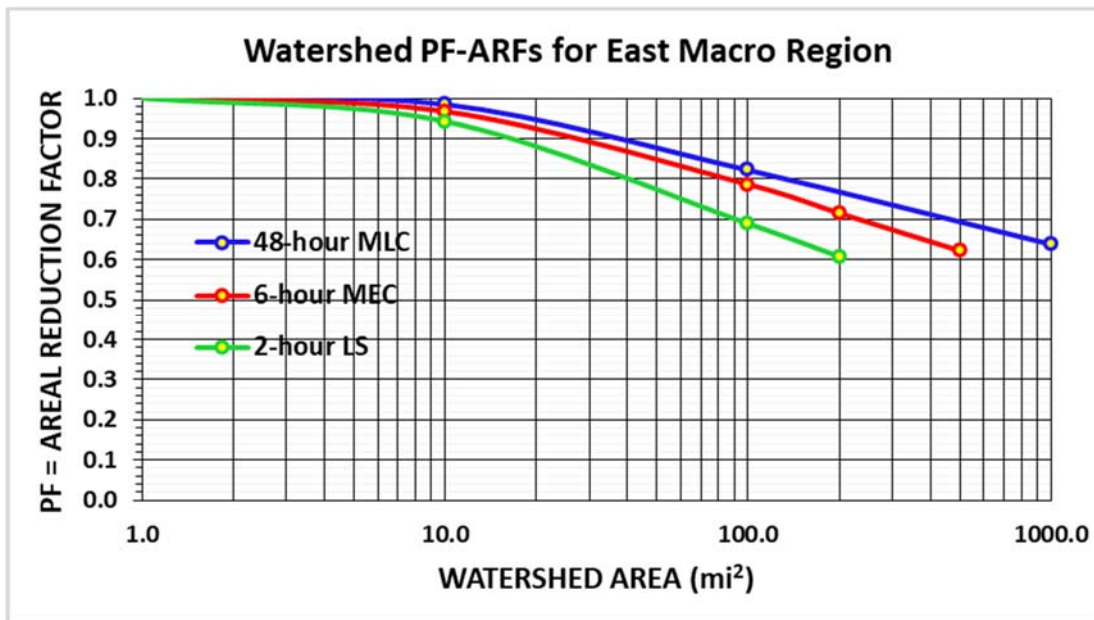


Figure 94. Watershed ARFs for LS, MEC, and MLC storm types for the East Macro Region

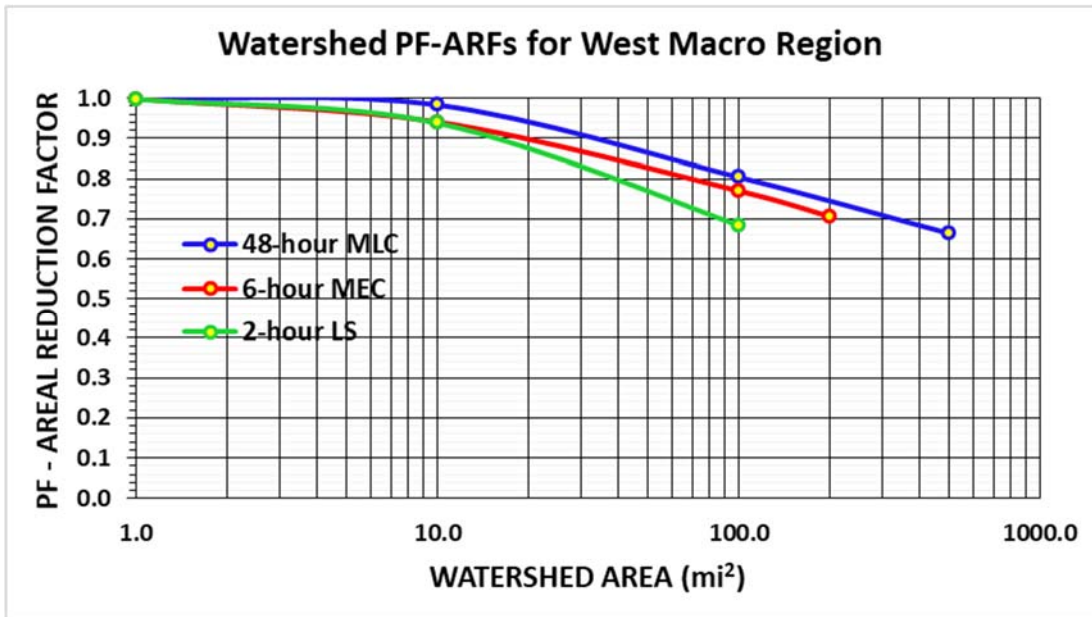


Figure 95. Watershed ARFs for LS, MEC, and MLC storm types for the West Macro Region

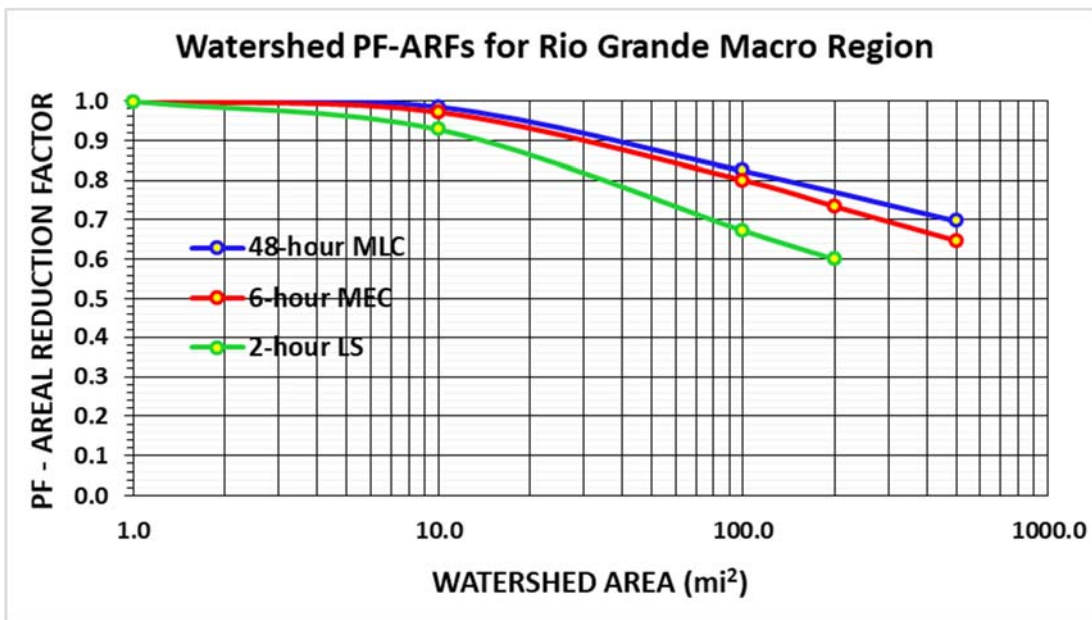


Figure 96. Watershed ARFs for LS, MEC, and MLC storm types for the Rio Grande Macro Region

As expected, there is significant areal reduction for convective thunderstorms (Local Storms) and less so with larger areal-coverage MLC storms. The ARFs provided are considerably different than those provided in NOAA Atlas 2, which are based on dense rain gauge networks across eastern portions of the United States where storm footprints are naturally much larger. The ARFs in this study are more consistent with the ARFs published in HYDRO-40 [Zehr and Myers (1984)], which is based on the Walnut Gulch dense rain gauge network in semi-arid Arizona and provides a good validation of these results.

In order to integrate the scalable ARFs into the MetPortal, it was necessary to translate the ARF curves into polynomial equations using watershed area (in square miles) as the explanatory variable; those are available in Table 39. When applying these, remember to impose the limits conveyed in Table 38.

Table 39. PF-ARF equations

Macro Region	Storm type	Watershed size (mi <sup>2</sup> )	Equation used where y=ARF; x=Log10(watershed area, sq mi)
East	MLC	1 - 1000	$y = -0.013257x^5 + 0.108832x^4 - 0.300585x^3 + 0.265403x^2 - 0.076466x + 1.000694$
East	MEC	1 - 500	$y = -0.009114x^5 + 0.078659x^4 - 0.228760x^3 + 0.198464x^2 - 0.072290x + 1.000464$
East	LS	1 - 200	$y = -0.019265x^5 + 0.146755x^4 - 0.371625x^3 + 0.278722x^2 - 0.092194x + 1.000226$
West	MLC	1 - 500	$y = -0.014771x^5 + 0.121212x^4 - 0.334808x^3 + 0.296515x^2 - 0.085609x + 1.000792$
West	MEC	1 - 200	$y = 0.010574x^3 - 0.088460x^2 + 0.020526x + 0.998281$
West	LS	1 - 100	$y = 0.013351x^4 - 0.058832x^3 - 0.013985x^2 - 0.000290x + 0.997799$
Rio	MLC	1 - 500	$y = -0.012973x^5 + 0.106852x^4 - 0.295968x^3 + 0.261726x^2 - 0.075402x + 1.000672$
Rio	MEC	1 - 500	$y = -0.008558x^5 + 0.071635x^4 - 0.200460x^3 + 0.156794x^2 - 0.047929x + 1.000196$
Rio	LS	1 - 200	$y = -0.018704x^5 + 0.129375x^4 - 0.282599x^3 + 0.131023x^2 - 0.030251x + 0.998530$

### 5.3. Representative Temporal, Spatial, and Temperature Patterns

Section 4.7 provides descriptions of the development of representative temporal and spatial patterns for each storm-type/Macro-Region pair and climatologies of freezing-level and 1000-mb temperature. These datasets are intended to be used in conjunction with a hydrologic/watershed model that resolves different precipitation phases (rain vs. snow) and snow melt. Refer to the Colorado-New Mexico MetPortal for access to the suite of data available and the User Guide for instructions on accessing these data.

#### 5.3.1 Temporal

Dimensionless time series of precipitation (i.e., temporal patterns) were developed as synthetic storm patterns for three Macro Regions: West (of the Continental Divide), East (of the Continental Divide), and the Rio Grande (south-central Colorado and central New Mexico) (Figure 7). In addition, dimensionless time series of precipitation for specific representative storms within each region are provided. Table 40, Table 41 and Table 42 provide the number of storms used to compute the temporal distribution statistics. The large sample size of

storms provides a total of 56 scalable historical and synthetic temporal patterns to use in hydrologic modeling simulations.

*Table 40. Number of Storms Analyzed (Total = 134) as part of Temporal Distribution Analysis*

Storm Types	West Macro Region	Rio Grande Macro Region	East Macro Region	Total Number Storms
LS	21	18	29	68
MEC	9	6	18	33
MLC/TSR	9	12	12	33

*Table 41. Number of scalable historical storms (Total = 44) for use in MetPortal*

Storm Types	West Macro Region	Rio Grande Macro Region	East Macro Region	Total Number Storms
LS	6	6	6	18
MEC	3	3	6	12
MLC/TSR	3	5	6	14

*Table 42. Number of scalable synthetic storms (Total = 12) for use in MetPortal*

Storm Types	West Macro Region	Rio Grande Macro Region	East Macro Region	Total Number Storms
LS	1	1	1	3
MEC	1	1	2	4
MLC/TSR	1	2	2	5

Synthetic storm temporal patterns provide general information on storm characteristics such as: the time to peak of the maximum precipitation rate, the order of precipitation magnitudes surrounding the maximum precipitation rate, tercile of the storm duration with the maximum precipitation volume, and a mass curve/incremental precipitation from depth-area relationships from a suite of storms. For individual specific storm patterns, the user will need to employ meteorological knowledge in selection of appropriate storms based on local geography, climatology, and dam safety considerations - high-intensity, short duration events for peak runoff sensitive locations and longer duration events for volumetric concerns, for example.

Appendix E provides a catalog of the storms used in the temporal analysis and figures of the available scalable patterns for reference.

### 5.3.2 Spatial

A uniform spatial distribution may be used for small watersheds (less than 50 square miles). Spatial variability is most important in larger watersheds with highly variable terrain. Representative spatial patterns are provided based on the PRISM mean monthly precipitation. The representative spatial pattern provides the relative contribution of each grid cell's mean monthly precipitation for the month selected. The ratio grid is then multiplied by the selected watershed precipitation-frequency amounts to produce a storm spatial pattern. Selecting the appropriate month depends on the seasonality of the particular storm type and Macro Region (Sections 5.1.1.5, 5.1.2.5 and 5.1.3.5).

### 5.3.3 Freezing Levels

Freezing levels are used to identify phase changes from liquid to solid precipitation. Temperature time series were generated only for mid-latitude cyclone (MLC) events. An assumption was made that for convective events (i.e., LS and MEC) the freezing level is sufficiently high that the precipitation is liquid-only due to their warm season nature. Tropical events should also assume liquid-only precipitation.

Temperatures may also be of concern to practitioners for snowmelt calculations, particularly in high elevation basins where rain-on-snow events are considered in dam safety decisions. To support snowmelt modeling, climatological information on 1000-mb temperatures and freezing-level heights are provided to calculate lapse rates for determination of the rain-snow line (i.e., precipitation phase of liquid vs frozen).

The representative temperature pattern provides climatological information based on month of the year. The user will decide on the most applicable quantile value to apply for the situation of concern; the best, or median, estimate is the 50th percentile value. Mean time series values for the MLC storm type are provided for both the 1000-mb temperature and freezing level heights.

## 6. Comparisons

### 6.1. NOAA Atlas 14

The hydrologic community is generally familiar with precipitation-frequency products contained in NOAA Atlas 14 [Bonnin et al. (2011); Perica et al. (2013)]. Note that New Mexico is included in Volume 1, while Colorado is included in Volume 8; and there is inconsistency in precipitation frequency estimates across the state border between the two in the Atlas due to different approaches and data available at the time of the Volumes' completion. The CO-NM REPS point PF analysis and results differ from NOAA Atlas 14 with regard to the use of storm typing to assemble the annual maxima datasets and the focus on estimation of very extreme precipitation applicable to dam safety flood analyses. See Overview Section 2 for further details.

There are three primary reasons for differences between the findings for this project and the findings from NOAA Atlas 14. These differences relate to the SWT methodology (Appendix C) that was designed to take advantage of regional information using homogeneous data sets. (1) Storm typing avoids mixed populations and allows analysis on a more homogeneous data set thereby decreasing uncertainty to allow estimation out to rarer AEPs. (2) The current approach groups stations within a narrow range of climatological/meteorological indices that satisfy homogeneity criteria which allows reduction of uncertainties by taking advantage of information from similar stations that are not necessarily near each other (e.g., upslope stations within a range of elevation). (3) Lastly, the spatial mapping approach takes advantage of regional behavior that reduces sampling variability at a given location.

In order to assess the degree to which the NOAA-14 annual maximum series (AMS) data at various durations contains a mixed population of storm types, seven representative, geographically-distributed stations with co-located daily and hourly observations were evaluated. For each annual maximum in the NOAA-14 series, the daily storm type from the Daily Database of Storm Types (DDST) was extracted at the grid cell corresponding to the

station for the date of occurrence, plus a buffer range (2 days for 2-day maxima; 1 day for 6-hour and 2-hour). Multiple storm types could therefore be present for each event across the duration; in cases of conflict, the largest-scale event was chosen for classification (i.e., MLCs > hybrids > MECs > local storms). Finally, for short duration (2-hour and 6-hour) AMS events, an “out-of-season” category was used to denote events that occurred between December and February, or outside the warm season. Such events were differentiated because they were generally low outliers in terms of magnitude and may not be reflective of the convective conditions that typically pose the greatest flood threat at short durations. Event statistics are summarized in Table 43, with the stations aggregated by Macro Region.

*Table 43. Summary of the number of events of each storm type for a given macro-region and duration contained within the sample set of NOAA Atlas 14 AMS. Ratios are expressed in station-years to the total station-years of record. Stations selected include Ft Collins, CO and Pueblo Memorial AP, CO (East); Rienhardt Ranch, NM and Santa Fe, NM (Rio Grande); Cedaredge, CO, Durango, CO, and Grand Junction Regional AP, CO (West).*

Duration	Macro Region	MLC Ratio	Hybrid Ratio	MEC Ratio	Local Ratio	Out-of-Season
2-day	East	66 / 202 (33%)	69 / 202 (34%)	32 / 202 (16%)	35 / 202 (17%)	-
	Rio Grande	43 / 155 (28%)	45 / 155 (29%)	44 / 155 (28%)	23 / 155 (15%)	-
	West	163 / 298 (55%)	83 / 298 (28%)	37 / 298 (12%)	15 / 298 (5%)	-
6-hour	East	5 / 109 (5%)	7 / 109 (6%)	12 / 109 (11%)	84 / 109 (77%)	1 / 109 (1%)
	Rio Grande	5 / 101 (5%)	5 / 101 (5%)	17 / 101 (17%)	72 / 101 (72%)	2 / 101 (2%)
	West	10 / 123 (8%)	9 / 123 (7%)	12 / 123 (10%)	81 / 123 (66%)	11 / 123 (9%)
2-hour	East	2 / 110 (2%)	5 / 110 (5%)	12 / 110 (11%)	91 / 110 (83%)	0 / 110 (0%)
	Rio Grande	4 / 101 (4%)	7 / 101 (7%)	19 / 101 (19%)	71 / 101 (71%)	0 / 101 (0%)
	West	7 / 121 (6%)	10 / 121 (8%)	11 / 121 (9%)	87 / 121 (72%)	6 / 121 (5%)

As evident from Table 43, the AMS data from NOAA-14 contains mixed populations of precipitation types at all durations. While some storm types clearly dominate certain durations, for no region/duration combination is there a complete consensus storm type (100 percent of events). There are also some evident regional differences, with MLCs being more prominent at all durations in the more arid West Macro Region than either of the Rio Grande or East Macro Regions. Accordingly, the West also recorded the highest number of the out-of-season events, with occasional years devoid of summer convection providing for the possibility that windows of peak precipitation associated with larger-scale (generally MLC) events end up constituting short-duration AMS events. Additionally, “up-scale contamination” may occur, with 2-day annual maxima resulting from extreme cases of short-duration, high-intensity precipitation. An excellent example of this phenomenon is the MEC that occurred over Santa Fe, New Mexico on July 25, 1968. That single event produced the greatest 2-hour (2.95”), greatest 6-hour (3.51”), and second-largest 2-day (3.71”) rainfall events on record for Santa Fe. The 2-day annual maximum that resulted is therefore not reflective of atmospheric processes than can produce extreme precipitation on 2-day timescales; it is more

appropriate to consider such an event in the context of short-duration/high-intensity rain events.

Sample plots showing the PF relationships for the 2-hour, 6-hour and 48-hour durations at selected locations are provided for illustrative purposes in Figure 97, Figure 98, and Figure 99. These demonstrate that differences between CO-NM REPs and NOAA-14 PF estimates can vary based on location and duration due to the reasons already discussed.

Lastly, maps of percent differences comparing gridded 1:100 AEP estimates between the two studies demonstrate that the CO-NM REPs PF estimates mostly fall within the uncertainty bounds of the NOAA-14 estimates (unshaded areas) with REPs estimates being generally lower (due to the mixed population of the NOAA-14 data) (Figure 100, Figure 101, Figure 102). The expectation is, then, that the SWT approach develops a relatively higher degree of certainty, especially at rarer AEPs, compared to the NOAA Atlas 14. This can be seen in Figure 103, Figure 104, and Figure 105 where NOAA-14 best estimates predominantly fall outside REPs uncertainty bounds.

The inherent differences between NOAA Atlas 14 and the results of this project make it impossible to make direct comparisons. However, the comparison maps do suggest the most wide-spread differences occur at the 48-hour MLC duration, which is the duration most impacted by mixed storm-types. The differences are generally less for the 2-hour LS and 6-hour MEC durations given more consistency (i.e., same storm-type) with the underlying AMS.

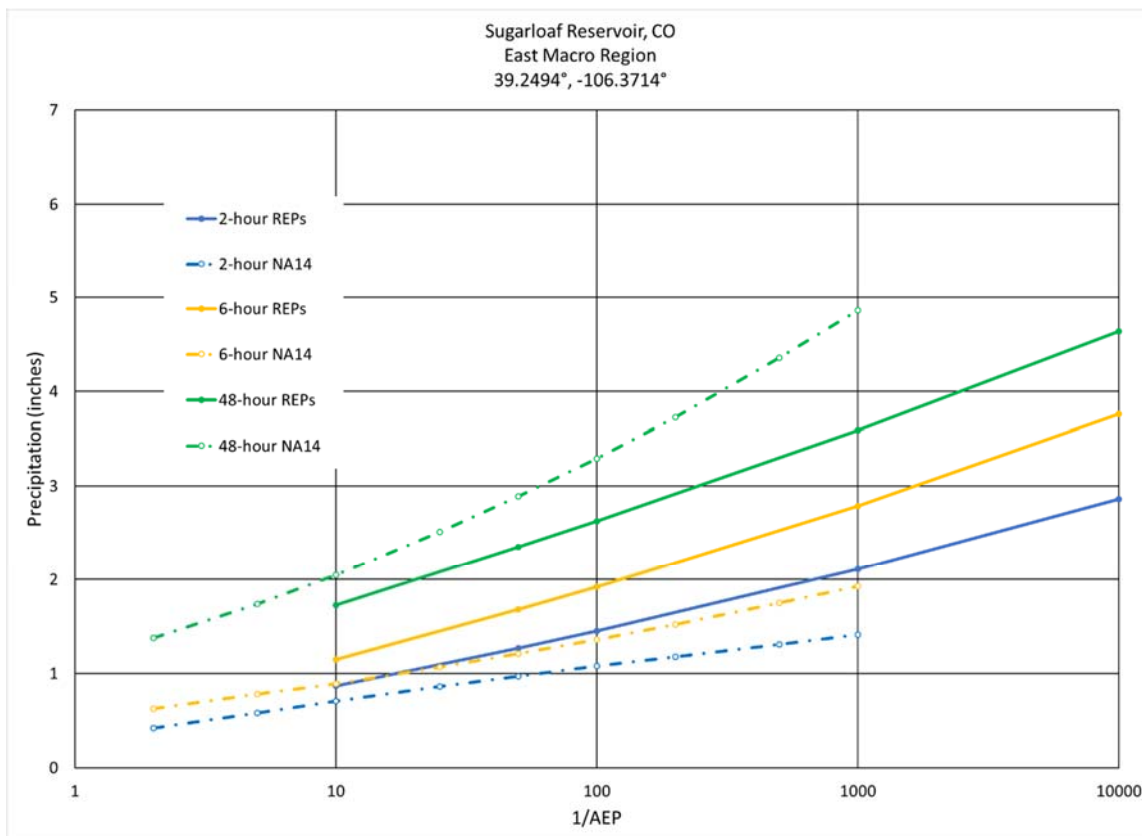


Figure 97. Point comparisons in each Macro Region between NOAA Atlas 14 and the results of CO-NM REPS (1 of 3)

CO-NM Regional Extreme Precipitation Study

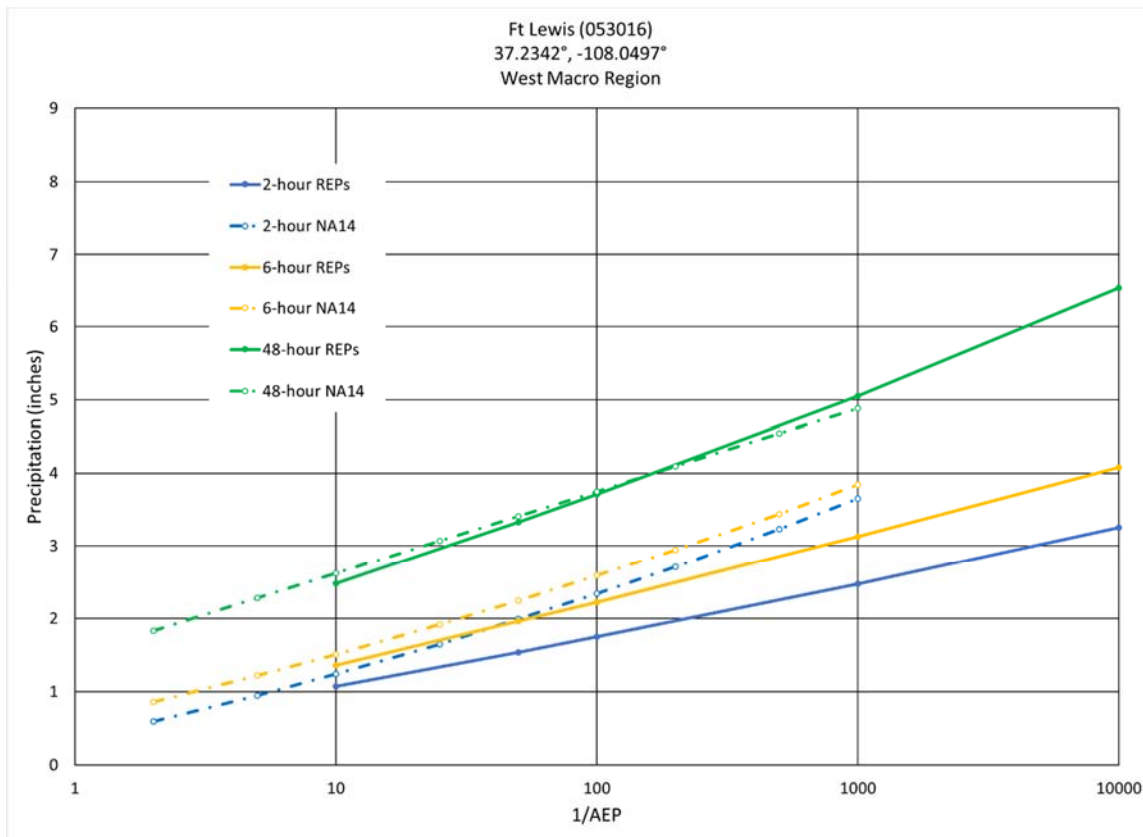


Figure 98. Point comparisons in each Macro Region between NOAA Atlas 14 and the results of CO-NM REPS (2 of 3)

CO-NM Regional Extreme Precipitation Study

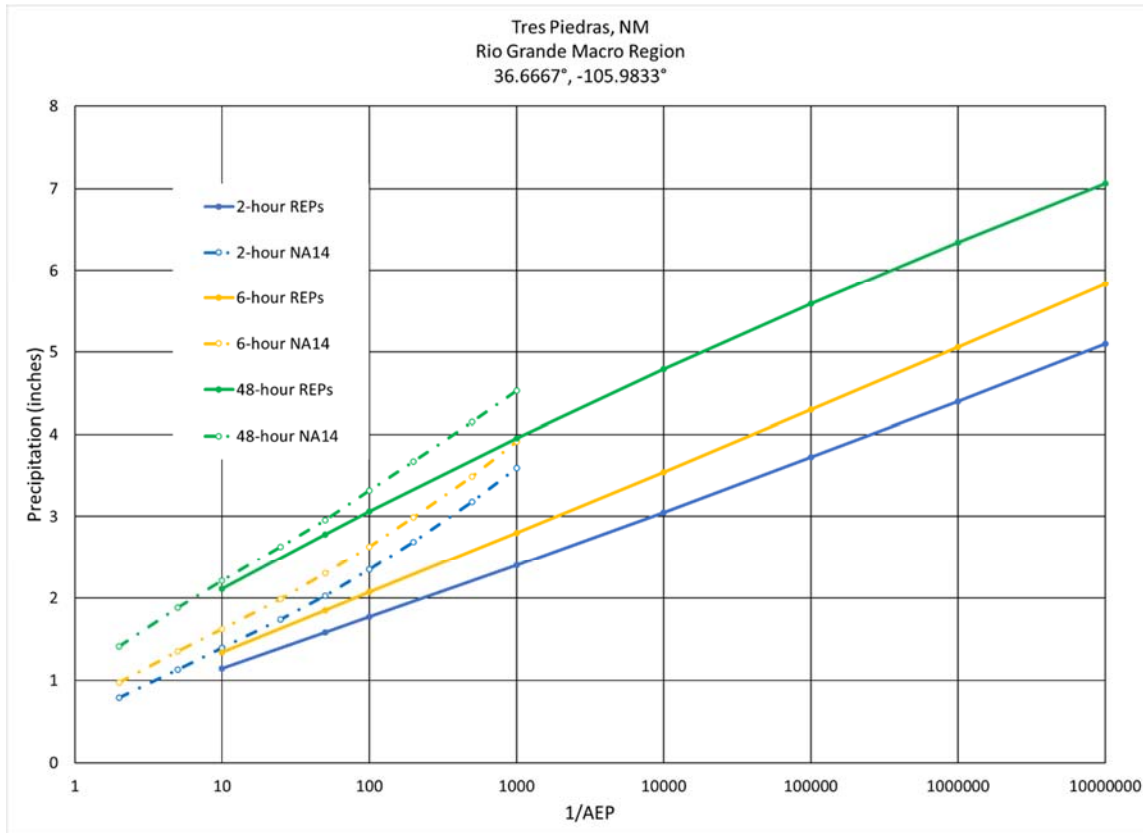


Figure 99. Point comparisons in each Macro Region between NOAA Atlas 14 and the results of CO-NM REPS (3 of 3)

CO-NM Regional Extreme Precipitation Study

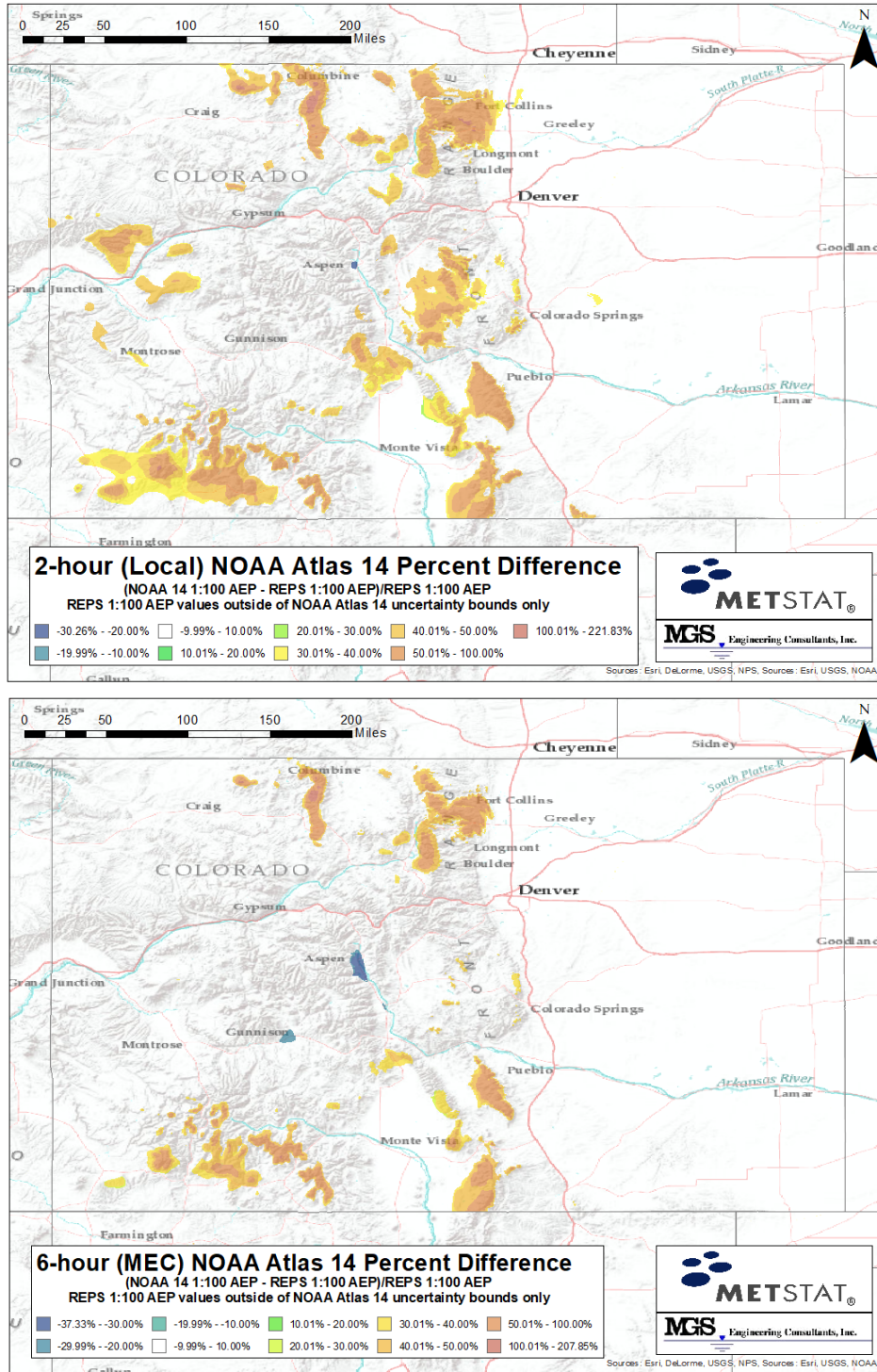


Figure 100. 1 in 100 AEP 2- and 6-hour LS and MEC comparison to NOAA Atlas 14 in Colorado; areas without color represent areas where REPs best estimates are within NOAA-14 confidence limits

# CO-NM Regional Extreme Precipitation Study

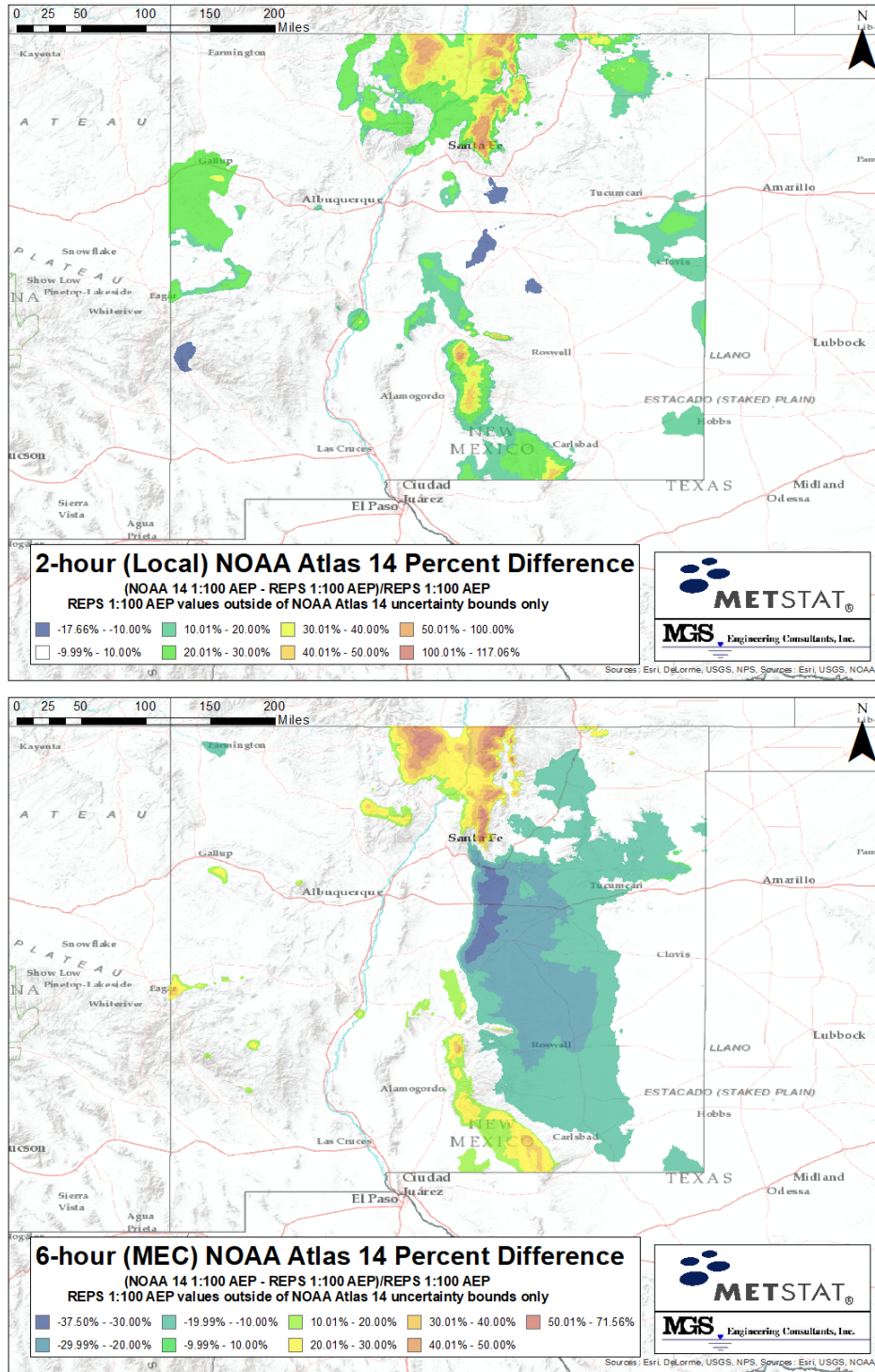


Figure 101. 1 in 100 AEP 2- and 6-hour LS and MEC Comparison to NOAA Atlas 14 in New Mexico; areas without color represent areas where REPs best estimates are within NOAA-14 confidence limits

# CO-NM Regional Extreme Precipitation Study

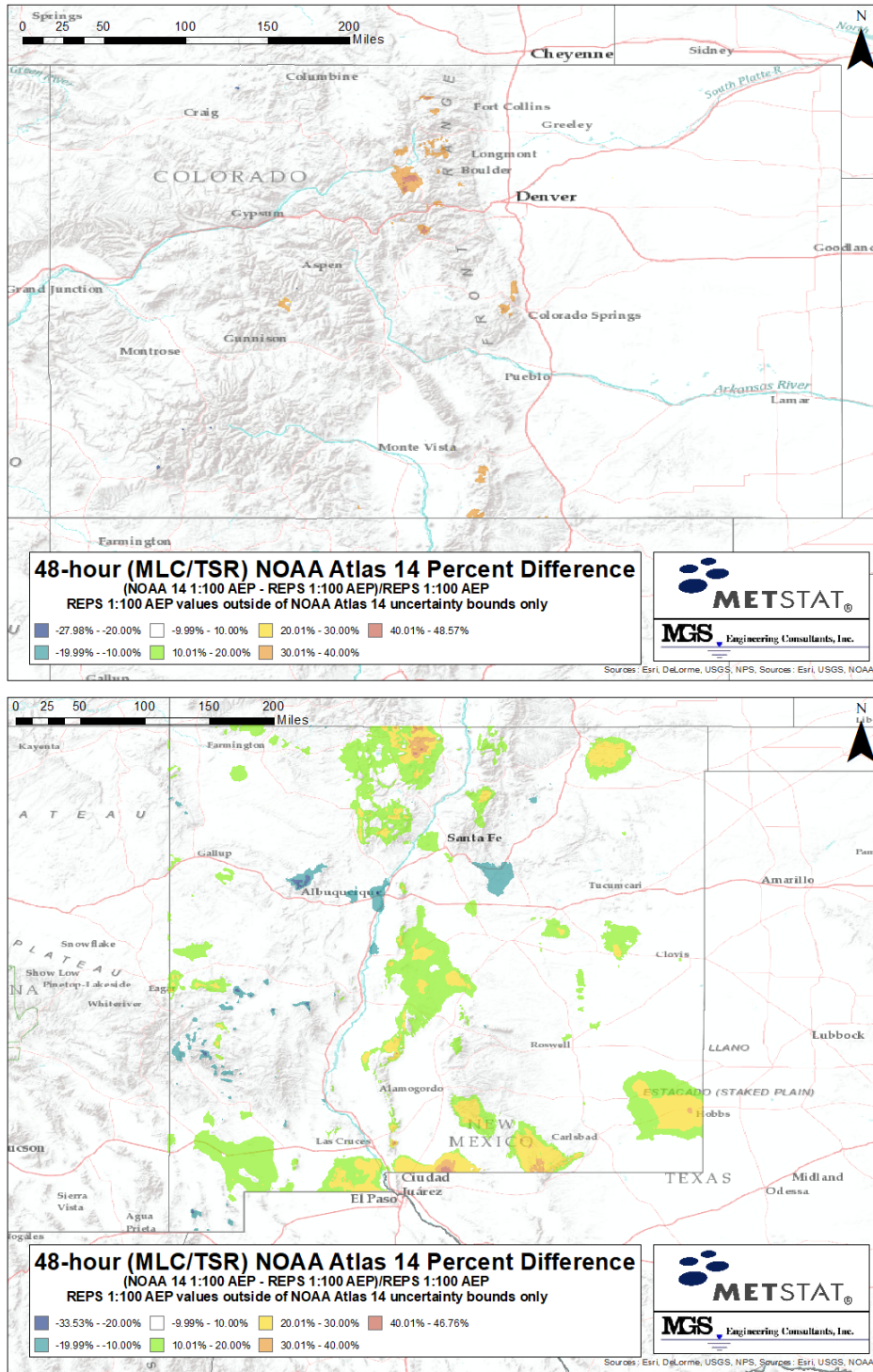


Figure 102. One in 100 AEP 48-hour MLC/TSR comparison to NOAA Atlas 14 in Colorado and New Mexico; areas without color represent areas where REPs best estimates are within NOAA-14 confidence limits

CO-NM Regional Extreme Precipitation Study

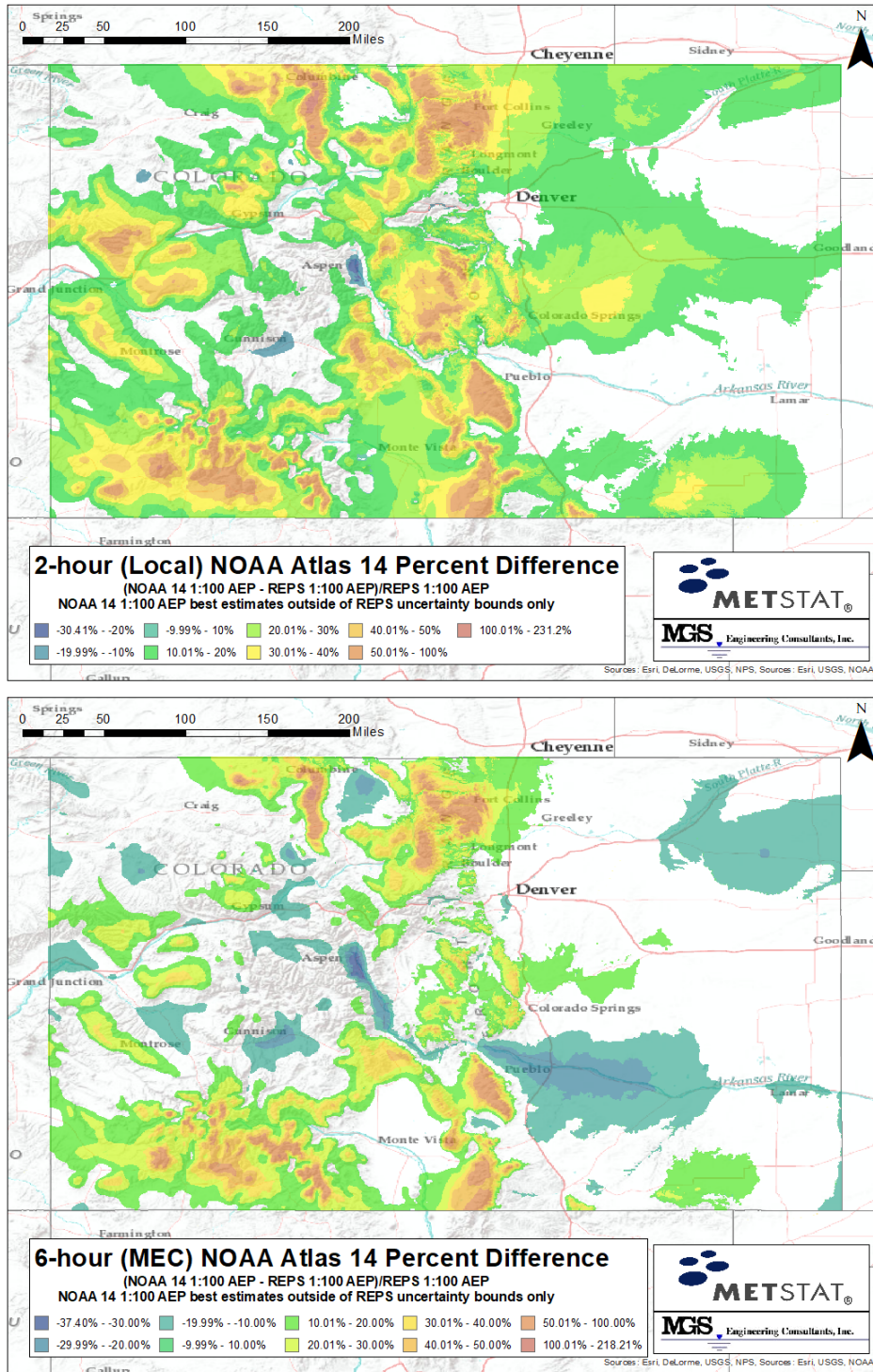


Figure 103. 1 in 100 AEP 2- and 6-hour LS and MEC comparison to NOAA Atlas 14 in Colorado; areas without color represent areas where NOAA-14 best estimates are within REPS confidence limits

CO-NM Regional Extreme Precipitation Study

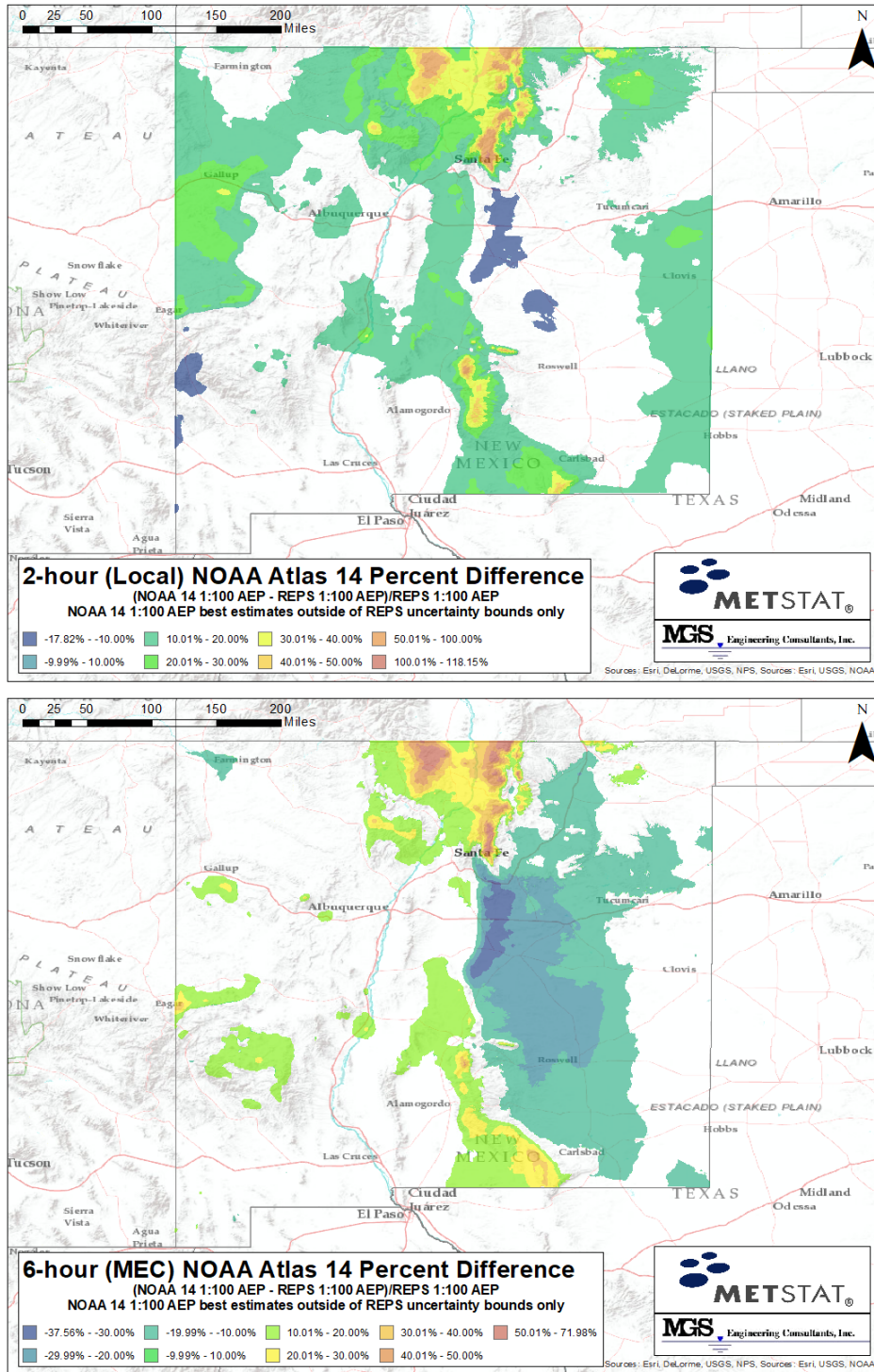


Figure 104. 1 in 100 AEP 2- and 6-hour LS and MEC comparison to NOAA Atlas 14 in New Mexico; areas without color represent areas where NOAA-14 best estimates are within REPS confidence limits

# CO-NM Regional Extreme Precipitation Study

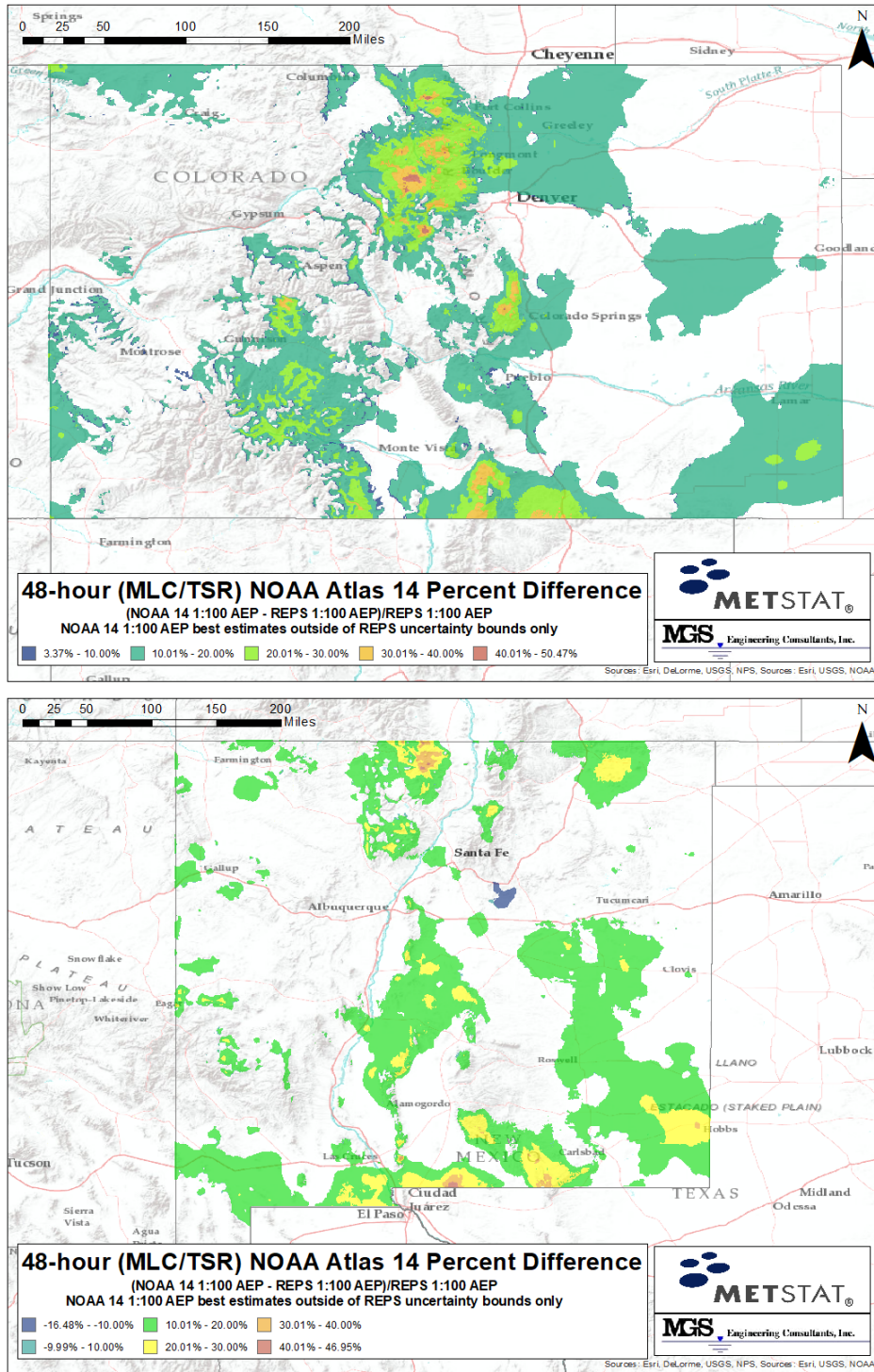


Figure 105. 1 in 100 AEP 48-hour LS and MEC comparison to NOAA Atlas 14 in Colorado and New Mexico; areas without color represent areas where NOAA-14 best estimates are within REPs confidence limits

## 6.2. Estimates of Annual Exceedance Probability for Historical Storms

Evaluating the AEP of extreme historical storms provides a perspective and frame of reference for Engineers and Dam Owners. The maximum point precipitation, for the key duration (2-hour, 6-hour or 48-hour), was determined for 29 of the most extreme storms identified in Volume 2 for PMP analysis that occurred within the precipitation-frequency analysis domain. Extracting at-site mean,  $\xi$ ,  $\alpha$ ,  $\kappa$  and Hondo values (Equation 2) from the PF gridded datasets provided the needed parameters for direct calculation of the equivalent point AEP. Similarly, the equivalent 95 percent percentile AEP is provided for each point storm precipitation value. A summary of the results is provided in Table 44.

*Table 44. AEPs for the most extreme historical storms observed in the project area. NA's indicate the storm center was outside of our spatial mapping domain. Local storms are 2-hours, MECs are 6-hour and MLCs 48-hour.*

Storm Name	Storm ID	Latitude	Longitude	Storm Type	Key Duration Point Precip. (inches)	Best Estimate AEP	95th Percentile AEP
Deer Creek Dam, UT (2010)	1241_2	41.360	-111.910	local	1.48	NA	NA
Rattlesnake, ID (1909)	1274_1	43.648	-115.744	local	1.92	NA	NA
Mt. Hope, CO (2007)	1149_4	37.540	-106.870	local	0.89	1.54E-01	NA
Tajique 121 to 264h, NM (1915)	1650B_1	34.746	-106.413	local	3.07	4.33E-03	1.00E-02
Pyramid, CO (1961)	1652_1	40.540	-106.721	local	0.86	8.96E-02	NA
Cheyenne Mountain, CO (2013)	1302_2	38.745	-104.865	local	6.62	5.50E-09	1.20E-06
Adelaide, CO (1921)	1294_2	38.564	-105.071	local	5.59	2.10E-06	8.00E-05
Aurora, CO (2013)	1302_3	39.705	-104.835	local	3.36	2.48E-03	6.00E-03
Guadalupe Pass, TX (2013)	1530_1	32.035	-104.555	local	3.93	4.51E-03	8.00E-03
Prairieview, NM (1941)	1587_1	33.138	-103.079	local	2.60	5.39E-02	NA
Elbert, CO (1965)	1293_3	39.188	-104.296	local	8.28	3.30E-07	9.00E-06
Plum Creek, CO (1965)	1293_4	39.221	-104.896	local	8.06	1.15E-08	1.20E-06
Penrose, CO (1921)	1294_1	38.464	-105.070	local	4.31	9.43E-04	5.00E-03

CO-NM Regional Extreme Precipitation Study

Storm Name	Storm ID	Latitude	Longitude	Storm Type	Key Duration Point Precip. (inches)	Best Estimate AEP	95th Percentile AEP
Tajique 121 to 264h, NM (1915)	1650B_1	34.746	-106.413	mec	4.89	2.62E-05	3.00E-04
Guadalupe Pass, TX (2013)	1530_1	32.035	-104.555	mec	7.46	1.09E-04	1.20E-04
Rattlesnake, ID (1909)	1274_1	43.648	-115.744	mec	4.18	NA	NA
Adelaide, CO (1921)	1294_2	39.705	-104.835	mec	8.70	2.89E-06	3.00E-05
McColleum Ranch, NM (1941)	1486_1	32.146	-104.746	mec	10.88	1.39E-08	3.00E-06
Carlsbad, NM (1966)	1568_1	32.254	-104.613	mec	7.50	5.31E-05	3.00E-04
Penrose, CO (1921)	1294_1	38.464	-105.070	mec	10.49	3.29E-06	3.00E-05
Rattlesnake, ID (1909)	1274_1	43.648	-115.744	mlc	11.41	NA	NA
Guadalupe Pass, TX (2013)	1530_1	32.035	-104.555	mlc	17.71	2.09E-05	1.00E-04
Tajique 121 to 264h, NM (1915)	1650B_1	34.746	-106.413	mlc	6.83	1.92E-04	1.00E-03
Coal Creek, CO (2013)	1302_5	39.865	-105.285	mlc	14.70	8.13E-07	1.20E-05
Adelaide, CO (1921)	1294_2	39.705	-104.835	mlc	10.08	6.10E-05	3.00E-04
Lake Moraine, CO (1894)	1614_2	38.804	-104.946	mlc	8.69	2.33E-04	1.00E-03
McColleum Ranch, NM (1941)	1486_1	32.146	-104.746	mlc	19.39	3.22E-06	3.00E-05
Penrose, CO (1921)	1294_1	38.464	-105.070	mlc	12.16	2.35E-06	3.00E-05
Lake Maloya, NM (1955)	1251_1	37.009	-104.341	mlc	14.74	3.16E-06	8.00E-05
Big Elk Meadow, CO (1969)	1253_1	40.270	-105.420	mlc	14.23	2.72E-07	1.00E-05
Ward District, CO (1894)	1614_1	39.804	-105.329	mlc	10.55	2.46E-05	1.20E-04

## 7. Uncertainty in Precipitation Frequency Estimates

It is expected that the majority of applications of point and watershed precipitation-frequency will be for rare to extreme storms. It is important in these situations to provide information on uncertainty along with the best-estimate of precipitation for a selected Annual Exceedance Probability (AEP). In this study, 90 percent uncertainty bounds are provided that identify the 5<sup>th</sup> and 95<sup>th</sup> percentiles for the best-estimate to alert the user of the magnitude of uncertainty associated with a design precipitation value.

Identifying sources of aleatoric and epistemic uncertainty and assessing the effects of uncertainty was one of the goals of the PF analyses for both point precipitation and watershed precipitation. Probability distributions were used to characterize epistemic uncertainty for point precipitation associated with estimating at-site means, regional L-Cv, regional L-Skewness, identification of the regional probability distribution, and solving for Hondo, the 2<sup>nd</sup> shape parameter, of the 4-parameter Kappa Distribution.

Probability distributions were also used in computation of watershed PF relationships using SST methods. This included aleatoric uncertainty in the number of storm events per year from which the annual maximum was obtained. It also included epistemic uncertainty through the manner in which spatial patterns intersected watershed shapes. Resampling methods were used to characterize epistemic uncertainty in the selection of spatial storm patterns and the magnitude of precipitation at the storm center for a given spatial pattern.

Characterization of uncertainties as described above allowed for uncertainty analyses to be conducted as part of the development of watershed PF relationships for a range of watershed sizes (8 mi<sup>2</sup> over 1,000 mi<sup>2</sup>) for the three storm types and three Macro Regions. All of these topics are described in Sections 4.4.7 and 4.5.1.

An example of the findings of uncertainty analyses for the MEC storm type are listed below. Figure 41 and Figure 80 are repeated from earlier in the report (as Figure 106 and Figure 107, respectively), where the square root of the height of the columns in the histogram are related to the width of uncertainty bounds in the East Macro Region.

Quantile estimates for selected AEPs for both point and watershed precipitation-frequency are provided to users via the MetPortal tool along with uncertainty bounds.

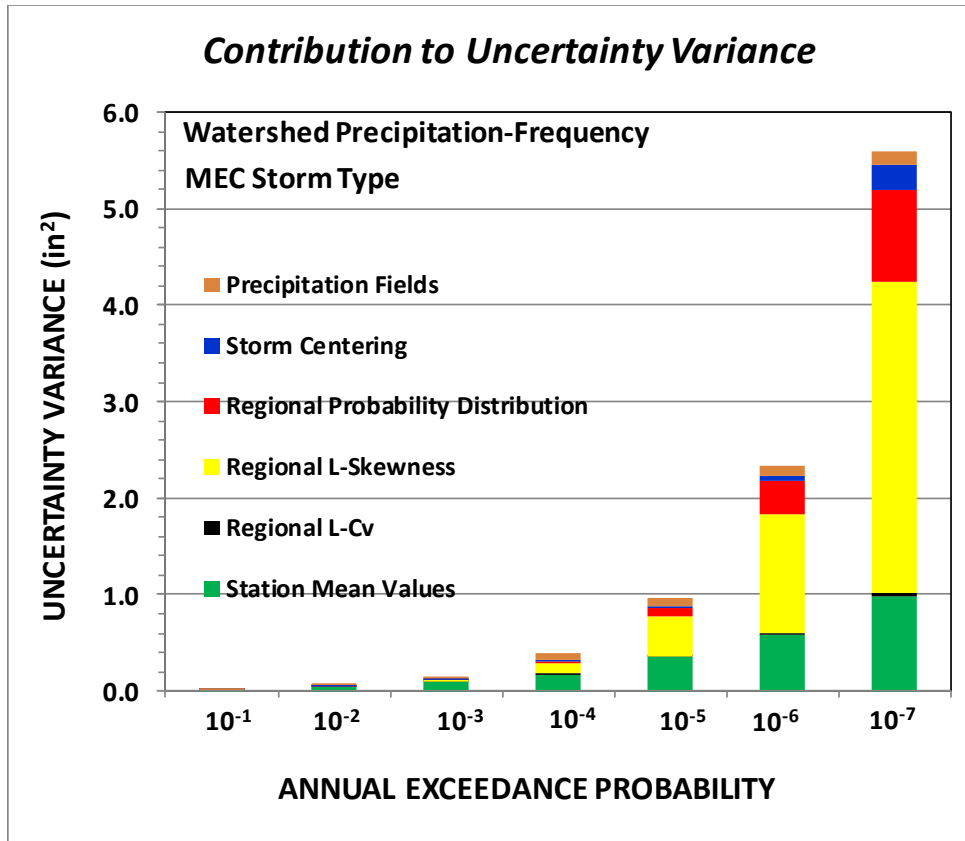


Figure 106. Example of relative contribution to total uncertainty from various sources of uncertainty in developing Watershed Precipitation-Frequency Relationship for the MEC Storm Type in the East Macro Region

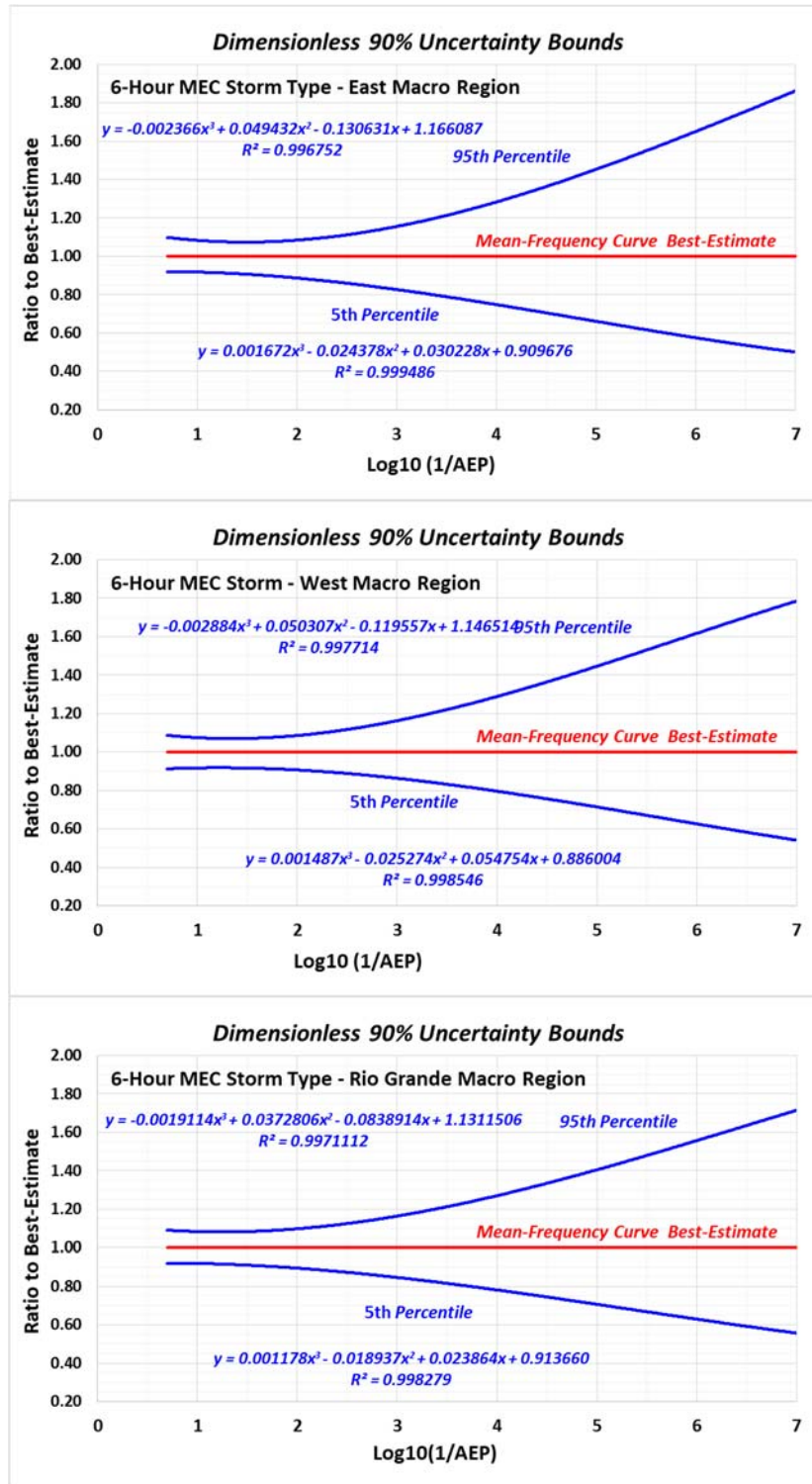


Figure 107. Probability graphics depicting magnitude of dimensionless uncertainty bounds for point MEC precipitation-frequency estimates

## 8. Limitations

These findings are based on the available historical record which dates to the late 19th century. They can be improved upon as more data become available and there is a greater understanding of the meteorological processes that produce extreme precipitation. Non-stationary climate considerations suggest that the findings from this project should be reevaluated in the future.

## 9. Conclusions and Applications

Successful probabilistic hydrologic modeling of extreme floods for dam safety applications depends on the use of representative storm characteristics. This includes:

- watershed-specific Precipitation-Frequency (PF) relationship,
- spatial and temporal storm patterns,
- storm seasonality information which helps inform the choice of:
  - representative antecedent soil moisture;
  - snowpack;
  - initial streamflow; and
  - initial reservoir level.

The watershed PF relationship must be developed for a specific storm type because synoptic scale, mesoscale, and local storms have different spatial and temporal storm patterns that produce different flood hydrographs. Compatibility must be maintained between the watershed PF relationship, spatial and temporal storm patterns, and storm seasonality.

Therefore, regional point PF analyses have been conducted in a manner that allows development of watershed PF relationships for a specific storm type. In addition, uncertainty bounds have been provided along with the best-estimate for a selected AEP that can be useful in accounting for precipitation-related uncertainties in hydrologic modeling of floods.

Representative temporal patterns have been provided comprised of both scalable historical storms and synthetic storms for use in flood modeling. The suite of historical storms is intended for use by consultants and dam safety staff for detailed flood analyses where greater scrutiny of spillway adequacy is warranted. The synthetic temporal patterns are anticipated for internal usage by the Dam Safety Program engineers for developing unbiased estimates of spillway performance. The synthetic patterns may also be used in either a standards-based approach or Risk-Informed Decision framework for sizing of spillways by consultants.

Information on storm spatial patterns has been provided which will be useful for larger watersheds where a storm spatial pattern can be an important contributor to flood magnitude.

Storm seasonality information has been provided for each storm type for locations throughout the Colorado and New Mexico areas. Seasonality information will be helpful for setting initial conditions for soil moisture, streamflow and reservoir level. Seasonality information will also be useful for assessing whether snowpack and rain-on-snow is a concern and for setting initial snow-water content for a given time of year.

Information on freezing levels has been provided to assist in hydrologic modeling for fall and spring storm events where snowmelt could be an important contribution to runoff.

In summary, storm-related information has been provided in this report and through the MetPortal tool that will support both standards-based and probabilistic flood modeling for operation of State Dam Safety activities.

## 10. Deliverables

Results are provided via the MetPortal - Precipitation Frequency CO-NM REPs (<https://conm-reps-gui.shinyapps.io/metportal>). This is an interactive, public-facing on-line Graphical User Interface (GUI) for data delivery and includes a downloadable User Guide. The MetPortal and User Guide will be updated occasionally with bug fixes, enhancements, and new functionality as necessary. Precipitation-frequency estimates and 90 percent uncertainty bounds for a point or for an uploaded watershed for each storm type-duration are available, listed again in Table 45. Precipitation Frequency Estimates are provided for annual exceedance probabilities (AEPs) ranging from  $10^{-1}$  to  $10^{-7}$ . Spatial and temporal precipitation patterns, together with freezing height climatologies are also available via the MetPortal for integration into watershed models.

*Table 45. List of Storm Types and associated durations available via the MetPortal*

Storm Type	Duration
Local Storms	2-hour
Mesoscale Storms with Embedded Convection	6-hour
Mid-Latitude Cyclones and Tropical Storms and Remnants (synoptic-scale)	24-hour 48-hour (key duration) 72-hour

## 11. References

- Benjamin, J.R. and C.A. Cornell, 1970: Probability and Statistics for Civil Engineers, McGraw-Hill. 640 pp.
- Bonnin, G.M., D. Martin, B. Lin, T. Parzybok, M. Yekta, and D. Riley, 2011: NOAA Atlas 14 Volume 1 Version 5.0, Precipitation-Frequency Atlas of the United States. NOAA, National Weather Service, Silver Spring, Maryland.
- Compo, G.P., and Coauthors 2011: The Twentieth Century Reanalysis Project. *Quarterly J. Roy. Meteorol. Soc.*, 137, 1-28, <http://dx.doi.org/10.1002/qj.776>.
- Dalrymple, D., 1960: Flood Frequency Analysis. Manual of Hydrology: Part 3, Water Supply Paper 1543-A, 86 pp, <https://pubs.usgs.gov/wsp/1543a/report.pdf>.
- Daly, C., 1994: PRISM, Parameter-Elevation Regression on Independent Slopes Model, Oregon State University, Oregon Climate Service.

- Daly, C., R.P. Neilson, and D.L. Phillips, 1994: PRISM, A Statistical-Topographic Model for Mapping Climatological Precipitation over Mountainous Terrain, *Journal of Applied Meteorology*, 33, 140-158.
- Efron B., 1979: Bootstrap Methods: Another Look at the Jackknife, *The Annals of Statistics*, 7, No. 1, 1-26.
- FEMA (Federal Emergency Management Agency), 2012: Summary of Existing Guidelines for Hydrologic Safety of Dams. 22 pp, [https://www.fema.gov/media-library-data/20130726-1849-25045-1538/01\\_hydrosafetydam\\_intro.pdf](https://www.fema.gov/media-library-data/20130726-1849-25045-1538/01_hydrosafetydam_intro.pdf).
- FERC (Federal Energy Regulatory Commission), 2014: FERC Engineering Guidelines Risk-Informed Decision-Making. Chapter R19 Probabilistic Flood Hazard Analysis, 61 pp, <https://www.ferc.gov/industries/hydropower/safety/guidelines/ridm/eng-guide/chapter-R19.pdf>.
- Hansen, E. M., D. D. Fenn, L. C. Schreiner, R. W. Stodt, and J. F. Miller, 1988: Hydrometeorological Report No. 55A: Probable Maximum Precipitation estimates - United States Between the Continental Divide and the 103<sup>rd</sup> Meridian. NOAA, National Weather Service, Silver Spring, Maryland.
- Hosking, J.R.M., 1990: L-Moments: Analysis and Estimation of Distributions using Linear Combinations of Order Statistics, *Journal Royal Statistical Society, Series B*, Vol 52, 105-124.
- Hosking, J.R.M., and J.R. Wallis, 1997: *Regional Frequency Analysis - An Approach Based on L-Moments*, Cambridge Press, 224 pp.
- Hydrometrics, Inc., 2010: Dam Safety Program, Tech Note 2, Loss of Life Determination for Spillway Capacity Analysis. Prepared for Montana Department of Natural Resources and Conservation, 39 pp, [http://dnrc.mt.gov/divisions/water/operations/docs/dam-safety/technical-references/technical\\_note\\_2.pdf/view](http://dnrc.mt.gov/divisions/water/operations/docs/dam-safety/technical-references/technical_note_2.pdf/view).
- ICOLD (International Committee on Large Dams), 2005: *Risk Assessment in Dam Safety Management: A Reconnaissance of Benefits, Methods and Current Applications*, 276 pp.
- Karl, T. R. and W.J. Koss, 1984: Regional and National Monthly, Seasonal, and Annual Temperature Weighted by Area, 1895-1983. *Historical Climatology Series 4-3*, National Climatic Data Center, Asheville, NC, 38 pp.
- Knapp, K. R., M. C. Kruk, D. H. Levinson, H. J. Diamond, and C. J. Neumann, 2010: The International Best Track Archive for Climate Stewardship (IBTrACS): Unifying tropical cyclone best track data. *Bulletin of the American Meteorological Society*, 91, 363-376. <http://www.ncdc.noaa.gov/ibtracs/>.
- Kuczera G., 1982: Combining Site-Specific and Regional Information: An Empirical Bayes Approach, *Water Resources Research*, 18, No. 2, 306-314.

- Kunkle, Kenneth, 2018: Personal communication. NOAA's Cooperative Institute for Climate and Satellites.
- Livneh B., T.J. Bohn, D.S. Pierce, F. Munoz-Ariola, B. Nijssen, R. Vose, D. Cayan, and L.D. Brekke, 2015: A spatially comprehensive, hydrometeorological data set for Mexico, the U.S., and southern Canada 1950-2013, *Nature Scientific Data*, 5:150042, doi:10.1038/sdata.2015.42. <http://ciresgroups.colorado.edu/livneh/data/daily-observational-hydrometeorology-data-set-north-american-extent>.
- McKay, M.D., W.J. Conover, and R.J. Beckman, 1979: A Comparison of Three Methods for Selecting Values of Input Variables in the Analysis of Output from a Computer Code, *Technometrics*, 221, 239-245.
- McKee, T. B. and N.J. Doesken, 1997: Colorado extreme storm precipitation data study. Final report: Summary of accomplishments and work performed February 15, 1995 through October 31, 1996. Climo Report 97-1, Dept. of Atmos. Sci., CSU, Fort Collins, CO, May, 107 pp. [https://ccc.atmos.colostate.edu/pdfs/Climo\\_97-1\\_Extreme\\_ppt.pdf](https://ccc.atmos.colostate.edu/pdfs/Climo_97-1_Extreme_ppt.pdf)
- MGS Engineering Consultants, MetStat, Applied Climate Services and Riverside Technology, 2015: Regional Precipitation-Frequency Analyses for Mid-Latitude Cyclones, Mesoscale Storms with Embedded Convection, Local Storms and Tropical Storm Remnant Storm Types in the Tennessee Valley Watershed, prepared for Tennessee Valley Authority (TVA). [http://www.mgsengr.com/damsafetyfiles/TVA\\_Point%20Precipitation-Frequency\\_2015-03-02\\_Release.pdf](http://www.mgsengr.com/damsafetyfiles/TVA_Point%20Precipitation-Frequency_2015-03-02_Release.pdf)
- Nathan, R.J., E.M. Weinmann, and P. Hill, 2003: Use of Monte Carlo Simulation to Estimate the Expected Probability of Large to Extreme Floods. *28th International Hydrology and Water Resources Symposium*, Wollongong, NSW, The Institution of Engineers, Australia, 105-122.
- National Atlas of the United States, 2002: Continental Divide of the United States. <https://www.sciencebase.gov/catalog/item/4f4e477ee4b07f02db480f8a>.
- NRC (Nuclear Regulatory Commission), 2014: Probabilistic Flood Hazard Assessment Research Plan Version 2014-10-23. 18 pp, <https://www.nrc.gov/docs/ML1429/ML14296A442.pdf>.
- Perica, S., D. Martin, S. Pavlovic, I. Roy, M. St. Laurent, C. Trypaluk, D. Unruh, M. Yekta, G. Bonnin, 2013: NOAA Atlas 14 Volume 8 Version 2, Precipitation-Frequency Atlas of the United States, Midwestern States. NOAA, National Weather Service, Silver Spring, Maryland.
- Schaefer, M.G., 1989: Characteristics of Extreme Precipitation Events in Washington State. Washington State, Department of Ecology, Water Resources Program, number, pages.
- Schaefer, M.G., 1997: Magnitude Frequency Characteristics of Precipitation Annual Maxima in Southern British Columbia, MGS Engineering Consultants, Inc.
- Schaefer, M.G., 1997: Data-Quality Checking Software for Precipitation Maxima. MGS Engineering Consultants.

- Schaefer M.G., 2015, Algorithm for Move-the-Earth Stochastic Storm Generation of Watershed Precipitation-Frequency Relationships for the Mesoscale Storm with Embedded Convection Storm Type, Technical Memorandum prepared for Tennessee Valley Authority.
- Schaefer, M.G. and B.L. Barker, 2005: Stochastic Modeling of Extreme Floods on the American River at Folsom Dam Flood-Frequency Curve Extension. MGS Engineering Consultants for US, US Army Corps of Engineers, Hydrologic Engineering Center, Davis CA, 54 pp.
- Schaefer, M.G. and B.L. Barker, 2009: L-Moments Regional Analysis Package (L-RAP). MGS Software LLC.
- Schaefer, M.G., B.L. Barker, G.H. Taylor, and J.R. Wallis, 2002: Regional Precipitation-Frequency Analysis and Spatial Mapping for 24-Hour and 2-Hour Durations for Western Washington, MGS Engineering Consultants and Oregon Climate Service for Washington State Dept. of Transportation, 93 pp.
- Schaefer, M.G., B.L. Barker, G.H. Taylor, and J.R. Wallis, 2006: Regional Precipitation-Frequency Analysis and Spatial Mapping for 24-Hour and 2-Hour Durations for Eastern Washington. MGS Engineering Consultants and Oregon Climate Service for Washington State Dept. of Transportation, 82 pp.
- Schaefer, M.G., B.L. Barker, G.H. Taylor, and J.R. Wallis, 2007: Regional Frequency Analysis and Spatial Mapping of 24-Hour Precipitation for Oregon. MGS Engineering Consultants and Oregon Climate Service for Oregon State Dept. of Transportation, 114 pp.
- SEFM, Stochastic Event Flood Model User's Manual, 2015: MGS Software LLC Olympia WA, developed by Schaefer MG and Barker BL, 2001, 2009, 2015.
- USBR (United States Bureau of Reclamation), 2011: Dam Safety Public Protection Guidelines, A Risk Framework to Support Dam Safety Decision-Making. 38 pp, <https://www.usbr.gov/ssle/damsafety/documents/PPG201108.pdf>.
- USBR (United States Bureau of Reclamation), 2012: Altus Dam Hydrologic Hazard and Reservoir Routing for Corrective Action Study. Bureau of Reclamation, Flood Hydrology and Consequences Group, 230 pp.
- U.S. Geological Survey, 2017, USGS NED 1 arc-second n19w067 1 x 1degree ArcGrid 2017: U.S. Geological Survey.
- US Weather Bureau, 1957: Rainfall Intensity-Frequency Regime, Part 2 - Southeastern United States. Tech Paper No. 29, US Dept. of Commerce, Washington, DC.
- Weiss, L.L., 1964, Ratio of True to Fixed Interval Maximum Rainfall, Journal Hydraulics, ASCE, 90(HY1), pp77-82.
- Zehr, R. M. and V. A. Meyers, 1984: NOAA Technical Memorandum NWS HYDRO-40: Depth-Area Ratios in the Semi-Arid Southwest United States. NOAA, National Weather Service, Silver Spring, Maryland.